Peptidoglycan Dynamics in *Bacillus subtilis*

Alaa Aljohani

A thesis submitted for the degree of **Doctor of Philosophy**

Newcastle University

Institute for Cell and Molecular Biosciences

September 2024

Abstract

Gram-positive bacterial cell morphology, growth, and division rely on a delicate balance of peptidoglycan synthesis and controlled degradation to maintain the structural integrity of the cell wall. The process of growth involves synthesising new wall material underneath the existing cell wall on the surface of the cell membrane. This growth requires the cell wall degrading enzymes to distinguish between the newly generated wall and the old wall, selectively degrading the outer layers of the wall to facilitate cell enlargement.

As the *B. subtilis* genome encodes 42 genes that are potentially involved in peptidoglycan degradation, systematic deletion of the known autolytic enzymes was used combined with phenotypic analysis for both cell morphological changes and the ability to become motile. From this work, it was found that only 1 of 2 specific autolytic enzymes is functionally required for growth (CwlO and LytE). Although these two autolytic enzymes exhibit a significant degree of functional redundancy, they are required for slightly different aspects of cell morphology. Only CwlO, in concert with CwlQ or CwlS, was also found to be required for the efficient insertion of flagella through the cell wall. Further analysis showed that CwlO activity with respect to cell growth required the activity of a peptidoglycan carboxypeptidase (DacA), but this was not required for flagellar insertion, suggesting that CwlO has two distinct modes of action.

In summary, the results of the work presented in this thesis show that the majority of the predicted cell wall degrading enzymes are dispensable, and only 2 enzymes, CwlO and LytE, have critical roles in maintaining normal cell morphology. Interestingly, this study also reveals that the two key autolytic enzymes seem to have distinct modes of action and potentially differ in their substrate specificity. In this respect, a model for cell growth is presented that tries to amalgamate the results of this work with previously published ideas to explain how cell growth is coordinated with respect to peptidoglycan synthesis and degradation without compromising cell integrity and maintaining cell morphology. This model potentially outlines the basic mechanism of cell wall metabolism in Gram-positive rod-shaped bacteria. It also seems that aspects of the mechanism are also conserved in other bacterial species with a different cell morphology as well as in Gram-negative bacteria. These results clearly indicate that the autolytic enzymes and their regulatory mechanisms are potentially interesting novel targets for the development of small molecule antibacterial compounds.

Acknowledgement

First and foremost, I would like to express my heartfelt gratitude to my thesis advisor, Dr. Richard Daniel, for helping me understand that science is a journey, not just a destination. Thank you for believing in me and never letting me become discouraged. Your willingness to open your office door whenever I encountered difficulties or had questions about my research or writing has been invaluable. I am grateful for consistently allowing this project to be my own work while guiding me in the right direction when necessary. Without your support, I would never have discovered and written this thesis. I would also like to extend my thanks to all members of the Daniel laboratory group, both past and present, for making my PhD journey an enjoyable experience. I genuinely appreciate the knowledge and support you have contributed to my time at Newcastle University.

I want to extend my deepest gratitude to my wonderful, supportive, loving, and ever-patient family and friends. To Mom and Dad, thank you for investing so much of your time in me. From continuous encouragement throughout my years of study, our countless video calls discussing the research and writing process, and your personal engagement in following my work mean more to me than words can express. I know that you will always be there to support me in everything I do. To my sisters, despite the physical distance, you have been my cheerleaders, and your unwavering support has meant the world to me. Amirah, you have been a constant source of support, both academically and personally. As a friend, listener, and constructive critic, you have been invaluable in my journey. To Taghreed, I appreciate your kind and patient nature, your consistent willingness to listen, and your enduring interest, even during the less exciting parts of my journey. I owe much of my success to each and every one of you.

I must acknowledge my colleagues at Newcastle University for their role in helping me become a better scientist through discussions, training, and valuable advice. I extend my thanks to Prof. Waldemar Vollmer, Dr. Daniela Vollmer, and Dr. Jacob Biboy for their assistance and guidance in HPLC analysis. I would also like to thank George Merces and Dr. James Grimshaw from the Bioimages Analysis department for their training and assistance with microscopy and image analysis. My appreciation extends to Tracey Davey and Ross Laws at the Electron Microscopy Research Services (EMRS) for their contributions to my training.

Last but certainly not least, I am deeply thankful to the government of Saudi Arabia for their financial support throughout my academic journey. Your assistance has made it possible for me to pursue my educational goals and achieve what I have today.

Contents

List of Figures

List of Tables

List of Abbreviations

B. subtilis	*Bacillus subtilis*
E. coli	*Escherichia coli*
S. aureus	*Staphylococcus aureus*
H. influenzae	*Haemophilus influenzae*
S. pneumoniae	*Streptococcus pneumoniae*
M. tb.	*Mycobacterium tuberculosis*
W/T or WT	Wild type
PG	Peptidoglycan
Glc*N*Ac or NAG	*N*-acetylglucosamine
Mur*N*Ac or NAM	*N*-acetylmuramic acid
L-Ala	L-alanine
D-Glu	D-glutamic acid
***m*-DAP or *meso*-DAP**	*meso*-diaminopimelic acid
L-Lys	L-lysine
L-Ser	L-serine
L-Hse	L-homoserine
D-Ala	D-alanine
Gly	Glycine
L-Orn	L-ornithine
PBPs	Penicillin-binding proteins
GTase	Glycosyltransferase
HMM	High molecular mass
LMM	Low molecular mass
DAC	D-alanyl-D-alanine carboxypeptidase
PBP5	Penicillin-binding protein 5
RP-HPLC	Reverse-phase high-performance liquid chromatography

HPLC	High-performance liquid chromatography
TnSeq	Transposon mutagenesis and high throughput sequencing
DD-peptidases	Cleave between two D-amino acids
LD- or DL-peptidases	Cleave between an L-amino acid and a D-amino acid
TA	Teichoic acid
WTA	Wall teichoic acid
LTA	Lipoteichoic acid
CPase	Carboxypeptidase
EPase	Endopeptidase
TCT	Tracheal cytotoxin
amp	Ampicillin
kan	Kanamycin
cat	Chloramphenicol
spec	Spectinomycin
zeo	Zeocin
ery	Erythromycin
neo	Neomycin
°C	Degree Celsius
min	Minute (s)
h	Hour (s)
O/N	Overnight
LB	Luria-Bertani broth
NB	Nutrient Broth
NA	Nutrient agar
mL	Millilitres
g	Gram
mg	Milligram
µg	Microgram

µL	Microlitre
L	Litre
mM	Millimolar
µM	Micromolar
M	Molar
IPTG	Isopropyl-β-D-thiogalactopyranoside
X-Gal	5-bromo-4-chloro-3-indolyl-β-D-galactopyranoside
$MgSO_4$	Magnesium sulfate
Mg^{2+}	Magnesium ion
WLM	Cell wall labeling medium
SMM	Spizizen minimal medium
$CaCl_2$	Calcium chloride
$MnSO_4$	Manganese sulfate monohydrate
NaCl	Sodium chloride
PTM	Pre-transformation medium
Fe-NH_4-citrate	Ferric ammonium citrate
OD	Optical density
OD_{600} nm	Optical density measured at a wavelength of 600 nanometers
FDAAs	Fluorescent D-amino acids
HADA	3-[[(7-Hydroxy-2-oxo-2H-1-benzopyran-3yl) carbonyl] amino]-D-alanine hydrochloride
RADA	TAMRA-based fluorescent D-amino acid
PBS	Phosphate-buffered saline solution
DNA	Deoxyribonucleic acid
gDNA	Genomic deoxyribonucleic acid
RNA	Ribonucleic acid
EDTA	Ethylenediaminetetraacetic acid
e.g.	Exempli gratia (for example)
PCR	Polymerase chain reaction

TAE	Tris-Acetate-EDTA
V	Voltage
UV	Ultraviolet
kb	Kilobase
kDa	Kilodalton
bp	Base pair
pH	Potential hydrogen
GFP	Green fluorescent protein
SDS	Sodium dodecyl sulfate
SCC	Sodium chloride-sodium citrate solution
Na_2CO_3	Sodium carbonate
ONPG	Ortho-Nitrophenyl-β-galactoside
DNase	Deoxyribonuclease
RNase	Ribonuclease
Tris/HCL	Tris hydrochloride
Tris	Tris(hydroxymethyl)aminomethane
NaN_3	Sodium azide
HF	Hydrofluoric acid
rpm	Revolutions per minutes
LiCl	Lithium chloride
NaH_2PO_4	Sodium dihydrogen phosphate
SDS-PAGE	Sodium dodecyl sulfate–polyacrylamide gel electrophoresis
Amp	Ampere (electric current)
PVDF	Polyvinylidene difluoride
PBS-T	Phosphate-buffered saline solution with 0.1% Tween™
FITC	Fluorescein isothiocyanate
FM5-95 and FM4-64	*N*-(3-Trimethylammoniumpropyl)-4-(6-(4-(Diethylamino)phenyl)hexatrienyl) pyridinium dibromide fluorescent membrane dye

DAPI	4′,6-Diamidino-2-phenylindole
SEM	Scanning electron microscopy
SIM	Structured illumination microscopy
TIRF	Total internal reflection fluorescence microscopy
MIC	Minimum inhibitory concentration
CFU	Colony-forming unit
µm	Micrometre
cm	Centimetre
mm	Millimetre

Chapter 1

Introduction

The intricate dynamics of bacterial cell wall synthesis and the remarkable assembly of appendages, such as bacterial flagella passing through the cell wall, represent complex engineering feats in the microbial world. Importantly, autolytic enzymes orchestrate the turnover and remodeling of the bacterial cell wall and, in combination with the synthesis of new material, are important fundamental aspects of bacterial physiology, encompassing cell growth, division, and pathogenicity. Furthermore, understanding these processes has a pivotal role in antibiotic development, as numerous antibiotics target bacterial cell wall synthesis or stability, and a comprehensive understanding of the mechanisms governing bacterial autolysis holds the key to forging new avenues in antibiotic development or refining existing therapeutic strategies. Also, from a different perspective, the involvement of these enzymes in biofilm formation and bacterial cell dispersal has applications for biotechnological processes, as well as clinical treatments. Here, unraveling the intricacies of autolytic enzyme function offers insights into biofilm dynamics, presenting promising strategies for combating chronic infections as well as averting biofouling in diverse industrial settings. In summary, the multifaceted roles of bacterial autolytic enzymes underscore their importance, and understanding their regulation has the potential to have a profound impact on diverse fields, from microbiology to biotechnology.

Various extracellular structures also pass through the cell wall and hence have to be intimately related to cell wall synthesis, the best example being bacterial flagella that emerge as dynamic appendages to allow motility. These whip-like structures, orchestrating the propulsion and navigation of bacteria through diverse environments, offer a gateway to unraveling fundamental aspects of microbial physiology. The mechanisms underpinning cell motility, chemotaxis, and biofilm formation have been well documented in their own right, but very little work has been done determining how they pass through the cell wall without compromising its structural integrity and/or presenting complications for cell growth. This thesis details the requirements for cell wall degradation to permit the extrusion of the flagellum as a functional entity and provides insight into the functional roles of the autolytic enzymes in this process.

This thesis sheds light on the multifaceted importance of investigating bacterial autolytic enzymes and flagella, elucidating their roles in modifying the cell wall while preserving its structural integrity. Through a comprehensive exploration, it aims to unveil the far-reaching

implications of dysfunction in this class of extracellular enzymes, perhaps pointing to new potential targets for developing antimicrobial agents.

1.1 Bacterial cell wall

A bacterial cell's integrity is maintained by an extracellular matrix known as a cell envelope, which encases the cytoplasmic membrane. This structure protects the cell from rupturing through its internal osmotic pressure. The major structural component of the cell envelope is a layered polymer of sugars and amino acids (peptidoglycan) that is assembled on the outer surface of the cytoplasmic membrane. It is constructed in such a way as to encase the cytoplasmic membrane, forming a sacculus that is essentially a single molecule. The thickness of the peptidoglycan layer is variable depending on the bacterial species, but in general, they can be divided into two classes: Gram-negative and Gram-positive bacteria. Gram-negative bacteria have a thin peptidoglycan layer that is sandwiched between the inner and outer cell membranes separated by a periplasmic space (Figure 1.1A) (11). The outer membrane consists of lipopolysaccharides (LPS) and phospholipids, serving as a permeability barrier and protecting the cell from antibiotics, disinfectants, and host immune defences. The outer membrane also contains porins, which allow the passage of small molecules through passive diffusion (2). Due to the presence of the outer membrane, Gram-negative bacteria are more resistant to antibiotics that target peptidoglycan synthesis. In contrast, Gram-positive bacteria have a thicker peptidoglycan layer through which wall teichoic acids and lipoteichoic acids permeate. However, it lacks an outer cell membrane, the structural part of the cell envelope, so the cell wall is exposed directly to the environment (3). This makes Gram-positive bacteria more susceptible to certain antibiotics, such as penicillin, that target peptidoglycan synthesis (Figure1.1B) (4). In both species, peptidoglycan is fixed, in that it defines the shape of the cell, and yet is dynamic, in that it is restructured as the cell grows. The dynamic features of the cell wall structure are essential for cell growth and cell division.

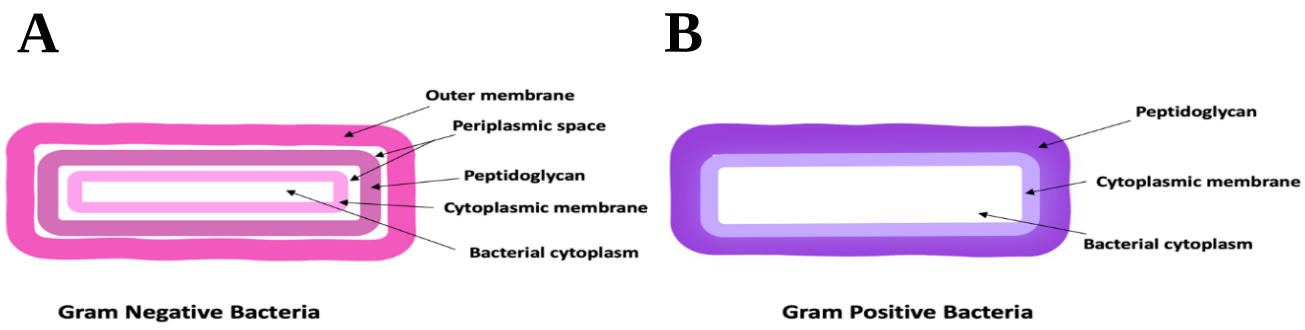

Figure 1.1 Gram-positive and negative cell structures

Differences in cell architecture among Gram-negative bacteria (**A-** e.g., *E. coli*) and Gram-positive bacteria (**B-** e.g., *B. subtilis*). This figure is derived from (5).

From extensive studies of cell wall biosynthesis, we now have a good understanding of how nascent peptidoglycan synthesis is coordinated to permit cell growth. However, much of our understanding is based on data derived from *Escherichia coli*, and these mechanisms do not easily transpose to Gram-positive bacteria, such as *Bacillus subtilis*. In both bacterial species, the sacculus, or cell wall, is composed of repetitive polymers of amino sugars, *N*-acetylglucosamine (Glc*N*Ac) and *N*-acetylmuramic acid (Mur*N*Ac), that are cross-linked by short peptide chains consisting of L-alanine (L-Ala), D-glutamic acid (D-Glu), *meso*-diaminopimelic acid (*m*-DAP) or L-lysine (L-Lys), D-alanine (D-Ala), and D-Ala (Figure 1.2B). This intricate network forms a 3D mesh-like structure (6). The key difference is the thickness of the cell wall, in that for *E. coli*, the sacculus is essentially a single layer (Figure 1.2A), whereas in *B. subtilis*, the sacculus is much thicker and is considered to be formed from multiple sheets of peptidoglycan cross-linked together (Figure 1.2C). A simple model to explain how the enlargement of the sacculus has been proposed for *E. coli* that relies on the differential activity of the autolytic enzymes acting in concert with the synthetic enzymes (7). The result is the controlled opening of the peptidoglycan matrix with the simultaneous insertion of new material to enlarge the structure. However, this mechanism for the enlargement of the sacculus is difficult to see operating when it is a multilayered structure, as is present in Gram-positive bacteria.

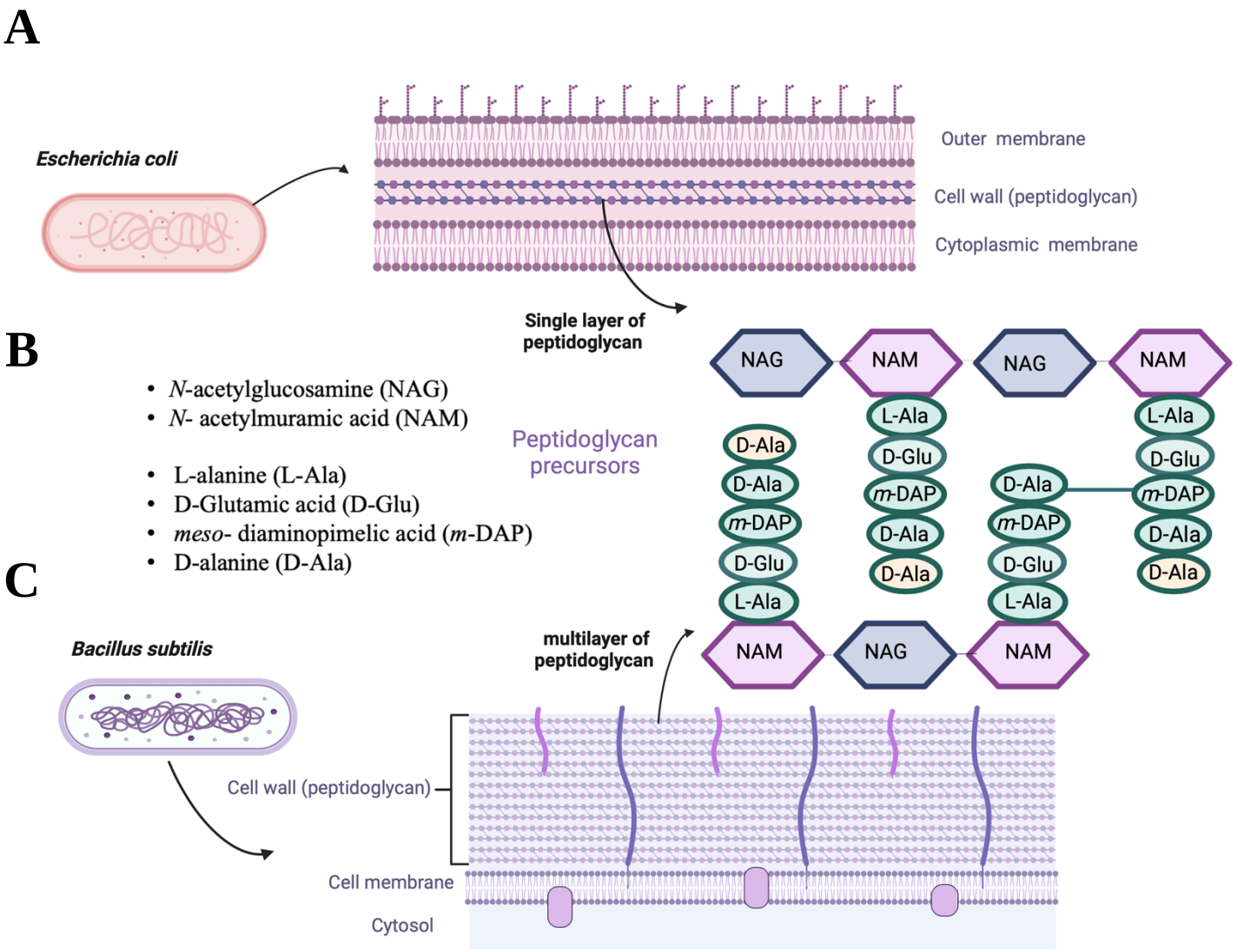

Figure 1.2 Cell wall composition

A- The cell wall structure of *E. coli* is a single-layer arrangement of peptidoglycan precursors. The regulation of peptidoglycan synthases and hydrolases in *E. coli* occurs by attaching the newly synthesised material to the preexisting strands at the time of rupturing the old covalent bonds, as shown by Höltje (7). **B-** Peptidoglycan precursors of both *E. coli* and *B. subtilis*: glycan strands (NAG and NAM) and the pentapeptide chains (L-alanine (L-Ala), D-glutamic acid (D-Glu), *meso*-diaminopimelic acid (*m*-DAP), D-alanine (D-Ala), and D-alanine). **C-** The cell wall structure of *B. subtilis* is a multilayer arrangement, suggesting that synthases are in the innermost layer, whereas hydrolases are in the outermost layer. The illustration was created with BioRender.com.

1.2 Cell wall modification of *B. subtilis*

The mechanisms for inserting nascent peptidoglycan into the cell wall in *B. subtilis* have been extensively studied, and an inside-to-outside model for growth has been developed to fit the data (8). For this model to work, cell enlargement requires dynamic processes of new wall synthesis close to the membrane and autolytic enzyme activities to cleave the covalent bonds within the older peptidoglycan to act in concert (9). Thus, the regulation of hydrolases and synthases of the cell wall should be accurately organized in order to prevent the random or uncontrolled breakdown of the peptidoglycan that would result in cell lysis. However, the mechanism(s) by which these enzymes are regulated is still obscure. Various hypotheses exist to explain how the autolytic enzymes selectively and specifically degrade the old outer wall; in simple terms, they tend to rely on two potential mechanisms. The first mechanism uses the properties or structure of the cell envelope as a way to restrict the activity of the enzymes, such that the autolytic enzymes are not active near the cell membrane, e.g., conformational changes in the enzymes structure and the availability of cofactors (metals) necessary for their activity (10, 11). Second, the physical structure of the peptidoglycan in the cell wall might be different depending on its relative position in the wall (12).

1.2.1 Peptidoglycan synthesis

The biosynthesis mechanism of peptidoglycan has been extensively studied across various organisms, including *Staphylococcus aureus*, *Micrococcus luteus*, *E. coli*, and more recently, several members of the Bacilli. Despite significant differences in morphology and the chemical composition of their peptidoglycans, the biosynthesis process in each organism shares enough common characteristics to outline the fundamental nature of the process. Modifications observed in the biosynthetic pathway of individual organisms are unique to each organism and likely reflect the evolution of specific enzymes tailored to their respective needs.

The peptidoglycan component of the bacterial cell wall requires Lipid II molecules that are derived from two types of sugar molecules: uridine diphosphate-*N*-acetylglucosamine (UDP-Glc*N*Ac) and uridine diphosphate -*N*-acetylmuramic acid (UDP-Mur*N*Ac) (Figure 1.3). The biosynthesis of UDP-*N*-acetylglucosamine, a crucial precursor in various metabolic pathways, initiates from fructose-6-phosphate, readily available from both glycolytic and gluconeogenic

pathways (13). This transformation is orchestrated by glucosamine-6-phosphate synthase (GlmS), a multifunctional enzyme possessing distinct glutaminase and synthetase activities (14). Within its active sites, glutaminase catalyses the hydrolysis of L-glutamine to L-glutamic acid, releasing ammonia, which subsequently couples with fructose-6-phosphate under the synthetase domain, yielding glucosamine-6-phosphate (15). Prokaryotic systems convert glucosamine-6-phosphate to glucosamine-1-phosphate through phosphoglucosamine mutase (GlmM), requiring ATP phosphorylation for activation (16). The subsequent steps involve the bifunctional enzyme GlmU, which undertakes *N*-acetylation using acetyl-CoA and uridylylation using UTP (17).

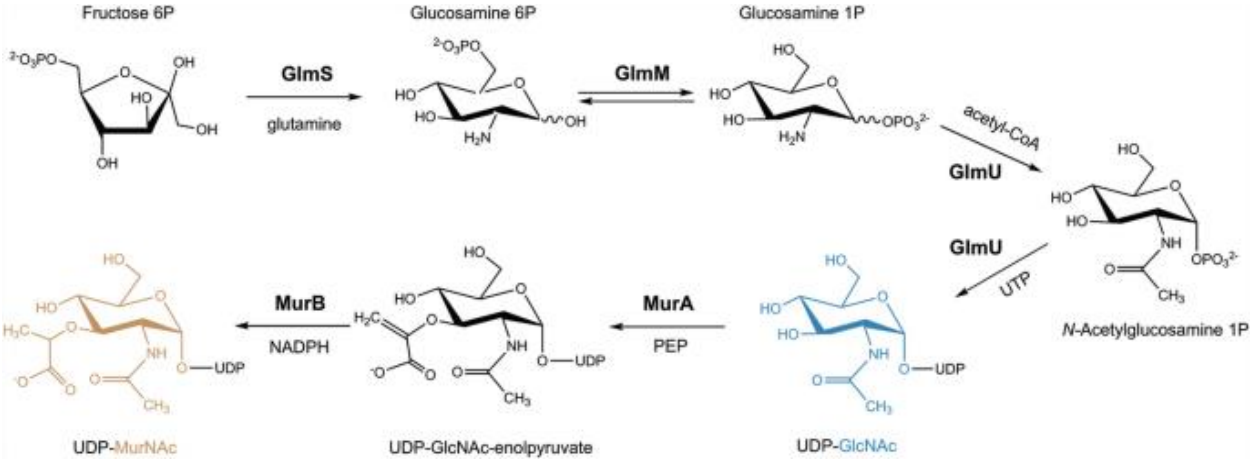

Figure 1.3 Synthesis of peptidoglycan components uridine diphosphate-*N*-acetylglucosamine (UDP-Glc*N*Ac) and uridine diphosphate-*N*-acetylmuramic acid (UDP-Mur*N*Ac).

The synthesis of UDP-Glc*N*Ac from fructose-6P is facilitated by the enzymes GlmSMU, incorporating an amino group from L-glutamine, an acetyl group from acetyl-CoA, and UTP. This is followed by the transformation of UDP-Glc*N*Ac to UDP-Mur*N*Ac by MurAB, which involves the addition of an enolpyruvate from PEP and subsequent reduction to form the D-lactyl residue of UDP-Mur*N*Ac. The figure is derived from (18).

In parallel, the biosynthesis of UDP-*N*-acetylmuramic acid, another key component in bacterial cell walls, unfolds through sequential enzymatic reactions (Figure 1.4). UDP-*N*-acetylmuramic acid synthesis is initiated by UDP-*N*-acetylglucosamine enolpyruvyl transferase (MurA), catalysing the transfer of an enolpyruvyl group from phosphoenolpyruvate to UDP-*N*-acetylglucosamine, forming an enol ether (19, 20). Some Gram-positive bacteria, like *S. aureus*,

Streptococcus pneumoniae, and *B. subtilis*, have two alleles of the *murA* gene. Each gene is controlled differently. This extra gene might help the bacteria make more cell wall material when needed, especially during cell wall stress (21-23). Subsequently, UDP-*N*-acetylenolpyruvylglucosamine reductase (MurB) reduces this enol ether to produce UDP-*N*-acetylmuramic acid (24).

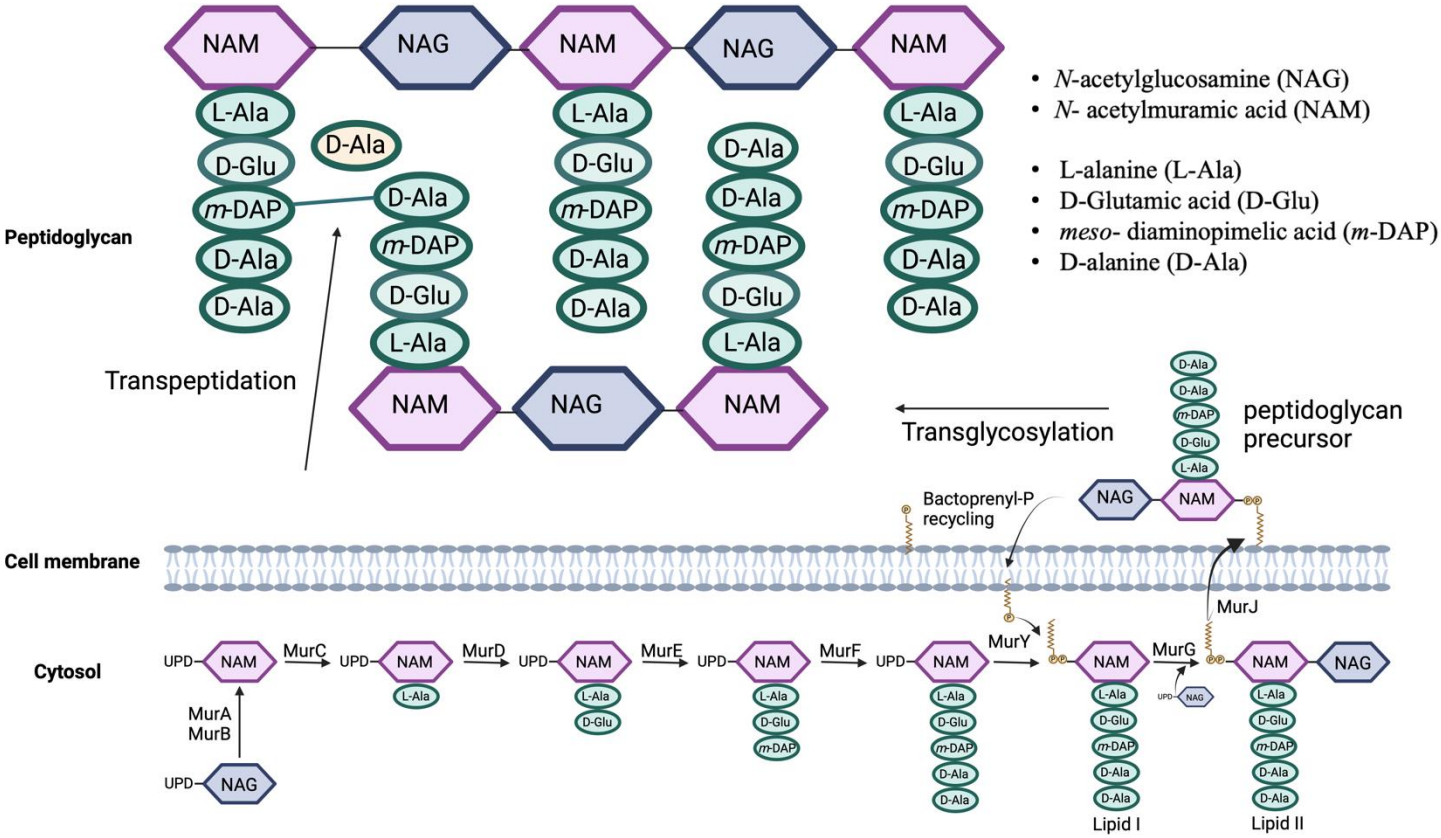

Figure 1.4 Peptidoglycan biosynthesis

A general scheme of peptidoglycan synthesis in *B. subtilis.* The peptidoglycan (PG) biosynthesis is initiated by the formation of disaccharide pentapeptide precursors (Glc*N*Ac-Mur*N*Ac-L-Ala-D-Glu-DAP-D-Ala-D-Ala) within the cytosol. Subsequently, these PG precursors are transported to the extracellular space between the cell wall and the cell membrane, which is facilitated by their association with bactoprenol, forming lipidic complexes. Upon reaching the extracellular space, the PG monomers are incorporated into the murein polymer through transglycosylation and transpeptidation reactions mediated by the enzymatic activity of penicillin-binding proteins (PBPs). The illustration was created by BioRender.com.

The pentapeptide chain assembly is facilitated by enzymes like MurC, MurD, and MurE, adding L-Ala, D-Glu, and *m*-DAP or L-lys, respectively (Figure 1.4) (25-28). The dipeptide D-Ala-D-Ala is formed by D-alanine racemase (Alr) and D-Ala-D-Ala ligase (Ddl), then added to UDP-Mur*N*Ac-tripeptide by MurF. Further steps involve lipid carrier transfer catalysed by MraY. However, *Mycobacterium smegmatis* uses decaprenylphosphate (29). Then, MurG facilitates the addition of Glc*N*Ac to form Lipid II (30, 31).

In cases where a peptide branch is present, the usual addition of necessary amino acids to Lipid II moiety is a common occurrence. However, notable exceptions exist, such as in *Lactobacillus viridescens*, where the first amino acid of the L-alanine-L-serine bridge directly incorporates into UDP-*N*-acetylmuramylpentapeptide (32). In *S. aureus*, enzymes like FemX, FemA, and FemB sequentially add one, two, and two glycines, respectively, to construct the pentaglycine chain, utilising glycyl-tRNA donors (33-36). Conversely, in other staphylococcal strains, the replacement of glycines with serines enhances resistance against lysostaphin, a glycylglycine endopeptidase (37, 38). The discoveries of similar enzymes in *E. faecalis* and *S. pneumoniae* underscores the evolutionary consistency of this mechanism across bacteria (39, 40). Unlike Mur ligases, which directly utilise ATP-activated amino acids, enzymes involved in branching peptides rely on charged tRNAs. The discoveries in the 1960s revealed the role of tRNAs as aminoacyl donors for peptidoglycan precursors, shifting understanding from their previous association solely with protein synthesis (41). It is now understood that both phospholipids and peptidoglycan precursors undergo aminoacylation through acyl-tRNAs.

There are some variations in the peptide stem among bacterial species. In most bacterial species, the first amino acid of the peptide stem is L-Ala, although in rare instances, glycine (Gly) or L-serine (L-Ser) may be incorporated instead. Notably, *Mycobacterium tuberculosis* (*M. tb.*) and *Mycobacterium leprae* enzymes exhibit similar specificity in vitro towards L-Ala and Gly, yet they differ in the amino acid found at the first position due to growth conditions (42). Another instance concerns *Chlamydia trachomatis*, where MurC adds L-Ala, L-Ser, and Gly with similar efficiencies in vitro, hindering the deduction of the putative chlamydial peptidoglycan's first amino acid (43).

The second position's amino acid is universally added as D-Glu by the MurD ligase. In many organisms, amidation of the α-carboxylate of iso-glutamic acid at position 2 of the peptide

chain occurs intracellularly after the formation of lipid-linked peptidoglycan precursors (6, 44). In *S. aureus*, the enzymes MurT and GatD were recently found to be involved in this process (45, 46).

The most variability lies at position 3, added by the MurE ligase. The MurE enzyme demonstrates a strong preference for the specific amino acid involved. This has been observed in *E. coli* and *S. aureus* for the addition of *meso*-DAP and L-Lys, respectively (47). However, in *Corynebacterium pointsettiae*, where L-homoserine (L-Hse) is located at position 3, MurE is precise not only about the amino acid but also about the nucleotide precursor UDP-Mur*N*Ac-Gly-D-Glu. This selectivity ensures the accurate formation of the peptide stem Gly-γ-D-Glu-L-Hse-D-Ala-D-Ala (6). Nonetheless, MurE's rigid specificity occasionally diminishes, impacting the final peptidoglycan makeup. For instance, certain Bifidobacterium species exhibit both L-Lys and L-ornithine (L-Orn) at position 3, with MurE from *Bifidobacterium globosum* able to incorporate both amino acids interchangeably (48). Similarly, MurE from *Thermotoga maritima*, a Gram-negative species, displays comparable efficiency in adding L-Lys, D-Lys, and *meso*-DAP (49). The absence of *meso*-DAP in *T. maritima* peptidoglycan is due to its limited intracellular pool compared to L- and D-Lys. Moreover, the presence of D-Lys results in the synthesis of two peptide stems, one conventional and one unusual, due to acylation by the γ-carboxylate of D-Glu on its ε-amino function.

A dipeptide consisting of amino acids at positions 4 and 5 is typically added, with D-Ala-D-Ala being the most common. The synthesis of this dipeptide is facilitated by the Ddl enzyme, and its integration into the peptide stem is managed by the MurF ligase. MurF exhibits a notable specificity for the C-terminal amino acid (50). In contrast, Ddl primarily focuses on the N-terminal amino acid, forming a "double-sieving" mechanism ensuring the predominance of a pentapeptide stem ending in D-Ala-D-Ala. D-Ala is predominantly situated at position 4 across species (50, 51). However, strains resistant to vancomycin may have D-lactate (D-Lac) or D-Ser at position 5, as their affinity for the antibiotic is considerably lower than that of the standard D-Ala-D-Ala moiety (52). Occasionally, Gly is found at positions 4 or 5, likely evading the double-sieving mechanism. While its occurrence is minimal in *E. coli* (around 1%), it can reach up to 19% in *Caulobacter crescentus* (6, 44).

Peptidoglycan synthesis occurs in the cylindrical cell wall to maintain thickness/ integrity and permit elongation. It also forms the division septum to allow the cell to divide. The synthesis starts with the formation of the peptidoglycan subunit, disaccharide-pentapeptide, in the cytoplasm close to the cell wall, where then it is flipped out to the cell wall by a lipid II flippase (MurJ) (53-55). When MurJ is absent in *B. subtilis*, another flippase known as Amj steps in to fulfill its role (56). Once Lipid II is outside the cell, this precursor is then polymerised to generate the glycan strands by a glycosyltransferase (GTase) activity, and these are then cross-linked into the existing peptidoglycan (57, 58) and then can undergo maturation. The cross-linkage reaction is carried out by penicillin-binding proteins, DD-transpeptidases and LD-transpeptidases, using the energy of the donor peptide D-alanine at position 5 of the pentapeptide chain to link the newly formed tetrapeptide to *meso*- diaminopimelic acid, position 3, of a neighbouring peptide chain (acceptor) (6, 9). The neighbouring peptide that serves as an acceptor of the cross-linkage reaction can be either a tri, tetra, or pentapeptide chain (7). The peptide chains that did not serve as acceptors are reduced to either tri- or tetrapeptides (59). In vegetative *B. subtilis*, approximately 30-40% of the peptide chains are cross-linked to the neighbouring chain, and this number increases slightly during the stationary phase to reach 33.2-44% (60).

In general, most modifications of the PG involve the action of penicillin-binding proteins (PBPs). Over the last 50 years, research has been conducted in various ways, often through amino acid sequence alignments and then in combination with structural knowledge and biochemistry, and has identified the number and types of PBPs in different bacteria (61-65). This has resulted in PBPs typically being classified into two categories: high molecular mass (HMM) and low molecular mass (LMM) proteins (66, 67). High molecular mass (HMM) proteins are further divided into class A that are bifunctional, having glycosyltransferase activity at the N-terminus domain (polymerisation) and transpeptidation at the C-terminus domain of the protein (cross-linking). The other class (B) seems to have an N-terminal domain assigned for transpeptidation activity and a presumed interaction domain in the N-terminal region and seems to be required for cell shape maintenance and septation (67). In contrast, low molecular mass (LMM) exhibits either a DD-carboxypeptidase, transpeptidase, or endopeptidase activity and has an unclear role in PG metabolism (68). It is also clear that there are other enzymes with these activities that do not bind to penicillin, e.g., LdcB (69). *E. coli* has 12 PBPs: three class A PBPs

(PBP1a, PBP1b, and PBP1c), two class B PBPs (PBP2 and PBP3), and seven low molecular mass (LMM) PBPs involved in cell separation, peptidoglycan maturation, or recycling (70-72). *Neisseria gonorrhoeae* possesses four PBPs, where PBP1 is analogous to *E. coli* PBP1a and PBP2 to *E. coli* PBP3 (63, 73, 74). PBP3 and PBP4 in *N. gonorrhoeae* share sequences with *E. coli* PBP4 and PBP7, respectively (75). *Listeria monocytogenes* has six PBPs: two class A PBPs (PBP1 and PBP4), three class B PBPs (PBP2, PBP3, and Lmo0441), and one class C PBP of type-5 (PBP5) (76-78). *M. tb.* produces two class A PBPs, two class B PBPs, and a lipoprotein with motifs similar to class B PBPs (79). Its set of PBPs includes six class C PBPs: one type-4, one type-5, one type-7, and three putative type-AmpH PBPs. *B. subtilis* has 16 extensively studied PBPs, with roles in vegetative peptidoglycan synthesis and sporulation.

1.2.2 Peptidoglycan maturation

In addition to the synthesis of the basic precursors of peptidoglycan, the disaccharide pentapeptide, other peptidoglycan modifications can occur, such as *O*-acetylation, amidation, and carboxypeptidation, either before export from the cytoplasm or post polymerisation. *O*-acetylation is a modification of the *N*-acetylmuramic acid at the C-6 position, providing the cell wall with resistance to endogenous autolysins, lysozyme, penicillin, and protection against macrophages killing (80, 81). Amidation occurs at the carboxy group of the amino acids of the peptide chain itself or of the cross-bridges linking two adjacent peptide chains. Amidation also occurs at the ε-carboxy group of the 3rd position *meso*-diaminopimelic acid (*m*-DAP) (60). Lastly, there are two types of carboxypeptation occurring in the peptidoglycan: LD-carboxypeptidation and DD-carboxypeptidation. LD-carboxypeptidation is the removal of the 4th position D-alanine of the tetrapeptide chain, mediated by the LD-carboxypeptidase (LdcB), producing a tripeptide chain (69). Meanwhile, DD-carboxypeptidation is the removal of the terminal D-alanine of the pentapeptide chains required for peptidoglycan maturation, although the precise roles of these processing events are unclear and not necessarily essential. *B. subtilis* genome encodes six genes expressing DD-carboxypeptidases that are known as low molecular mass proteins. Four of them have high sequence similarity and are proposed to be D-alanyl-D-alanine carboxypeptidase, and they are known as *dac* genes: *dacA*, *dacB*, *dacC*, and *dacF*. The remaining two (*pbpE* and *pbpX*) have low sequence similarity and have not been assigned a biochemical activity, so they may or may not carry out this activity.

DacA is composed of 443 amino acids and is a class C penicillin-binding portion 5 (PBP5) that shows sensitivity to β-lactams antibiotics (82). PBP5 is the major D-alanyl-D-carboxypeptidase during vegetative growth and is required for peptidoglycan maturation (6, 60, 83). HPLC analysis of muropeptides showed that a null mutant in *dacA* resulted in an abundance of pentapeptide chains compared to the wild type, which normally has an abundance of tetrapeptide chains (60). A cell diameter screening study revealed that DacA plays an important role in cell width control, and the absence of DacA generated wider and shorter cells compared to the wild type (83). Otherwise, a null *dacA* mutant does not show any morphological abnormalities during exponential growth, and the cells got shorter at the end of the exponential phase (84). A transposon mutagenesis and high-throughput sequencing (TnSeq) analysis showed that DacA is also involved in motility, and the absence of DacA resulted in a defect in swarming motility (85).

DacB (PBP5*) and DacF are also class C penicillin binding protein, but they are specifically expressed during sporulation and presumed to control the peptide cross-linking of spore peptidoglycan (86). DacB (382 amino acids) is only expressed in the mother cell compartment of the sporulating cell (87). In contrast, DacF (389 amino acids) is only expressed in the forespore compartment of a sporulating cell. A null mutant in the sporulation-specific DD-carboxypeptidase *dacB* showed a fourfold increase in the cross-linking of the spore cortex compared to the wild type of *B. subtilis* (86). Moreover, a double mutant *dacB dacF* showed an increase in the cross-linking in cortical peptidoglycan with a failure in normal spore dehydration (88). However, there is no phenotype nor change in spore peptidoglycan structure in a null *dacF* mutant.

DacC is the final DD-carboxypeptidase and is also called penicillin-binding protein 4A (PBP4). It is significantly larger than the others, comprising of 491 amino acids, and is expressed during stationery and sporulation phases. Deletion or point mutations in the gene showed no morphological effects (89) and so seems to have no important role in cell viability under normal conditions or is functionally redundant (90).

1.2.3 Peptidoglycan hydrolyses

In all bacteria, the genome encodes diverse groups of peptidoglycan hydrolases that are specialised in hydrolysing different bonds within the cell wall. Bioinformatic analysis of the *B. subtilis* genome and protein sequences, employing alignment and PHMMER tools, reveals three classes of autolytic enzymes based on their hydrolytic bond specificities: muramidases and *N*-acetylglucosaminidases act on the sugar backbone of the peptidoglycan, whereas amidases, endopeptidases, and carboxypeptidases work on the peptide side chains (Figure 1.5) (62, 91). The end result of the action of these enzymes is a complete degradation of the complex peptidoglycan molecule into essentially single subunits.

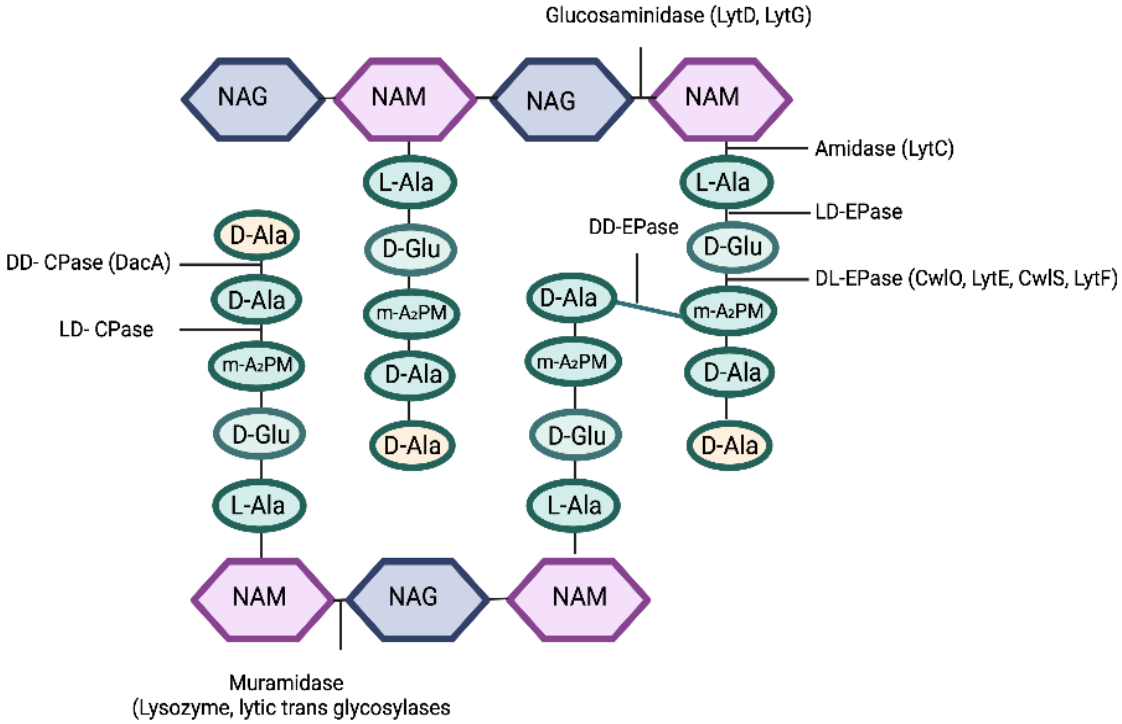

Figure 1.5 Autolytic enzymes of *B. subtilis* during vegetative growth

Autolytic enzyme classifications: amidase, glucosaminidase, and muramidase, LD-endopeptidases (LD-EPase), DL-endopeptidases (DL-EPase), DD-endopeptidases (DD-EPase), LD-carboxypeptidases (LD-CPase) and DD-carboxypeptidases (DD-CPase). The small black lines indicate the active sites of the autolytic enzymes. The illustration was created with BioRender.com.

In total, the *B. subtilis* genome encodes 42 genes that have been considered to be peptidoglycan hydrolases (91). These autolytic enzymes play specific roles or could have multiple roles in cell wall synthesis and growth, e.g., recycling of old wall material, specific degradation to permit new synthesis, or cell wall modifications in order to facilitate cellular appendage insertions (92). Some of these have been shown to be important in the vegetative growth and cell separation of *B. subtilis*, although their precise roles are unclear due to functional redundancy (Table 1.1).

Table 1.1 Autolytic enzymes in *B. subtilis*

Autolytic enzyme locations, expressions, activities, and functions in *B. subtilis.* Adapted from (93) and modified based on (94) and SubtiWiki.

Protein	location	Expression *	Sigma factor (σ)	activity	function
LytD (CwlG)	Cell wall	Vegetative	D	Glucosaminidase	Major autolysin, cell separation, cloxcillin-induced cell lysis
YubE (LytG)	Secreted	Vegetative		N-acetylglucosaminadase	Cell wall turnover
YjbJ (CwlQ)		Vegetative	D	Muramidase, lytic	Cell wall turnover
LytF (CwlE, YhdD)	Cell wall	Vegetative	D	Endopeptidase	Cell separation
YwtD (Pgds)	Extracellular	Vegetative	D	Endopeptidase	Cell separation
LytE (CwlF, YhdD)	Cell wall	Vegetative	A, H, I	Endopeptidase	Major autolysin, cell separation, cell lysis
CwlO (YzkA, YvcE)	Cell membrane	Vegetative, sporulation	A	Endopeptidase	Cell wall synthesis, cell wall elongation
YojL (CwlS)	Cell wall	Vegetative, sporulation	D, H	Endopeptidase	Cell wall separation
LytC (CwlB)	Cell wall	Vegetative sporulation	A, D	Amidase	Major autolysin, cell separation, wall turnover, cell lysis, mother cell lysis
YrvJ		Vegetative, sporulation		Amidase	Cell wall metabolism
YocH	Extracellular	Vegetative sporulation	A	Amidase	Cell wall turnover
CwlC	Mother cell wall	Sporulation	K	Amidase	Mother cell lysis
CwlD	Secreted	Sporulation	E, G	Amidase	Formation of muramic δ- lactam structure in spore cortex, spore germination
YqeE (CwlH)	Cell membrane	Sporulation	K	Amidase	Cell wall metabolism, mother cell lysis
YqgT	Cell wall	Sporulation		Endopeptidase	Cell wall metabolism
YkfC		Sporulation		Endopeptidase	Cell wall metabolism
YunA (LytH, YutA)		Sporulation	E, K	Endopeptidase	Endospores cortex maturation
YdhD	Spore wall	Sporulation	E	Glycosylase	
SleB (ypeA)	Outer surface of the spore cortex	Sporulation	G	Lytic	Germination
CwlJ (YcbQ)	Outer edge of the spore cortex	Sporulation	E, K		Germination
SpoIIQ (YwnL)	Membrane protein	Sporulation	F		Perspore engulfment
YqiI (MmgA)	Mother cell wall	Sporulation	E, V		Mother cell lysis
CwlA		Apparently silent		Amidase	Minor autolysin
YkvT		Silent		Lytic	
YomI (CwlP)	Cell membrane			Tranasglycosylase	Cell wall turnover
YcdD (CwlK)	Cell membrane			Endopeptidase	Cell wall turnover
YddH (CwlT)	Secreted			Endopeptidase	Cell wall hydrolase conjugative transfer ICEBs1
YpbE	Cell membrane				
YsbB (PftB)	Cell membrane			Pyruvate transport	Uptake of pyruvate
YwbG				Holin-like auxilary protein	
YxaC	Cell membrane			Holin-like auxilary protein	
XlyA	Extracellular	PBSX induction	XPF	Amidase	PBSX prophage-mediated lysis
XlyB	Secreted	PBSX induction		Amidase	PBSX prophage-mediated lysis
BlyA (YomC)		SPB induction		Amidase	SPB-mediated lysis

* Autolytic enzyme expression is the separator of which enzymes could be essential for cell growth. The degree of shading (white, light grey, and dark grey) represents the time of the autolytic enzyme expression: vegetative, sporulation, remains silent, or belongs to bacterial phage, respectively.

1.3 Repertoire of autolytic enzymes in *B. subtilis*

1.3.1 Endopeptidase and carboxypeptidase

Peptidases cleave the bonds within the peptide chain itself, specifically at various LD, DL, and DD bonds. Peptidoglycan peptidases can be categorized into two main types: carboxypeptidases and endopeptidases. Carboxypeptidases are responsible for removing a C-terminal amino acid from the peptide chain. Conversely, endopeptidases cleave within the peptide. There are specific subtypes of peptidoglycan peptidases exist based on the amino acid composition of the cleavage site. DD-peptidases cleave between two D-amino acids, while LD- or DL-peptidases cleave between an L-amino acid and a D-amino acid (Figure 1.6) (6). Regarding endopeptidases: LD-endopeptidase cleaves the bond between L-Ala and D-Glu, DD-endopeptidase hydrolyses the cross-bridges linking D-Ala to *meso*-DAP, and DL-endopeptidase cleaves the bond between D-Glu and *meso*-DAP (Figure 1.6). As for carboxypeptidases: LD-carboxypeptidase cleaves between *meso*-DAP and D-Ala in tetrapeptides, DD-carboxypeptidase cleaves between D-Ala and D-Ala, and DL-carboxypeptidase cleaves the bond between D-Glu and *meso*-DAP of tetrapeptides (Figure 1.6) (6).

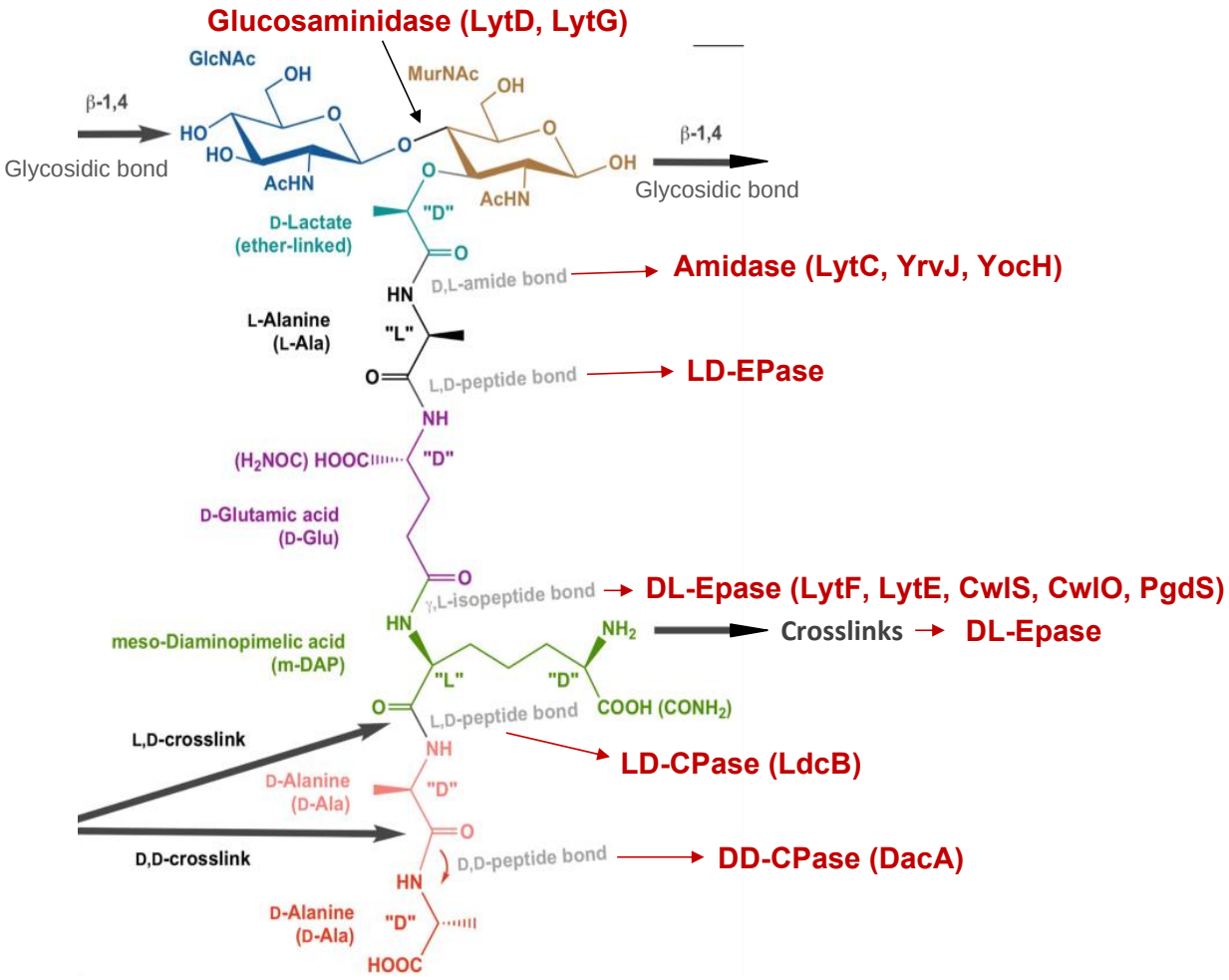

Figure 1.6 Chemical structure of peptidoglycan and autolytic enzyme activities

The chemical structure of the Glc*N*Ac-Mur*N*Ac-pentapeptide building block of the peptidoglycan and modes of cross-linkage (black arrows) are shown. Hydrolases cleave specific bonds within the peptidoglycan (red arrows), such as the bonds within the pentapeptide chain (L-Ala, D-Glu, *m*-DAP, D-Ala, D-Ala), the bond linking the amino sugar (Mur*N*Ac) with the first amino acid of the pentapeptide chain, or the bond linking the amino sugars Glc*N*Ac and Mur*N*Ac. Peptidoglycan peptidases are classified by the amino acid composition of the cleavage site: DD-peptidases cleave between two D-amino acids. In contrast, LD- or DL-peptidases cleave between an L-amino acid and a D-amino acid. LD-endopeptidase (LD-EPase) cleaves between L-Ala and D-Glu, DD-endopeptidase (DD-EPase) hydrolyses the cross-bridges linking D-Ala to *m*-DAP, and DL-endopeptidase (DL-EPase) cleaves between D-Glu and *m*-DAP. LD-carboxypeptidase (LD-CPase) cleaves between *m*-DAP and D-Ala in tetrapeptides, and DD-carboxypeptidase (DD-CPase) cleaves between D-Ala residues. The amino group at the stereochemical D-site of *m*-DAP (green) facilitates the generation of peptidoglycan cross-linkages with the D-Ala residues of neighbouring strands. These cross-linkages occur via transpeptidation reactions, driven by the cleavage of a terminal D-Ala residue (red), resulting in a DD-(4,3) peptide bond. The figure is adapted from (95).

The DL-endopeptidase family in *B. subtilis* comprises 7 hydrolases targeting D-γ-glutamyl-*meso*-diaminopimelic acid bond sites within peptide chains of the peptidoglycan sacculus (Figure 1.6). Five of them have been shown to be produced during the vegetative phase of growth: PgdS, LytE, LytF, CwlS, and CwlO (Table 1.1). Each autolytic enzyme has an N-terminal signal peptide that suggests it is secreted (96). Sec-type signal peptides direct the secretion of the preproteins via the Sec pathway, which is essential for cell wall remodeling. These signal peptides typically comprise three main domains (97, 98). The N-domain contains positively charged residues, such as lysine or arginine, which are recognized by the signal recognition particle (SRP) in the cytoplasm and facilitate interaction with the Sec translocation machinery (99). The SRP guides the ribosome-nascent chain complex to the Sec translocon, which is embedded in the cytoplasmic membrane. This process is mediated by the SRP receptor (FtsY) that interacts with the membrane-bound Sec translocon (100). The hydrophobic core, or H-domain, usually spans around 19 residues and often includes helix-breaking residues like glycine. This domain integrates into the membrane. This hydrophobic domain anchors the preprotein into the Sec translocon, facilitating its passage through the membrane (101). Finally, the C-domain of Sec-type signal peptides ends with a type I signal peptidase (SPase) cleavage site, featuring a consensus sequence like A-S-A at positions -3 to -1 relative to the cleavage site domains (97, 102). Approximately 50% of these signal peptides also contain a helix-breaking residue, such as proline or glycine, at positions -7 to -4 relative to the cleavage site, aiding in proper cleavage and activation of the mature protein. These structural features ensure that preproteins are accurately processed into mature secreted proteins.

The DL-endopeptidase PgdS has been found to be involved in poly-γ- glutamic acid degradation, an extracellular polysaccharide (44, 96). In contrast, the other DL-endopeptidases, LytE, LytF, CwlS, and CwlO, have been found to have roles in the morphogenesis of the rod-shape (103). These four autolytic enzymes possess a catalytic domain structure belonging to the NlpC/P60 family, as their C-terminus is suggestive of the DL-endopeptidase function. LytE, LytF, and CwlS carry different numbers of LysM domains in their N-termini: three, five, and four, respectively (6, 96, 104). The LysM domain is an essential PG-binding domain determining the subcellular localisation of these enzymes at the poles and division sites, which might be related to their role in cell separation (105). Previous studies have observed that cells with *lytE lytF cwlS* triple mutations are defective in cell separation and growth, resulting in a

chaining morphology (104). LytE has also been detected at the lateral cell wall, which might suggest its role in cell elongation (106). CwlO has a unique N-terminal, two coiled-coil domains, and is proposed to be activated at the innermost layer of the lateral cell wall near the cell membrane by interaction with other membrane proteins (FtsEX and SweCD) (96, 103, 105, 107).

Genetically, it appears that CwlO and LytE have overlapping functions in the essential elongation machinery (6, 105). According to previous studies, a double mutation in the DL-endopeptidase genes relating to these two enzymes (*lytE* and *cwlO*) leads to lethal defects in cell elongation (11, 96, 105, 108). Biochemically, both CwlO and LytE are implicated in mediating the cleavage of the bond linking gamma D-glutamine (second position) to *meso*-diaminopimelic acid (third position). CwlO is a 473-amino-acid protein expressed by SigA, the major housekeeping sigma factor of *B. subtilis* (109). In contrast, LytE (a 334 amino acid protein) is expressed by SigA, SigH, and SigI, depending on the cells' status. A single mutation in *lytE* or *cwlO* genes has been previously studied and suggested to result in different cell morphologies compared to a wild type. A null mutation for *cwlO* generated shorter, bent, and wider cells, and this mutant did not become competent (107). Meanwhile, a strain with a single mutation in *lytE* resulted in slightly longer and thinner cells compared to the wild type. However, other analyses seem to suggest that these phenotypes are not present, which is perhaps conditional on the growth condition. Although CwlO and LytE have similar DL-endopeptidase domains, they clearly act differently in cell growth, and one acting alone seems to be able to support cell growth (110).

It has been proposed that the DL-endopeptidase family of enzymes is physiologically activated depending on their subcellular localisation (103, 105). CwlO is a cell membrane protein that is activated by FtsEX, an ABC transporter-like multiplex in combination with other proteins. The FtsEX complex potentially restricts CwlO activity at the inner cell wall layer, and so once CwlO is separated from the cell membrane, it will be inactivated and unable to hydrolyse the outer layers of the peptidoglycan. Consequently, depletion of either CwlO or FtsEX in a *lytE* mutant will result in a growth defect (111). However, LytE is a cell wall hydrolase that needs to interact with the actin-like protein MreBH and probably MreB prior to its secretion in order to be directed to the cylindrical wall and division sites (106). A null mutation of either *lytE* or *mreBH*

leads to similar morphological defects in growth when combined with a *cwlO* mutant (6, 11). LytE also seems to play an important role when the cell envelope is under stress. For this role, its expression is mediated by the stress response factor that is regulated by SigI and also the possibility of SigH (generally active in late stationary phase growth) in addition to the general housekeeping sigma factor (SigA) (111).

The DL-endopeptidases LytF (488 amino acids) and CwlS (414 amino acids) are primarily localised at the septal and polar sites. In contrast, the DL-endopeptidases CwlO and LytE seem to be present in the cylindrical wall, and depletion impacts on the elongation machinery of the cell. In a study conducted by Hashimoto (105), it was discovered that LytF and CwlS were unable to compensate for the growth defects caused by the depletion of both CwlO and LytE. The researchers attempted to address this issue by swapping the N-terminal regions, which contain LysM domains of LytE or CwlO to LytF or CwlS, thereby redirecting LytF and CwlS to target the sidewall of the cell. However, even with this manipulation, LytF and CwlS could not fulfill the role of CwlO and LytE in supporting cell growth. Thus, supporting the idea that the N-terminus domain of the DL-endopeptidase family determines their subcellular localisation and their function in cell morphogenesis.

1.3.2 Amidase

The amidase family consists of enzymes responsible for cleaving the amide bond between the amino sugar *N*-acetylmuramic acid and the N-terminal of the first peptide, L-alanine, of the peptide chain (Figure 1.6) (6). These proteins have a signal peptide that suggests they are secreted, and the best characterised one is LytC. LytC (formerly CwlB) is a 496 amino acid enzyme that is considered to be the major amidase active during the vegetative phase of growth in *B. subtilis*. It is localised to the cell wall where the flagella are predicted to be present (Table 1.1) (112). LytC is a product of the *lytABC* operon that requires the lipoprotein LytA and the modifier protein LytB to promote its activity (113). The *lytABC* operon expression is regulated by both SigA during vegetative growth and is 70-90% upregulated by SigD during the late stationary growth phase (92, 113).

The other enzymes found belonging to the amidase family, YrvJ and YocH, are poorly characterised. YrvJ possesses an amidase-3 domain like LytC, but no functional data are

available for this enzyme (Table 1.1). YocH was found to play a role in facilitating survival in the post-exponential phase in the liquid culture of *B. subtills* (114), but it is unclear how this is mediated.

1.3.3 Glycosaminidase

The N-Acetyl-β-D-glucosaminidase family targets the glycosidic bond linking N-acetyl-β-D-glucosamine residues with their adjacent monosaccharides (Glc*N*Ac to Mur*N*Ac) (Figure 1.7) (6, 44). In *B. subtilis*, LytD (an endo-acting enzyme) and LytG (an exo-acting enzyme) belong to the glycosyl hydrolase 73 family (GH73) (115). LytD is an 880 amino acid protein that is localised in the cell wall and is produced during vegetative growth under the control of SigD, a sigma factor that transcribes genes responsible for motility and chemotaxis (Table 1.1). This enzyme is considered one of the major autolysins involved in cell wall turnover, cell separation, cell lysis, and motility (60, 92). LytG is also a member of the vegetative autolysin family of *B. subtilis*. It is a 282 amino acid protein, and its expression is regulated by a single promoter that is probably transcribed by sigma factor A (Table 1.1) (115). It has been proposed that LytG is a novel glucosaminidase that may play a role in motility, chemotaxis, cell lysis, and cell division (115). However, the precise role of the glucosaminidase LytG is still unclear.

1.3.4 Muramidase

The muramidase family comprises enzymes that cleave glycan strands by hydrolysing the glycosidic bond at the point where *N*-acetylglucosamine is attached to (1,4) *N*-acetylmuramic acid (Figure 1.7) (6). The muramidase family is composed of lysozymes and lytic transglycosylases, both targeting the glycan strands at the same site but resulting in two different products. Lysozyme hydrolyses the glycosidic bonds linking *N*-acetylmuramic acid (Mur*N*Ac) to *N*-acetylglucosamine (Glc*N*Ac) by adding water, resulting in a reduced Mur*N*Ac product. On the other hand, lytic transglycosylase catalyses the C-6 hydroxyl group of Mur*N*Ac, leading to the production of anhydromuropeptide (1,6-anhydro-*N*-acetylmuramic acid). In contrast, *N*-acetylglucosaminidase is also a glycoside hydrolase, but it is responsible for cleaving the other glycosidic linkage between *N*- acetylglucosamine and *N*-acetylmuramic acid.

The *B. subtilis* genome encodes *cwlQ*, a bifunctional protein with soluble-lytic transglucosylase and muramidase activities that produce 1,6-anhdro-*N*-acetylmuramic acid and *N*-acetylmuramic acid products, respectively (116). CwlQ (formerly YjbJ) is a 181 amino-acid protein that is regulated by the motility sigma factor SigD during the exponential phase (Table 1.1) (117). Cells lacking CwlQ activity show a severe defect in swarming motility, even though the absence of CwlQ does not affect the assembly of the flagellum (118), so the effect of the absence of this activity on swarming is unclear.

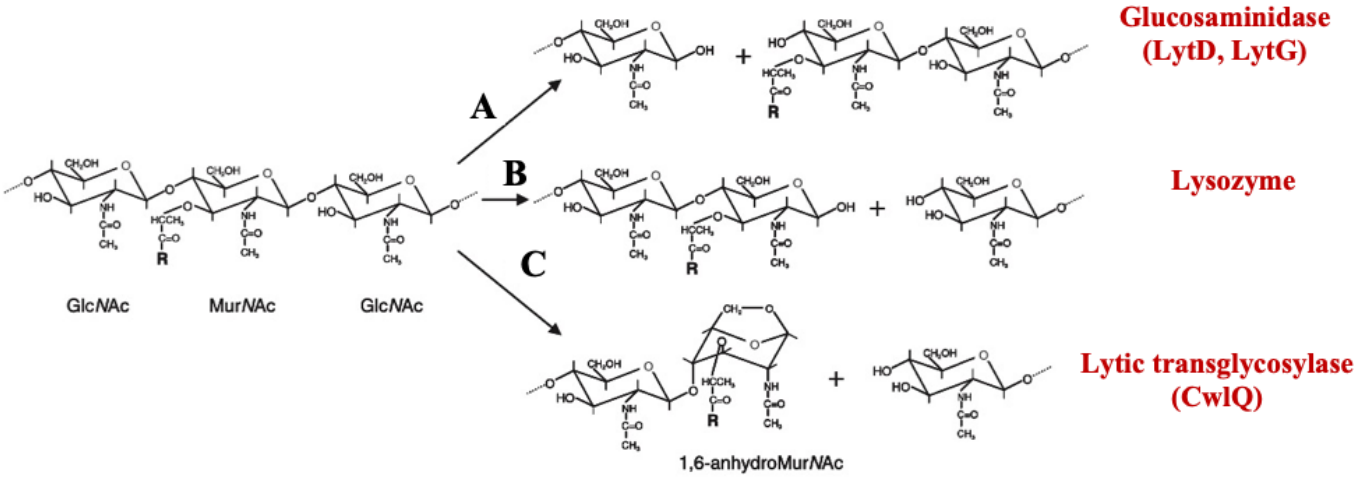

Figure 1.7 The biosynthesis pathway of peptidoglycan components UDP-Glc*N*Ac and UDP-Mur*N*Ac

Breakdown of glycosidic bonds in peptidoglycan between Glc*N*Ac and Mur*N*Ac by **A-** glucosaminidase (LytD and LytG) or between Mur*N*Ac and Glc*N*Acby muramidase, either **B-** lysozyme or **C-** lytic transglycosylases. Lysozyme hydrolyses by adding water, resulting in a reduced Mur*N*Ac product. Lytic transglycosylases specifically break the glycosidic bond between Mur*N*Ac and Glc*N*Ac, forming a 1,6-anhydro ring at Mur*N*Ac via an intramolecular transglycosylation reaction. R indicates the peptide linked to the lactyl residue of Mur*N*Ac. This figure is adapted from (6).

1.4 Cell elongation and division

The rod-shaped *B. subtilis* propagates basically by a short life cycle requiring complicated protein-to-protein interactions and cell wall modification. A single cell grows by an elongation of the cylindrical portion of the cell until its length is doubled. Concomitantly with this, the DNA in the parent cell is duplicated and then separated into two discrete units. Then, cell

division and separation occur at the middle of the parent cell to produce two identical daughter cells (first generation). Remodeling the cell wall during cell elongation and division implicates the need for specific hydrolytic activities, but the biochemical activities, or specific enzymes involved are not well defined due to the autolytic enzyme redundancy.

1.4.1 Role of autolytic enzymes in cell elongation and division

Extensive studies on the autolytic enzymes of *B. subtilis* have identified four key enzymes involved in cell separation during vegetative growth: the glucosaminidase (LytD), the amidase (LytC), and the endopeptidases (LytE and LytF) (93). Previously, multiple, single, and double mutations have been constructed of these enzymes in order to discover which enzymes are responsible for cell separation. From these analyses, a single mutation in *lytC* was found to result in a slight increase in cell chain length compared to the wild type, and when combined with a *lytD* mutant, the cell chains became even longer, which is perhaps the first indication of the overlapping roles of autolytic enzymes in cell separation (92). However, a study by Chen (112) stated that the main autolytic enzyme in cell separation is LytF. A complication of the early work stems from the fact that defining increased cell length versus cells joined together in a chain can be problematic. Hence, a defect in cell division will result in a filamentous cell, whereas a cell separation defect results in a chain of multiple cells connected at the poles. Discriminating between the two, particularly when the effect is subtle, is difficult without the use of membrane dyes combined with fluorescence microscopy or EM. Cell division was later suggested to be most affected by the absence of *lytF* compared to the minor defect caused by the double mutant in *lytC lytD*. Margot (104) found that the depletion of the four major autolysins LytC, LytD, LytE, and LytF resulted in very long chains of cells, and a consequence of this was the apparent loss of motility. Consequently, there is a need to systematically delete enzymes and evaluate the consequences carefully.

1.5 Cell wall turnover and recycling

Inside-to-outside remodeling of the wall seems to provide a simple explanation for the growth of Gram-positive cells (Figure 1.8). The newly synthesised materials, PG monomers, are inserted into the innermost surface of the cell wall, polymerised, and then cross-linked. The new

synthesis pushes outward and stretches the older wall both through the action of deposition of the newest material and cell turgor, respectively. By the time a layer reaches the outer surface, it becomes susceptible to degradation by the action of autolytic enzymes (8, 110). *B. subtilis* cylindrically elongates in order to grow, while the poles serve as fixed support points and do not seem to be subject to significant turnover of the PG (8). It was suggested by Reith and Mayer (110) that complete cylindrical cell wall PG turnover takes about two generations; during this time, a newly synthesised layer would progress to the outer surface and become degraded. This seems to be consistent with other wall turnover analyses where the shift from teichuronic to teichoic acids was visualised by differential metal staining EM (119).

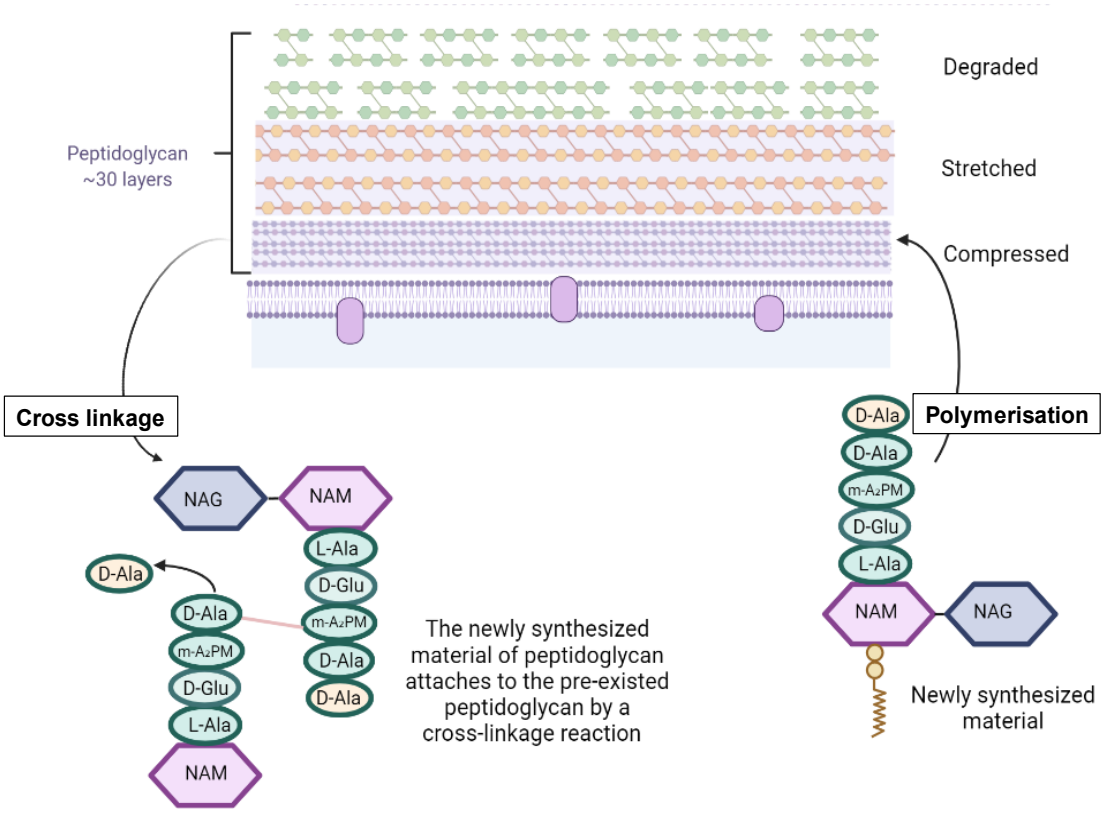

Figure 1.8 Cell wall synthesis and turnover

The mechanism of cell wall synthesis and turnover in *B. subtilis* starts by polymerization of newly synthesised material of peptidoglycan deposited at the innermost layer of the cell wall (compressed layers), followed by a cross-linkage reaction between the new and the pre-existed peptidoglycan materials. The middle layers are stretched because of the cell turgor and are pushed outward to reach the outer surface, which is then degraded by autolytic enzymes. The illustration was created with BioRender.com.

1.5.1 Muropeptides

Naturally produced muropeptides are the products released as a result of peptidoglycan remodeling during cell growth. This process involves degrading mature peptidoglycan into muropeptide fragments, which are dictated by specific autolytic enzymes. Depending on the enzyme activity, different muropeptides would be released from the cell wall into the surrounding environment, such as disaccharide tripeptide, *m*-DAP -type peptidoglycan (tripeptide, tetrapeptide and pentapeptide), monomeric NAG sugar, muramyl-dipeptide, anhydro-murotetrapeptide (tracheal cytotoxin, TCT), anhydro-murmayltripeptide, disaccharide pentapeptide, dipeptide, dipeptide D-Glu- *m*-DAP (mono and disaccharide peptides, and muramyl-dipeptide (disaccharide di-, tri-, tetrapeptides) (60, 120). In contrast, the analysis of the cell wall composition generally uses the enzymatic degradation of the peptidoglycan to permit the complex structure to be broken up to permit their characterisation. This is usually referred to as muropeptide analysis and exploits chromatography methods (HPLC and UHPLC) in combination with mass spectrometry (MS) to allow the identification of the fragment, and the results provide an overall understanding of the level of cross-linkage and modification of the sacculus structure. However, the data obtained is the average of the entire "molecule". Consequently, there is little information available about the structural difference between newly synthesised and "old" peptidoglycan or the cylindrical vs. cell pole PG structure.

The degradation of the cell wall components is undeniably important for cell growth, but it could be a waste of resources if not recovered. Approximately 45% of the peptidoglycan material is turned over per generation in both *B. subtilis* and *E. coli.* However, the cell wall turnover and recycling in *E. coli* have been to some degree better elucidated as the products are retained by the outer membrane; little work has been done with *B. subtilis* as it is presumed that the degradation products are released into the growth medium and consequently are hard to analyse. For *E. coli*, it was found that about half of the old wall was recycled and reinserted as a new wall per generation. In contrast, as *B. subtilis* lacks the ability to retain its turnover products, it has been presumed that little is recovered by the cell. Recently, it has been found that *B. subtilis* recovers about 5-10% of its degraded material (110, 121), but the role of the autolytic enzymes involved in this process was not analysed in detail.

1.5.2 Role of autolytic enzymes in cell wall turnover

LytC and LytD have been extensively studied in terms of cell wall turnover in *B. subtilis*. A former study by Blackman (92) reported that LytC was the essential autolytic enzyme in cell wall turnover since a *lytC* mutant decreased the rate of this process and that a double mutant in *lytC lytD* resulted in a significant decrease in the rate of cell wall turnover when compared with the *lytC* mutant. In contrast, a single mutant in *lytD* did not affect the cell wall turnover rate compared to its wild-type parent. Consequently, LytD may slightly compensate for LytC in wall turnover at the cylindrical portion of the cell, while LytC completely substitutes LytD (92, 122). Saman Nayyab (123) suggested that depletion of the glucosaminidase LytG is thought to impair the tension release of the outermost layers of the PG that is necessary for the insertion of the newly synthesised material, consequently hindering the nascent components from being pushed into the stress-bearing layers. A consequence of this is that the division process is impaired (123).

1.6 Extracellular appendage insertion through a cell wall

Peptidoglycan dynamics must also be modified somehow to permit cellular complexes such as pili and flagella to pass through the cell wall. Pili are a type IV system required for cellular adhesion, gene transfer (conjugation), natural transformation, colonization, biofilm formation, and even twitching motility in some bacterial species (124). However, the flagella are the best characterised, involving a type III secretion system, and the functional complex is required for cell movement either by swimming in a liquid medium or swarming on a solid medium (Figure 1.9) (125).

In Gram-positive bacteria, these two assembly systems are synthesised in the cytoplasm, embedded in the cell membrane, and extended through the thick peptidoglycan layers. However, how these structures can pass through the cell wall to the outside of the cell has not been analysed in detail and needs further investigation.

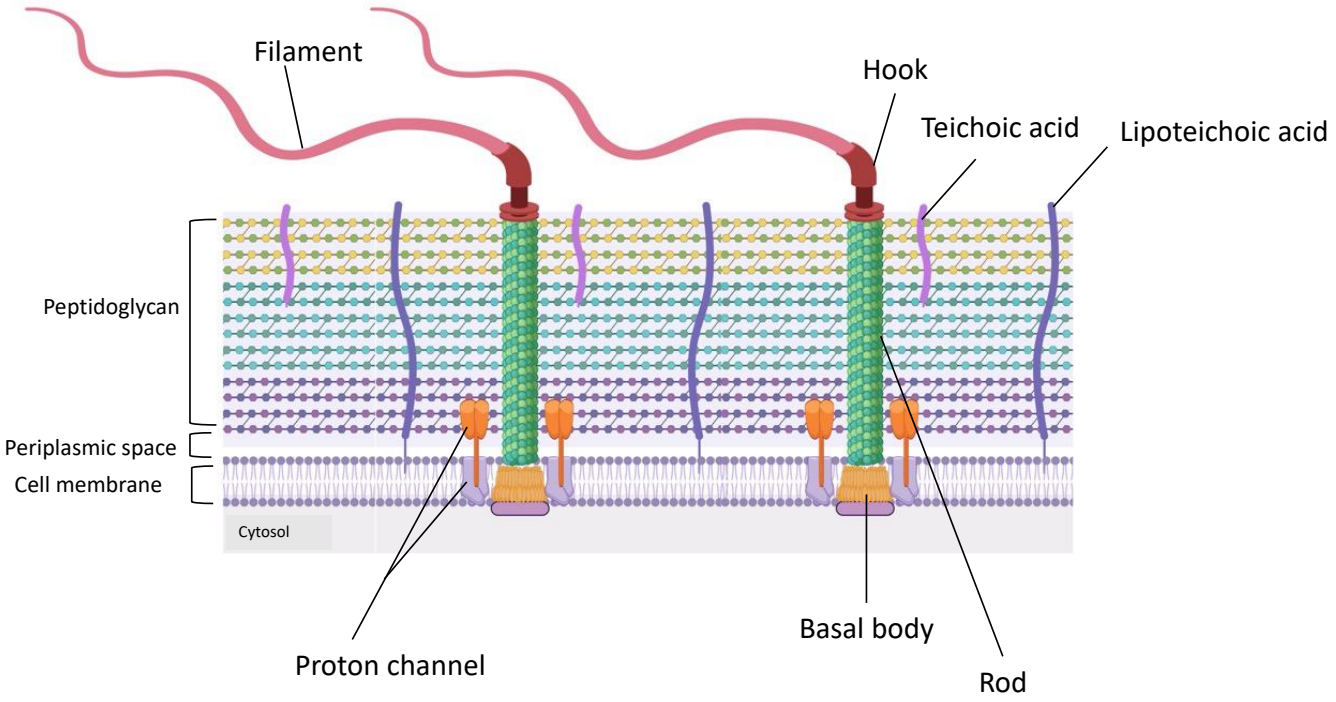

Figure 1.9 Flagellar structure of Gram-positive bacteria

Flagellar structure: the basal body, rod that passes through the thick peptidoglycan layers, hook, and filament. The three colours (purple, blue, and yellow) of peptidoglycan represent the compressed, stretched, and degradable layers of peptidoglycan, respectively. The illustration was created with BioRender.com.

1.6.1 Flagellum structure and regulation

Flagella are composed of a basal body, rod, hook, and filament (Figure 1.9). The basal body is the part of the flagellum that is integrated into the cell membrane and serves as the structural anchor combined with a gear-like rotor. The rod is the part that crosses through the peptidoglycan layers and links the basal body with the external structures: the universal joint (hook), and the propeller-like filament (126). Flagellar torque is generated by a proton motive force pumping through the stator MotA/MotB that is associated with a flagellar rotor FliG (127).

Extensive genetic and biochemical investigations have been carried out on the flagellum in the Gram-negative bacterial species *Salmonella enterica* serovar Typhimurium and *E. coli* (128). These studies have uncovered that over 50 gene products play roles in the assembly and

operation of the flagellum in both species (129). This knowledge has been then instrumental in understanding how flagella are structured and function in the Gram-positive *B. subtilis*. In *B. subtilis*, the flagella closely resemble those of *E. coli* and *S. enterica*, with the notable difference being the absence of the top pair of rings of the basal body: the *p*eptidoglycan ring (P-ring) and the *s*upramembrane ring (S-ring) (130). Moreover, *B. subtilis* does not encode homologs of the bushing proteins found in the basal body structure of both *E. coli* and *S. enterica* (131-133).

B. subtilis synthesises approximately 20 rotary flagella along the length of the cell. The assembly process of a rotary flagellum is complicated and involves a variety of proteins that are built in an organized and regulated sequence extending from the cytoplasmic membrane to the external surface of the cell body. Most of the genes corresponding to flagellar proteins are encoded in a 32-gene long *fla/che* operon (Figure 1.10A). The expression of the *fla/che* operon is mediated initially by SigA, and then by the activation of SigD that is encoded at the end of the *fla/che* operon, increasing the expression of the operon. SigD is also needed for the transcription of the final component of the structure, flagellin (Hag), and acts in the regulation of chemotaxis, motility, and some autolysins (LytC, LytD, and LytF). A previous study by Mukherjee and Kearns (134) showed that cells lacking the sigma factor D (SigD) exhibited long chains and were impaired in swarming motility. The activity of SigD is controlled by FlgM, which acts as an anti-sigma factor that inhibits its homolog σ^{28} (135-137). FlgM coordinates the expression of the flagellar genes involved in the assembly of the flagellar hook and basal body by binding to SigD and preventing its association with RNA polymerase (138).

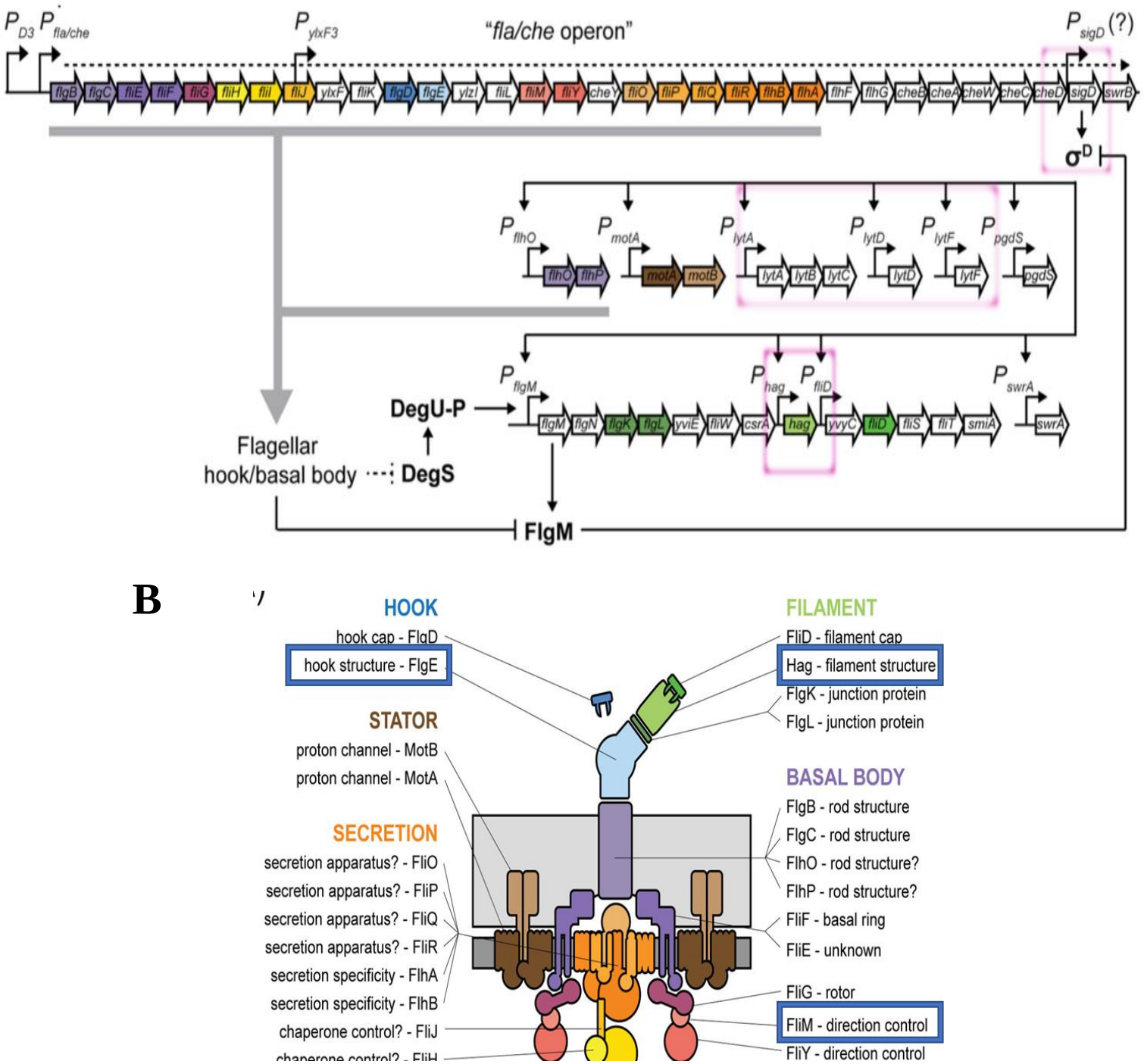

Figure 1.10 Flagellar proteins and composition

A- The genetic hierarchy of the flagella in *B. subtilis*. Open arrows represent the flagellar genes, while bent arrows indicate the promoters. The pink boxes denote the sigma factor SigD that controls the expression of flagellin Hag and autolytic enzymes LytC, LytD, and LytF. **B-** Flagellar composition proteins. The blue boxes highlight the proteins used to monitor the flagellar assembly in this study. This figure is adapted from (134).

The core of the basal body is similar to the type III secretion apparatus, serving as an export gate for proteins required for the assembly of the more distal flagellar components (rod, hook, and filament). This export gate comprises six proteins, including FliO, FliP, FliQ, FliR, FlhA, and FlhB (Figure 1.10B) (139-141). Five of these proteins, FliP, FliQ, FliR, FlhA, and FlhB, are comparable to the type III pathogenic injectisome. The remaining protein, FliO, seems to be involved in the flagellar secretion and stabilization of the FliP protein (142). FlhA interacts with the ATPase (FliI), the negative regulator (FliH) of FliI, and the putative general chaperone (FliJ), which are crucial in the secretion process (128, 143, 144). FliJ interacts with both FliI and FliH (145).

The basal body is made up of the polymerised FliF subunits that serve as a membrane anchor, denoted the inner *m*embrane ring (M-ring) (Figure 1.10B) (146, 147). FliF contains a large central extracellular domain attached to FliE, which may play a role in providing a fitting for the flagellar rod (148, 149). FliG is attached to FliF and polymerised to form a cytoplasmic gear-like rotor (150, 151). FliM is polymerised below FliG to build the cytoplasmic ring (C-ring) (133, 152), which is essential for the chemotaxis system and controlling the direction of the flagellar rotation (Figure 1.10B). In *B. subtilis*, FliY is part of the switch complex that constitutes the flagellar C-ring (153). In *E. coli* and *S. enterica*, this switch complex includes a large number of FliG, FliM, and FliN proteins (154). In addition to the role of FliG in flagellar biosynthesis, its C-terminal interacts with the MotA protein of the Mot complex to generate the torque necessary for the flagellar rotation (155, 156). This torque is then transmitted through FliF to the flagellar rod, enabling the rotational movement of the flagella (157).

Rod formation in *S. enterica* has undergone extensive investigation. Initially, it was found that FlgB, FlgC, FlgF, and FlgG are indispensable for rod assembly (152, 158, 159). These proteins, acting as structural components, are secreted via the flagellar type III secretion system and exhibit polymerisation in *vitro* (146, 160). The rod spans the cell envelope, penetrating the peptidoglycan and outer membrane through the "P" and "L" rings, potentially aiding rod rotation within the envelope (130, 161). The sequential assembly of the *Salmonella* rod has been demonstrated. FlgB is believed to initiate rod polymerisation as it interacts with FliE, which is closely linked to the basal body protein FliF (148, 162, 163). FlgG is likely the final protein added to the rod, as indicated by mutations in FliF, which causes rod shearing and

releases FlgG with the flagellar hook (164). Hence, the proposed assembly order, from cell proximal to distal, is FlgB, FlgC/FlgF, and FlgG, with recent evidence suggesting FlgF might precede FlgC. The predictive accuracy of the assembly order was constrained by the inability to form intermediate structures upon mutation of individual subunits.

In *B. subtilis*, the flagellar rod composes four similar putative proteins: FlgB, FlgC, FlhO, and FlhP (Figure 1.10B) (133, 165, 166). The first two (FlgB and FlgC) are encoded within the *fla/che* operon (Figure 1.10A), while FlhO and FlhP are likely part of the upstream region of the hook assembly and are expressed separately as a putative dicistron (166). The absence of any of these proteins leads to defects in flagellar assembly and loss of swarming motility (126). The assembly order of the flagellar rod proteins is as follows: FlgB, FlgC, FlhO, and FlhP from the proximal (FliF) to the distal end (FlgE) (Figure 1.10B). FliE serves as a connecting platform between the basal body protein FliF and the rod protein FlgB. The absence of FliE results in a defect in swarming motility, as well as defects in the assembly of the filament and hook. However, the basal body structure itself appears to remain intact (126).

The hook is a focal joint that links the basal body to the filament in the flagellar structure, and it is composed of repeating subunits of FlgE (Figure 1.10B) (133, 167, 168). The hook assembly involves several steps: first, the hook cap FlgD is secreted and placed on top of the rod, and then the protein FlgE is secreted by a type III-like secretion apparatus (159, 169). FlgE undergoes polymerisation to form a 70 nm curved cylindrical tube in *B. subtilis*, which is longer than the hook of *S. typhimurium* (133, 170). The length of the hook is tightly regulated by two proteins: FliK, a secreted protein, and FlhB, a proteolysis protein (170-172). The absence of either of these proteins leads to the formation of an extended hook structure, known as a polyhook, which disrupts the production of the flagellar filament (166, 173, 174). The construction of the hook is designed in such a way that it expands from one side and compresses from the other. This unique structure allows the transfer and reorientation of motor torque to the propeller-like filament, enabling flagellar rotation (175).

The filament, an extracellular component of the flagella, plays a crucial role in cell movement as it rotates like a propeller. A single filament may contain up to 20,000 subunits of one protein, known as flagellin (referred to as FliC or FljB in *Salmonella* species) (176). The *B. subtilis* filament comprises approximately 12,000 flagellin monomers that assemble through the

interactions between the N-terminal and C-terminal of flagellin monomers (177). This assembly process results in the formation of a cylindrical tube with a diameter of 20 nm (134). The synthesis of flagellin (Hag) occurs in the cytoplasm, after which it binds to FliS to facilitate its delivery to the secretion apparatus (178, 179). Subsequently, it is exported through the secretion apparatus via a partner-switch system involving FliW and CsrA proteins (179, 180). The extracellular chaperone protein FliD plays a crucial role in the polymerisation of flagellin monomers, forming a structure known as the filament cap (181). In the absence of FliD, flagellin monomers accumulate in their monomeric form in the extracellular environment.

In *B. subtilis*, each stage of the flagellum assembly has a defined time, with cells found to be capable of motility about 40-60 minutes after initiation. The basal body, the initial stage of flagellar assembly, is rapidly constructed within about 5 minutes. Next, the hook stage takes 10-20 minutes to be completed. Finally, the last stage of assembly, forming the filament, appears to start after 15 minutes and is fully formed after approximately 45 minutes of the flagellar initiation (182).

The distribution of flagella on the cell surface is a defined characteristic of bacterial species. Species that synthesise flagella along the lateral cell wall of the cell are called peritrichous or medial bacteria (as is seen for *B. subtilis*). In contrast, other species that restrict flagellar assembly to the poles of the cell are called polar or lophotrichous bacteria. The number of flagella also varies among the bacterial species. A study by Patrick (183) demonstrated that SwrA is responsible for controlling the expression of basal body number in *B. subtilis*. Furthermore, the placement of basal bodies on the cell surface is coordinated with a distance between basal bodies that is regulated by proteins FlhF and FlhG (182).

1.6.2 Role of autolytic enzymes in flagellum insertion and motility

Since the peptidoglycan layers are very strong and characterised by their criss-cross structure, the flagellum rod would need autolytic enzymes to pave its way through these layers (Figure 1.9). In *Salmonella typhimurium* and *E. coli*, FlgJ serves as a peptidoglycan hydrolase that creates a path for flagellar rod assembly (184, 185). However, in *B. subtilis*, it is unknown how the rod assembly crosses the peptidoglycan layers or if a specific autolytic enzyme is required.

Multiple autolytic enzymes have been implicated in flagellar motility and chemotaxis mechanisms in *B. subtilis*, and these enzymes are tightly regulated by a number of regulatory proteins (e.g., Spo0A, SwrA, CodY, DegU, and also SigD). LytD, LytC, lytF, and LytG have all been implicated in flagellar function somehow, and it is possible that these autolytic enzymes substitute for each other in case of the absence of one (92, 112, 115). However, most of the previous studies focused on motility, primarily in terms of the ability of the cells to migrate and not in terms of the presence of flagella. This is important since some of these mutations result in chains of cells, and this might have an impact on physical motility even if flagella are present and functional. To distinguish between these differences, plates with less than 0.5% (w/v) agar are referred to as 'swim plates,' where the individual cell movements in the liquid consistency of soft agar's liquid-filled channels allow the spreading of the culture. Conversely, plates with 0.5% (w/v) agar or more are termed 'swarm plates'. Here the thicker agar inhibits individual swimming and requires a more collective action for the cells to migrate across the surface, often referred to as swarming.

The following paragraph is a summary of previous analyses using the authors' terminology, and consequently, the definition of the lack of motility in relation to the absence of flagella is, to some degree, open to question. There is also a possibility that the genetic backgrounds of the strains analysed differ in key aspects and, consequently, may explain some of the variations observed.

LytC is the autolytic enzyme that has been demonstrated as the primary hydrolase for flagellar motility efficient function (112). A previous study reported that the absence of both *lytC* and *lytD* genes resulted in non-motile cells on soft agar (0.3%, w/v), while the individual mutations only resulted in a reduction in motility (92). In contrast, Rui Chen and his co-worker (112) elucidated that a mutant in *lytD* did not affect the swarming motility (swarm plate 0.7% (w/v) agar). Swarm motility was also unaffected by the absence of LytF. In contrast, the *lytC lytF* double mutant was non-motile, as well as the *lytC lytD lytF* mutant. However, this might be because cells were not separated and were generally observed as extremely long chains (104, 112). Moreover, Rui Chen and colleagues (112) demonstrated that both *lytC* and *lytD* mutants displayed a comparable decrease in swimming motility on 0.3% (w/v) agar. However, the *lytF* mutant exhibited slightly more impairment, likely due to the challenge faced by its long chains in

navigating through the agar pores. Another study by Horsburgh (115) reported that a *lytG* mutant also resulted in a reduction in swarm motility and that the *lytC lytD lytG* triple mutant and *lytC lytD* double mutant were observed to be non-motile on a soft agar plate (0.3%, w/v). The three autolytic enzymes LytC, LytD, and LytF have been examined in relation to flagellar assembly, and results show that the loss of these autolytic enzymes had no effect on flagellar assembly (112). A more recent study by Sandra (118) showed that cells without CwlQ activity experienced a severe defect in swarming motility. In contrast, cells without CwlO activity had a moderate defect on swarm plates (0.5% (w/v) agar). However, mutant *cwlQ* exhibited the swimming phenotype of the wild-type cells on soft agar (0.3%, w/v). This study also revealed that cells of the mutant *lytC lytD lytF cwlO cwlQ* were capable of flagellar biosynthesis. Thus, how the flagella basal bodies are made and how the structure passes through the PG remains unclear.

1.6.3 Competence pilus

Many bacteria naturally exhibit competence for transformation, enabling the bacterium to uptake DNA from its environment and thus enhancing its adaptation and genetic diversity. This process is tightly regulated and depends on their physiological state (186). Among the various bacterial competence systems, *B. subtilis* has been studied most extensively. During the transition from exponential growth to the stationary phase, *B. subtilis* cells undergo a critical juncture where they can either enter the stationary phase and induce sporulation or, alternatively, they can initiate competence. Notably, only a fraction of the cells, up to 20%, opt for competence under conditions favorable for this developmental pathway. This indicates that both competence and sporulation are actively determined decisions made by a distinct subpopulation of cells within the bacterial community. These decisions are governed by bistable switches, highlighting an intriguing phenomenon in bacterial populations where cells adopt different developmental fates based on environmental cues and internal regulatory mechanisms (187).

Numerous genes have been linked to the development of competence in this bacterium, divided into early genes, which are thought to have regulatory roles, and late genes, whose products appear to be involved in the transformation process itself. Proteins encoded by several late genes show significant homology to the pullulanase family of secretory systems (188). This

similarity suggests that the uptake of transforming DNA is mediated by a pseudopilus similar to the pullulanase system (186). A notable difference is that in Gram-negative bacteria, the pseudopilus is anchored between two membranes, whereas in Gram-positive bacteria, it extends from the cytoplasmic membrane into the peptidoglycan wall.

The transformation model outlines a six-step process for DNA uptake in *B. subtilis* and *S. pneumoniae*. Initially, transforming DNA (tDNA) binds reversibly across the cell wall, followed by the pilus assembly, facilitated by the ATPase ComGA (189, 190) and anchored by scaffold protein ComGB. Subsequently, the pilus, composed of ComGC, retracts, pulling DNA into the periplasm; the term periplasm in the context of Gram-positive bacteria refers to the extracellular space located between the cell wall and the cell membrane, which is believed to function similarly to the membrane-enclosed periplasm found in Gram-negative bacteria (191). Then the tDNA is stabilized by association with ComEA, a membrane-anchored DNA binding protein at the polar sites, facilitating its uptake into the cytosol before undergoing processing by membrane DNase NucA (192-194). The BdbD and BdbC proteins are functioning as thiol-disulfide oxidoreductases. Their primary role is to catalyse the formation of both intramolecular and intermolecular disulfide bonds within ComGC and ComEC, which plays a vital role as a component of the transformation permease. Through their enzymatic activity, BdbD and BdbC contribute to the proper folding and stability of these essential proteins, ultimately facilitating the efficient process of DNA uptake and transformation (195). Here, one DNA strand is degraded, and the other is transported through the channel with the help of ATPase ComFA. A study by Kilb (191) has revealed the localisation of competence machinery and recombination proteins at various sites within the cell. This study has also shed light on the dynamics of pilin ComGC and the mechanical forces involved in DNA uptake, demonstrating the retraction of pili by *B. subtilis* cells.

1.6.4 Role of autolytic enzymes in pilus insertion

There are indications that the assembly of the competence apparatus requires peptidoglycan rearrangements. In the early 1960s, a study by Young (196) found a correlation between autolytic activity and competence in *B. subtilis*. Young proposed that autolytic enzymes might create local gaps in the peptidoglycan for DNA uptake. This correlation was also observed in

group H streptococci (197). Later studies showed that competence development is co-regulated with autolytic activity and flagellar assembly (65). An indirect link between competence and peptidoglycan metabolism in *S. pneumoniae* was identified through a signal-transducing pathway that regulates both PBP activity and competence (198).

While the competence mechanisms differ between Gram-negative and Gram-positive bacteria, the systems appear related, as shown by the similarity between competence genes in *Haemophilus influenzae* and *B. subtilis* (199). An interesting connection between Gram-negative competence and peptidoglycan metabolism is mapping the *H. influenzae* PBP1a gene within a cluster of open reading frames involved in transformation, where gene inactivation significantly reduces transformation efficiency (200). In *Neisseria gonorrhoeae*, natural transformation competence is closely linked to piliation, with several genes involved in type IV pili assembly also required for transformation, supporting the idea of a pseudopilus in *B. subtilis* competence (201, 202).

Recently, researchers identified two crucial proteins in *Neisseria gonorrhoeae* that are necessary for transformation: Tpc and the peptidoglycan-linked lipoprotein ComL (201, 202). Mutations in the *tpc* gene lead to defects in cell division, suggesting that Tpc may act as a peptidoglycan hydrolase. Both Tpc and ComL are believed to assist in transporting DNA across the peptidoglycan layer. Additionally, Tpc is involved in the process of cellular invasion and may be required for the effective export of virulence factors, similar to the role of the LytA peptidoglycan hydrolase in *S. pneumoniae* (203).

1.7 Aims of the project

The initial direction of research would be to understand the role of autolytic enzymes involved in cell wall degradation, which is essential for the growth of bacterial cells. This can be achieved by developing methods to detect cell wall degradation products or phenotypes resulting from the loss of specific biochemical activities and generating multiple autolytic mutants.

In cases where the loss of autolytic enzyme activity leads to lethal phenotypes, conditional mutants will be constructed, introducing conditional promoters to regulate the expression of the genes encoding the autolytic enzymes or by introducing temperature-sensitive

mutations in the enzymes. These conditional mutants will allow the controlled expression of autolytic enzymes and, hence, their activity, providing insights into their role and regulation.

Another aspect that this work will explore is whether the insertion of cellular appendages, such as flagella and pili, requires dedicated autolytic activity or if they are passively incorporated into the newly synthesised cell wall and rely on the existing autolytic apparatus during growth to reach the outer surface. Investigating this phenomenon can shed light on the interplay between cell wall synthesis, degradation, and the assembly of cellular appendages and would exploit the strains constructed in the earlier work.

In addition, the combination of manipulated autolytic activity and the ability to detect the assembly of the structure crossing through the cell wall will provide tools to understand peptidoglycan dynamics, an example being the fact that flagella should be fixed landmarks. Thus, by differential fluorescent labeling of peptidoglycan and flagella, their relative positions and movement over time can be monitored. This will allow for the investigation of how cell wall remodeling occurs in relation to the movement of the PG as the cell expands, providing insights into the coordination between cell wall degradation and synthesis.

In summary, the research aims to develop a comprehensive understanding of the role of autolytic enzymes in cell wall degradation, the mechanism of flagellar insertion, and the dynamics of peptidoglycan. The overall aim is to significantly contribute to our knowledge of bacterial cell growth in relation to the regulation of cell wall metabolism.

Chapter 2
Material and Method

2.1 Strains, plasmids, and oligonucleotides

All strains used in this study are listed in (Table 2.1). Primers for PCR and sequencing are listed in (Table 2.2). Primers were designed using Clone Manager software (https://www.scied.com/dl_cm10.htm) and constructed by Eurogentec (www.eurogentec.com/life-science.html). Plasmids and the functions they were used for in this study are listed in (Table 2.3). All genes that have been deleted or inserted are indicated within the strain genotype. Plasmid genotypes also indicate the origin of replication, reporters, promoters, and resistance markers (antibiotic cassettes) that are present in the strain where appropriate. The resistance cassettes that were inserted into the strains as selective markers are abbreviated as follows: *amp* (Ampicillin), *kan* (Kanamycin), *cat* (Chloramphenicol), *spec* (Spectinomycin), *zeo* (Zeocin), *neo* (neomycin), and *ery* (erythromycin). All confirmed strains were stored in 20% (v/v) glycerol solution at -80 °C.

Table 2.1 Strains used in this study

Strain	Genotype	Source
168CA	*trpC2 Bacillus subtilis*	Laboratory collection
BKK35620	Δ*lytC::kan*	(204)
BKK35780	Δ*lytD::kan*	(204)
BKK09420	Δ*lytE::kan*	(204)
BKK09370	Δ*lytF::kan*	(204)
BKK31120	Δ*lytG::kan*	(204)
BKK34800	Δ*cwlO::kan*	(204)
BKK19410	Δ*cwlS::kan*	(204)
BKE00100	Δ*dacA::ery*	(204)
BKK34800	Δ*cwlQ::kan*	(204)
BKK16310	Δ*fliM::kan*	(204)
BKK16290	Δ*flgE::kan*	(204)
BKK35360	Δ*hag::kan*	(204)
AA001	*trpC2* Δ*lytC::kan*	This study
AA002	*trpC2* Δ*lytD::kan*	This study
AA003	*trpC2* Δ*lytE::kan*	This study
AA004	*trpC2* Δ*lytF::kan*	This study
AA005	*trpC2* Δ*lytG::kan*	This study
AA006	*trpC2* Δ*cwlO::kan*	This study
AA007	*trpC2* Δ*cwlS::kan*	This study
AA070	*trpC2* Δ*cwlQ::kan*	This study
AA008	*trpC2* Δ*fliM::kan*	This study
AA009	*trpC2* Δ*flgE::kan*	This study

AA010	*trpC2 Δhag::kan*	This study
AA011	*trpC2 ΔlytE ΔlytF::kan*	This study
AA012	*trpC2 ΔlytF ΔcwlO::kan*	This study
AA013	*trpC2 ΔlytD ΔlytG::kan*	This study
AA014	*trpC2 ΔlytD ΔlytG ΔlytC ΔlytF ΔcwlO::kan*	This study
AA015	*trpC2 ΔlytD ΔlytG ΔlytC ΔlytE ΔLytF::kan*	This study
AA016	*trpC2 ΔlytD ΔlytG ΔlytC::kan*	This study
AA017	*trpC2 ΔlytD ΔlytG ΔlytC ΔlytF::kan*	This study
AA018	*trpC2 ΔlytD ΔlytG ΔlytC ΔlytF ΔcwlS::kan*	This study
AA019	*trpC2 ΔlytD ΔlytG ΔlytC ΔlytF ΔcwlS ΔcwlQ::kan*	This study
AA020	*trpC2 ΔlytD ΔlytG ΔlytC ΔlytF ΔcwlS ΔcwlQ ΔlytE::kan*	This study
AA021	*trpC2 ΔlytD ΔlytG ΔlytC ΔlytF ΔcwlS ΔcwlQ ΔcwlO::kan*	This study
AA064	*trpC2 ΔdacA::ery*	This study
AA022	*trpC2 ΔlytD ΔlytG ΔlytC ΔlytF ΔcwlS ΔcwlQ::kan ΔdacA::ery*	This study
AA023	*trpC2 ΔlytD ΔlytG ΔlytC ΔlytF ΔcwlS ΔcwlQ ΔdacA::ery ΔcwlO::kan*	This study
AA024	*trpC2 ΔlytE ΔlytF::kan ΔdacA::ery*	This study
AA025	*trpC2 ΔlytE::kan ΔdacA::ery*	This study
AA026	*trpC2 ΔlytF::kan ΔcwlS::kan*	This study
AA027	*trpC2 ΔlytF::kan ΔcwlS ΔlytE::kan*	This study
DS8521	*ΔfliM amyE::*$P_{fla/che}$*-fliM-gfp spec*	(126)
AA030	*trpC2 amyE::*$P_{fla/che}$*-fliM-gfp spec*	This study
AA028	*trpC2 ΔfliM:kan amyE::*$P_{fla/che}$*-fliM-gfp spec*	This study
AA029	*trpC2 ΔflgE thrC::*$P_{fla/che}$*-flgE*^{T123C} *ery*	This study
DS8996	*ΔfliM ΔflgE amyE::*$P_{fla/che}$*-fliM-gfp spec thrC::*$P_{fla/che}$*-flgE*^{T123C} *ery*	(182)
AA035	*trpC2 amyE::*$P_{fla/che}$*-fliM-gfp spec thrC::*$P_{fla/che}$*-flgE*^{T123C} *ery*	This study
DS1916	*amyE::*P_{hag}*-hag*^{T209C} *spec*	(126)
AA043	*trpC2 amyE::*P_{hag}*-hag*^{T209C} *spec*	This study
AA031	*trpC2 Δhag:kan amyE::*P_{hag}*-hag*^{T209C} *spec*	This study
DS7673	*ΔflgE amyE::*$P_{fla/che}$*-flgE*^{T123C} *cat*	(126)
AA032	*trpC2 ΔflgE:kan amyE::*$P_{fla/che}$*-flgE*^{T123C} *cat*	This study
AA033	*trpC2 lacA::*P_{hag}*-hag*^{T209C} *ery*	This study
AA034	*thrC::*$P_{fla/che}$*-flgE*^{T123C} *ery*	This study
AA035	*trpC2* $P_{fla/che}\Omega P_{xyl}$*-fla/che cat*	This study
AA036	*trpC2* $P_{fla/che}\Omega P_{spac}$*-fla/che kan*	This study
AA037	*trpC2 ΔfliM ΔflgE:kan*	This study
AA038	*trpC2 ΔlytF::kan ΔcwlS ΔcwlO::kan*	This study
AA039	*trpC2* $P_{fla/che}\Omega P_{xyl}$*-fla/che cat amyE::*$P_{fla/che}$*-fliM-gfp spec*	This study
AA041	*trpC2 thrC::*$P_{fla/che}$*-flgE*^{T123C} *ery*	This study
AA042	*trpC2* $P_{fla/che}\Omega P_{xyl}$*-fla/che cat thrC::*$P_{fla/che}$*-flgE*^{T123C} *ery*	This study

AA043	*trpC2* Δ*lytD* Δ*lytG* Δ*lytC* Δ*lytF* Δ*cwlS* Δ*cwlQ::kan amyE::*P_{hag}*-hag*^{T209C} *spec*	This study
AA044	*trpC2* Δ*cwlO::kan amyE::*P_{hag}*-hag*^{T209C} *spec*	This study
AA045	*trpC2* Δ*lytD* Δ*lytG* Δ*lytC* Δ*lytF* Δ*cwlS amyE::*P_{hag}*-hag*^{T209C} *spec*	This study
AA046	*trpC2* Δ*lytD* Δ*lytG* Δ*lytC* Δ*lytF* Δ*cwlS* Δ*cwlQ amyE::*P_{hag}*-hag*^{T209C} *spec* Δ*lytE kan*	This study
AA047	*trpC2* Δ*lytD* Δ*lytG* Δ*lytC* Δ*lytF* Δ*cwlS* Δ*cwlQ amyE::*P_{hag}*-hag*^{T209C} *spec* Δ*cwlO kan*	This study
AA048	*trpC2 amyE::*$P_{fla/che}$*-fliM-gfp spec lacA*::P_{hag}*-hag*^{T209C} *ery*	This study
AA049	*trpC2* Δ*LytE* P_{spac}*-lacZ pLOSS -lytE spec*	This study
AA050	*trpC2* Δ*lytD* Δ*lytG* Δ*cwlQ::kan*	This study
AA051	*trpC2* Δ*lytD* Δ*lytG* Δ*lytC* Δ*lytF* Δ*cwlS* Δ*cwlQ amyE::*$P_{fla/che}$*-fliM-gfp spec*	This study
AA052	*trpC2* Δ*LytF* Δ*dacA::ery*	This study
PDC519	*trpC2 amyE::* P_{xyl}*-gfp-cwlO spec*	(11)
AA053	*trpC2* Δ*lytD* Δ*lytG* Δ*lytC* Δ*lytF* Δ*cwlS* Δ*cwlQ* Δ*dacA::ery* Δ*lytE::kan*	This study
AA054	*trpC2* Δ*lytF* Δ*lytE* Δ*dacA::ery amyE::*P_{xyl}*-gfp-cwlO::spec*	This study
AA055	*trpC2* Δ*LytF* Δ*LytE::kan* P_{spac}*-lacZ pLOSS-lytE spec*	This study
AA056	*trpC2* Δ*lytD* Δ*lytG* Δ*lytC* Δ*lytF* Δ*cwlS* Δ*cwlQ* Δ*pgdS::kan*	This study
AA057	*trpC2* Δ*lytF* Δ*cwlS* Δ*pgdS::kan*	This study
AA058	*trpC2* Δ*lytD* Δ*lytG* Δ*lytC* Δ*lytF* Δ*cwlS* Δ*cwlQ amyE::*$P_{fla/che}$*-fliM-gfp spec lacA*::P_{hag}*-hag*^{T209C} *ery*	This study
AA059	*trpC2* Δ*lytD* Δ*lytG* Δ*lytC* Δ*lytF* Δ*cwlS* Δ*cwlQ amyE::*$P_{fla/che}$*-fliM-gfp spec lacA*::P_{hag}*-hag*^{T209C} *ery* Δ*lytE kan*	This study
AA060	*trpC2* Δ*lytD* Δ*lytG* Δ*lytC* Δ*lytF* Δ*cwlS* Δ*cwlQ amyE::*$P_{fla/che}$*-fliM-gfp spec lacA*::P_{hag}*-hag*^{T209C} *ery* Δ*cwlO kan*	This study
AA061	*trpC2* Δ*LytF* Δ*LytE* Δ*dacA::ery* P_{spac}*-lacZ pLOSS -lytE spec*	This study
AA062	*trpC2* Δ*LytE* P_{spac}*-lacZ pLOSS -lytE spec* Δ*dacA::ery*	This study
AA063	*trpC2 amyE::*$P_{fla/che}$*-fliM-gfp spec aprE::*P_{spac} *- mChary- cheA::kan*	This study
BKK19620	Δ*ldcB::kan*	(204)
AA065	*trpC2* Δ*ldcB::kan*	This study
AA066	*trpC2* Δ*lytE* Δ*ldcB::kan*	This study
AA067	*trpC2* Δ*lytF* Δ*ldcB::kan*	This study
AA068	*trpC2* Δ*lytE* Δ*lytF* Δ*ldcB::kan*	This study
MGNA-B737	*yxkC lacZ'* P_{spac} *lacI-ery*	(205)
AA069	*trpC2 yxkC lacZ'* P_{spac} *lacI-ery*	This study
AA071	*trpC2* Δ*sigD yxkC lacZ'* P_{spac} *lacI-ery*	This study
AA073	*trpC2* Δ*flgM yxkC lacZ'* P_{spac} *lacI-ery*	This study
AA075	*trpC2* Δ*flgM yxkC lacZ'* P_{spac} *lacI-ery* Δ*cwlQ::kan*	This study
AA076	*trpC2* Δ*sigD yxkC lacZ'* P_{spac} *lacI-ery* Δ*cwlQ::kan*	This study

AA077	*trpC2 ΔflgM yxkC lacZ'* P_{spac} *lacI-ery ΔcwlS::kan*	This study
AA078	*trpC2 ΔsigD yxkC lacZ'* P_{spac} *lacI-ery ΔcwlS::kan*	This study
AA079	*trpC2 ΔflgM yxkC lacZ'* P_{spac} *lacI-ery ΔcwlQ*	This study
AA080	*trpC2 ΔflgM yxkC lacZ'* P_{spac} *lacI-ery ΔcwlS*	This study
AA081	*trpC2 ΔsigD yxkC lacZ'* P_{spac} *lacI-ery ΔcwlS*	This study
AA082	*trpC2 ΔsigD yxkC lacZ'* P_{spac} *lacI-ery ΔcwlQ*	This study
AA083	*trpC2 ΔsigD yxkC lacZ'* P_{spac} *lacI-ery ΔcwlQ ΔcwlO kan*	This study
AA084	*trpC2 ΔsigD yxkC lacZ'* P_{spac} *lacI-ery ΔcwlS ΔcwlO kan*	This study
AA085	*trpC2 ΔflgM yxkC lacZ'* P_{spac} *lacI-ery ΔcwlQ ΔcwlO::kan*	This study
AA086	*trpC2 ΔflgM yxkC lacZ'* P_{spac} *lacI-ery ΔcwlS ΔcwlO::kan*	This study
AA087	*trpC2 yxkC lacZ'* P_{spac} *lacI-ery ΔcwlQ ΔcwlO kan*	This study
AA088	*trpC2 yxkC lacZ'* P_{spac} *lacI-ery ΔcwlS ΔcwlO kan*	This study
AA089	*trpC2 ΔcwlQ*	This study
AA090	*trpC2 ΔcwlS*	This study
BKK16470	*ΔsigD::kan*	(204)
BKK35430	*ΔflgM::kan*	(204)
AA091	*trpC2 ΔsigD::kan*	This study
AA092	*trpC2 ΔflgM::kan*	This study
AA093	*trpC2 ΔsigD*	This study
AA094	*trpC2 ΔflgM*	This study
AA095	*trpC2 ΔcwlQ amyE::*$P_{fla/che}$*-fliM-gfp spec*	This study
AA096	*trpC2 ΔcwlS amyE::*$P_{fla/che}$*-fliM-gfp spec*	This study
AA097	*trpC2 ΔcwlQ amyE::* P_{hag}*-hag*^{T209C} *spec*	This study
AA098	*trpC2 ΔcwlS amyE::*P_{hag}*-hag*^{T209C} *spec*	This study
AA099	*trpC2 ΔcwlQ amyE::*P_{hag}*-hag*^{T209C} *spec ΔcwlO::kan*	This study
AA100	*trpC2 ΔcwlS amyE::*P_{hag}*-hag*^{T209C} *spec ΔcwlO::kan*	This study
AA101	*trpC2 dacA'* P_{xyl}*-dacA::cat*	This study
AA102	*trpC2 ΔlytF ΔlytE dacA'* P_{xyl}*-dacA::cat*	This study
BKK14470	*trpC2 ΔmreBH::kan*	(204)
AK045B	*trpC2 Δmbl::zeo*	(206)
3725CA	*trpC2 ΔmreB::neo*	(207)
AA103	*trpC2 Δmbl::zeo ΔdacA::ery*	This study
AA104	*trpC2 Δmbl::zeo dacA'* P_{xyl}*-dacA::cats*	This study
AA105	*trpC2 ΔmreB::neomycin ΔdacA::ery*	This study
AA106	*trpC2 ΔmreB::neomycin dacA'* P_{xyl}*-dacA::cats*	This study
AA107	*trpC2 ΔmreBH::kan ΔdacA::ery*	This study
AA108	*trpC2 ΔmreBH::kan dacA'* P_{xyl}*-dacA::cats*	This study
AA109	*trpC2 ΔcwlS ΔcwlQ::kan*	This study
AA110	*trpC2 ΔcwlS ΔcwlQ*	This study
AA111	*trpC2 ΔcwlS ΔcwlQ amyE* P_{hag}*-hag*^{T209C} *spec*	This study
PDC484	*ΔftsEX::neo::spec*	(11)
PDC4501	*ΔftsX::neo*	(11)
PDC4503	*ΔftsE::neo*	(11)
AA112	*trpC2 ΔftsEX::spec ΔdacA::ery*	This study
AA113	*trpC2 ΔftsX::neomycin ΔdacA::ery*	This study

AA114	*trpC2 ΔftsE::neomycin ΔdacA::ery*	This study
AA115	*trpC2 ΔcwlQ amyE::*P_{hag}*-hag*^{T209C} *spec ΔdacA::ery*	This study
AA116	*trpC2 ΔdacA::ery amyE::*P_{hag}*-hag*^{T209C} *spec*	This study
AA117	*trpC2 ΔcwlS ΔcwlQ amyE::*P_{hag}*-hag*^{T209C} *spec ΔdacA::ery*	This study
AA118	*trpC2 ΔlytF ΔcwlO::kan*	This study
AA119	*ΔdacA::ery ΔcwlO::kan*	This study
AA120	*trpC2 amyE::*P_{xyl}*-dacA::spec*	This study
AA121	*trpC2 amyE::*P_{xyl}*-dacB::spec*	This study
AA122	*trpC2 amyE::*P_{xyl}*-dacC::spec*	This study
AA123	*trpC2 amyE::*P_{xyl}*-dacF::spec*	This study
AA124	*trpC2 ΔlytF ΔlytE ΔdacA::ery amyE::*P_{xyl}*-dacB::spec*	This study
AA125	*trpC2 ΔlytF ΔlytE ΔdacA::ery amyE::*P_{xyl}*-dacC::spec*	This study
AA126	*trpC2 ΔlytF ΔlytE ΔdacA::ery amyE::*P_{xyl}*-dacF::spec*	This study
AA127	*trpC2 ΔdacA::ery amyE::*P_{xyl}*-dacB::spec*	This study
AA128	*trpC2 ΔdacA::ery amyE::*P_{xyl}*-dacC::spec*	This study
AA129	*trpC2 ΔdacA::ery amyE::*P_{xyl}*-dacF::spec*	This study
PDC639	*ΔcwlQ::spec aprE::*P_{xyl}*-cwlO::ery*	(11)
AA131	*trpC2 ΔlytF ΔlytE ΔdacA::ery amyE::*P_{xyl}*-dacA::spec*	This study
AA132	*trpC2 ΔdacA::ery amyE::*P_{xyl}*-dacA::spec*	This study
Crw369	*trpC2 amyE::*P_{xyl}*-walp23-gfp-spec*	
AA136	*trpC2 ΔcwlS amyE::*P_{hag}*-hag*^{T209C} *spec aprE::*P_{xyl}*-cwlO::ery*	This study
AA137	*trpC2 ΔcwlQ amyE::*P_{hag}*-hag*^{T209C} *spec aprE::*P_{xyl} *-cwlO::ery*	This study
AA138	*trpC2 ΔcwlS amyE* P_{hag}*-hag*^{T209C} *spec aprE::*P_{xyl}*-cwlO::ery ΔcwlO::kan*	This study
AA139	*trpC2 ΔcwlQ amyE* P_{hag}*-hag*^{T209C} *spec aprE::*P_{xyl}*-cwlO::ery ΔcwlO::kan*	This study
AA140	*trpC2 ΔcwlS amyE::*$P_{fla/che}$*-fliM-gfp spec thrC::*$P_{fla/che}$*-flgE*^{T123C}*::ery*	This study
AA141	*trpC2 ΔcwlQ amyE::*$P_{fla/che}$*-fliM-gfp spec thrC::*$P_{fla/che}$*-flgE*^{T123C}*::ery*	This study
AA142	*trpC2 ΔcwlS amyE::*$P_{fla/che}$*-fliM-gfp spec thrC::*$P_{fla/che}$*-flgE*^{T123C} *::ery ΔcwlO::kan*	This study
AA143	*trpC2 ΔcwlQ amyE::*$P_{fla/che}$*-fliM-gfp spec thrC*::$P_{fla/che}$*-flgE*^{T123C}*::ery ΔcwlO::kan*	This study
AA144	*trpC2 amyE::*P_{xyl}*-walp23-gfp-spec thrC*::$P_{fla/che}$*-flgE*^{T123C}*::ery*	This study

Table 2.2 Primers used in this study

Name	Sequence	Amplified gene	Restriction site
oAA001	5' GTTCCGGACGAGGG '3 5' CACAGACTGTCGCTGC '3	*lytC*	NA
oAA002	5' GCAGGCGCGACTTTAG '3 5' CTGTTGCAAATGGCCC '3	*lytD*	NA
oAA003	5' GCGGCTGTTGATCATG '3 5' CGGAAATCGCGTCAC '3	*lytE*	NA
oAA004	5' GCCGTCTGCGTCAGTAAAG '3 5' CTGGCTGCAGAGCGTC '3	*lytF*	NA
oAA005	5' GGCGAAGTGTTTACAGGG '3 5' CATGCTTGCAGCGGGAAC '3	*lytG*	NA
oAA006	5' GCACCTGCAGCAATGATG '3 5' CGGCTGCTGACGTTTC '3	*cwlO*	NA
oAA007	5' GCTGGCTGATACGAATG '3 5' CCGCGTCACTTTGTTCCAC '3	*fliM*	NA
oAA008	5' GTCGACGAACAACAGCAG' 3 5' CATTCGTATCAGCCAGC' 3	*flgE*	NA
oAA009	5' GGCTTATATCAGGGCGAG' 3	*flgB*	NA
oAA010	5'GTGCAACTTACTTACAATATGTCTAGAGGCTTATATCAGGG CGAG' 3	*flgB*	Overlapping sequence (flagellar induction)
oAA011	5'CTCACATTTGTGCCACCCCTAGGCTCGCCCTGATATAAGCC' 3	*codY*	overlapping sequence (flagellar induction)
oAA012	5' GGACACAGATAATATCGGTG' 3	*codY*	NA
oAA013	5' GCACAAGGACGTGCC' 3 5' GTGACAGGATGAGGAATG' 3	*hag*	NA
oAA014	5' CCCATATCGAGCGGAGCATC' 3 5' GCGGAACGAAGGGCTAAGAG' 3	*lacA*	NA
oAA015	5' GCCATCCGCATGACG' 3 5' CCATGATGACGCCGCC' 3	*dacA*	NA
oAA016	5' GGATGGCCGTGTTCCTCAG '3 5' CCCTGTGAAGGACCAGC '3	*cwlQ*	NA
oAA017	5'AGGAGGTCGACTACGGAGGTGAGGAAAATGTCAGG'3 5'CTCCTGGTACCTGAGATAATCTATTATTCTCCATCTTG'3	*FliM*	*Sal*I-*FliM* *FliM -Kpn*I (Halo-tag)
oAA018	5'AGGAGGCATGCTTGCTGACCGTGTCGGCATTACCC'3 5'CTCCTGTCGACTCAGTTTTTTTCACCCTCAATATCCT'3	$P_{fla/ch}$	*sph*I-$P_{fla/ch}$ $P_{fla\text{-}ch}$- *sal*I (Halo-tag)
oAA019	5'GTGACATTTGCATGCTTCAAAG 5'CGATGGGATGTCACGC	Halo-tag	NA
oAA020	5'GGCGCAAACCTCTTCAGG 5'CCGTAGCCATCGTGTTCA	*pgdS*	NA

oAA021	5'GGACGCAGGCTGTTTGCGG 5'CCGATGGGAGGCGACC	*cwlS*	NA
oAA023	5'GGGCTTGCCATCCCTG'3 5'CCATGTCCCACCCCTCC'3	*ldcB*	NA
oAA024	5'CGCTAATCTTGTCATGGAGGATATG'3 5'GAAATACTCCCGTCGTATCGC'3	*mreB*	NA
oAA025	5'GGGCGGCTCAAGCGGCCGG'3 5'CTGCAGCGAGCCTCG'3	*sigD*	NA
oAA026	5'GCATATGCCCGGATGAG'3 5'CAAGCTCCCGATCGC'3	*tagO*	NA
oAA027	5'GGTCATCTTCTGTCTGCG'3 5'CTGCAAGGCTTGCCAGTC'3	*flgM*	NA
oAA028	5'AGGATGGGTACCCTGCAGATGAAGAAAATGAAATACGGAG GTCG'3 5'TAATTCGCGGCCGCTCTAGAACCCCTAACATCCATCAGAGC '3	*dacA*	*Knp*I- *dacA* *dacA- Eag*I (Cloning)
oAA029	5'AGGATGGGTACCCTGCATTGTACAAACCACCACAAGG'3 5'TAATTCGCGGCCGCTCTAGAACGCACATCGCAAAAACGAG'3	*dacB*	*Knp*I- *dacB* *dacB- Eag*I (Cloning)
oAA030	5'AGGATGGGTACCCTGCAGATGAAGCGCAGAGAGGCGGGGAA'3 5'TAATTCGCGGCCGCTCTAGAACCGACAAAGCGTTATTACAG'3	*dacC*	*Knp*I- *dacC* *dacC- Eag*I (Cloning)
oAA031	5'AGGATGGGTACCCTGCAGGATTATGAAATGGAGGGCTTTTG'3 5'TAATTCGCGGCCGCTCTAGAACCCGTGACAAAACTAGTGGTC'3	*dacF*	*Kpn*I- *dacF* *dacF- Eag*I (Cloning)

Table 2.3 Plasmids used in this study

Plasmid	Genotype	Function	Reference
pDR244	Cre/*lox* recombination *spec amp*	Markerless	(204)
pKB142	*lacA::*P_{hag}*-hag*^{T209C} *ery amp*	Hag Cysteine labeled	(182)
pSG68	*thrC::*$P_{fla/che}$*-flgE*^{T123C} ery *amp*	FlgE cysteine labeled	(182)
pRD96	*lacZ::*P_{xyl} *cat amp*		Laboratory collection
pSG441	*lacI::*P_{spac} *kan amp*		Laboratory collection
pLOSS	P_{spac} *lacZ pLOSS-lytE amp spec*	LytE Complementary	Laboratory collection
pAK12	*amyE'* P_{xyl} *-linker-halo- spec amp*	Halo-tag	(208)
pAA001	*amyE'* $P_{fla/che}$ *fliM-linker-halo- spec amp*	FliM label	pAK12
pSG1729	*amyE::*P_{xyl}*-gfp-spec amp*	GFP detection	(209)
pAA002	*amyE::*P_{xyl}*-dacA-spec amp*	DacA Complementary	pSG1729
pAA003	*amyE::*P_{xyl}*-dacB-spec amp*	DacB expression	pSG1729
pAA004	*amyE::*P_{xy}*-dacC-spec amp*	DacC expression	pSG1729
pAA005	*amyE::*P_{xyl}*-dacF-spec amp*	DacF expression	pSG1729

2.2 Culture and growth conditions

All bacteria strains were grown at 30 °C in nutrient agar plates (NA) (Oxoid) or otherwise tested on defined medium plates if needed. Strains were grown at 30 or 37 °C in Luria- Bertani (LB), Nutrient Broth (NB), or defined mediums when needed with continuous shaking (horizontally or orbital). Overnight *E. coli* or *B. subtilis* cultures were cultivated in test tubes with a volume of 5 millilitres (mL). However, for experimental purposes, cultures were grown in 125 mL Erlenmeyer flasks, with the culture volume being approximately 15-20% of the flask capacity. Antibiotics were added when required at the following concentrations: 5 μg/mL chloramphenicol, 60 μg/mL spectinomycin, 1 μg/mL erythromycin, 5 μg/mL kanamycin, and 10 μg/mL zeocin. Nutrient agar or LB medium with 100 μg/mL ampicillin was used for growing *E. coli* stains. Supplements were added when required to the culture medium as the following concentrations: 1 mM Isopropyl-β-D-thiogalactopyranoside (IPTG), 2 ml xylose (25%, w/v), 100 μg/mL X-Gal, and 25 mM magnesium sulfate ($MgSO_4$).

2.2.1 Cell wall labeling medium (minimal medium)

Cell wall labeling medium (WLM) was used by maxing 100 mL of SMM with: 2 mL Casamino acids (20%, w/v), 2 mL glucose (40%, w/v), 1 ml Tryptophan (2 mg/mL), 0.5 mL $MgSO_4$ (1 M), 0.5 mL $CaCl_2$ (100 mM), and 0.01 mL $MnSO_4$.

2.2.2 Pre-transformation medium (semi-defined medium)

Pre-transformation medium (PTM) was used by mixing 10 mL of SMM with: 250 μL glucose (40%, w/v), 200 μL Casamino acids (20%, w/v), 100 μL Tryptophan (2 mg/mL), and 100 μL of the previously prepared mixture of (25 mL $MgSO_4$, 5 mL $CaCl_2$, 100 μL $MnSO_4$, and 70 mL H_2O MilliQ).

2.2.3 Competence medium

Competence medium was prepared by mixing 10 mL of SMM with: 125 μL of glucose (40%, w/v), 100 μL Tryptophan (2 mg/mL), 60 μL $MgSO_4$ (1 M), 10 μL Casamino acids (20%, w/v), and 5 μL Fe-NH_4-citrate (0.22%, w/v).

2.2.4 Starvation medium

Starvation medium was prepared by mixing 10 mL of SMM with: 125 μL of glucose (40%, w/v) and 60 μL $MgSO_4$ (1 M).

2.2.5 Swarm and swim agar plates (soft agar)

Swarm and swim agar plates were freshly prepared by adding 0.5% and 0.15% (w/v) Bacteriological agar no 1 (Oxoid) to 100 mL PTM, respectively. After setting, the plates were dried for 20 min in a hood before inoculating them with tested strains.

2.2.6 β-lactam antibiotic plates

Concentrations of β-lactam antibiotics were used as 0.04 μg/mL Oxacillin, 0.002 μg/mL Cephalexin, 0.005 μL/mL Penicillin G, 0.002 μL/mL Meropenem, and 1 μg/mL Moxalactam. Plates were papered by pouring 100 mL NA with the desired β-lactam antibiotic in a square plate a day before the experiment. The plates were then left to dry for an hour before inoculating them with diluted cultures. Cultures are prepared by inoculating 5 mL NB with a single colony of the desired strain and incubated at 30 °C overnight, shaking. The next day, the overnight cultures were diluted in 1/100 NB and incubated at 37 °C, shaking until they reached the exponential phase (3:30-4 hours). Then, the samples were normalized at OD600 nm~0.3, and 1/5 dilution series were prepared before inoculating the prepared plates with 5 μL of each diluted culture. Once all the strains were added to the plate, allowing the 5 μL drops to be fully absorbed, the plates were incubated at 37 °C and then scanned by an Epson scanner in 24 hours of incubation. The plates were also monitored for 72 hours.

2.3 Growth curve determination

A strain culture of *B. subtilis* was prepared by inoculating 5 mL NB, LB, or defend medium with a single colony, and 25 mM $MgSO_4$ was added to the culture medium when needed. The culture was incubated overnight at 30 °C and diluted back the following day in 5 mL fresh medium (OD600 nm~0.05) with the addition of 25 mM $MgSO_4$ if required. The diluted culture was incubated at 37 °C (shaker), and the samples were collected every 30-60 minutes, depending on

the experiment condition, for 4-5 hours. Optical density (OD) was monitored by a spectrophotometer (Thermofisher Genesys 20) at 600 nm. Each time point was plotted later in a graph to indicate the bacterial stages of growth: lag, exponential, stationary phases, and decline phases. A spectrometer was set to zero (blanked) by a sterile medium, and then a 1 mL volume or a 10-fold dilution of culture was measured for a correct reading. Most samples were experimentally tested at the time of the exponential phase, where bacterial populations were growing uniformly.

2.4 Fluorescent D-amino acid labeling

Fluorescent D-amino acids (FDAAs) were used to label peptidoglycan in live bacteria. HADA (HCC-amino-D-alanine) that is emitting light in blue (excitation/emission λ ~405/450 nm), and RADA, a red TAMRA-based fluorescent D-amino acid (excitation/emission λ ~554/580 nm), were used at concentrations of 20 μM, 16 μM, 12 μM, and 9 μM. For cell wall labeling, a *dacA* background was used as the wild type to enable efficient labeling of nascent peptidoglycan.

2.5 Fixation

100 μl of prepared culture was spun down and suspended in 100 μl fixation solution, which is a mix of 0.42 mL 16% (w/v) paraformaldehyde with 2.08 mL PBS. The samples were then put on ice for 1 hour and left at 4 °C for further use. An alternative method for cell fixation, 500 μl of the cell culture was spun down and fixed by treating it with 70% (v/v) ice-cold ethanol, followed by incubating it in an ice bath for 1 h and stored in 4 °C. For microscopy imaging, 20 μL of the fixed cells were washed twice with 4 °C 1x PBS via centrifuge at 13,300 x *g* for 3 min. Then, 1 μL was mounted on a 1.2% (w/v) agarose pad to permit visualisation (Sections 2.18 and 2.19). All ethanol-fixed cells were imaged no more than three hours after mounting.

2.6 DNA methods

2.6.1 Purified and quick Chromosomal DNA extraction

To extract purified genomic DNA, 5 mL LB was inoculated by bacterial cells and left to grow for 3-4 hours at 37 °C, shaking. Then, 2 mL of the growing culture was centrifuged for 2 min at

13,300 x *g*, and the supernatant was discarded as much as possible. The cell pellets were suspended in 60 µL EDTA (50 mM) and lysed by adding 6 µl lysozyme (10 mg/mL) for 20 min at 37 °C. Then, 600 µl nuclei lysis solution (Promega) was added and mixed gently before incubating for 5 minutes at 80 °C, followed by 2 minutes of incubation on ice. 200 µL protein precipitation solution (Promega) was added to the mixture, followed by 20-seconds vortex. The sample was centrifuged for 10 minutes at 13,300 x *g*, and the supernatant was transferred to a clean Eppendorf tube and mixed with 600 µl isopropanol (99.99%). The mixture was centrifuged for 6 minutes at 13,300 x *g*, the supernatant was discarded, and then 600 µl ethanol (70%, v/v) was added to the sample, followed by centrifugation for 3 minutes at 13,300 x *g*. The supernatant was carefully poured off the Eppendorf tube. The inverted tube was blotted off onto a tissue and air-dried for 10 minutes. The purified DNA was suspended in 100 µl H_2O MilliQ and stored at -20 °C as a stock for further use.

For a quick prep genomic DNA, 5 mL LB was inoculated by a single colony of bacterial cells and incubated for 3-4 hours at 37 °C, shaking. The growing culture was then centrifuged for 5 min at 9000 x *g*, and the supernatant was discarded. The cells pellets were suspended in 1 mL SSC (1 L H_2O MilliQ, 0.15 M Sodium chloride, and 0.01 M Sodium tri-citrate at pH 7.0) and lysed by adding 20 µl lysozyme (10 mg/mL) for 20 min at 37 °C. Then, 500 µL NaCl (4 M) was added, followed by a filter sterilization to the mixture using a 0.45 µM syringe filter into a sterile Eppendorf tube. The quick prep genomic DNA was stored at -20 °C for further usage.

2.6.2 Polymerase chain reaction (PCR)

Polymerase chain reaction (PCR) is prepared to amplify a specific fragment located at a genome DNA or a plasmid to confirm gene deletion, modification, or cloning purposes.

PCR reactions were prepared utilising a Q5 High-fidelity DNA Polymerase kit (NEB, UK) or a GoTaq DNA Polymerase kit (Promega, UK).

Colony PCR was done using a GoTaq® DNA polymerase (Promega) following the manufacturer's instructions. For *B. subtilis*, a single colony was suspended in 300 µl 50% (v/v) Dimethyl sulfoxide (DMSO) and heated at 65 °C for 20 minutes before applying 1 µl to the reaction mix.

DNA purification (clean-up) was processed as needed utilising a QIAquick PCR Purification kit or a QIAquick Gel Extraction kit (Qiagen, Germany).

2.6.3 Agarose gel electrophoresis

PCR fragments or digested plasmids were loaded into 1% (w/v) agarose gel made of agarose with 1x Tris-Acetate-EDTA (TAE) buffer (2 M Tris/HCL pH 8.3, 50 mM sodium acetate, 5.7% (w/v) acetate). A final concentration of 0.12 μg/mL Nancy-520 DNA gel stain was added into the cooled-down agarose gel for DNA detection and quantification. Then, the loaded agarose gel ran for an hour with a constant voltage of 100 V, where then a fluorescent image of the gel was taken by a UV transilluminator with a Lumenera USB 2.0 camera to confirm the fragment size by comparison to a 1 kb DNA ladder.

2.6.4 DNA restriction and ligation

Restriction enzymes from New England or Promega were used as directed by the manufacturer's instructions. The sample was prepared utilising the desired digested enzyme with its recommended buffer added to a template. The mixture was then incubated at 37 °C for 3 hours or O/N, followed by enzyme inactivation.

The compatible ends of DNA fragments were ligated by T4 DNA ligase with a ligase buffer and then incubated at 4 °C overnight, or NEBuilder HiFi DNA assembly was used according to the manufacturer's instructions. After the ligation, plasmid or fragments were transformed into *E. coli* or *B. subtilis* as required.

2.6.4 DNA sequencing and analysis

Genomic DNA extractions were isolated by a GenElute ™ Bacterial Genomic DNA Kit (Sigma-Aldrich/MeRCK). The absorbance ratio (260 nm-280 nm) was checked by NanoDrop™ spectrophotometer (Thermo Fisher Scientific), and it was close to ~1.8. The concentration was measured by Qubit Fluorometric Quantification (Thermo Fisher Scientific) following the instructions of optimised Qubit Assay. The chromosomal DNA concentrations were somewhere between 3.5-16.5 ng/μL in MilliQ H_2O. The whole genomic DNAs were sequence analysed by

MiSeq System-Illumina sequencing platform (NU-OMICS, Northumbria University), and the results were analysed compared to the reference genome sequence of *Bacillus subtilis* 168 (AL009126.3) using a CLC genomics Workbench (Qiagen Bioinformatics).

Plasmids or PCR products were sequenced using Sanger sequencing at the MRC PPU unit, DNA Sequencing and Services, at Dundee University (www.dnaseq.co.uk). The sequencing results were then analysed and compared to a reference DNA using Clone Manager or SnapGene softwares.

2.7 Transformation

2.7.1 *Bacillus subtilis*

The chromosomal DNA of all single mutant strains utilised in this study were transformed into 168CA using the method of Anagnostopoulos and Spizizen (210) as modified by (210, 211). To prepare a competent culture, cells were freshly streaked on an NA plate and incubated overnight at 30 °C. The following day, a touch of the growing cells was inoculated into 10 mL of competence medium (see Section 2.2.3) and incubated at 37 °C with vigorous shaking overnight. The next morning, 0.6-1 mL of the overnight culture was diluted into 10 mL of fresh competence medium and grown for 3 hours. Then, 10 mL of starvation medium (see Section 2.2.4) was added, and the culture was incubated for an additional 2 hours with shaking.

The transformation was performed by mixing 2-3 µL of DNA (10-100 ng/µL) (see Section 2.6.1) with 300 µL of the prepared competent culture and incubating for 1 hour at 37 °C with shaking. After 1 hour of incubation, 100 µL of the transformation culture was plated on a selective medium. Sterilized glass plating beads were used to spread the bacterial culture evenly over the plates. For control plates, 10 µL of the genomic DNA was tested on the selective medium plate to detect sporulation, and 100 µL of the competent culture was plated on the same selective medium to test resistance before the transformation.

2.7.2 *Escherichia coli*

All plasmids were transformed to *E. coli* (DH5α) by chemically competent cells using the method of Hanahan (212), and heat shock transformations were performed using the methods

described by Bergmans (213). Then, the plasmids were extracted by a Qiagen Miniprep kit when needed, following the manufacturer's instructions.

2.8 Strain manipulation

2.8.1 Construction of isogenic autolytic mutant strains

Initial strains with a defined null mutation in an autolytic gene were constructed as kanamycin resistance cassette replacements of the coding sequence of the gene derived from the Koo collection (204). To ensure characterisation was done with isogenic strains, the chromosomal DNA of all single mutant strains was transformed into 168CA using the method of Anagnostopoulos and Spizizen (210) as modified by Hamoen (211). The initial approach was to use these antibiotic cassette deletions and generate marker-less deletions by Cre/lox recombinase (expressed from a temperature-sensitive plasmid, pDR244) and then introduce another autolytic gene deletion utilising the same transformation method and build strains with multiple mutations in autolytic genes.

After transforming pDR244 (see Section 2.7.1 for plasmid extraction) into a *B. subtilis* strain (see Section 2.7.1 for *B. subtilis* transformation), the temperature-sensitive plasmid pDR244 was eliminated by streaking transformants from an overnight plate onto one side of a fresh NA plate and incubating at 45 °C for 3 hours. This higher temperature promotes the loss of the plasmid. After this incubation period, the growing side of the plate was streaked across the entire surface to isolate single colonies, and the plate was then incubated overnight at 45 °C. The following day, individual colonies were screened by streaking onto kanamycin, spectinomycin, and ampicillin plates. Colonies that grew only on the NA plate but not on the antibiotic plates indicate successful loss of the plasmid, confirming that the generated strain is now marker-less. The marker-less strains were subsequently confirmed by PCR.

2.9 Plasmid construction

2.9.1 Construction of strains expressing labeled flagella subunits

To construct strains that permit monitoring the flagellar subunits, we obtained strains DS8521 (Δ*fliM: amyE::*$P_{fla/che}$*-fliM-gfp spec*), DS1916 (*amyE::*P_{hag}*-hag*^{T209C} *spec*) and DS7673 (Δ*flgE*

amyE::$P_{fla/che}$-$flgE^{T123C}$ *cat*) from Kearns (182). These flagellar strains were transferred to 168CA and other backgrounds as appropriate to permit the visualisation of the assembly of the basal body of the flagellum (FliM-GFP), the hook (FlgE) and the assembly of the flagellum (Hag) in single cells. Details of how individual strains were constructed are provided in Table 2.1.

2.9.2 Xylose and IPTG inducible flagella expression constructs

To generate an inducible *fla/che* operon, two constructions were generated using different promoters: a P_{xyl} promoter linked to a chloramphenicol cassette (isolated from pRD96 utilising *Bam*IH and *Xba*I restriction enzymes) or a P_{spac} linked with both a constitutively expressed *lacI* gene and a kanamycin resistance cassette (liberated from pSG441by *Bgl*II and *Xba*I digestion). These promoters containing the fragments were then linked to a PCR-amplified DNA fragment corresponding to a *codY* gene (the gene upstream of the *fla* operon) and a fragment corresponding to a *flgB* gene (the first gene of the *fla* operon) by ligation. The fused fragments were then transformed into 168CA, selecting the appropriate resistance marker. The transformants obtained were then checked by PCR and sequencing to confirm the correct insertion of the construction into the genome. Phenotypically, it was also confirmed that the insertion resulted in xylose or IPTG-dependent motility in rich media (AA035 and AA036). The xylose inducible promoter (P_{xyl}) is a high expression promoter, but it is leaky. While the IPTG inducible promoter (P_{spac}) is tightly regulated, it is not a strong promoter.

2.9.3 Xylose inducible DD-carboxypeptidase gene expression constructs

To generate inducible DAC protein (for DacA, DacB, DacC, or DacF) constructs, the coding sequences were cloned into pSG1729. This plasmid contained the upstream and downstream of *amyE* loci linked to a P_{xyl} promoter, *gfp* sequence, and spectinomycin cassette (Table 2.2). The GFP coding sequence was replaced with one of the *dac* genes (*dacA, dacB, dacC*, or *dacF*). For this, the plasmid was digested utilising *Kpn*I and *Eag*I restriction enzymes that cut before and after the *gfp* sequence. The *dac* genes were amplified utilising the appropriate DAC primer pairs containing *Kpn*I and *Eag*I tails (Table 2.3). The digested plasmid was then ligated to each PCR amplified DNA fragment corresponding to the *dac* genes by overlapping PCR utilising the HIFI method, resulting in the generation of pAA001, pAA002, and pAA004 plasmids. These

constructed plasmids were then transformed into *E. coli* (DH5α) cells, selecting for the appropriate resistance marker, ampicillin. The obtained plasmids were verified by PCR and sequencing to confirm the correct insertion of the desired constructs (see Section 2.6.5). Subsequently, the plasmids were transformed into *B. subtilis* strains. Then, the presence of DAC proteins was assessed using SDS PAGE utilising Bocillin fluorescent labeling of cells growing in the presence or absence of xylose.

2.10 β-galactosidase assay (Transcriptional regulation of flagellum subunits)

To detect SigD activity in strains lacking CwlO and CwlQ or CwlS in either *sigD* or *flgM* backgrounds, using the integrational plasmid *lac* reporter, 5 mL LB tubes were inoculated and incubated at 37 °C overnight. The growing cultures were then diluted back in 20 mL PTM (OD600 nm ~0.05). 200 µL of the samples were collected at this time point and every 20 mins for 2 hours, frozen in liquid nitrogen, and stored at -80 °C for β-galactosidase assay. For the β-galactosidase assay, the 200 µL samples were defrosted in a 30 °C water bath and lysed by 400 µL lysis solution (200 µg/mL lysozyme, 100 µg/mL DNase, 1.25% (w/v) Triton-X100) for approximately 10 minutes. Then, the reaction was started in 10-second intervals from sample to sample by adding 200 µL substrate solution (4 mg/mL 2-Nitrophenyl β-D-galactopyranoside (ONPG-Sigma), mixed, and returned to the water bath. The reaction was stopped by adding 400 µL Na_2CO_3 (1M), and that was when the samples started to turn yellow or if the reaction exceeded 3 hours.

To calculate β-galactosidase activity, the equation of specific β-galactosidase activity = (A420 x V1)/(V2 x OD600 nm x T x 0.00486) was used. Here, A420 represents the blank (water) absorbance, V1 is the volume of the reaction mixture, V2 is the volume of the culture used for lysis, OD600 is the optical density at 600 nm, and T is the reaction time in minutes. The molar extinction coefficient of ONP is 4860 at pH 10.

A sample of sterile medium mixed with assay reagents was incubated for the maximum time and was used to provide a background value that was subtracted from all assay readings, thus obtaining the correct absorption value of the samples. The calculated β-galactosidase activity was expressed in nmoles 2-nirophenyl (ONP). min^{-1}. $OD600^{-1}$.

Miller Units = (A420 x 6 x 1000) / (t_{ONPG} reaction time x OD600 nm)

2.11 Cell wall preparation for muropeptide analysis

The method of Atrih (60), modified by Bisicchia (214), was used for cell wall purification. Overnight cultures of *B. subtilis* were prepared by inculcating 50 mL of NB with a single colony and incubated at 30 °C. The following day, the cultures were diluted back to OD600 nm of 0.001 in 500 mL NB medium, with the addition of 25 mM $MgSO_4$ if required. The cultures were incubated with shaking at 37 °C until reaching an OD600 nm of 0.5- 0.6 and then cooled down in an ice bath to 4 °C. The samples were centrifuged at 4 °C 7500 x *g* for 15 min using pre-cooled centrifuge tubes. The resulting pellet was suspended in 15 mL ice-cold Tris/HCL (50 mM, pH 7.0). The cell suspensions were dropped into 60 mL of hot SDS (5%, w/v), boiled for 30 min, and then left to cool down at room temperature. The next day, the lysate was transferred into 50 mL round bottom tubes (Nalgene ™ PPCO) and centrifuged at 250000 x *g* (JA25-50) for 30 min at room temperature until the supernatant was clear. The supernatant was discarded, and the pellet was suspended in 20 mL NaCl (1M), vortex with a glass stick, and centrifuged again, as above twice. Then, the pellet was washed 4-5 times with H_2O MilliQ (suspend, vortexed with glass stick, and centrifuged at 250000 x *g* (JA25-50) for 30 min at room temperature) until the suspension was free of SDS (no foam). The pellet was suspended in 2 mL H_2O MilliQ, and the tube was rinsed with another 2 mL H_2O MilliQ to ensure nothing was left. The suspension was then transferred into a 2 mL screwcap tube that was filled to 1/3 with glass beads and pulsed using Precellys 24 lysis homogenizer with max speed (6500) for 30 seconds, which works for three pulses in one run. After 3 pulses, the tubes were cooled down on ice for 5 min until the machine could be used again; then, this step was repeated for 18 pulses altogether. The cell debris was filtered through a glass frit to remove the glass beads, and the beads were washed with 10-20 mL H_2O MilliQ. The filtrate was then transferred into 50 mL falcon tubes and centrifuged for 5 min 2000 x *g*. The supernatant was then transferred into a 50 mL round bottom tube (Nalgene ™ PPCO), and the remaining pellet was suspended in 25 mL H_2O MilliQ, centrifuged as above, and added to the tube. The supernatant containing broken cells was then centrifuged for 30 min 25.000 x *g* (JA25-50) at room temperature. The broken cell pellets were then suspended in 10 mL buffer (Tris/HCL (100 mM) pH 7.5, $MgSO_4$ (20 mM)) with the addition of 100 µL DNase (10 µg/mL, Sigma) and 100 µL RNase (50 µg/mL, Sigma). The suspension was stirred at 37 °C for 2 hours, to which 100 µL $CaCl_2$ (10 mM) and 100 µL Trypsin (100 µg/mL) from porcine pancreas (Novagen/Merck) were added. The suspension was

then stirred for another 18 hours at 37 °C. After this, H_2O MilliQ and 8% (w/v) SDS-solution were added to reach a final SDS concentration of 1% (v/v) and a final volume of 20-30 mL. The samples were then incubated for 15 min at 80 °C (water bath) and then left to cool down for 10-15 min before being centrifuged at 25000 x *g* for 30 min RT. The pellets were then suspended in 10 mL LiCl (8M), incubated for 15 min at 37 °C, and centrifuged as above. A white precipitate might form on top of the solution, which should be discarded with the supernatant. The pellets were then suspended in 10 mL EDTA (100 mM, pH 7.0), incubated for 15 min at 37 °C, and centrifuged as above. The pellets were washed twice (suspended and centrifuged) in 20-30 mL H_2O MilliQ. The final pellets were then suspended in 1-3 mL H_2O MilliQ and transferred in a suitable container (a snap cap glass vial, which was empty weighted before used), frozen at -80 °C for an hour, and finally lyophilized for two days via Alpha 1-2 freezer dryer (Biopharma). The dry-weight was determined and stored at -20 °C (This permitted an estimation of how much material was obtained and allowed for sample variation to be corrected for later use).

These processes of cell wall preparation can be stopped anytime, but the addition of 2 µL-3 µL/ 1 mL of 10% (w/v) sodium azide (NaN_3) to the sample is recommended for storage at 4 °C to prevent microbial contamination. The next day, the 10% (w/v) NaN_3 should be washed out using H_2O MilliQ and centrifugation.

2.11.1 Purification of murein by removing wall teichoic acid

5 mg cell wall of each strain was transferred to polyallomer tubes for 100.3 Rotor (desktop-UZ) dissolved in 2.7 mL Ice-cold hydrofluoric acid (HF). The tubes were closed with double Parafilm and stirred at 4 °C for 48 hours. After 28 hours, the parafilm was removed carefully, and the samples were centrifuged in pre-cooled Rotor TLA 100.3 centrifuged at 70000 rpm, 4 °C for 45 minutes. The supernatant (HF) was carefully transferred to an HF-waste bottle. The tube was filled up with ice-cold H_2O MilliQ and centrifuged as above; these steps were repeated twice. Then, the pellets were suspended in ice-cold Tris/HCL (100 mM, pH 7.0) and centrifuged as above. The samples were twice washed in H_2O MilliQ, suspended in 250 µL ice-cold H_2O MilliQ, and later transferred into a 2 mL screwcap tube. Also, the centrifuge tube was washed with another 250 µL ice-cold H_2O MilliQ and added to the screwcap tube. 1 µL NaN_3 (0.05%, v/v) was added to the samples and stored at 4 °C.

2.11.2 Isolating muropeptides from Murein (Cellosyl-digestion)

Purified murein samples were vortexed, and 180 µL was transferred into a 1.5 mL Eppendorf tube. 60 µL 4x Cellosyl buffer ((NaH_2PO_4 (80 mM, pH 4.8) with NaN_3) and 14 µL Cellosyl (0.7 mg/ml)) were added into the murein. The samples were incubated with low shaking (850 rpm) at 37 °C overnight. The next day, another 14 µL Cellosyl was added and incubated with shaking for another night at 37 °C. The following day, the samples boiled at 100 °C for 10 min, left to cool at room temperature, and centrifuge for 10 min high speed (14,000 rpm). The supernatant was then transferred to a new 1.5 mL Eppendorf tube and stored at -20 °C. The supernatant was recovered, and the volume was reduced to 50-100 µL in a pre-chilled speed Vac at 100 °C. Where then 100 µL of Sodium borate (0.5 M, pH 9.0) and 1 mg of solid sodium borohydride were added to the samples (foaming can occur, so pierce a hole on the top of the Eppendorf to release the H_2 gas produced during the reduction step). The samples were then incubated for 30 min at room temperature with centrifugation at 3000-4000 rpm (centrifugation prevents contents from spilling out if foaming occurs). The pH of samples was adjusted between pH 3.5 and pH 4.5 (best pH 4.0) using 20% (v/v) phosphoric acid. The samples were then centrifuged at 14,000 rpm and directly used for HPLC analysis or stored at -20 °C while covering the Eppendorf lid with parafilm to plug the hole.

2.11.3 Reverse-phase high-performance liquid chromatography (RP-HPLC)

Reverse-phase high-performance liquid chromatography (RP-HPLC) is a technique used to separate and analyse components within a liquid sample based on their hydrophobicity. The process involves injecting the sample into a column packed with hydrophobic porous particles, known as the "stationary phase." The sample components are then carried through the column by a liquid, referred to as the "mobile phase." The separation of these components occurs due to the differential interaction of each component with the stationary and mobile phases, based on their hydrophobic properties (214-216).

After preparing the *B. subtilis* PG samples, the analysis began with setting up the RP-HPLC system. The mobile phase buffers were prepared as follows: solvent A consisted of a 40 mM sodium phosphate buffer with 0.0003% (v/v) NaN_3, and solvent B consisted of a 40 mM sodium phosphate buffer with 20% (v/v) methanol, pH 4.5. These solvents are crucial for the

gradient elution process that separates the muropeptides based on their hydrophobicity (214). The RP-HPLC system used was an Agilent Technologies Series 1200, equipped with a reverse-phase column (Prontosil 120-3-C18-AQ 3 μM, Bischoff), was configured. The column was initially equilibrated with 100% solvent A to ensure a stable baseline and consistent reproducibility of results.

Solubilized muropeptide samples were placed in autosampler vials, and the autosampler injected 10 μL of each sample into the HPLC system. The system programmed to run a gradient elution, designed specifically for *B. subtilis* PG samples. A linear gradient was employed, transitioning from 100% solvent A to 100% solvent B over a period of 5 hours at 55°C. Inside the reverse column, the muropeptides interacted with the hydrophobic stationary phase. The gradient elution gradually changed the composition of the mobile phase, leading to the separation of the muropeptides based on their hydrophobicity. More hydrophobic compounds interacted more strongly with the stationary phase and eluted later, while less hydrophobic compounds eluted earlier. As the muropeptides eluted from the column, they passed through a UV detector set at 205 nm. The detector measured the absorbance of UV light by the muropeptides, generating a signal proportional to their concentration, allowing for qualitative and quantitative analysis.

2.11.4 Muropeptide analysis

Signals from the UV detector were processed using an HPLC data system to generate chromatograms, where each peak represented a different muropeptide. The peaks were identified and quantified based on their retention times using Radiochromatography software v4.1.7.70 (Laura, LabLogic Systems Ltd). The UV signal integration in the chromatograms determined the total peak area. To assess the relative concentrations of muropeptides in different sacculi preparations, a comparison was made by analysing the total peak area from the UV signal integration in the HPLC chromatograms and comparing the results with reference chromatograms from previous studies (60, 217).

2.12 Cell wall labeling and cell wall turnover

Culture of *B. subtilis* strains (e.g., a mutant *dacA* and 168CA) was prepared by inoculating cell wall labeling media (WLM) or LB with a single colony, and 25 mM $MgSO_4$ was added to the culture medium if required. The culture was incubated overnight at 30 °C and diluted back the following day in 20 mL of the same medium (OD600 nm ~0.05) with or without the addition of 25 mM $MgSO_4$ if required. The diluted culture was incubated at 37 °C with shaking until it reached the exponential phase (OD600 nm ~0.1), where then 20 μM FDAAs (HADA) were added. The sample was incubated at 37 °C for an hour. After that, the cells were centrifuged for 3 minutes at 13,300 x *g* and washed in WLM or LB (no FDAAs). The cell pellets were then suspended in 20 mL of WLM or LB and incubated at 37 °C. The samples were taken in 30-minute intervals for both measuring the optical density (OD) and cell fixation for later visualisation (Section 2.5).

For long-pulse labeling, exponential cells were diluted with fresh LB broth containing 20 μM FDAAs (RADA) and grown at 37 °C for 1 h. Then, the cells were spun down, washed with fresh media, and suspended in fresh medium with the second label, 20 μM HADA. The samples were collected at regular time points and fixed for further use.

2.13 Cell growth statistical analysis

Statistical analysis of cell growth was conducted by calculating the mean and standard deviation across three experimental replicates (a detailed procedure of cell growth curve determination can be found in Section 2.3). The average growth was plotted on growth curves, with the standard error of the mean (SEM = $\sigma/\sqrt{n}$) used to represent the variability among replicates, where σ is the standard deviation and n is the number of observations (three). This approach ensures that the data accurately reflect the differences in growth patterns between strains while accounting for experimental variability.

2.14 Flagellum assembly

2.14.1 Sample preparation for monitoring the flagellum assembly

Strain cultures of *B. subtilis* were prepared by inoculating LB with a single colony. The cultures were incubated overnight at 30 °C. The overnight cultures were then diluted back in 5 mL of LB (OD600 nm ~0.05) and incubated at 37 °C with shaking to reach OD600 nm ~1. Cells were then induced to be motile by shifting mediums from LB to pre-transformation medium (PTM). The samples were collected over a specific period of time to permit visualisation of the cells and to determine if the labeled flagellum subunits could be detected by fluorescence microscopy.

2.14.2 Flagella staining procedure

Hook (FlgE) and filament (Hag) structures were stained by either Alexa Fluor 594 C_5-maleimide dye (red) or Alexa Fluor 488 C_5-maleimide dye (green) utilising the method of Kearns (126).

2.15 Motility assays

Samples were prepared by inoculating LB with a single colony of *B. subtilis* strains and incubated overnight at 30 °C. The overnight cultures were then diluted back in 5 mL of LB (OD600 nm ~0.05) and incubated at 37 °C with shaking until reaching the exponential phase OD600 nm ~0.1. Freshly prepared swarm and swim agar plates were inoculated with 5 µl of the exponentially growing cultures. After inoculating the plates, they were left to dry for 20 minutes and then incubated at 37 °C for an appropriate period of time: 12h for swimming and 24 hours for swarming. Following the incubation period, the growth diameters of the tested strains were compared to positive and negative control strains to assess swarm and swim motilities.

Swimming and swarming motility were determined by measuring the growth diameters in millimeters (mm) across 5 repeated experiments (n). The mean and standard deviation (σ) of the strains were calculated, with the standard error of the mean $\sigma/\sqrt{n}$ used to represent variability. The growth diameters were compared relative to the wild type (168CA), providing insights into the comparative motility characteristics across different strains.

2.16 Protein separation and identification

2.16.1 Sodium dodecyl sulfate-polyacrylamide gel electrophoresis (SDS-PAGE)

SDS-PAGE was used to separate proteins depending on their molecular weight. To generate a sample, 5 mL LB was inoculated by a single colony and grown overnight at 30 °C with shaking. The next day, the overnight culture was diluted back into OD600 nm ~0.05 and incubated at 37 °C to reach OD600 nm ~1. Then, 1 mL of the culture was centrifuged, and the supernatant was discarded. The cell pellet was then frozen in liquid nitrogen for later use.

Cell pellets were suspended in 200 µl SDS-PAGE loading buffer (10 g SDS (10%, w/v), 25 mL Tris-HCL (0.125 M, pH 6.8), Bromophenol blue (0.01%, w/v), 40 mL glycerol (40%, w/v), and 25 mL H_2O MilliQ). The samples were then sonicated at 4 °C for 40 seconds using a needle probe and then heated for 4-8 minutes at 60-80 °C prior to loading onto a gel. The samples were loaded into a 4-12% gel (Invitrogen) and run in 20X MOPS SDS- running buffer at 180 constant voltages (V) for Western blot or 50 constant currents (Amp) for Bocillin detection. The amount of sample loaded was generally normalized at the time of loading by adjusting the loading volume according to the optical density of the culture at the time of sampling; where necessary, the effectiveness of this was checked by running an identically loaded gel, staining with Coomassie blue (Section 2.16.2), and checking the intensity of the stained bands (total protein) were similar for each sample.

2.16.2 Coomassie staining

Coomassie protein stain (Abcam, InstantBlue®) was used according to the manufacturer's instructions when needed for clear visualisation of protein bands using an Epson scanner.

2.16.3 Western blotting

To detect the presence or relative abundance of a protein of particular interest, a semi-wet Western blot analysis was used to separate proteins using an SDS-PAGE gel electrophoresis technique. For this, resolved proteins were transferred into a 0.45 µm PVDF membrane by a Turbo Biorad transfer machine and that by sandwiching the SDS-PAGE gel and an activated PVDF membrane between wet layers of filter paper (the wet filter papers being soaked in

transfer buffer made of (1 L of H_2O MilliQ mixed with 72.68 g Tris (300 mM), 45.04 g glycine (300 mM), 50.16 g Tricine (140 mM), 5 mL SDS (0.05%, w/v), and 5 mL EDTA (2.5 mM)). The PVDF membrane was activated by being immersed in methanol for 1 minute prior to assembly for the transferring step. This was then electro-transferred in the blotting machine according to the manufacturer's instructions. On completion, the PVDF membrane was incubated for 1 hour at room temperature in 40 ml blocking buffer (5 g milk (5%, w/v) mixed with 100 ml of PBS-T, which is made of 10 dissolved tablets of PBS in 1 L of H_2O MilliQ and 1 mL of Tween^{20} (0.1%, v/v). Then, the blocking buffer was removed and replaced with a primary antibody diluted in 20 mL PBS-T with 5% (w/v) milk (as described in Table 2.4), and the PVDF membrane left at 4 °C overnight. The following day, the membrane was washed by PBS-T for 4X 8 minutes on rocking and shaking before adding a secondary antibody diluted in 20 mL PBS-T with 5% (w/v) milk and left shaking at room temperature for an hour. Then, the washing steps were repeated as described previously. A mixture of 10 mL solution A and 250 µL solution B was prepared using a Pierce ECL Plus Western Blotting Substrate Kit (Thermo Scientific, Ref 32132). The mixture was poured above the membrane and incubated for 5 minutes. The membrane was then dried on white tissue to remove any remaining solution and placed inside a plastic sheet for visualisation. Detected bands were visualised by ImageQuant LAS 400 mini biomolecular imager (GE Healthcare).

Table 2.4 Primary and secondary antibodies used for Western blot assay

Expressed protein	Genotype	Primary antibody	Secondary antibody	Molecular wight
GFP	*amyE::*P_{xyl}*-gfp*	GFP antibody 1/10000 dilution	anti-rabbit 1/10000 dilution	27.00 kDa
DacA	*dacA'*P_{xyl}*-gfp-dacA*	GFP antibody 1/10000 dilution	anti-rabbit 1/10000 dilution	48.47 kDa
CwlO	*amyE::*P_{xyl}*-gfp-cwlO*	GFP antibody 1/10000 dilution	anti-rabbit 1/10000 dilution	50.87 kDa,
Flagellin (Hag)	Wild-type (168CA)	Hag antibody 1/10000 dilution	anti-rabbit 1/10000 dilution	32.47 kDa
PBP2B	Wild-type (168CA)	PBP2B antibody 1/10000 dilution	anti-rabbit 1/10000 dilution	79.12 kDa

2.17 Bocillin stain procedure to detect penicillin-binding proteins (DACs)

To detect penicillin-binding proteins (PBPs), Bocillin FL (Invitrogen) was used as a labeling reagent (218). For sample preparation, 5 mL LB was inoculated with a single colony of *B. subtilis* strains and grown at 37 °C overnight. The growing culture was diluted back in fresh LB (OD600 nm ~0.05) the next day and incubated until reaching (OD600 nm ~0.1). 1 mL of the culture was labeled by 2 µL Bocillin FL penicillin stain (Invitrogen) and left for 2 minutes, after which it was centrifuged for 3 minutes at 13,300 x *g*. The supernatant was discarded, and the cell pellets were thrown into liquid nitrogen and stored at -20 °C for further use. Later, the sample was sonicated as described previously and resolved via SDS-PAGE. The labeled penicillin-binding proteins were visualised via a Typhoon scanner - FITC channel (488 nm-blue) with an absorbance peak of 490 nm.

2.18 Slide preparation and microscopy imaging

2.18.1 Agarose pad immobilization of cells

Agarose pads were prepared to prevent cell movement and orientate them to have a long axis in the focal plane under a microscope. This simple pad of agarose was made by dissolving and heating 1.2 g of agarose powder in 10 mL H_2O MilliQ. Then, 600 µL of the molten agarose was placed on top of a glass slide between two coverslips, where then the molten agarose was squashed by another glass slide to have a smooth, flat surface. The agarose pads were left to set before applying 1 µL of culture on top, which was briefly left to soak into the pad and then covered by a coverslip. A drop of immersion oil was added to allow visualisation under the 100x objective of the microscope.

2.18.2 Time-lapse microscopy

Time-lapse microscopy slides were prepared utilising a GeneFrame (Thermofisher). 600 µL of molten 1.2% (w/v) agarose (agarose dissolving in competence medium) was set into GeneFrame and sandwiched between slides. The surface of the pad was allowed to air dry before adding 1 µL culture, followed by a coverslip and immersion oil, respectively. Images were acquired every 5 minutes or less as needed at one or multi-positions.

2.18.3 Membrane dye

Fluorescent membrane dyes FM5-95 or FM4-64 (Molecular Probes) were used when needed by mixing a 1 μl of membrane dye with 30 μl of culture. Then 1 μl of the mixture was applied to an agarose pad for visualisation.

2.19 Microscopy

2.19.1 Fluorescence Microscopy

Fluorescence microscopy was used with Nikon Eclipse Ti with a phase-contrast objective Nikon Plan Apo 100x/1.40 and a cool LED pE-300 white light source. HADA fluorescent signals were visualised using DAPI Filter Cube (EX350/50, DM400Ip, EM460/50). Alexa Fluor 594 C_5-maleimide fluorescent, RADA, FM5-95, and FM4-64 signals ware viewed using m-Cherry Flitter Cube (EX560/40, DM585Iprx, EM630/75). GFP and Alexa Fluor 488 C_5-maleimide fluorescent signals were viewed with GFP Filter Cube (EX470/40, DM495Iprx, EM525/50). Fluorescence microscopy was fitted with a Sony Cool-Snap HQ2 CCD camera (Roper Scientific).

2.19.2 Scanning Electron Microscopy (SEM)

A Tescan Vega LMU Scanning Electron Microscope (part of the EM Research Service facility of Newcastle University) was used to examine the cell service. Digital images were collected using Tescan-supplied software.

Cultures of *B. subtilis* were prepared by inoculating 5 mL LB with a single colony and incubating overnight (approximately 9 hours) at 30 °C. The overnight culture was then diluted back in 20 ml LB or pre-transformation medium (PTM) (OD_{600} nm~0.005) and incubated at 37 °C with shaking for an hour. A 500 μL sample was collected from both cultures and centrifuged for 3 minutes at 13,300 x *g*. The cell pellets were fixed in 500 μL 2% (v/v) Glutaraldehyde in Sorenson's Phosphate Buffer at 4 °C overnight. Dehydration and coating processes were done by EM technicians.

2.19.3 Transmission Electron Microscopy (TEM)

B. subtilis strain cultures were prepared by inoculating 5 mL of LB medium with a single colony and incubating overnight at 30 °C. If required, 25 mM $MgSO_4$ was added to the medium. The overnight cultures were then diluted in LB medium to an OD600 nm of 0.05 and incubated at 37 °C with shaking for 2 hours. Samples of 500 µl were collected and centrifuged at 13,300 x *g* for 3 minutes. The resulting cell pellets were fixed in 2% (v/v) Glutaraldehyde in Sorenson's Phosphate Buffer at 4 °C overnight. Subsequent steps, including dehydration, monitoring, sectioning, and coating, were performed by electron microscopy (EM) technicians. The sections were visualised on a Tescan Vega LMU Transmission Electron Microscope housed within EM Research Services, Newcastle University. Digital images were collected using a Tescan-supplied camera and software.

2.19.4 Structured Illumination Microscopy (SIM)

This imaging method employed the Nikon N-Sim/-Storm, equipped with Nikon intensilight light source, laser, and Andor iXon DU-897 camera.

2.20 Image analysis and processing

Microscopy images were acquired by Metamorph 7.10 Imaging Software (Universal imaging). The images were then processed and analysed via the program Fiji-ImageJ (https://fiji.sc).

2.20.1 Cell morphology measurement and statistical analysis

Strain cultures of *B. subtilis* were prepared by inoculating LB with a single colony (with 25 mM $MgSO_4$ as mutant required). The cultures were incubated overnight at 30 °C. The overnight cultures were then diluted back to OD600 nm ~0.05 in 5 mL of LB and incubated at 37°C with shaking to reach OD600 nm ~0.1 (exponential phase) and OD600 nm ~1.5 (late stationary phase). At regular time points, samples were visualised under a fluorescence microscope after being stained with a fluorescent membrane dye (Sections 2.15 and 2.16).

Cell measurements were conducted manually using the ObjectJ tool in the Fiji-ImageJ software, measuring the width and length of approximately 300 cells for each strain. The means,

standard deviations, and standard error of the mean of these measurements were calculated to summarize the data. To compare the cell widths and lengths between two strains, unpaired t-tests (two-tailed) with Welch's correlation were conducted. Additionally, one-way ANOVA followed by post hoc (Tukey's HSD) tests were performed to compare these dimensions among multiple strains. This approach ensures a comprehensive statistical analysis of cell size variations.

2.20.2 Fluorescence intensity measurements of the cell wall labeling

The fluorescence intensity of FAADs (HADA and RADA) was quantified using a macro language developed in ImageJ, specifically designed for use with FIJI (https://imagej.net/software/fiji/downloads). This macro was capable of analysing individual images obtained from microscopy data and processing them based on their respective channels, determined by the saved image file names.

Chapter 3
Characterisation of Cell Wall Degradation

3.1 Introduction

The cell wall of *B. subtilis* is dynamic, with degradation of old layers and the insertion of nascent peptidoglycan into the cell wall occurring to permit growth. The synthetic process has been extensively studied, and an inside-to-outside transition model for wall material has been developed to fit the data (8). Previous studies utilising radioactive substrates and/ or suicide probes have contributed to a good understanding of peptidoglycan modification (219, 220). However, these methods were limited as they were toxic to live bacteria.

More recently, fluorescently modified D-amnio acid analogues have been extensively used to expand our understanding of cell wall synthesis and turnover in various live bacterial species (221). Fluorescent D-amino Acids (FDAAs) are designed as biomolecular fluorescent probes, featuring three primary components: a carrier moiety with a D-amino acid backbone for specific target binding, a fluorophore that emits light upon excitation, and a linker to connect the two (222). These FDAAs are biocompatible, allowing them to integrate seamlessly into biological systems. When used, they provide a fluorescent readout that indicates peptidoglycan (PG) synthesis and remodeling activity within bacterial cell walls (221, 223, 224). The D-amino acid backbone binds specifically to the peptidoglycan structure, and upon excitation by an external light source, the fluorophore emits light at a different wavelength (221). This emitted light is detected through fluorescence microscopy, offering a visible signal that reflects the activity of peptidoglycan processes, enabling real-time observation and analysis of bacterial cell wall dynamics (221, 225). FDAAs are incorporated with nascent peptidoglycan by exchange with the 5^{th} D-alanine of the peptidoglycan after it has been assembled by transglycosylation and is not crosslinked to other peptide side chains. Previous studies have shown that these fluorescent probes are efficiently incorporated into the entire cell wall in the absence of DacA activity, the major DD-carboxypeptidase responsible for peptidoglycan maturation during vegetative in *B. subtilis* (60, 226). In the absence of DacA, the abundance of pentapeptide chains significantly increases in the cell wall, with a proportional decrease in tetrapeptide chains compared to the wild type. Surprisingly, the absence of carboxypeptidase activity had no apparent phenotype, suggesting that peptidoglycan maturation is not an essential process. Using this property as a way to directly incorporate FDAAs into nascent peptidoglycan facilitated the tracking of cell wall synthesis and turnover in live bacteria. The results supported the inside-

outside model of growth, where nascent peptidoglycan is inserted into the innermost layer of the cell wall. As the bacterium grows, this layer progresses to the outer surface, where cell wall degradation seems to occur. For this model to work, cell enlargement requires synthases and hydrolyses to be accurately regulated to maintain cell integrity and prevent cell autolysis (9). However, the understanding of how peptidoglycan synthesis and turnover mechanisms link together is still limited.

This chapter focuses on the autolytic enzymes that have been shown to be expressed during the vegetative growth of *B. subtilis.* Using systematic deletions of the genes encoding these autolytic enzymes, we sought to define the minimum activities necessary for normal function in cell elongation, division, and cell wall turnover. This chapter shows that cell viability was dependent on either CwlO or LytE and revealed an interesting new insight into the requirements for CwlO to function in cell growth.

3.2 Construction of autolytic mutants

To evaluate the role of specific enzyme activity, strains lacking amidase, glucosaminidase, and DL-endopeptidase, as well as multiple autolytic mutants were constructed using the antibiotic knockout mutations from the Koo collection (204) as a starting point. These antibiotic knockout mutations were transferred to the 168CA background, and then the Cre *lox* recombination system was used to remove the kanamycin antibiotic cassette, 1.1 kDa (Figure 3.1A). This resulted in marker-less deletion mutations for the gene, into which it was possible to introduce another deletion mutation using the same resistance marker (Figure 3.1B). This process was repeated, allowing the generation of strains with multiple deletion mutations and strains lacking specific types of biochemical activity (Figure 3.1). Confirmation that the strains generated contained the expected deletions was done by PCR amplification of the loci using PCR oligonucleotides complementary to regions of ~500 bp upstream and downstream of the gene of interest and agarose gel electrophoresis to confirm that the resulting DNA fragment was the expected size (Figure 3.2). Here, the expectation was that PCR amplification of the marker-less deletion mutants would result in smaller DNA fragments than those obtained for the wild-type strain, where the difference in size corresponds to the known size of the deleted gene.

A

Make a kanamycin marker-less by pDR244

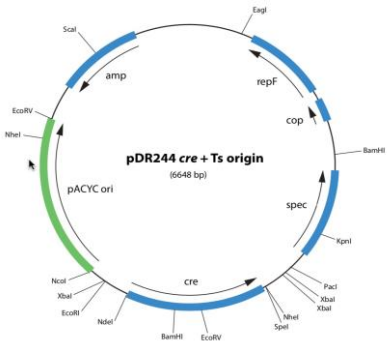

(Cre-recombinase)

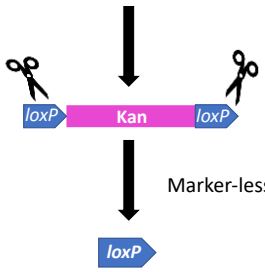

B

Introducing a new genomic DNA with a kanamycin marker

Multiple autolytic mutants

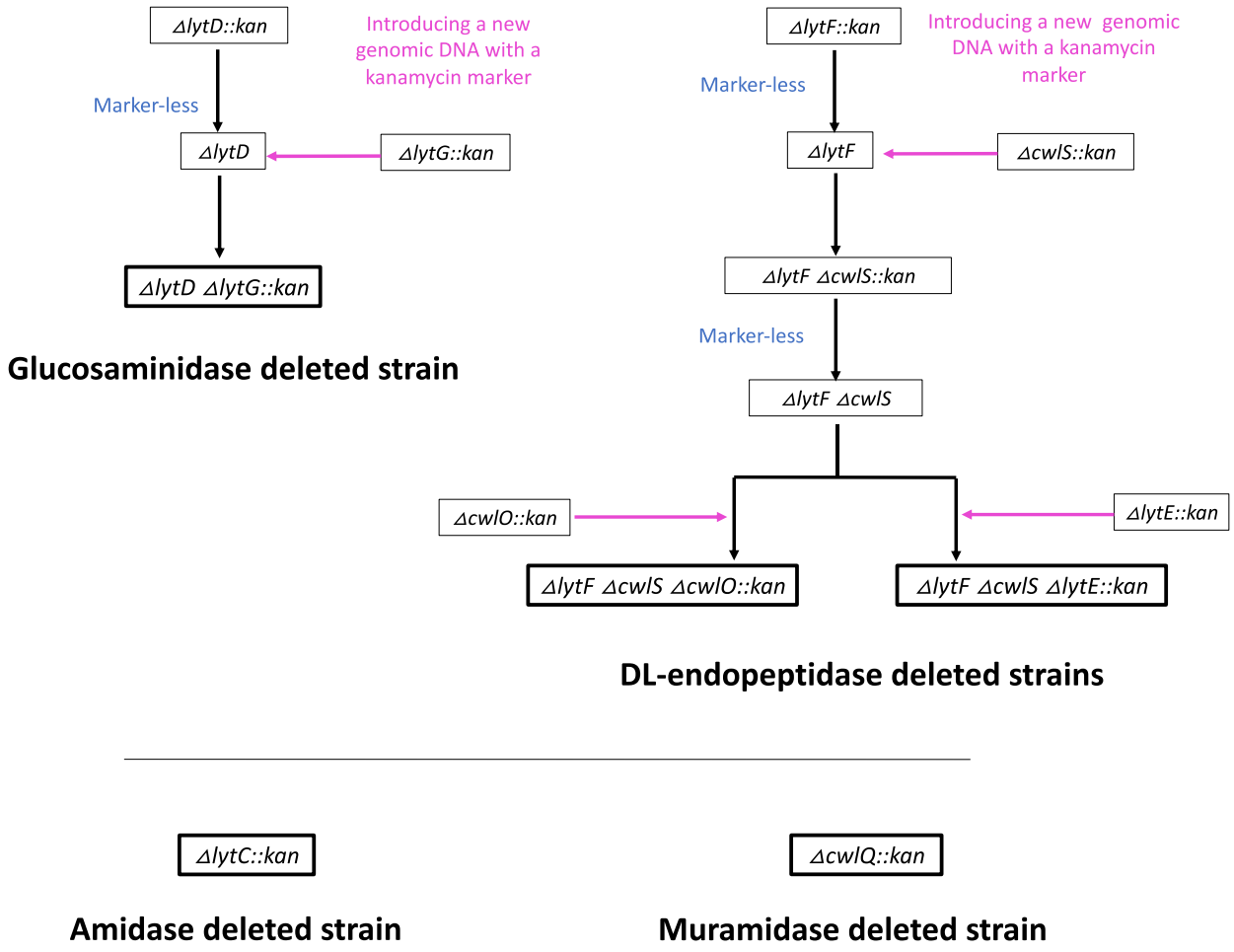

Figure 3.1 A family tree of the constructed autolytic mutations

A family tree depicts the construction of autolytic mutants as multiple autolytic mutants and autolytic mutants lacking a specific class of biochemical activity. Strains were constructed by introducing a strain with a kanamycin marker from the Koo collection (204) on the right side (pink). A marker-less strain was created using the pDR244 plasmid with the Cre *lox* recombination system on the left side (Blue). These processes were repeated to construct the final desired strains in black boxes: the multiple vegetative autolytic mutants (Δ*lytD* Δ*lytG* Δ*lytC* Δ*lytF* Δ*cwlS* Δ*cwlQ* Δ*lytE::kan* and Δ*lytD* Δ*lytG* Δ*lytC* Δ*lytF* Δ*cwlS* Δ*cwlQ* Δ*cwlO::kan*), the glucosaminidase deleted strain (Δ*lytD* Δ*lytG::kan*), the DL-endopeptidase deleted strains ((Δ*lytF* Δ*cwlS* Δ*lytE::kan* and Δ*lytF* Δ*cwlS* Δ*cwlO::kan*), the amidase deleted strain (Δ*lytC::kan*) and the muramidase deleted strain (Δ*cwlQ::kan*).

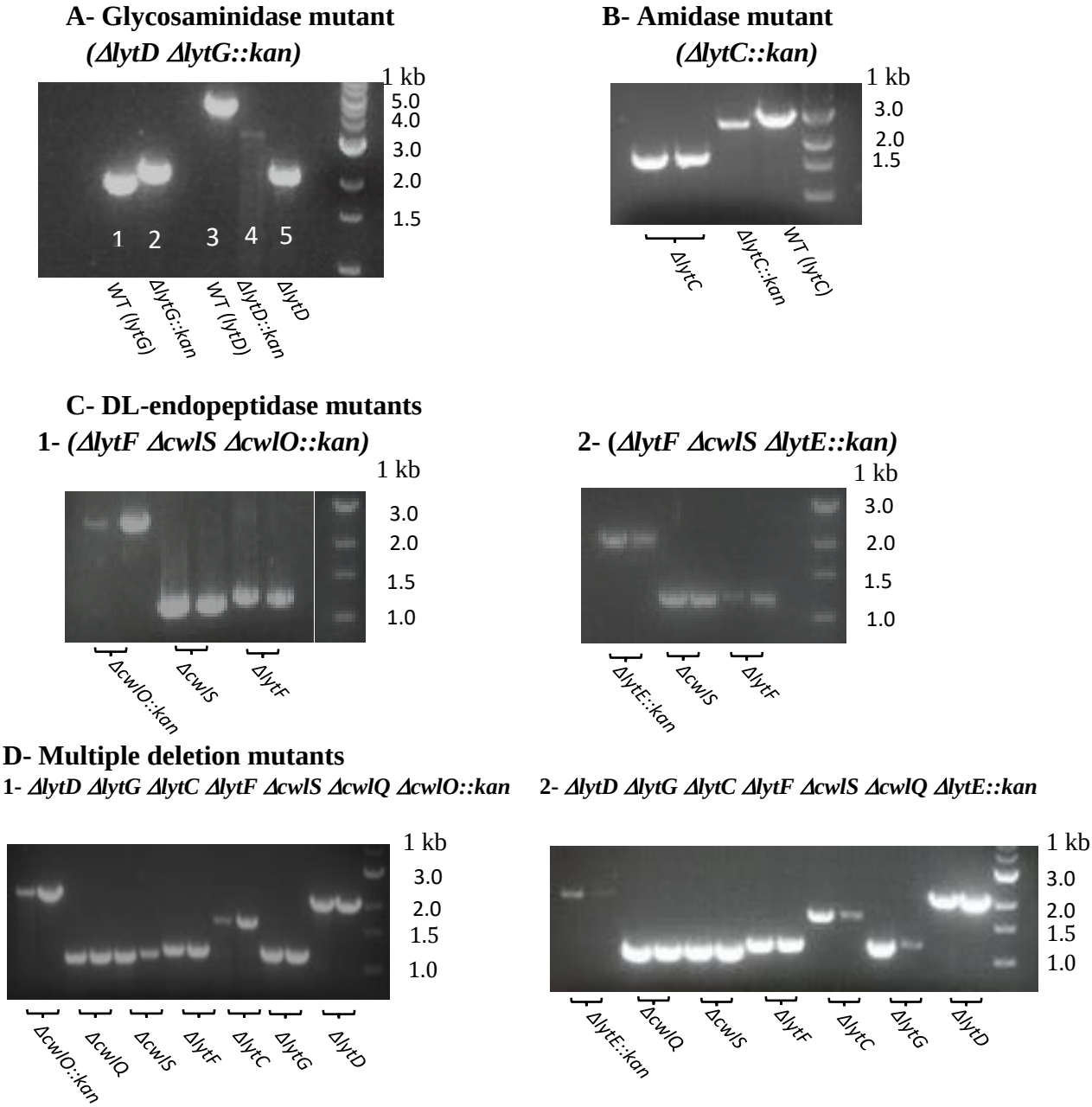

Figure 3.2 Autolytic strain constructions

Agrouse gel electrophoresis of PCR products of the following strains: **A-** Glucosaminidase, *ΔlytD ΔlytG::kan.* **B-** Amidase *ΔlytC::kan.* **C-** DL-endopeptidase: 1- *ΔlytF ΔcwlS ΔcwlO::kan,* 2- *ΔlytF ΔcwlS ΔlytE::kan.* **D-** Multiple autolytic mutants: 1- *ΔlytD ΔlytG ΔlytC ΔlytF ΔcwlS ΔcwlQ ΔcwlO,* 2- *ΔlytD ΔlytG ΔlytCΔlytF ΔcwlSΔcwlQ ΔlytE.* Each band indicates the size of the gene, as shown below it. The DNA ladder is 1 kilobase pair (1kb).

To demonstrate that the expected mutations were present and validate the strain genotypes, PCR and gel electrophoresis were used. The agarose gel electrophoresis images in Figure 3.2 are examples of this method of analysis where distinct band sizes corresponding to the amplified loci of different strains were obtained, which corresponded to the expected genetic manipulations, the replacement of a coding sequence with the kanamycin resistance cassette, a marker-less recombination product, or the wild type. For example, the validation of a glucosaminidase-deleted strain is shown in Figure 3.2, representing the PCR product generated by amplification of panel A, lane 1 shows the PCR product generated by amplification of the *lytG* locus of the wild-type strain, lane 2 is the *lytG* locus but it replaced by a kanamycin cassette (*ΔlytG::kan*), lane 3 is the *lytD* locus of the wild-type strain, lane 4 is the *lytD* locus but it replaced by a kanamycin cassette (*ΔlytD::kan*), and lane 5 is the marker-less mutant *lytD* used as a background to generate the double mutant *lytD lytG::kan.* This mutation confirmation process was repeated for each new knockout mutation introduced, generating strains lacking specific classes of biochemical activity, such as the glucosaminidase-deleted strain containing a double mutant in Δ*lytD* Δ*lytG::kan* (Figure 3.1 & 3.2A); the amidase-deleted strain composed of Δ*lytC::kan* (Figure 3.1 & 3.2B). Since a double mutant in *lytE cwlO* is lethal (105), two strains for DL-endopeptidase deletion were constructed: Δ*lytF* Δ*cwlS* Δ*lytE::kan* mutant and Δ*lytF* Δ*cwlS* Δ*cwlO::kan* mutant (Figure 3.1 & 3.2 C1-2). A consequence of this essential pair also means that two multiple vegetative autolytic mutants were also constructed (Figure 3.1 & 3.2D). It was also found that the construction of the strains in some cases had to be done by introducing *lytE* or *cwlO* mutations as a final step; as consistent with Liu (227), the introduction of either *lytE* or *cwlO* mutations resulted in strains that were difficult to transform by conventional methods.

Strains constructed lacking all of the known autolytic enzymes expressed in vegetative growth except for *lytE* and *cwlO* were viable and grew in a way that was comparable to the wild type, indicating that most of the autolysins are not required for normal growth (Figure 3.3, green line). Since a double mutant *lytE cwlO* is lethal, the effect of the absence of one of these enzymes, in combination with the multiple autolytic deletions was tested separately. Optical densities of cultures of the multiple autolytic mutants were plotted in both logarithmic (Figure 3.3A) and linear graphs (Figure 3.3B). From this representation, it was clear that subtle differences were best indicated using a linear scale for optical density. Thus, all future graphs representing growth in this study were generated using linear scales.

Consistent with the cell growth of the multiple autolytic mutant, when LytE was absent in this background, the culture grew similarly to the wild type (Figure 3.3B, yellow line). However, when CwlO was absent, there was an initial period of slow growth or a lag phase at an early phase for two hours. However, ultimately, the growth reached the same final optical density as the wild type later (Figure 3.3B, red line). Since these multiple autolytic mutants are still viable, it confirms that CwlO and LytE are to some degree redundant to each other (as suggested previously by Hashimoto (105)) and are the only known enzymes essential for cell growth, or that there could be other autolytic enzymes that have yet to be identified.

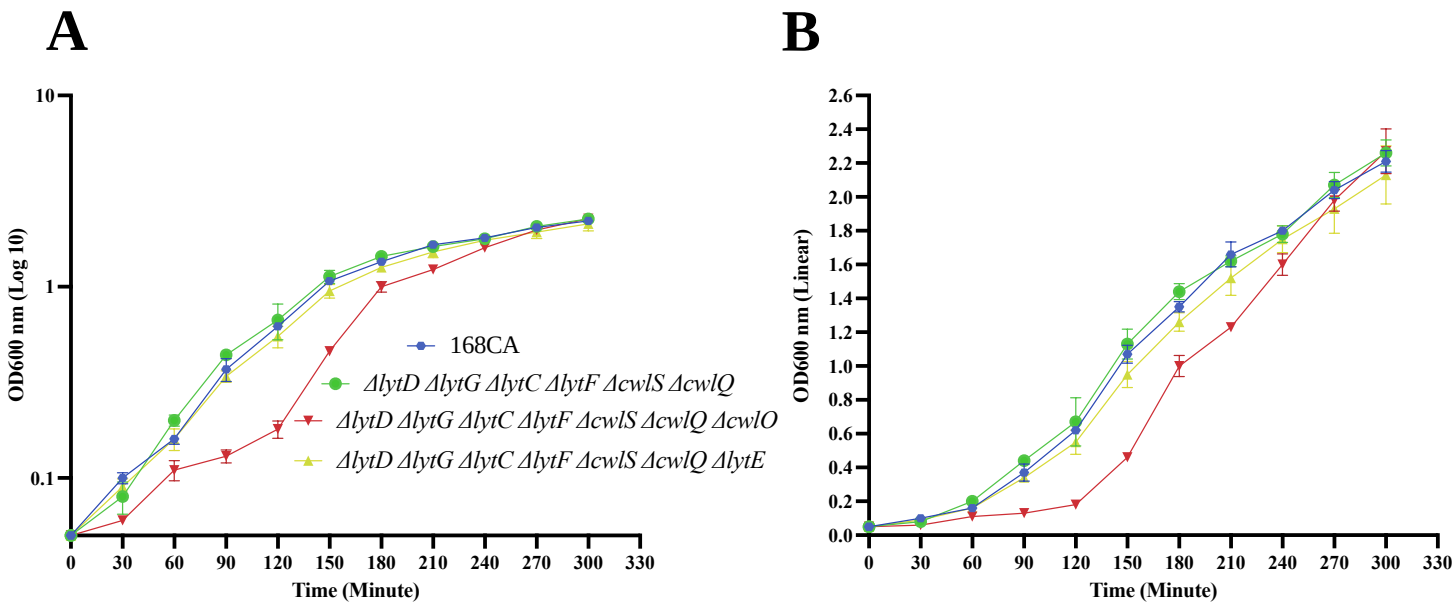

Figure 3.3 Cell growth in the absence of autolytic enzymes

Cell growth of multiple autolytic mutants compared to the wild type (168CA, blue lines). The green lines are *ΔlytD ΔlytG ΔlytC ΔlytF ΔcwlS ΔcwlQ*, the red lines are *ΔlytD ΔlytG ΔlytC ΔlytF ΔcwlS ΔcwlQ ΔcwlO* and the yellow lines are *ΔlytD ΔlytG ΔlytC ΔlytF ΔcwlS ΔcwlQ ΔlytE*. Same data represented in: **A-** Log10 Graph. **B-** linear Graph. Each plotted point corresponds to the average of cell growth (OD600 nm) based on three experimental replicates at the indicated time. Error bars represent the standard error of the mean.

3.3 Phenotypic characterisation of mutant strains

Single mutants for most of the gene expressing autolytic enzymes have previously been characterised and have shown relatively mild phenotypes, suggesting either non-essential or

redundant functions. Taking this into account, this study focused initially on strains lacking specific biochemical activities and then strains with multiple autolytic genes deleted. As an initial characterisation of the strains, cells were visualised from the mid-exponential and stationary growth phases in LB medium (corresponding to OD600 nm ~0.1 and 1, respectively) and compared to equivalent samples of the wild-type strain (168CA). Fluorescence microscopy images and size distribution measurements were obtained using membrane dyes to permit differentiation between filamentous cells where division is delayed and chains of cells where cell separation has yet to occur (Figure 3.4).

Analysis of cells imaged in this way permitted the overall average morphology of the cell population to be determined for each strain sample in the exponential and stationary phase growth (Figure 3.5). Statistically significant differences between the means of each strain compared to the wild type were assessed using independent t-tests (unpaired t-tests) with Welch's correlation. To quantify the variability in cell size distribution, the percentage of mean variation in length and width was calculated for each autolytic strain relative to the wild-type strain. The amidase-deleted strain (*ΔlytC*) appeared shorter in both the mid-exponential and stationary phases, with a variation of 25.47 to 29.50%, respectively, compared to the wild type ($p < 0.0001$, unpaired t-test) (Figure 3.4A/B & Figure 3.5). Additionally, this strain appeared slightly thinner in the stationary phase (4.51%, $p < 0.0001$, unpaired t-test). Although the significance of these differences is questionable as in most other respects (growth rate, colony morphology on plate and transformability, etc.), the strain seemed to be comparable to the wild type. Similarly, the glucosaminidase-deleted strain (*ΔlytD ΔlytG*) displayed a 4.88% decrease in cell length during the mid-exponential phase ($p = 0.01$, unpaired t-test) but a 10.82% increase in length in the stationary phase ($p = 0.04$, unpaired t-test). Whereas these cells were 8.25% wider than the wild type during the mid-exponential phase, their width was close to the wild type in the stationary phase with a variation of 1.97% ($p < 0.0001$, unpaired t-test) (Figure 3.4A/C & Figure 3.5).

In the case of the endopeptidase-deleted strain combined with the *lytE* mutant, cell length was 16.59% longer, and cell width was 3.19% thinner during the mid-exponential phase ($p < 0.0001$, unpaired t-test) (Figure 3.4A/D & Figure 3.5). However, in the stationary phase, both cell length and width were comparable to the wild type, with a slight decrease in width (1.33%, $p = 0.007$, unpaired t-test) and a very minor, non-significant increase in length (0.26%, $p = 0.8$,

unpaired t-test). In contrast, the endopeptidase-deleted strain combined with the *cwlO* mutant exhibited significantly shorter cells (33.39-42.23% variation, $p < 0.0001$, unpaired t-test) and wider cells (23.24-21.55% width variation, $p < 0.0001$, unpaired t-test) compared to 168CA in both phases (Figure 3.4A/E & Figure 3.5). These strains were also seen to have short chains with a well-defined division/constriction in the middle of the chain of cells (Figure 3.4D/E).

The multiple autolytic mutant strains exhibited more significant variation in cell size distributions. The strain with multiple autolytic deletions, including the *lytE (*Δ*lytD* Δ*lytG* Δ*lytC* Δ*lytF* Δ*cwlS* Δ*cwlQ* Δ*lytE*), was generally seen as long chains of cells; these chains tangled, forming a net-like appearance (Supplementary 4.1A). This strain exhibited cell length comparable to the wild type in the mid-exponential phase with minor, non-significant cell length variation (1.68%, $p = 0.43$, unpaired t-test); however, in the stationary phase, cells were longer than the wild type (9.95%, $p < 0.0001$, unpaired t-test). Moreover, cells of this strain were slightly thinner (8.67%, $p < 0.0001$ unpaired t-test) in the mid-exponential and (1.40%, $p = 0.006$, unpaired t-test) in the stationary phase (Figure 3.4A/F & Figure 3.5). On the other hand, the multiple knockout strain with the *cwlO* deletion (Δ*lytD* Δ*lytG* Δ*lytC* Δ*lytF* Δ*cwlS* Δ*cwlQ* *Δcwl**O*) was wider (31.29-24.09% variation in width, $p < 0.0001$, unpaired t-test) and shorter (39.28-32.30% variation in length, $p < 0.0001$, unpaired t-test), although the cells were also seen in the form of long chains (Figure 3.4A/G & Figure 3.5). These observations suggest that most of these autolytic enzymes are redundant for cell separation and division. The absence of CwlO or LytE appears to primarily influence cell length and width in these mutants (Figure 3.5). Whereas the absence of CwlO generated shorter and wider cells, the absence of LytE generated longer and thinner cells compared to the wild-type strain.

In this chapter, CwlQ was not investigated as a single mutant because it is not expressed in normal vegetative growth. However, it was incorporated into the multiple deletion strain and was investigated in relation to flagellar insertion (see Chapter 4).

A

168CA

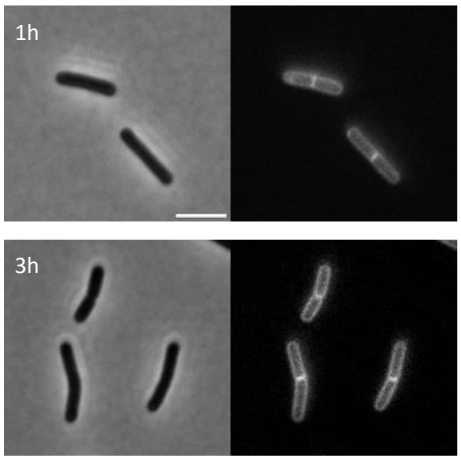

B

Amidase-deleted strain

ΔlytC

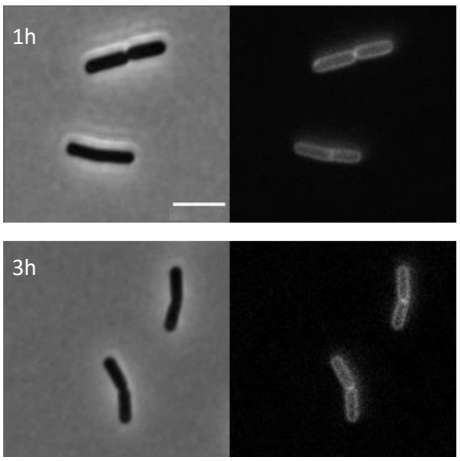

C

Glucosaminidase-deleted strain

ΔlytD ΔlytG

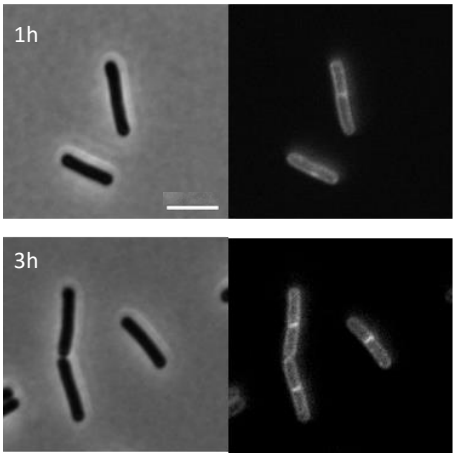

D

Endopeptidase-deleted strain

ΔlytF ΔcwlS ΔlytE

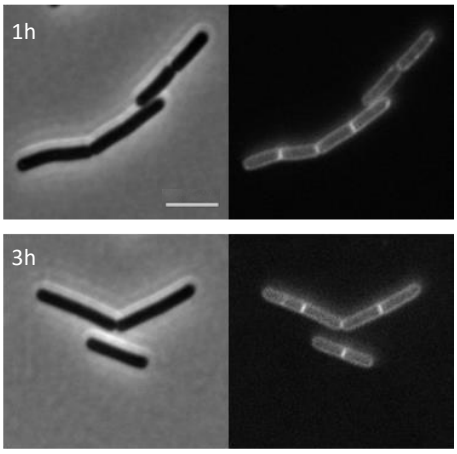

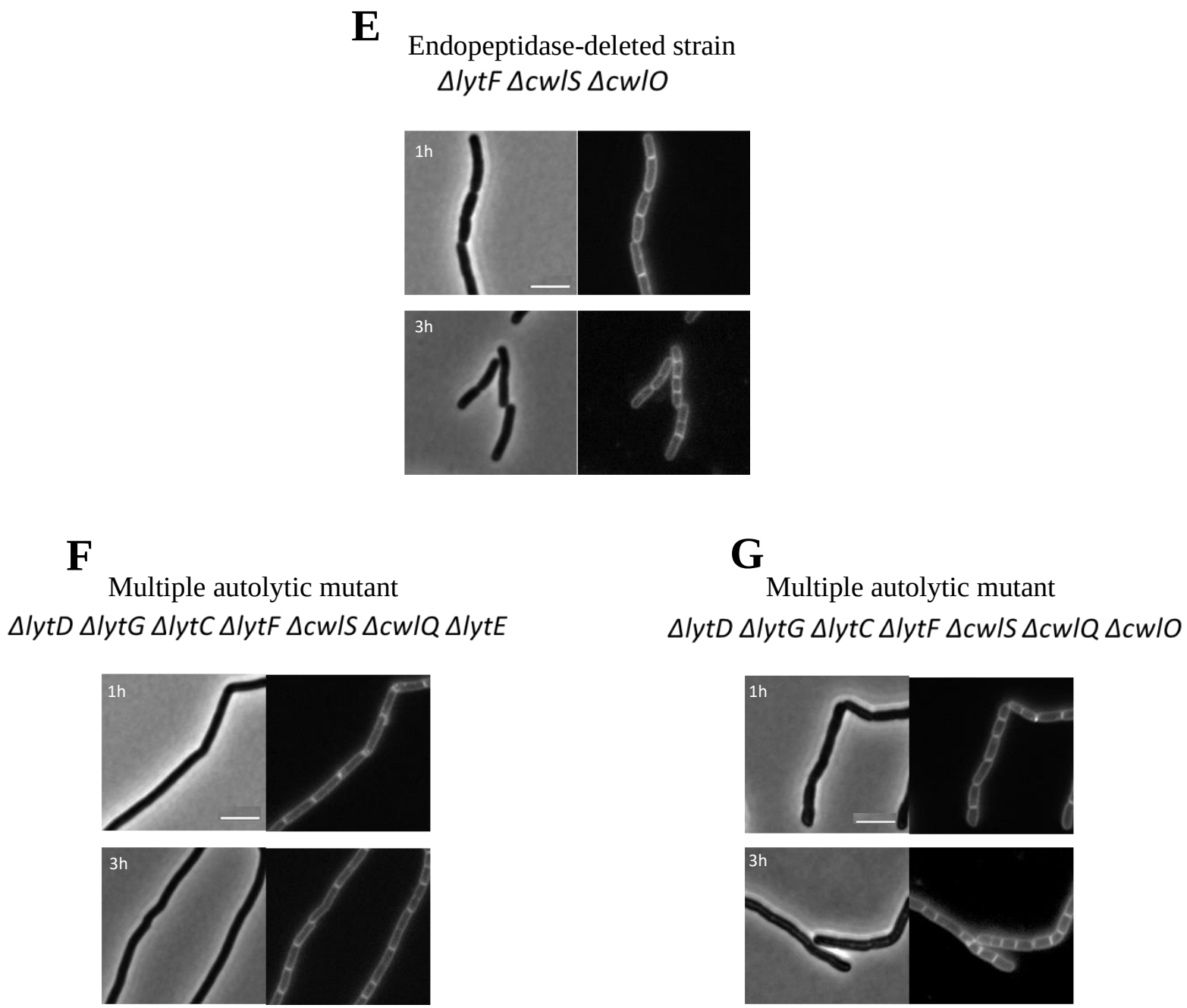

Figure 3.4 Phenotypic characterisation of autolytic mutants

Fluorescence microscopic images showing characteristic cells observed in exponentially (1h) and stationary (3h) growing cultures of the following strains: **A-** Wild type (168CA), **B-** Amidase-deleted strain (Δ*lytC*), **C-** Glucosaminidase-deleted strain (Δ*lytD* Δ*lytG*), DL-endopeptidase-deleted strains: **D-** (Δ*lytF* Δ*cwlS* Δ*lytE*) and **E-** *(*Δ*lytF* Δ*cwlS* Δ*cwlO)*, and multiple vegetative autolytic mutants: **F-** (Δ*lytD* Δ*lytG* Δ*lytC* Δ*lytF* Δ*cwlS* Δ*cwlQ* Δ*lytE*) and **G-** (Δ*lytD* Δ*lytG* Δ*lytC* Δ*lytF* Δ*cwlS* Δ*cwlQ* Δ*cwlO*). Scale bars represent 4 microns. The cells were stained with FM5-95 dye.

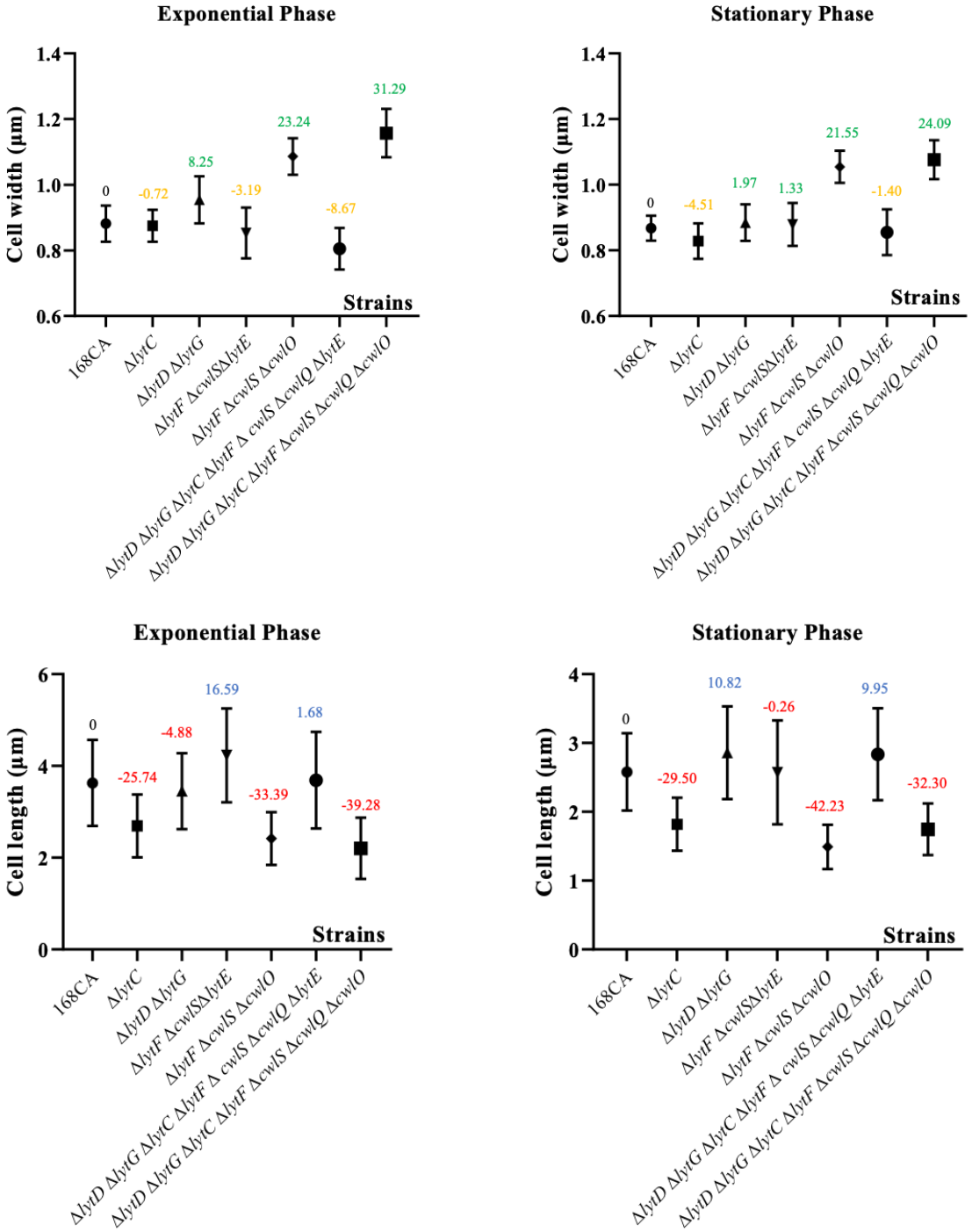

Figure 3.5 Cell diameters of autolytic mutants

The graphs indicate cell size distributions of cells lacking specific classes of biochemical activity: the amidase-deleted strain (Δ*lytC*), glucosaminidase-deleted strain (Δ*lytD* Δ*lytG*), DL-endopeptidase- deleted strains (Δ*lytF* Δ*cwlS* Δ*lytE* and Δ*lytF* Δ*cwlS* Δ*cwlO)*, and multiple vegetative autolytic mutants: (Δ*lytD* Δ*lytG* Δ*lytC* Δ*lytF* Δ*cwlS* Δ*cwlQ* Δ*lytE* and Δ*lytD* Δ*lytG* Δ*lytC* Δ*lytF* Δ*cwlS* Δ*cwlQ* Δ*cwlO*). The strains were measured in exponential and stationary

phases. The graphs represent the average and standard division of cell diameters from approximately 300 cells for each strain. Coloured numbers represent the percentage of width or length mean variations compared to 168CA. Yellow numbers indicate thinner cells, while green numbers are wider cells relative to 168CA. Blue numbers are longer cells compared to the wild type, while red numbers are shorter cells. Cell measurements are in microns (μm).

3.4 Cell wall turnover and synthesis

To evaluate the contribution of the individual autolytic enzymes to cell wall turnover *in vivo*, two approaches were initially planned. The first approach was to track cell wall turnover at the single cell level, and the second was to analyse the muropeptide composition of the PG to determine if the cell wall composition was altered or if the culture medium of autolytic mutants contained detectable fragments of the cell wall. For both the first and last objective, a preliminary goal was to efficiently label the cell wall to permit the visualisation of any changes in local turnover of the wall in living cells and to allow easy detection of cell wall fragments released into the culture medium during growth.

To visualise the newly synthesised peptidoglycan materials at the site of wall formation, fluorescent D-amino acids (FDAAs) were utilised in a *dacA* background to enable the efficient incorporation of FDAAs into the cell wall (60). These FDAAs specifically replace the 5^{th} amino acid (D-alanine) in the peptidoglycan structure (as illustrated in Figure 3.6A). This labeling was achieved using two types of FDAAs: 3-[[(7-Hydroxy-2-oxo-2H-1-benzopyran-3yl) carbonyl] amino]-D-alanine hydrochloride (HADA), emitting blue light on excitation, and TAMRA-based fluorescent D-amino acid (RADA), emitting red light. Different concentrations of these FDAAs were employed as 20 μM, 16 μM, 12 μM, and 9 μM (Figure 3.6B) to determine if the level of labeling had any effect on the cells. Through these tests, it was determined that a concentration of 20 μM of either HADA or RADA, when incorporated into the cell wall labeling medium or LB, produced a satisfactory fluorescent signal that could be detected using a fluorescence microscope. Higher concentrations were problematic due to increased background noise. Thus, it was concluded that 20 μM of HADA or RADA was sufficient for effectively labeling the newly synthesised peptidoglycan inserted into the cell wall (Figure 3.6B).

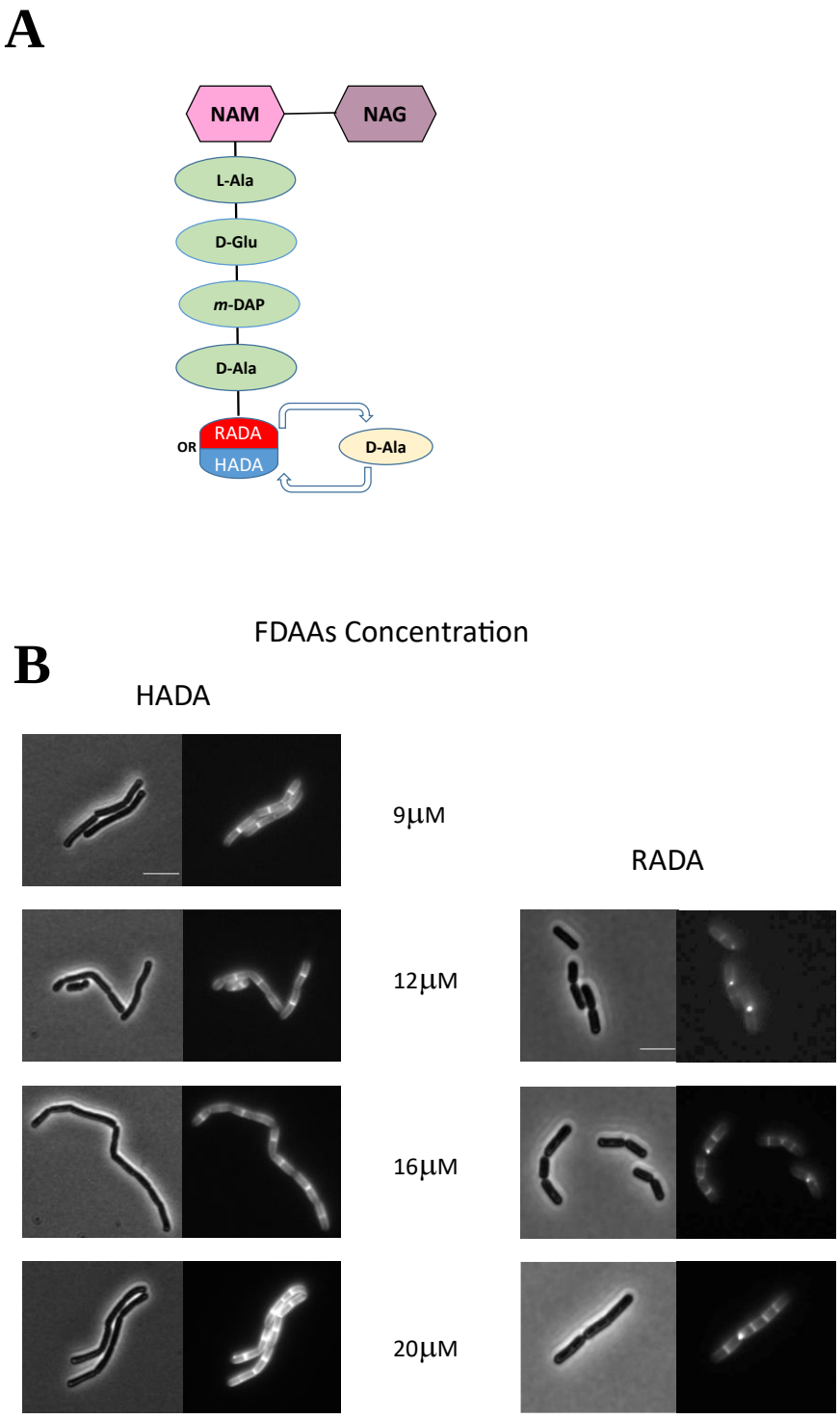

Figure 3.6 Efficient cell wall labeling

A- Fluorescent D-amino acids (HADA and RADA) are designed to take place the 5th peptide of the pentapeptide chain of newly synthesised peptidoglycan materials. **B-** Fluorescence microscopy images of the *dacA* mutant that incubated in LB with different concentrations of HADA (9 µM, 12 µM, 16 µM, and 20 µM) and RADA (12 µM, 16 µM, and 20 µM) for an hour, followed by washing to remove the excess FDAAs. Scale bar is 4 microns.

The cell wall turnover in the *dacA* mutant (wild type) was evaluated using 20 μM of HADA in live bacteria, followed by removing the labeling compound. Fluorescent images demonstrated changes in HADA signals overtime at the lateral cell wall, while the poles retained labeling for a longer duration, suggesting a slower turnover rate at the cell poles (Figure 3.7A). HADA is specifically attached to newly synthesised peptidoglycan and progresses as the cell grows, eventually reaching the outermost layer of the cell wall where degradation enzyme activities take place. It was also evident that using this level of labeling that there was minimal reincorporation of the FDAA as it was shed into the culture medium, presumably as muropeptide fragments.

To assess the time course of cell wall turnover, the HADA signals were monitored, and it was observed that the HADA signals at the lateral cell wall diminished within approximately two hours, indicating complete turnover of the lateral cell wall within this time frame under the given conditions (Figure 3.7B). In contrast, the cell poles that were labeled seemed to retain their fluorescent signal and were detectable over the duration of the experiment, although their signal seemed to gradually diminish, and none of the "new" cell poles formed after removal of the label exhibited any signal. This appeared to align with about two generations of bacterial growth, resulting in the complete turnover of the lateral cell wall. However, it should be noted that the growth curve was not optimal due to interruptions caused by culture manipulation. Nevertheless, the labeling approach proved successful in indicating the timeframe during which analysis would be feasible for the wild-type strain.

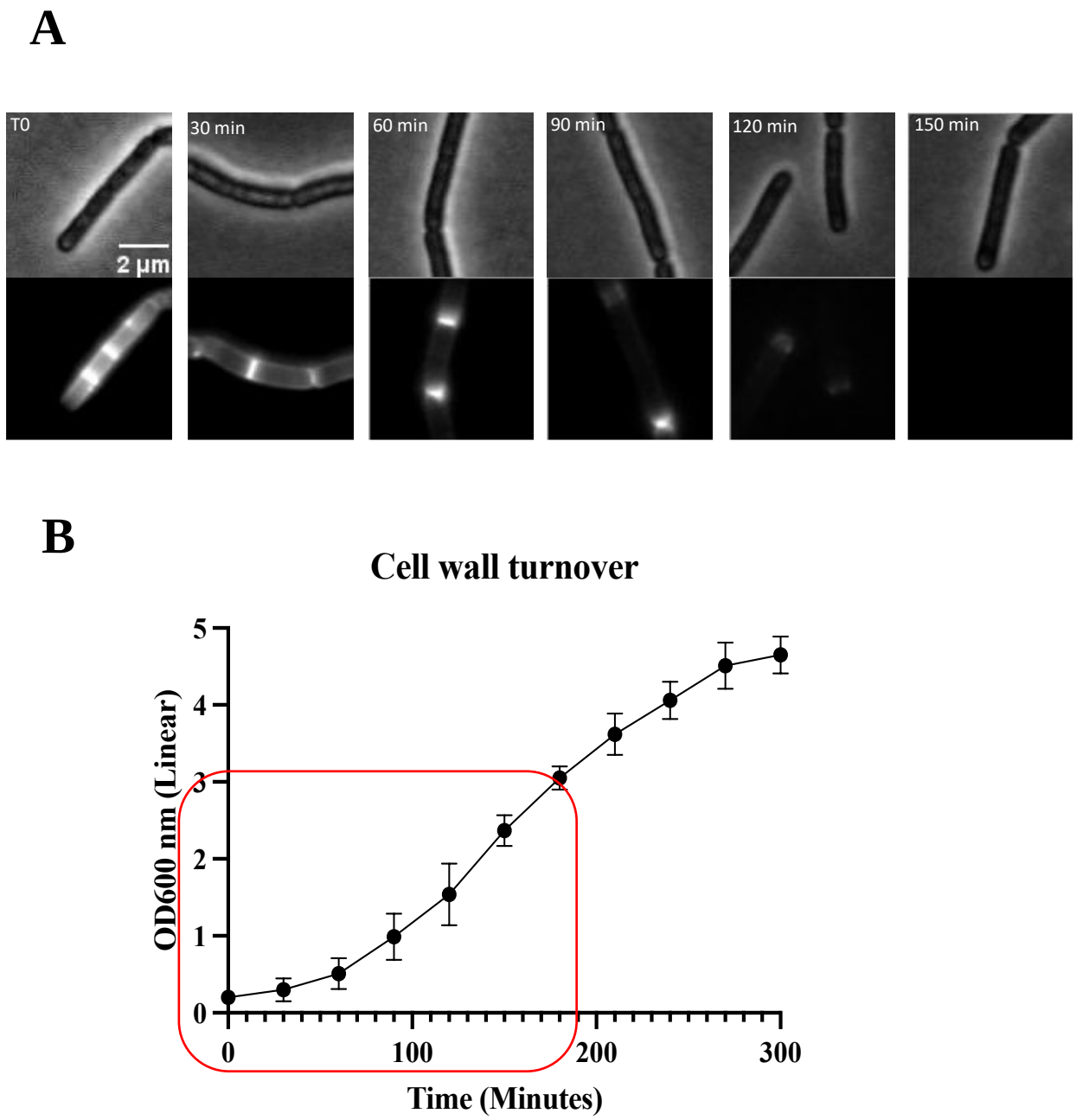

Figure 3.7 Time-course of cell wall turnover

A- Fluorescence microscopy images of the *dacA* mutant, incubated in LB with 20 µM HADA, then washed and allowed to grow in the absence of HADA to monitor cell wall turnover during growth time. Scale bar is 2 microns. **B-** Cell growth of the *dacA* mutant after the start of labeling with HADA. The red box indicates the time when the cells were visualised under fluorescence microscopy. Each plotted point corresponds to the average of cell growth (OD600 nm) based on three experimental replicates at the indicated time. Error bars represent the standard error of the mean.

3.5 Construction of strains to characterise altered cell wall turnover

The *dacA* deletion (*dacA::ery*) was successfully introduced into the Δ*lytD* Δ*lytG* Δ*lytC* Δ*lytF* Δ*cwlS* Δ*cwlO::kan* strain. However, difficulties were encountered when attempting to transform the *dacA* deletion into the Δ*lytD* Δ*lytG* Δ*lytC* Δ*lytF* Δ*cwlS* Δ*lytE::kan* multiple deletion strain. Only a few transformants were obtained, and it was discovered that these transformants had regained functional copies of either *lytF* or *lytE*. To determine if these gene deletions were incompatible with the *dacA* deletion or if multiple deletions were required, transformations were performed to generate the mutation combinations of *dacA* with all the single autolytic null mutations tested, but the results will focus on the construction of Δ*lytE* Δ*dacA,* Δ*lytF* Δ*dacA,* and Δ*lytF* Δ*lytE* Δ*dacA*. Both transformation directions were attempted, meaning that competent cells were generated for each of the single mutant strains, and they were transformed with the required second null mutation. Through this work, it was observed that the *dacA* mutant did not efficiently become competent for transformation. As a result, strain constructions were predominantly carried out by introducing the *dacA* mutant. However, it became apparent that introducing *dacA* into the *lytE* or *lytF* backgrounds resulted in very few transformants, and those that were obtained grew poorly on nutrient agar (Figure 3.8A/C). A few transformants regained functional copy of *lytE* back when attempting to knock *dacA* out (Figure 3.8A, big colonies in the NA plate). In contrast, the mutant *dacA* could be easily introduced into all other single autolytic mutations without significant phenotypic effects on the transformants' growth on plates. However, subsequent microscopic analysis revealed morphological changes in these strains compared to the 168CA strain (details are provided in Section 3.9). Interestingly, a more severe synthetic lethality was observed when attempting to transform a strain deleted for both *lytE* and *lytF* with any *dacA* allele (Figure 3.8B/C).

Since this synthetic lethality appeared to specifically involve strains where CwlO was present as the main or sole autolytic function, it was hypothesized that elevated concentrations of Mg^{2+} might suppress the growth defect in these strains. Therefore, the transformations were repeated, and selection on plates containing 25 mM $MgSO_4$ was compared to standard nutrient agar (Figure 3.8A/B). It was evident that the presence of 25 mM $MgSO_4$ significantly improved the growth of transformant colonies. Under these conditions, it was consistently observed that introducing *dacA* into the *lytE* null strain yielded transformant colonies that were less lytic, and

the *lytE lytF* double mutant, when transformed with the *dacA* knockout, resulted in culturable colonies. Single colonies from each transformation were streaked out on NA plates with and without the addition of 25 mM $MgSO_4$ (Figure 3.8C). Both the double mutants, *lytE dacA* and *lytF dacA*, exhibited impaired growth on the NA plate compared to the wild type, while their growth was improved in the NA plate with the addition of Mg^{2+}. On the other hand, for the triple mutant *lytF lytE dacA*, the addition of Mg^{2+} to the medium was required for the strain to be able to grow. The double mutant *mreB dacA* was lethal and required the addition of Mg^{2+} to survive. MreB is involved in the LytE system, which is discussed in detail in Section 3.9.

The growth of the double mutants *lytE dacA* and *lytF dacA* was also analysed in liquid medium, where it was found to be slower without the addition of 25 mM $MgSO_4$ compared to the wild type (168CA) and the single mutant *dacA* (Figure 3.9A/B). In contrast, the cell growth of the triple mutant *lytE lytF dacA* was also slow compared to the wild type, even when the media was supplemented with $MgSO_4$, and never reached the final/stationary phase optical density achieved by the wild-type strain. In the absence of the additional $MgSO_4$, growth slowed after about 2.5 h and by 3 h appeared to enter the stationary phase (Figure 3.9C).

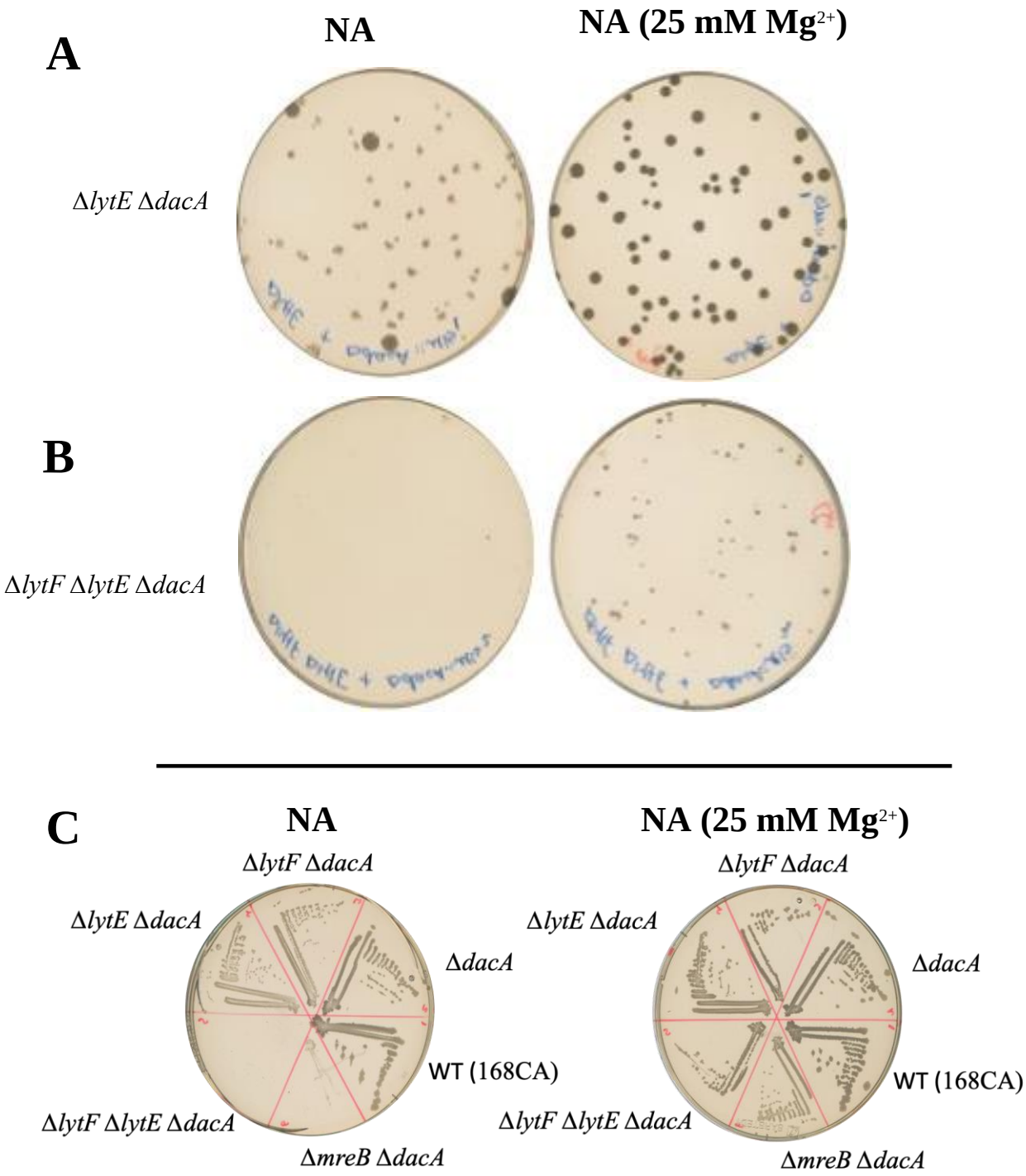

Figure 3.8 Strain constructions for cell wall turnover in a *dacA* background

Transformations with and without the addition of 25 mM Mg^{2+} of: **A-** *ΔlytE ΔdacA*, **B-** *ΔlytE ΔlytF ΔdacA*. **C-** Nutrient agar plates with and without the addition of 25 mM Mg^{2+} were inoculated with the following strains: 168CA, *ΔdacA*, *ΔlytE ΔdacA*, *ΔlytFΔdacA*, *ΔlytE ΔlytF ΔdacA*, and *ΔmreB ΔdacA*.

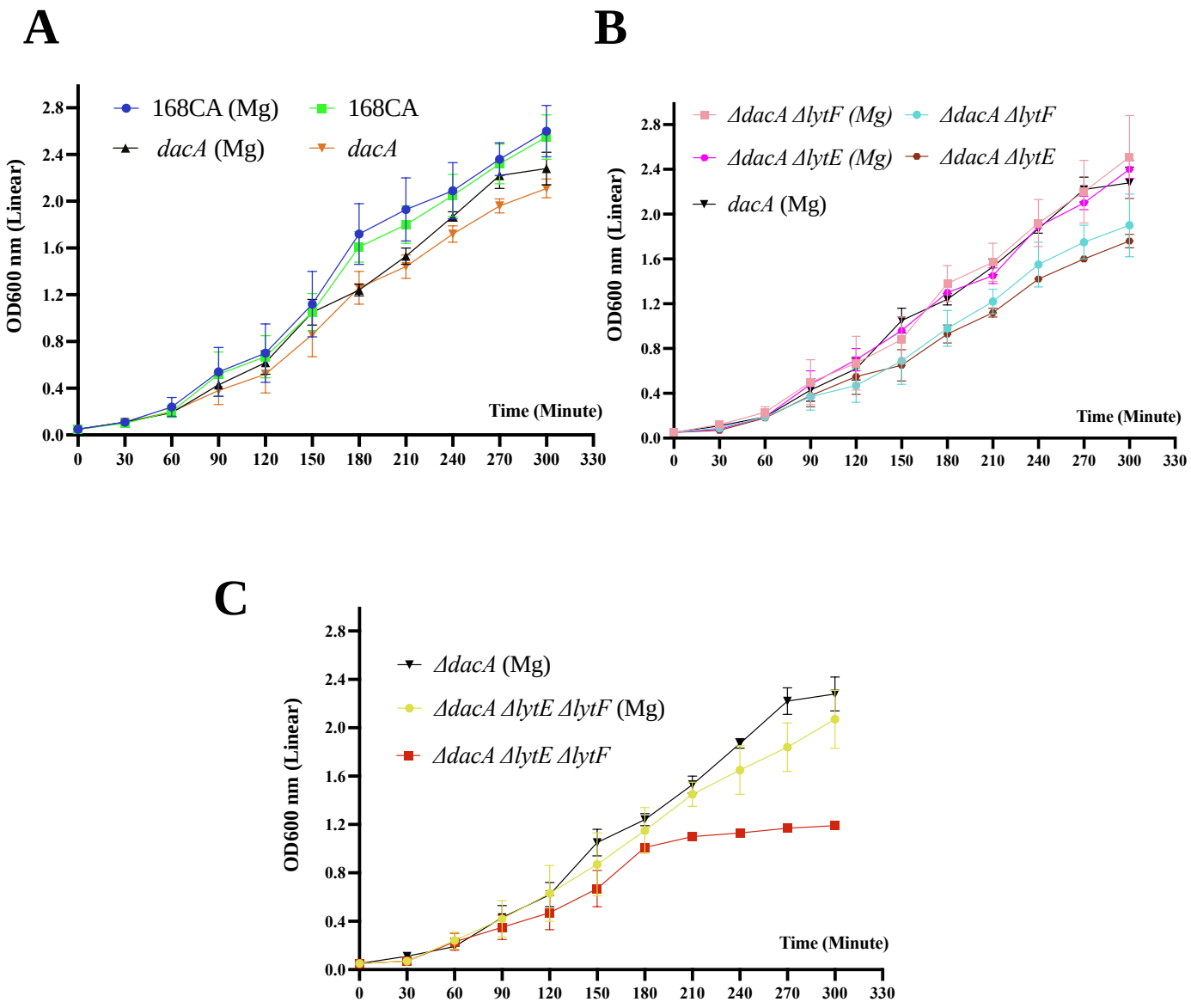

Figure 3.9 The impact of DacA absance in cell growth in different mutantation combinations

Growth curves graphs of strains growing with and without the addition of 25 mM Mg^{+2}. **A-** Control strains: 168CA and Δ*dacA*. **B-** Δ*lytE* Δ*dacA, and* Δ*lytF* Δ*dacA*. **C-** Δ*lytF* Δ*lytE* Δ*dacA*. Each plotted point corresponds to the average of cell growth (OD600 nm) based on three experimental replicates at the indicated time. Error bars represent the standard error of the mean.

Since this phenotype was unexpected, to check that the phenotype was caused by the absence of DacA in the *lytE lytF* background, a xylose-induced promoter was introduced at the native *dacA* gene in the double mutant *lytE lytF* generating AA102. Characterisation of this strain showed that when *dacA* was expressed, the cell growth of the double mutant *lytE lytF* in liquid medium with xylose was restored and grew as the wild type (Figure 3.10A). However, the cells stopped growing after about 2.5 hours when grown in the absence of xylose (Figure 3.10B). Cell morphology was assessed in the presence and absence of xylose under fluorescence microscopy after staining the cells with a membrane dye. It was found that this strain grew as expected when the cell culture was supplemented with xylose, showing the phenotype of the double mutant *lytE lytF* (Figure 3.10C). However, without DacA expression, the strain generated twisted cell chains that ultimately lysed, potentially explaining why the apparent growth defect seen in Figure 3.10D took a long time to be detected after DacA expression was repressed by the removal of xylose. These results confirmed that the phenotypes observed were specifically due to the absence of DacA in the *lytE* and/or *lytF* backgrounds and were not caused by the insertional deletion of *dacA* in the chromosome altering the genetic context of that region.

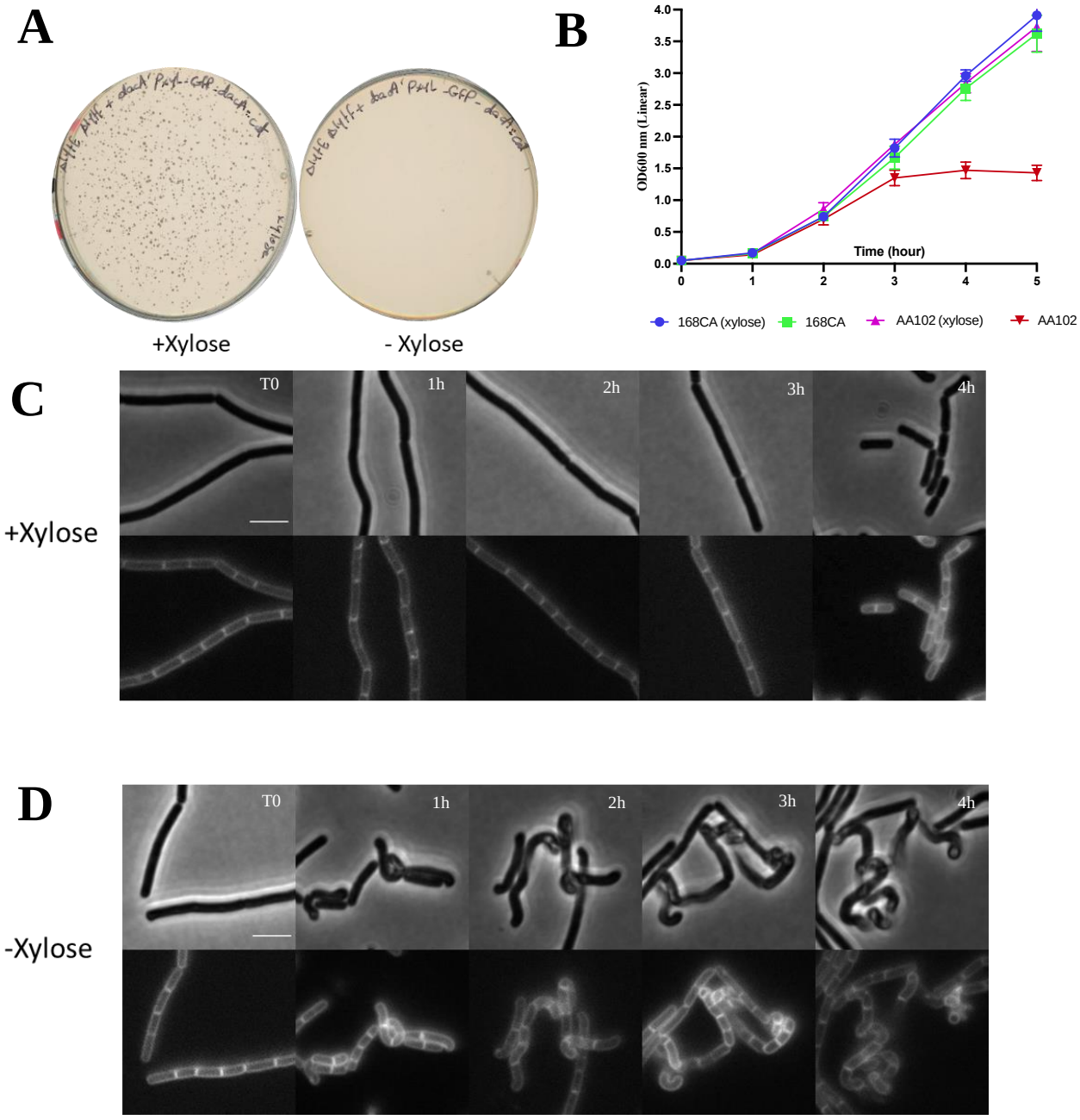

Figure 3.10 Complementing DacA-P_{xyl} regulated in strain lacking LytE and LytF activities

A- Transformation with and without xylose of the complementing *dacA*-P_{xyl} constructed into the double mutant *lytE lytF*. (AA102). **B-** Growth curves of the constructed strain with and without xylose compared to the wild type (168CA). Each plotted point corresponds to the average of cell growth (OD600 nm) based on three experimental replicates at the indicated time. Error bars represent the standard error of the mean. Fluorescence microscopic images to show the phenotype resulting of: **C-** DacA expression and **D-** its absence in the double mutant *lytE lytF*. Scale bar is 4 microns. The strains were stained with FM5-95 dye.

3.6 The biochemical function of DacA is essential in the *lytE lytF* double mutant

Previous results have indicated that DacA has an important role in a strain where CwlO is the only key autolytic enzyme (Section 3.5). Later results seem to confirm this and also show that LytE and LytF together are required to "functionally replace" the loss of DacA.

It has been shown previously that β-lactam antibiotics meropenem and moxalactam have a high affinity for DacA, inhibiting its biochemical function (228, 229). Using these β-lactam antibiotics provided a way to have a catalytically inactive DacA. When using concentrations of meropenem and moxalactam below the minimum inhibitory concentration (MIC) for these antibiotics, initial results showed that strains lacking LytE and/or LytF were significantly more sensitive to these β-lactam antibiotics than the wild-type strain (Figure 3.11). This was demonstrated by the fact that on NA plates with meropenem or moxalactam, the single mutants *lytE* and *lytF* exhibited significantly decreased plating efficiency (number of colony-forming units CFUs) relative to an NA plate, while the double mutant *lytE lytF* was even more significantly impaired (Figure 3.11A). In contrast, the wild-type strain was unaffected by the presence of the antibiotics at these concentrations. Penicillin G and cephalexin, which have a general affinity for all PBPs, or more specifically, target other PBPs respectively (229, 230), were used as controls to assess if the increased sensitivity of these strains was specific for the inhibition of DacA or there was a general increase in sensitivity to perturbation of cell wall synthesis. Here, the plating efficiency of the various strains was not significantly altered (Figure 3.11B), indicating that the *lyt* mutants were not more susceptible than the wild type to inhibition of cell wall synthesis. For both of these spot assays, although cells were standardized to the same optical density (OD) in all plates, both strains of multiple autolytic mutants (*+cwlO* or *+lytE*) had fewer CFUs on the NA plate. This correlated with the fact that multiple autolytic mutants form very log chains due to a separation defect, resulting in a reduced apparent CFU (see Section 3.3 & Supplementary Figure 4.1). Interestingly, on the meropenem or moxalactam plates, the multiple autolytic mutant (*+cwlO*) was essentially inviable, suggesting that the loss of the other autolytic enzymes further increases the dependence on active DacA to permit growth. Thus, our findings suggest that the biochemical activity of *dacA* is essential for cell growth in a double mutant *lytF lytE*, and that LytF has an activity that is able to compensate to a degree for the absence of LytE.

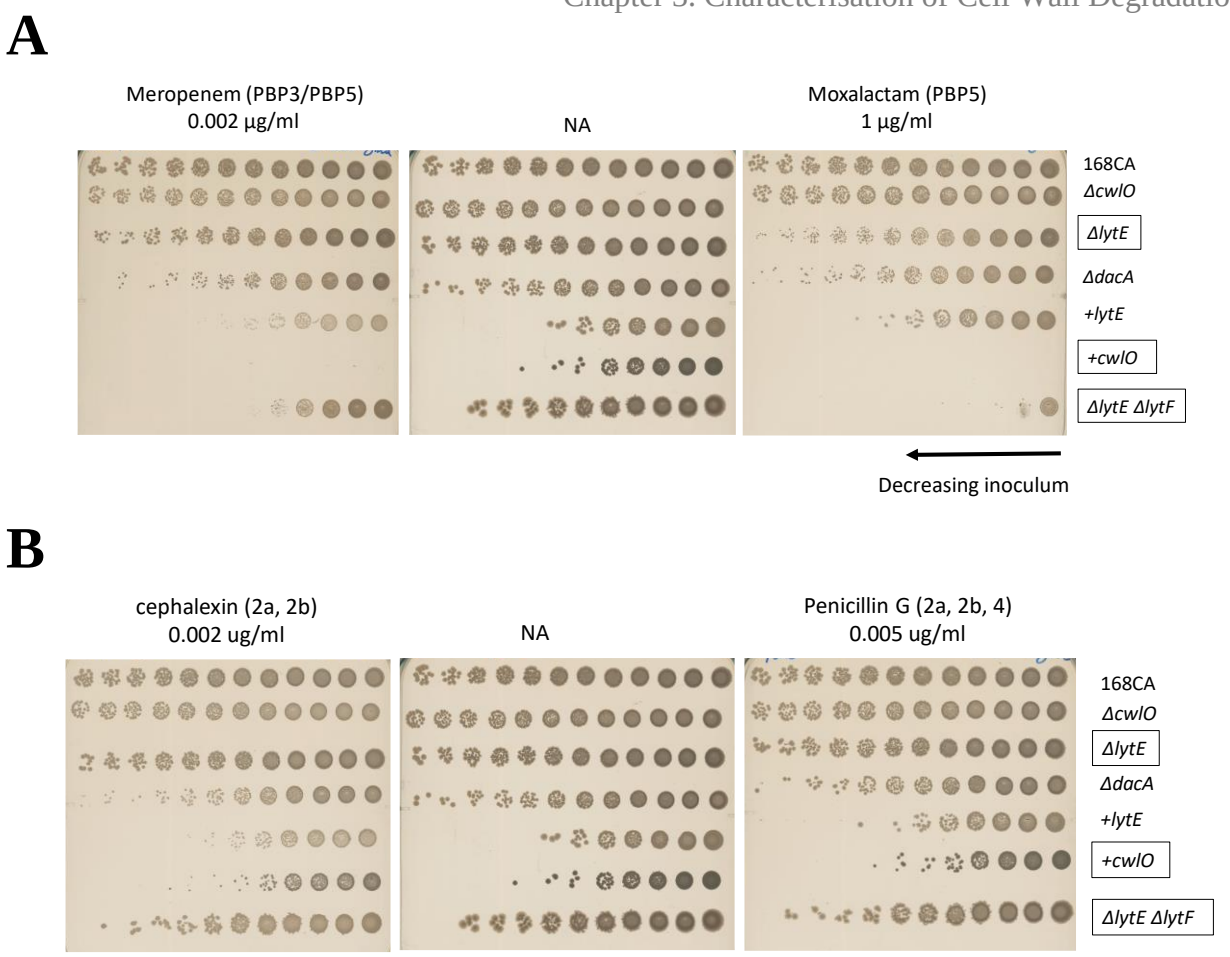

Figure 3.11 Inhibiting the function of DacA using β-lactam assay

Nutrient agar (NA) plates with different β-lactam antibiotics: **A-** 0.002 µg/mL meropenem and 1 µg/mL moxalactam, **B-** 0.002 µg/mL cephalexin and 0.005 µg/mL penicillin G that target specific penicillin-binding proteins. The following strains were inoculated: 168CA, *ΔcwlO*, *ΔlytE*, *ΔdacA*, *ΔlytD ΔlytG ΔlytC ΔlytFΔcwlS ΔcwlQ ΔcwlO* (*+lytE*), *ΔlytD ΔlytG ΔlytC ΔlytFΔcwlS ΔcwlQ ΔlytE* (*+cwlO*), and *ΔlytEΔlytF*. Black boxes indicate the strains that are affected by the inhibition of penicillin-binding protein 5 (DacA) function by the β-lactam antibiotics. The cultures were prepared in a series of five-fold dilutions, and 5 µL of each dilution was spotted onto the plates.

3.7 Morphological effect of the absence of DacA in specific strains

The absence of DacA activity in strains lacking *lytE* and/or *lytF* clearly had a significant effect on the viability of these strains. To determine if this was because cell growth or division was impacted, fluorescence microscopy images were taken of cells using membrane dyes to ensure the cell dimensions were easily determined (Figure 3.12). From the fluorescent images, different

cell morphologies were detected in mutation combinations of *dacA* with *lytE* and /or *lytF* (Figure 3.12 & 3.13). Cell measurements indicated that the cells were shorter and wider compared to the wild type (utilising unpaired t-tests with Welch's correlation for comparison). Additionally, the cells were shorter and wider compared to the single mutants of *lytE*, *lytF*, and *dacA* (utilising one-way ANOVA followed by Tukey HSD tests for comparison) (Figure 3.15 & Supplementary Tables 3.1). Previous studies have shown that *ΔlytE* cells are thinner and longer than the wild type (11), which is consistent with our findings showing a slight decrease in thickness by (6.37%, $p < 0.0001$, unpaired t-test) and an insignificant increase in length by (2.64%, $p = 0.18$, unpaired t-test) compared to the wild-type strain in mid-exponential phase. However, *ΔlytE* cells were dramatically longer in stationary phase (25.98%, $p = 0.001$, unpaired t-test). In this study, cell measurements indicated that *ΔdacA* cells were 34.71% shorter and 14.96% wider ($p < 0.0001$, unpaired t-test), while *ΔlytF* cells exhibited an increase in length by 17.43% and a decrease in thickness by 2.36% compared to the wild type ($p < 0.0001$, unpaired t-test) (Figure 3.15*).* The double mutant *lytE dacA* cells were 32.21% wider and 35.52% shorter than the wild type ($p < 0.0001$, unpaired t-test). Furthermore, when comparing the mean variations (cell length and width) of this double mutant *lytE dacA* to the single mutants *lytE*, *dacA*, and *lytF*, the cells were 43.53% wider and 37.18% shorter than *ΔlytE* ($p < 0.0001$, one-way ANOVA followed by Tukey's HSD test), 35.41% wider and 21.90 shorter than *ΔlytF* ($p < 0.0001$, one-way ANOVA followed by Tukey's HSD test), and (15.01%, $p < 0.0001$, one-way ANOVA followed by Tukey's HSD test) wider and not significantly shorter than *ΔdacA* (1.23%, $p = 0.99$, one-way ANOVA followed by Tukey's HSD test). Similarly, the double mutant *lytF dacA* cells were 39.55% wider and 16.59% shorter than the wild type ($p < 0.0001$, unpaired t-test), 51.80% wider and 35.02% shorter than *ΔlytE* ($p < 0.0001$, ANOVA with Tukey HSD test), 43.22% wider and 19.22% shorter than *ΔlytF* ($p < 0.0001$, ANOVA with Tukey HSD test), and (21.64%, $p < 0.0001$ one-way ANOVA followed by Tukey's HSD test) wider and not significantly longer than *ΔdacA* (2.16%, $p = 0.97$, one-way ANOVA followed by Tukey HSD test) (Figure 3.15 & Supplementary Tables 3.1).

Fluorescent images also revealed that the double mutant *lytF dacA* cells were in twisted filaments with and without the addition of 25 mM $MgSO_4$ (Figure 3.12 & 3.13). While the double mutant *lytE dacA* cells were bent, the bending phenotype was corrected by the addition of

25 mM $MgSO_4$ (Figure 3.12 & 3.13). The triple mutant *lytE lytF dacA* cells needed Mg^{2+} to survive, but even under these conditions, they were still very twisted filaments and appeared to have abnormal division sites (Figure 3.12 & 3.13). One consequence of this morphology was that reliable cell measurement was impossible for the *ΔlytF ΔlytE ΔdacA* and the double mutant *lytE dacA* in the absence of supplementary Mg^{2+}. However, the double mutant *lytF dacA* cells were carefully picked from the middle of the cell filaments, where the length and width were manually measured to permit comparison, avoiding interpretation combined with the twisting phenotype. Thus, these values are potentially biased and may not be representative of the population.

To try and obtain a better understanding of the morphology of these twisted cells, transmission electron microscopy (TEM) images were used on thin sections of fixed cells. The triple mutant *lytE lytF dacA* cells exhibited thick and deformed septa when supplemented with Mg^{2+}, and they had asymmetrically positioned division sites when depleted of $MgSO_4$ (Figure 3.13). This division defect was also observed under fluorescence microscopy but was challenging to quantify due to cell twisting and lysis (Figure 3.12). The double mutant *lytE dacA* appeared too short and wide, and the cells were binding without $MgSO_4$; this phenotype was corrected with the addition of $MgSO_4$ (Figure 3.13). The TEM images clearly indicated the presence of thick, deformed septa in *lytF dacA* mutant cells combined with cell morphology analysis, showing that DacA is required for the maintenance of the cell's diameter.

A closer inspection of the TEM images suggested that there was potentially some alteration in the cell wall thickness. The differences are difficult to quantify in a reliable way as the possibility of sectioning knife artefacts combined with variation in the contrast stain (lead citrate) in the preparation of the samples made cell-to-cell variations too significant; however, as an attempt to visually indicate the differences, a set of images for each strain was used to compile a set of pictures of the cell wall for the strains concerned, where they appeared to have been cleanly cut and minimal cell deformation was present. For clarity, the images shown here have been inverted such that the cellular material is white (Figure 3.14). The images, enlarged significantly, are aligned next to each other, allowing comparison. It is possible to see that the wild-type strain (168) seemed to have a clearly defined structure to the wall, in cross-section, with 2 clear white layers defined by thin black lines, resulting in roughly equal spacing. In

comparison, the *dacA* null mutant has a similar overall structure, but the outer layer seems thicker. This difference becomes more significant in cells where LytE or both LytE and LytF are absent when grown in a medium low in magnesium; elevated Mg^{2+} concentration in the culture medium seems to restore a cell wall structure that is more similar to the wild-type strain.

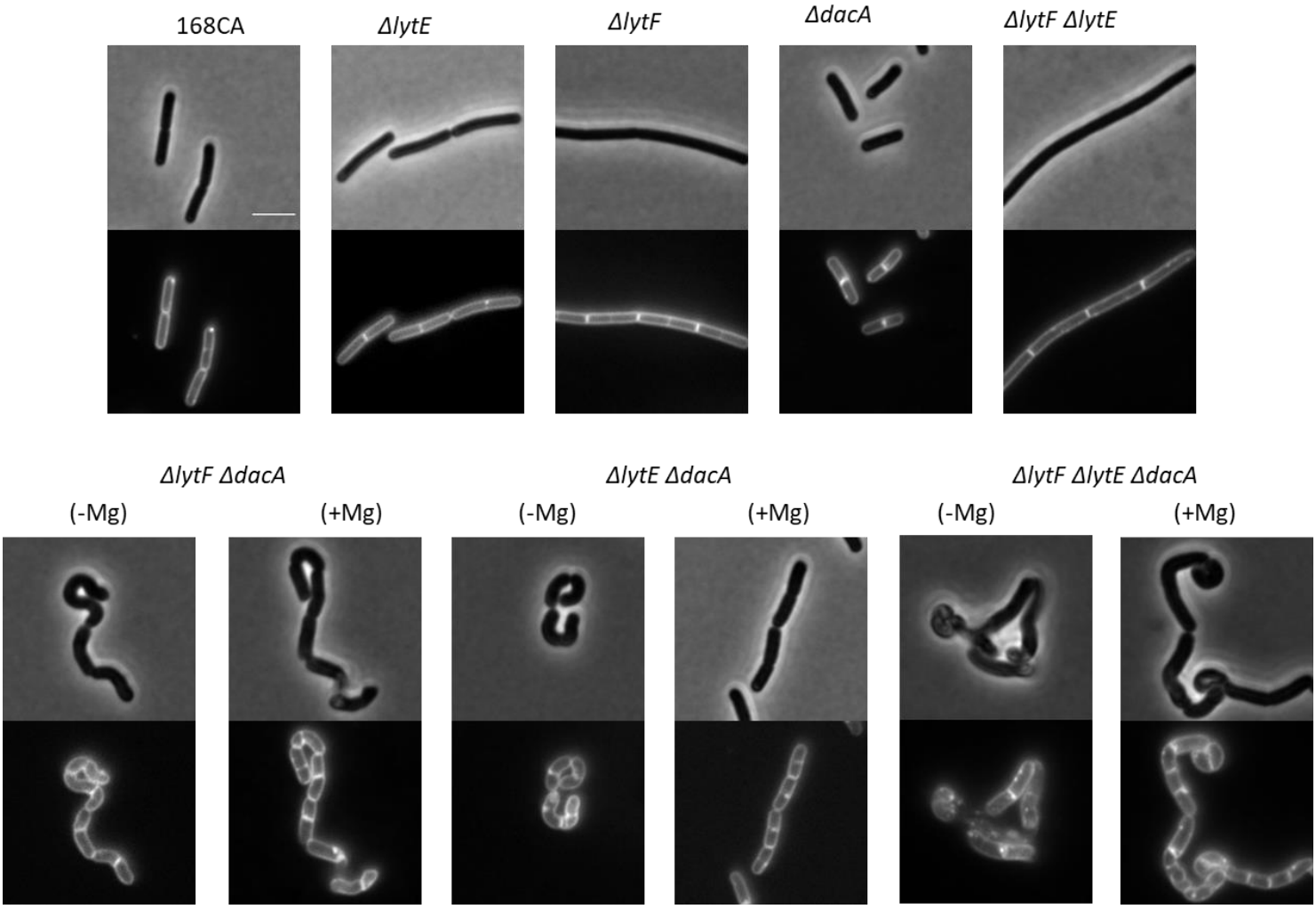

Figure 3.12 Morphological effect of the absence of DacA in different mutant combinations using fluorescence microscopy

Fluorescence microscopy images of exponentially growing cells of *(ΔlytF ΔdacA*, *ΔlytE ΔdacA*, and *ΔlytF ΔlytE ΔdacA*) with and without the addition of 25 mM Mg^{2+}, compared to the wild type (168CA), the null mutants *lytE*, *lytF* and *dacA*, and the double mutant *lytE lytF*. Scale bar is 2 microns. The cells were stained with FM5-95 dye.

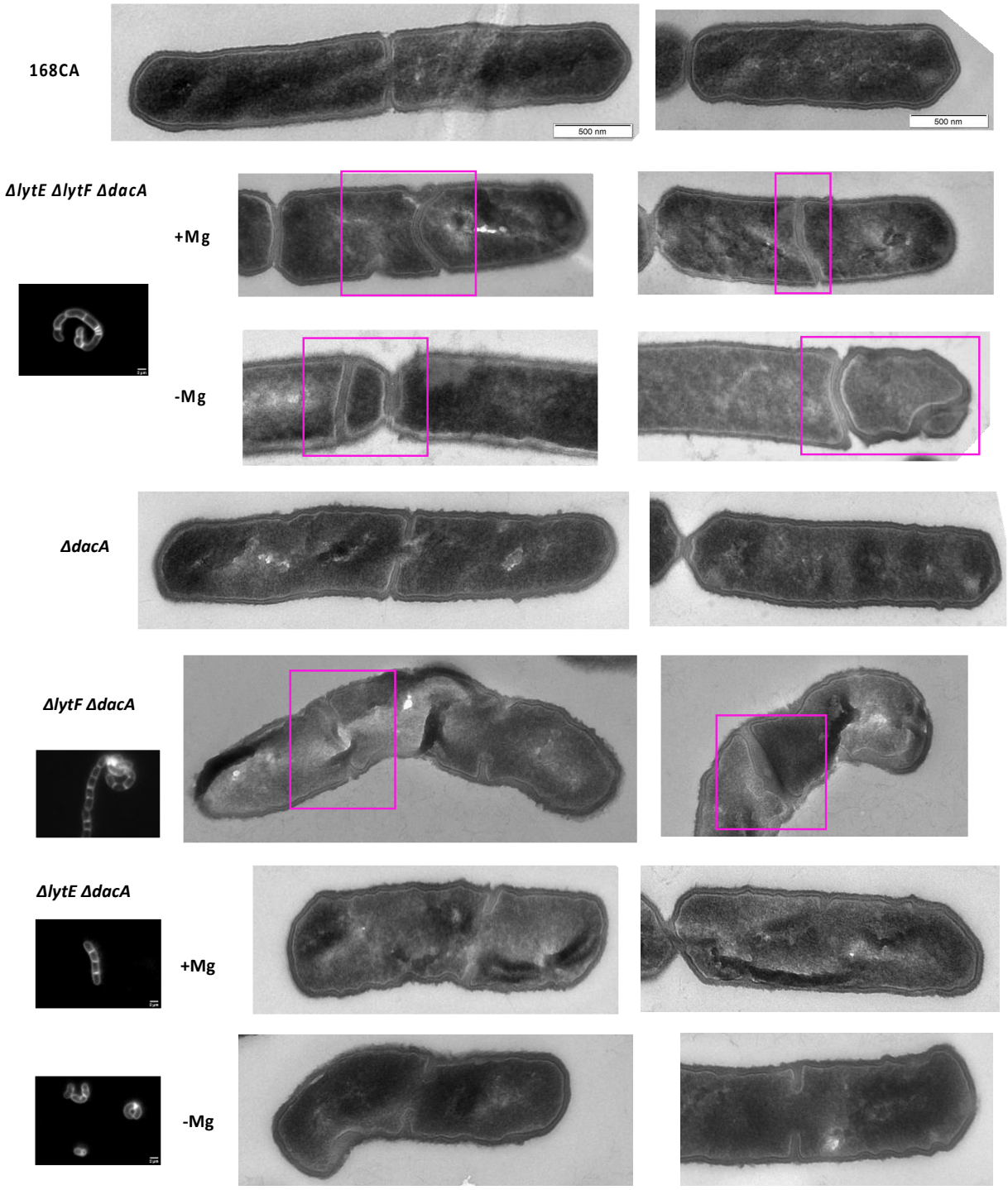

Figure 3.13 Morphological effect of the absence of DacA in different mutant combinations using transmission electron microscopy

Transmission electron images showing a closer look up to the cell wall and division sites of 168CA (WT), *ΔdacA*, *ΔlytFΔlytE ΔdacA* (-/+ 25 mM Mg^{2+}), *ΔlytE ΔdacA* (-/+25 mM Mg^{2+}), and

ΔlytF ΔdacA. The pink boxes show the abnormal changes of division sites compared to the wildtype. Bent and division defect phenotypes were also obvious by a fluorescence microscopy imaging. Scale bars represent 500 nm.

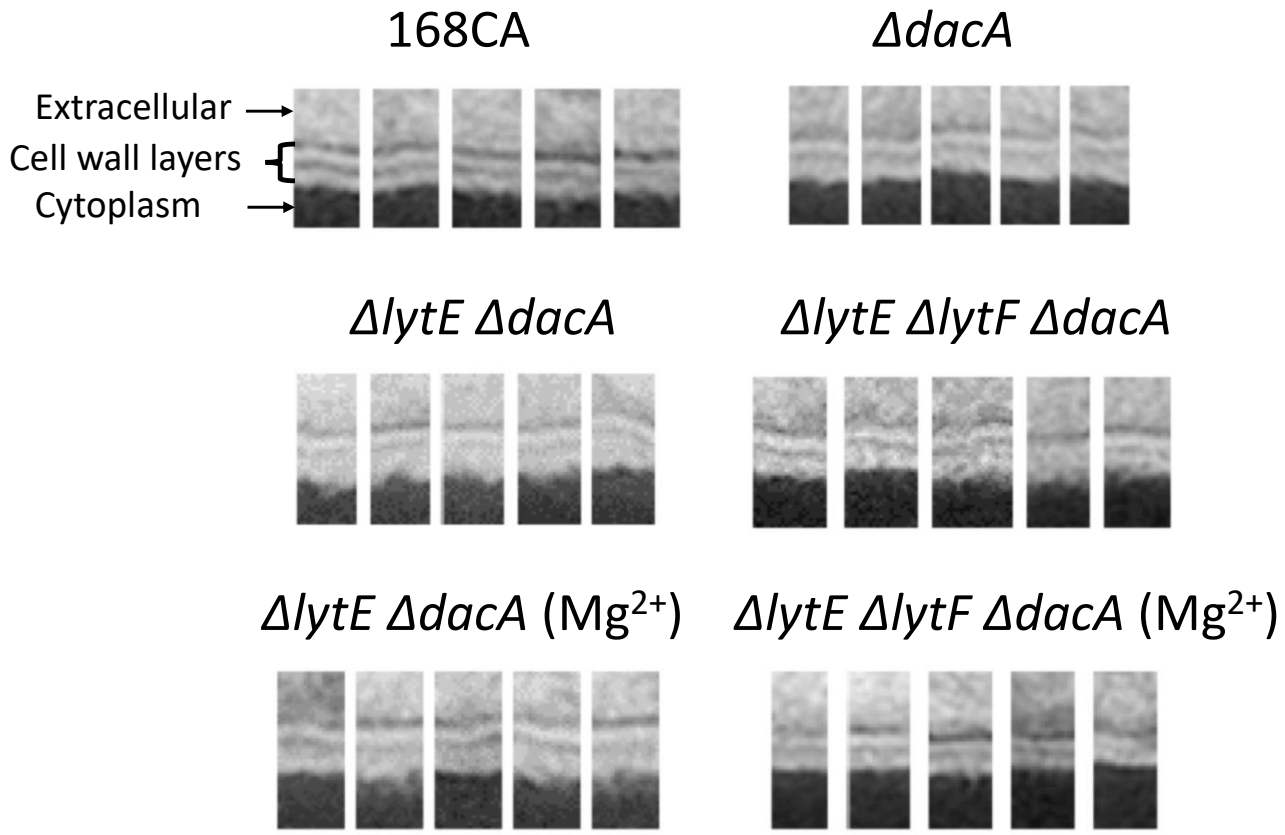

Figure 3.14 A closer inspection of the TEM images

A representative set of enlarged images of the cell wall as visualised by TEM for the following strains: 168CA (WT), *ΔdacA*, *ΔlytFΔlytE ΔdacA* (-/+ 25 mM Mg^{2+}), and *ΔlytE ΔdacA* (-/+25 mM Mg^{2+}). These images were cropped out of a collection of individual cell images for the strains. Close inspection was used to identify regions of the cell wall that appeared to have been cleaning sectioned. Each one was then rotated so it was orientated such that the cytoplasm of the cell was at the top of the image, and the extracellular material was at the bottom. In doing so, it was found that inverting the images resulted in easier visualisation of the subtle variations in grey scale, for each strain as a set of 5 cell wall sections is shown that come from different cells imaged from the same TEM grid using the same magnification and exposure settings and the images processed in the same way. Due to the processing steps used no reliable scale bar could be generated, but the features represented are clearly evident in the TEM images shown in Figure 3.13.

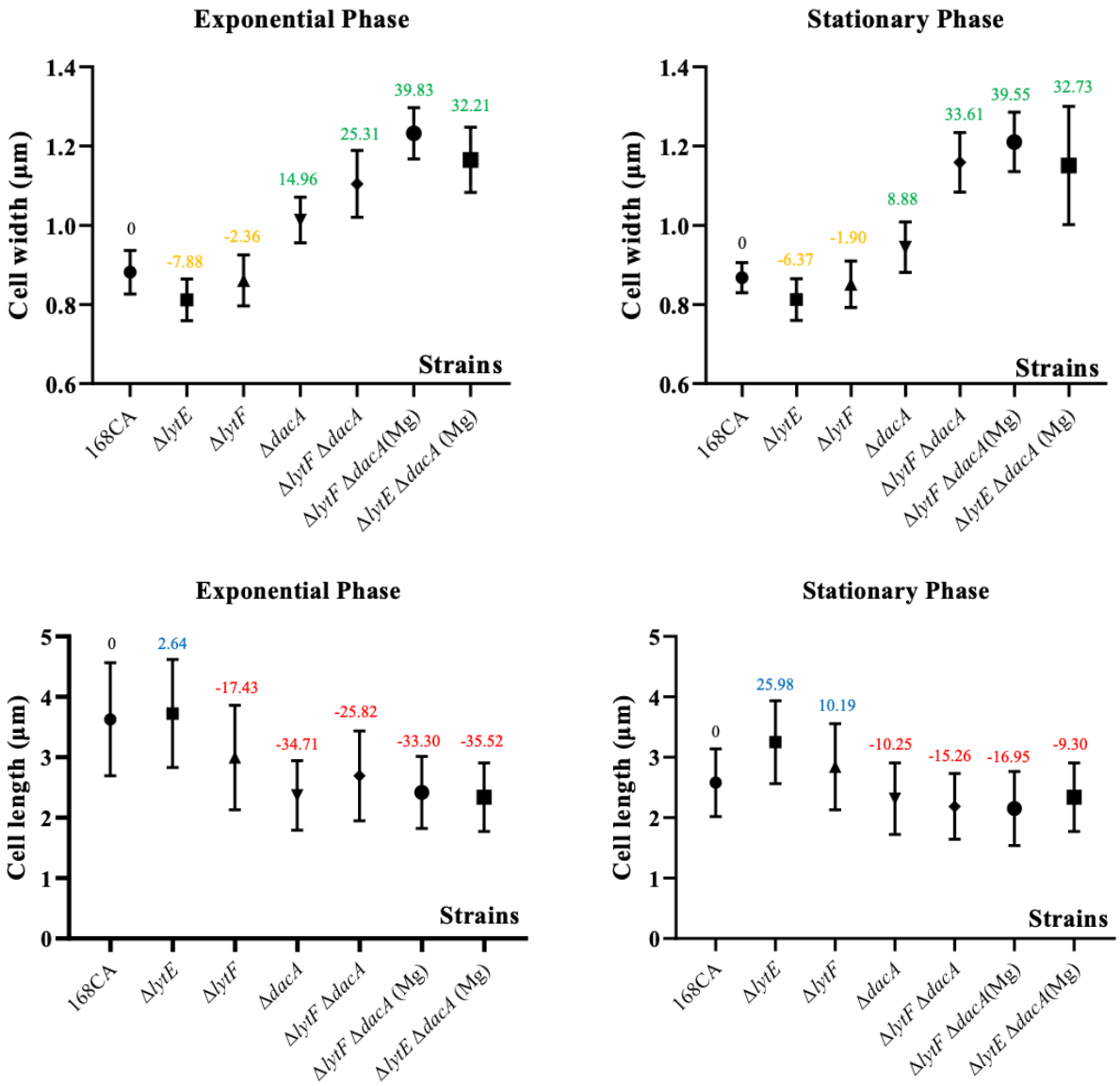

Figure 3.15 Cell size distributions of strains in *dacA* background

The graphs represent cell size distributions in mid-exponential and stationary phases of double mutants *ΔlytF ΔdacA*, *ΔlytF ΔdacA* (25 mM Mg^{2+}), and Δ*lytE ΔdacA* (25 mM Mg^{2+}) compared to 168CA and single mutants *ΔlytE*, *ΔlytF*, and *ΔdacA*. The graphs show the average and standard division of cell diameters from approximately 300 cells representing each strain. Cell measurements are in microns (µm). Coloured numbers represent the percentage of the width or length variations to 168CA. Yellow numbers indicate thinner cells, while green numbers are wider cells than 168CA. Blue numbers are longer, and red numbers are shorter cells compared to the wild type (168CA).

3.8 Muropeptide analysis

Considering the significant morphological effects seen in the mutant strains, the obvious suggestion was that the structure of the peptidoglycan was altered to some degree. To determine if this was the case, RP-HPLC analysis was used to determine the muropeptide composition of the mutant strains. For this, the cell wall of the multiple autolytic mutants was isolated and analysed in parallel with the wild type grown under the same conditions. Surprisingly, there were no significant differences between the muropeptide compositions of the multiple autolytic mutants and the wild type (Table 3.1 & Supplementary 2.1). Muropeptide identification and quantification were also done for the triple mutant *lytE lytF dacA* compared to the wild type and the single mutant *dacA*. The only noticeable difference here was the relative abundance of pentapeptide side chains, which was expected as it had been previously reported to be significantly increased in strains lacking DacA (Table 3.1 & Supplementary 2.1) (60).

Table 3.1 Muropeptide idintifications and quantitications from peptidoglycan of *B. subtilis*

Muropeptides/ strains	**168CA**	**168CA (25 mM Mg)**	***ΔdacA***	***ΔlytE ΔlytF ΔdacA* (25 mM Mg)**	***+lytE****	***+cwlO****
Sum monomers	24.59	27.66	31.59	38.12	24.27	27.74
Sum dimers	60.93	60.18	61.00	56.44	65.33	59.56
Sum trimers	10.52	9.13	6.48	4.47	6.07	6.80
Sum tetramers	1.95	1.94	1.47	0.89	1.61	2.08
Sum dipeptides	2.46	2.36	3.09	2.11	2.83	4.07
Sum tripeptides	56.32	57.41	32.57	30.91	57.03	57.89
Sum tetrapeptides	40.43	38.73	37.70	32.78	39.32	37.46
Sum pentapeptides	0.79	1.13	26.46	34.18	0.82	0.58
Degree of cross-linkage 1	38.94	37.63	35.92	31.87	37.93	35.88
% Peptides in cross-linkage 2	75.41	72.34	68.41	61.88	75.73	72.26

* Multiple vegetative autolytic mutants were created by lacking vegetative autolytic enzymes but expressing only either LytE or CwlO as the double mutant is lethal. These mutants are designated as "*+lytE*" that lacked LytD, LytG, LytC, LytF, CwlS, CwlQ, and CwlO enzymes (*ΔlytD ΔlytG ΔlytC ΔlytF ΔcwlS ΔcwlQ ΔcwlO*) or designated as "*+cwlO*" that lacked LytD, LytG, LytC, LytF, CwlS, CwlQ, and LytE (*ΔlytD ΔlytG ΔlytC ΔlytF ΔcwlS ΔcwlQ ΔlytE*).

3.9 Phenotypic effects of introducing the *dacA* mutation into other strain backgrounds

Previous studies have reported that the double mutant *lytE cwlO* is synthetic lethal (105). Another study showed that the cell shape-determining protein (MreB) is required for LytE activity (11, 231). In this study, genetic analysis has suggested that DacA might be required for CwlO activity. To be consistent with previous work, it was expected that the double mutant *mreB dacA* would be lethal or at least significantly altered. Therefore, a strain of double mutant *mreB dacA* was constructed, which appeared to grow conditionally in the presence of increased Mg^{2+} similar to the triple mutant *lytF lytE dacA* (Figure 3.16A & Figure 3.8C). It was previously known that a single mutant *mreB* exhibits minimal growth without Mg^{2+} supplementation. This phenotype was observed on the NA plate, where mutant *mreB* exhibited poor growth without the addition of Mg^{2+} as did the double mutants *lytE dacA* and *lytF dacA* compared to the wild type (168CA), mutant *dacA*, and mutant *lytE lytF* (Figure 3.16A & Figure 3.8C). Consequently, the single mutants of *mreB* and *dacA*, along with the double mutant, were tested in the presence and absence of 25 mM $MgSO_4$ in liquid and solid media to see if the growth defect was related to the absence of MreB was altered by the loss of DacA (Figure 3.16A/B). Although the growth of the single mutant *mreB* was slightly disrupted at a low level of Mg^{2+}, the double mutant *mreB dacA* was unable to grow on solid medium compared to the wild type (Figure 3.16A). The same results were observed in liquid medium; the cell growth of the single mutant *mreB* was slower than the wild type and the single mutant *dacA* (Figure3.16B, green line), and it improved when Mg^{2+} was added to the culture medium (Figure 3.16B, orange line). However, no cell growth was detected in the double mutant *mreB dacA* without the addition of Mg^{2+} (Figure 3.16B, red line). When Mg^{2+} was added to the culture medium of the double mutant *mreB dacA*, growth was observed but was slow and never reached the optical density of the other strains (168CA, *ΔdacA*, and *ΔmreB)* (Figure 3.16B, purple line). It was also found that the synthetic lethality of the double *mreB dacA* mutant was corrected by the introduction of a conditional allele of *dacA*, provided expression was permitted (AA106 strain) (Figure 3.17).

The cell morphology of the double *mreB dacA* mutant was determined by microscopy, which immediately indicated that the cells were swollen with Mg^{2+} supplementation and showed a polymorphic phenotype that appeared almost spherical when depleted of Mg^{2+} compared to the single mutant *mreB*, which exhibited only mild morphological defects (Figure 3.16C). More

detailed analyses of the cell morphology of the double mutant *mreB dacA* suggested that the cell length and width were both dramatically altered, resulting in very short and wide cells (48.08% length variation and 102.21% width variation, $p < 0.0001$, unpaired t-test) compared to the wild type and the single mutants of *mreB* (29.83% length variation and 47.05% width variation, $p < 0.0001$, one-way ANOVA followed by Tukey's HSD test) and to *dacA* (20.47% length variation-75.90% width variation, $p < 0.0001$, one-way ANOVA followed by Tukey's HSD test) (Figure 3.18 & Supplementary Tables 3.2). Thus, the synthetic lethality of the double mutant *mreB dacA* further suggested that the DD-carboxypeptidase (DacA) is involved in the CwlO system.

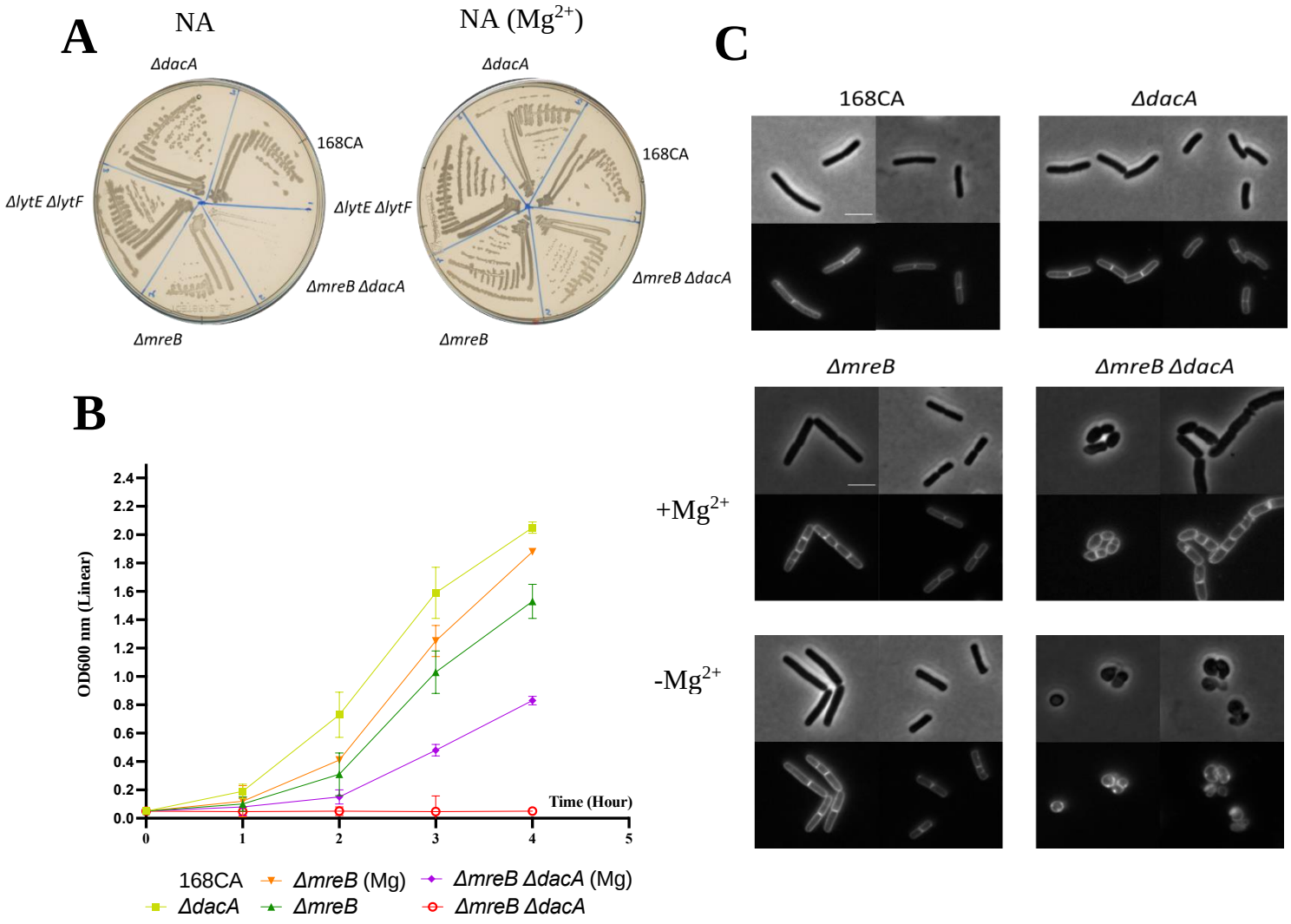

Figure 3.16 Synthetic lethality of a strain lacking both DacA and MreB

Growth comparison of 168CA, *ΔdacA*, *ΔmreB* and *ΔdacA ΔmreB* growing on: **A-** Nutrient agar plates with and without the addition of 25 mM Mg^{2+}. **B-** Growth curve of the same strains in LB cultures showing that the double mutant *dacA mreB* is lethal and dependent on Mg^{2+} to survive. Each plotted point corresponds to the average of cell growth (OD600 nm) based on three experimental replicates at the indicated time. Error bars represent the standard error of the mean. **C-** Fluorescence microscopic images show the phenotypic characterisations of 168CA, *ΔdacA*, *ΔmreB* (-/+Mg^{2+}) and *ΔdacA ΔmreB* (-/+Mg^{2+}). Scale bar is 4 microns. The cells were stained with FM5-95 dye.

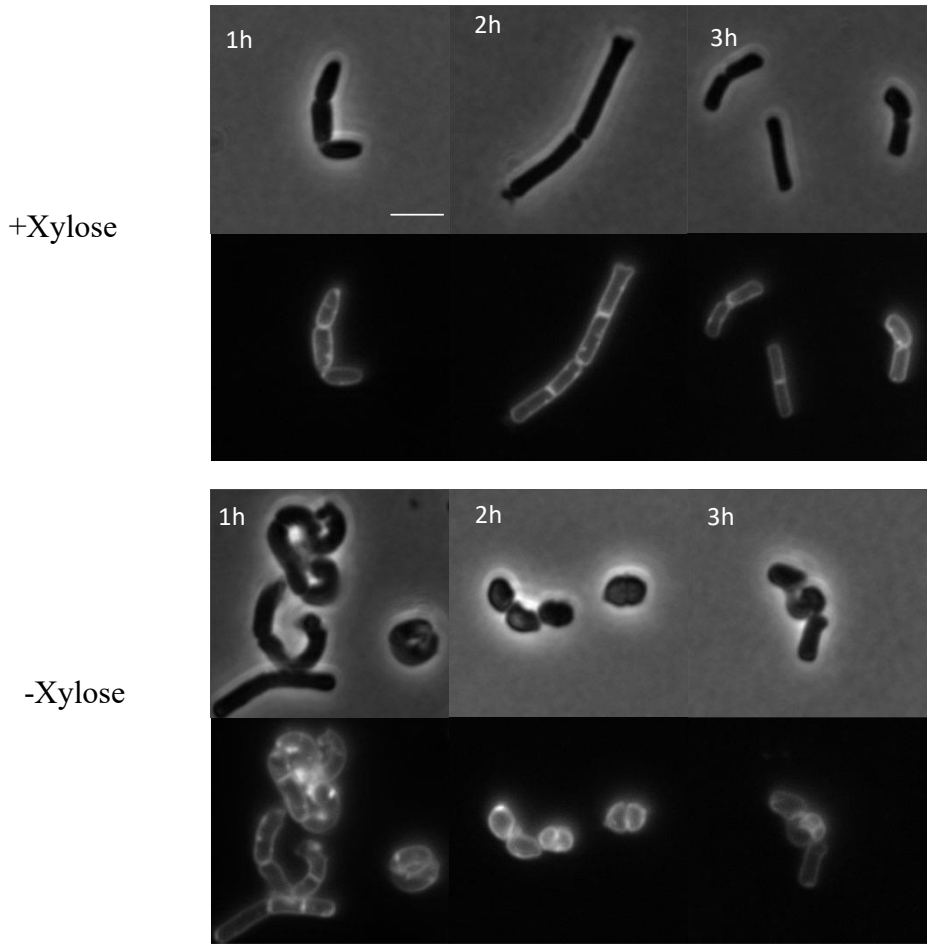

Figure 3.17 Complementing *dacA* in a mutant *mreB*

Fluorescence microscopy images of the AA106 strain, showing the *mreB* mutant with and without the expression of DacA, which is controlled by xylose induction. The imaged cells were stained with FM5-95 dye. Scale bar is 4 microns.

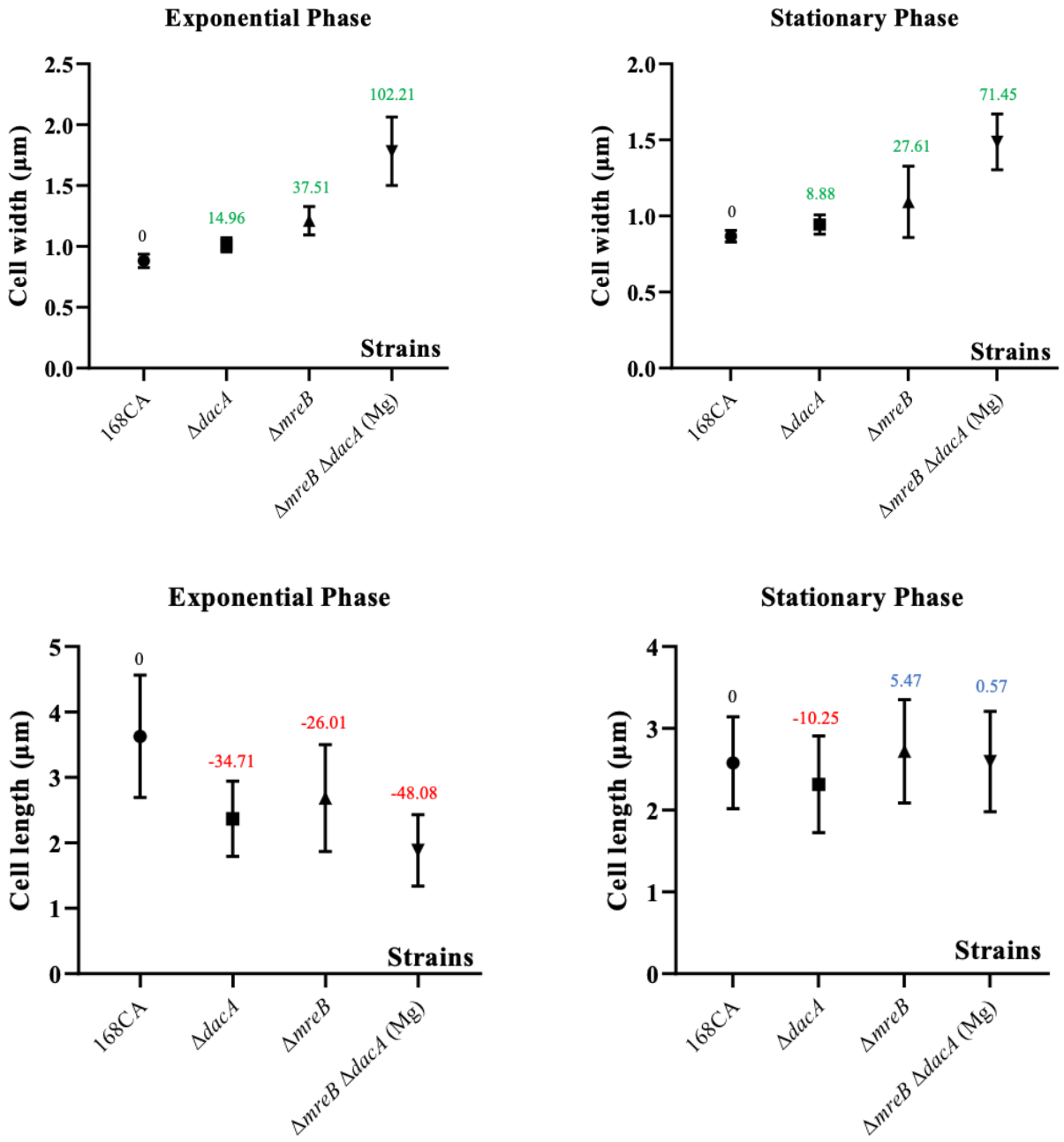

Figure 3.18 Cell size measurements of single and double mutants *dacA* and *mreB*

Cell size distributions of the double mutant *ΔmreB ΔdacA* (25 mM Mg^{2+}) measured in exponential and stationary phases compared to the single mutants *ΔmreB* and *ΔdacA*, and to the wildtype 168CA. The graphs show the average and standard division of cell diameters from approximately 300 cells representing each strain. Cell measurements are in microns (µm). Coloured numbers represent the percentage of width or length variations to 168CA. Yellow numbers indicate thinner cells, while green numbers are wider cells than 168CA. Blue numbers are longer, while red numbers are shorter cells.

3.10 Correlating the function of DacA to the CwlO-system

The earlier genetic data indicated that DacA is required for CwlO activity. In addition, when comparing the cell morphology of the *cwlO* mutant with that of the *dacA* mutant, similarities could be observed (Figure 3.19 & Supplementary Tables 3.3). The cell diameters in both strains were 18-14% wider, and in general, the cell length was 34-38% shorter compared to the wild type ($p < 0.0001$, unpaired t-test with Welch's correlation). A comparison of other mutation combinations, *lytF* with *cwlO* and *lytF* with *dacA*, showed that the length and width of the cells were very similar, with minor variation between them (3.69% width and 2.43% length, $p < 0.0001$, one-way ANOVA followed by Tukey's HSD test) and that both tended to be seen as short filaments of cells (Figure 3.20 & Supplementary Tables 3.3). However, the cell filaments of the double mutant *lytF dacA* were twisted, a phenotype that was found to be corrected to some degree by the addition of Mg^{2+}. Surprisingly, cells of the double mutant *cwlO dacA* were fatter and shorter compared to the single mutants.

These observations indicate that the CwlO autolytic enzyme could be dependent on cell wall modification, and its activity is impaired when the peptidoglycan has pentapeptides (in the absence of DacA, which removes the terminal D-alanine from the pentapeptide chain).

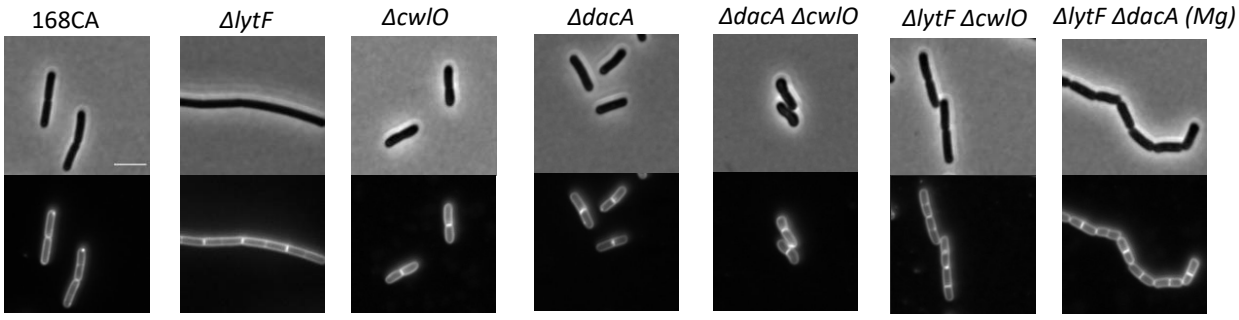

Figure 3.19 Phenotypic characterisations of *dacA* and *cwlO* strains

Fluorescence microscopy images show the cell morphology of strains lacking *cwlO*, *dacA* or both (*ΔdacA ΔcwlO*, *ΔlytF ΔdacA*, and *ΔlytF ΔcwlO*) compared to the wild type (168CA) and null mutants (*ΔlytF*, *ΔcwlO*, and *ΔdacA*) of exponentially growing cultures. Scale bar is 4 microns. The cells were stained with FM5-95 dye.

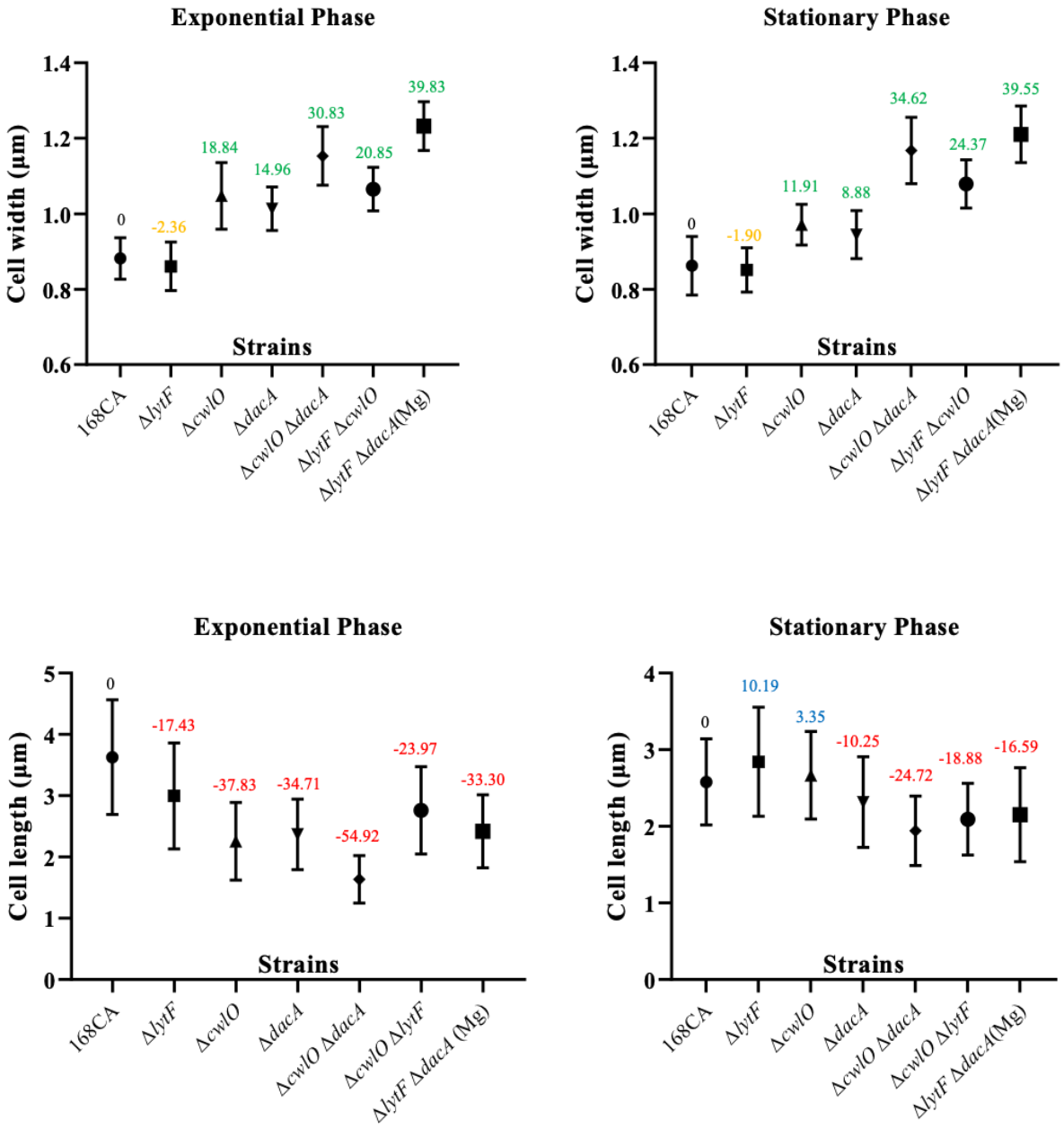

Figure 3.20 Cell size measurements

Graphs showing cell size distributions for both cell length and width. Strains of double mutants *ΔcwlO ΔdacA*, *ΔlytF ΔcwlO*, and *ΔcwlO ΔdacA* were measured and compared to single mutants *ΔcwlO*, *ΔlytF*, and *ΔdacA*, and to the wildtype 168CA in mid-exponential and stationary phases. The graphs show the average and standard division of cell diameters from approximately 300 cells representing each strain. Cell measurements are in microns (µm). Coloured numbers represent the percentage of width or length variations to 168CA. Yellow numbers indicate thinner cells, and green numbers are wider cells than 168CA. Blue numbers are longer, and red numbers are shorter cells.

However, it was also possible that, for some reason, the activity of CwlO was reduced in the absence of DacA, and the overexpression of CwlO might rescue the lethal effect of the triple mutant *lytE lytF dacA*. To test this, a second functional copy of the *cwlO* gene (fused to a *gfp*) (11) under the control of the P_{xyl} promoter was introduced at the *amyE* locus of the triple mutant *lytE lytF dacA*. The overexpression of CwlO was confirmed in the triple mutant *lytE lytF dacA* by SDS-PAGE and propped by a GFP antibody in a Western blot analysis. Two bands were detected in the wild type and the triple mutant representing the GFP-CwlO fusion (upper band) and the degraded GFP (lower band) (Figure 3.21). The phenotype resulting from the overexpression of CwlO was then initially determined on NA plates with and without xylose and compared to an NA plate supplemented with 25 mM $MgSO_4$, a condition that was known to permit growth of the triple mutant. When CwlO was expressed (on a plate with xylose), growth was partially restored compared to the other plates, although it was evident that some growth occurred on the NA plate without xylose (Figure 3.22A), which was difficult to understand. To try and resolve this and obtain a better understanding of the effects, growth was monitored in a liquid medium with and without xylose. This showed the overexpression of CwlO rescued the lethal effect of the triple mutant *lytE lytF dacA* to a limited degree compared to the wild type (Figure 3.22B, light blue line), with the culture lacking xylose eventually lysing (Figure 3.22B, red line). The cell morphology of this strain was also monitored by microscopy at the same time in the presence and absence of xylose, revealing long filamentous cells without division sites, suggestive of a division defect (Figure 3.22C).

The results obtained from the growth of the strain in liquid culture suggest that CwlO function is directly impacted by the absence of DacA activity, and it is not corrected by increasing the abundance of CwlO, implying that the dysfunction is probably related to the PG structure rather than limited enzyme activity. The fact that the growth on solid surfaces did not give the same result is concerning, but one possibility was that under these conditions, another DD-carboxypeptidase is expressed (a point addressed in the next section).

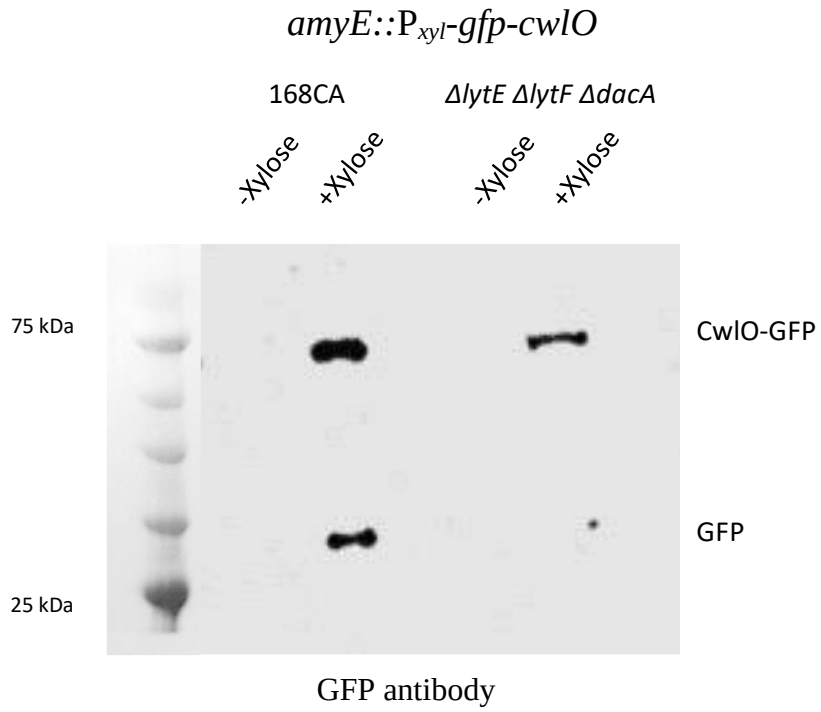

Figure 3.21 CwlO overexpression

Western blot analysis of cell lysates is shown to detect the level of GFP-CwlO expression in the following strains: *amyE::*P_{xyl}*-gfp-cwlO* and *ΔlytE ΔlytF ΔdacA amyE::*P_{xyl}*-gfp-cwlO* using a 1/1000 dilution GFP antibody. The upper bands indicated GFP-CwlO (molecular weight 77.87 kDa), while lower bands were an indication of cleaved GFP (molecular weight 27 kDa).

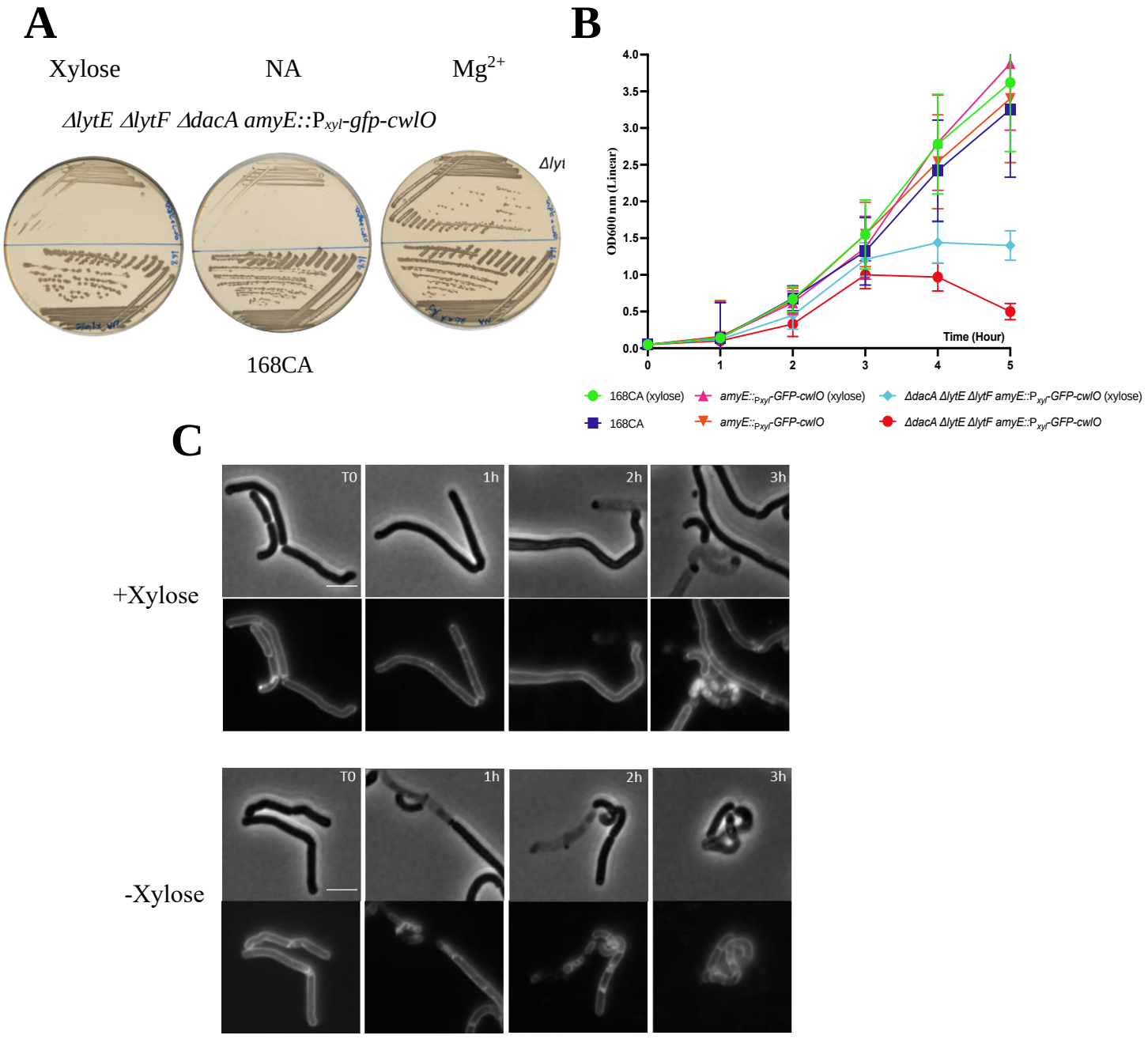

Figure 3.22 Overexpression of CwlO in a strain lacking LytE, LytF and DacA

A- Nutrient agar plates with and without xylose were inoculated with *amyE*::P$_{xyl}$-*gfp-cwlO* and *ΔlytE ΔlytF ΔdacA amyE*::P$_{xyl}$-*gfp-cwlO* strains, compared to an equally inoculated nutrient agar plate with 25 mM Mg^{2+}. **B-** Growth curves of 168CA, *amyE*::P$_{xyl}$-*gfp-cwlO* and *ΔlytE ΔlytF ΔdacA amyE*::P$_{xyl}$-*gfp-cwlO* were measured in LB with and without xylose. Each plotted point corresponds to the average of cell growth (OD600 nm) based on three experimental replicates at the indicated time. Error bars represent the standard error of the mean. **C-** Cell morphology of *ΔlytE ΔlytF ΔdacA amyE*::P$_{xyl}$-*gfp-cwlO* was monitored with and without xylose by fluorescence microscopy. Scale bar is 4 microns. The cells were stained with FM5-95 dye.

3.11 Ectopic expression of DD-carboxypeptidases

The *B. subtilis* genome encodes 4 DD-carboxypeptidases, DacA, DacC, DacB, and DacF, which are very similar. However, unlike DacA, both DacB and DacF are implicated in the correct formation of the spore wall. Conversely, DacC is a larger protein that appears to be structurally different and has no defined function. Thus, to determine if the observed effects of DacA are specific to this enzyme or if other DD-carboxypeptidase could correct the phenotype of the LytE/LytF mutants, an ectopic copy of each *dac* genes (*dacB, dacC, dacF,* and *dacA* as a control*)* was introduced under the control of the P_{xyl} promoter at the *amyE* locus in the *dacA* background, generating four different strains: AA127, AA128, AA129, and AA132 respectively. The expression of these proteins was tested by growing these strains in the presence of xylose and then using SDS PAGE in combination with Bocillin FL staining to determine the penicillin-binding protein profiles (Figure 3.23). The image of SDS PAGE gel revealed bands representing the expressed penicillin-binding proteins in cells grown in the presence or absence of xylose. Red arrows indicate bands corresponding to the position where the DAC proteins would migrate (DacA with a molecular weight of 48.47 kDa, DacB with 42.92 kDa, and DacC with 52.72 kDa). When DacC was expressed, two bands appeared; the upper band corresponded to DacC, while the lower band could be due to a secretion problem, inefficient signal peptide cleavage, or a degradation intermediate. However, these possibilities could not be further investigated as the level of expression determined was very low, making it impossible to validate the identity of the protein by any simple MS technique without significant enrichment of the protein. Nevertheless, PCR and sequencing confirmed that the gene was correctly inserted and should result in xylose-dependent expression, as was seen by Bocillin labeling. Additionally, later experiments indicated that DD-carboxypeptidase activity was potentially present (see Section 3.12).

From this test, it was evident that the ectopic constructs were functional in the presence of xylose. Bands corresponding to both DacB and DacC were also detectable in the absence of xylose in the culture medium but were minimal. Unfortunately, DacF was undetectable by Bocillin labeling, but since it has not been previously shown to bind penicillin and the sequence of the construct was correct, it is possible that expression was occurring.

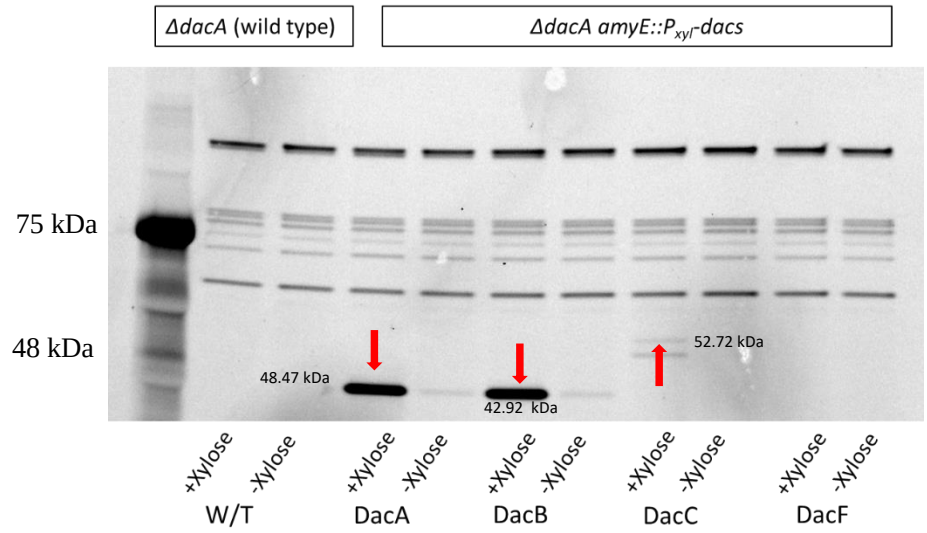

Figure 3.23 DD-carboxypeptidases expression

SDS-PAGE gel showing the PBPs labeled by Bocillin FL stain in the following strains *ΔdacA* (wild type*)*, *ΔdacA amyE*::P$_{xyl}$-*dacA*, *ΔdacA amyE*::P$_{xyl}$-*dacB*, *ΔdacA amyE*::P$_{xyl}$-*dacC*, and *ΔdacA amyE*::P$_{xyl}$-*dacF* in presence and absence of xylose. Red arrows indicate bands corresponding to the DAC proteins. The molecular weights are as follows: DacA (48.47 kDa), DacB (42.92 kDa), and DacC (52.72 kDa).

To evaluate whether the DAC proteins could substitute for DacA, the ectopic expression constructs for these proteins were introduced into the *lytF lytE dacA* strain in the presence of Mg^{2+} to ensure growth (Figure 3.24A). The obtained strains were then streaked out on NA plates with and without xylose and compared to those growing in a Mg^{2+} supplemented plate (Figure 3.24B/C). Using this test, none of the Dac proteins were found to be able to rescue the lethal effect of the triple mutant *lytF lytE dacA*, as the strains did not grow on the NA plates without Mg^{2+} or with xylose (Figure 3.24C). Thus, it has to be assumed that they either do not have the same biochemical activity as DacA or are unable to interact/localise in the cell wall in the same way as DacA.

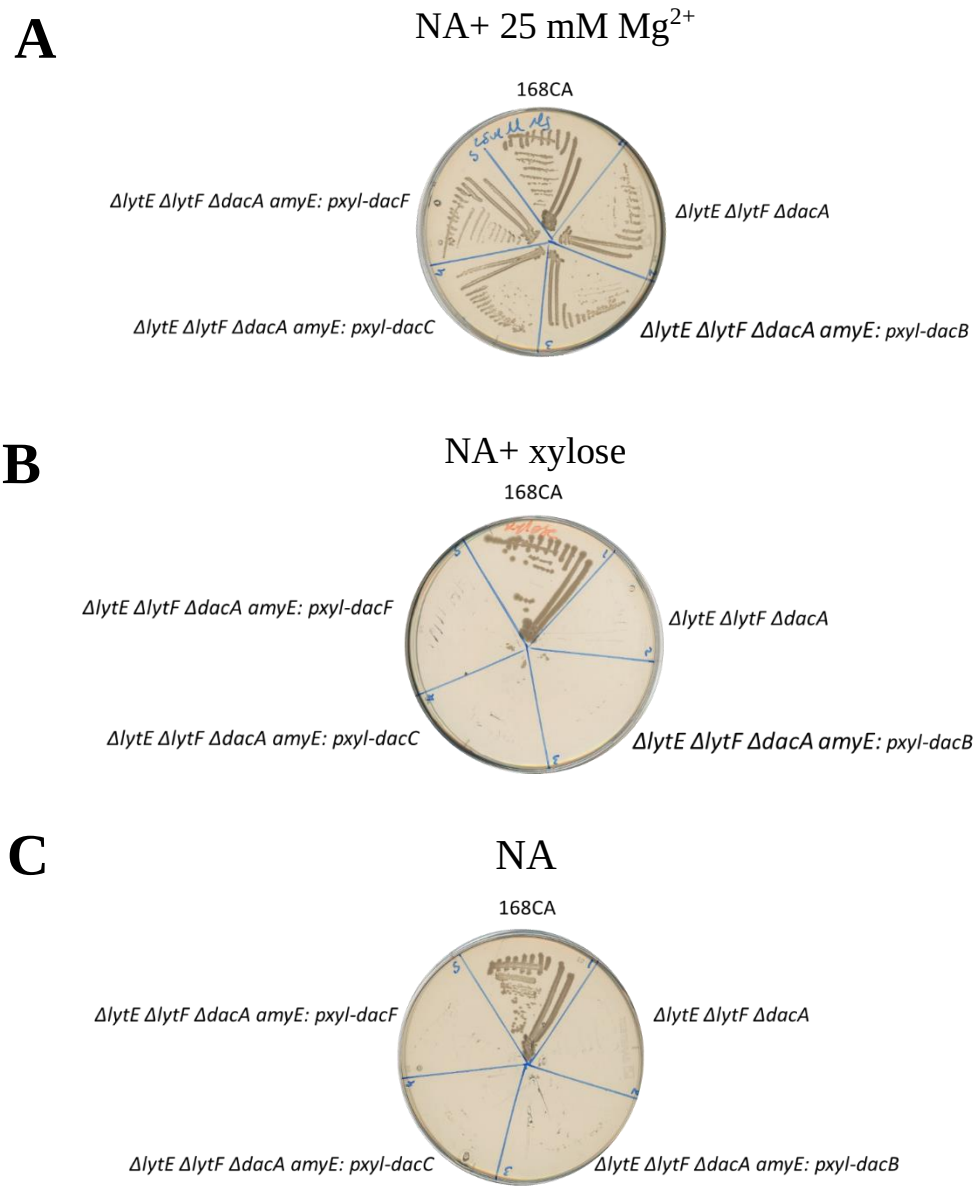

Figure 3.24 Expression of other DD-carboxypeptidases in a strain lacking LytE, LytF and DacA

Nutrient agar plates with **A-** 25 mM $MgSO_4$ or **B-** xylose were inoculated with 168CA, Δ*lytE* Δ*lytF* Δ*dacA,* Δ*lytE* Δ*lytF* Δ*dacA amyE::*P_{xyl}*-dacB,* Δ*lytE* Δ*lytF* Δ*dacA amyE::*P_{xyl}*-dacC,* and Δ*lytE* Δ*lytF* Δ*dacA amyE::*P_{xyl}*-dacF* and compared to **C-** those growing on an NA plate.

3.12 Cell wall labeling in different DD-carboxypeptidase backgrounds

To determine if the expressed Dac proteins were functional during vegetative growth, a cell wall labeling approach similar to the one used with *dacA* (as shown in Figure 3.7A) was employed. Here, the hypothesis was that if the ectopic expression of these DD-carboxypeptidases should result in the processing of the cell wall from the pentapeptide to the tetrapeptide form and the labeling of the cell wall by the fluorescent D-alanine derivative, HADA, would be altered compared to cells of a strain lacking this activity (the *dacA* null mutant). This "change" could then be detected by epifluorescence microscopy of the cells.

The strains were incubated with and without xylose for an hour, and then 20 µM of HADA was added. The cells incubated for an additional hour, allowing the incorporation of HADA with the cell wall. Excess HADA was then washed away, and the level and pattern of cell wall labeling were compared to that obtained using the same method for 168CA, *ΔdacA*, and *ΔdacA amyE::*P_{xyl}*-dacA* control strains (Figure 3.25A/B/C). From this analysis, it was clear from the images obtained that the expression of DacB resulted in a significantly reduced level of labeling (Figure 3.25D). In comparison, when DacC or DacF-expressing strains were labeled in the presence and absence of xylose, the cell wall was evenly labeled by HADA, and both culture conditions were essentially identical (Figure 3.25E/F). Interestingly, strong signals of HADA were reproducibly evident as spots on the cell wall when DacF was expressed, suggesting that the expression of *dacF* was having some effect on the cell wall but not comparable to that obtained when *dacA* was expressed (Figure 3.25F). It was also evident that mild cell morphological differences were evident in cells where DacC or DacF were expressed in vegetative growth (Figure 3.25E/F), implying that these proteins were active in a way that had consequences for cell wall metabolism but not in a way that was able to correct for the absence of DacA.

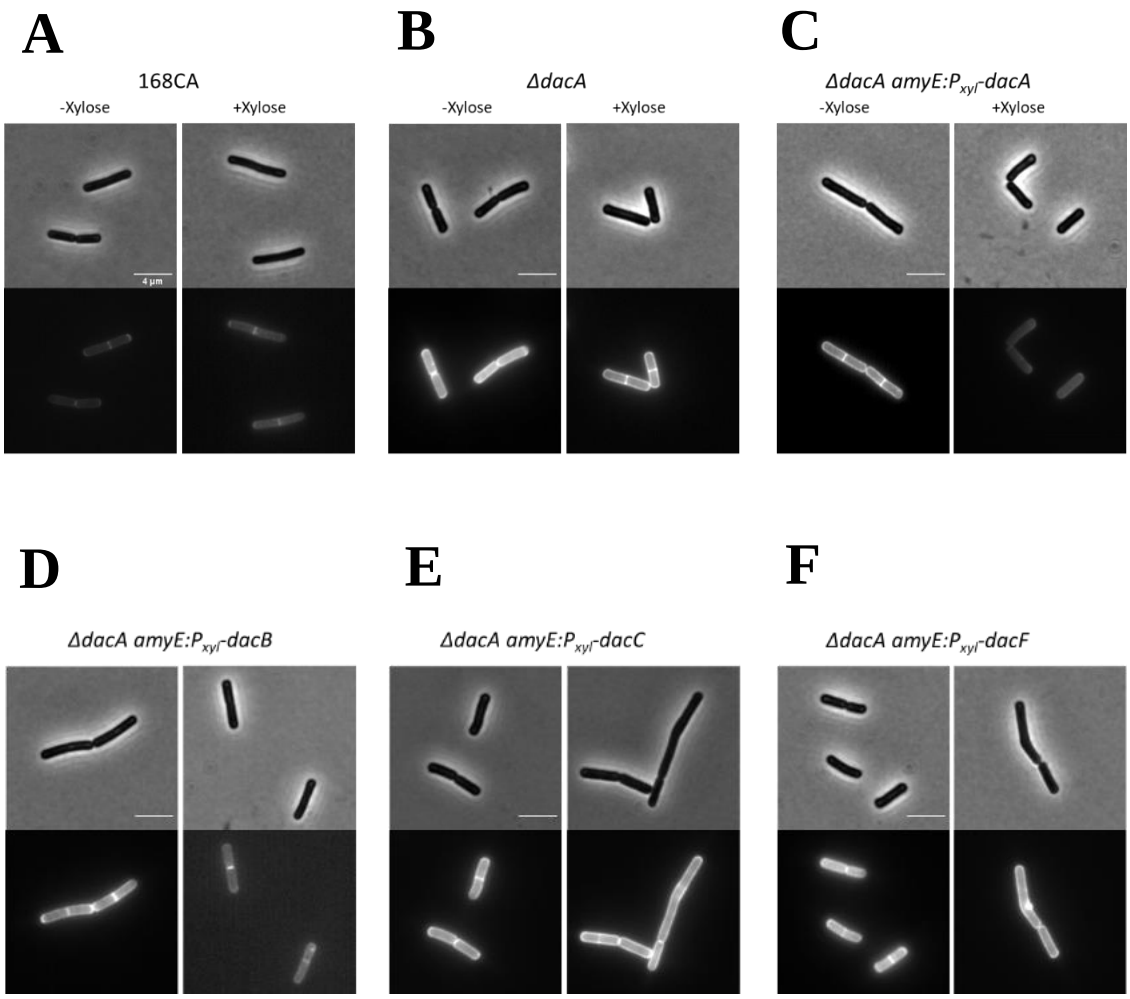

Figure 3.25 Cell wall labeling in DD-carboxypeptidase backgrounds

Fluorescence microscopy images of the cell wall labeled by 20 µm HADA of the following strains: **A-**168CA, **B-** *ΔdacA*, **C-** *ΔdacA amyE::*P_{xyl}*-dacA*, **D-** *ΔdacA amyE::*P_{xyl}*-dacB*, **E-** *ΔdacA amyE::*P_{xyl}*-dacC*, and **F-** *ΔdacA amyE::*P_{xyl}*-dacF*. HADA emits blue light. Scale bar is 4 microns. The strains incubated in LB with 20 µM of HADA for an hour, followed by washing to remove the excess HADA.

3.13 Cell wall turnover in the absence of autolytic enzymes

Since autolytic mutants can be generated in a *ΔdacA* background either normally or conditionally by adding 25 mM $MgSO_4$, we proceeded with our plan to monitor cell wall turnover in the absence of most of the autolytic enzymes expressed in vegetative *B. subtilis*. For this, we employed RADA and HADA (FDAAs) at a concentration of 20 µM (see Section 3.4).

Exponentially growing cells were first incubated with RADA for an hour to allow their incorporation with the cell wall. The excess RADA was then washed away before adding HADA to the medium. Samples were then collected at 10-minute intervals and imaged by epifluorescence microscopy. Since some strains require the addition of Mg^{2+} to survive, all samples were analysed in the presence and absence of additional Mg^{2+} as a way to have viable cells that were under the same conditions in all cases and to potentially gain an insight into the effect of Mg^{2+}.

Fluorescent images of the cells were then processed to allow the visualisation of both fluorophores in the same cell. Here, the expectation was that the red signal (RADA) would diminish as the old cell wall was lost, and the blue (HADA) would gradually increase as the new wall was synthesised and this label was incorporated. Figure 3.26A shows characteristic images of cells of the *dacA* null mutant strain sampled over time. The RADA signal was strong at T0 in all strains and reduced during cell growth until it entirely disappeared after about 60 minutes of growth. This indicated that the RADA label was not significantly recycled as the "old" wall was progressively replaced by a new synthesis. In contrast, no HADA signal was detected at T0 in any of the strains as was expected, but it started to appear as the cells grew and reached their strongest signal after about 50 minutes of growth (Figure 3.26A). This suggests that the cells were incorporating HADA from the culture medium, presumably into the newly synthesised PG. In accordance with expectations, the time taken for full HADA labeling corresponded with a generation time of the culture and more or less the time taken for the RADA signal to be lost.

The addition of Mg^{2+} on the wild-type strain (*ΔdacA)* enhanced the HADA signal, and the signal became visible sooner, suggesting that Mg might play a role in promoting cell wall synthesis or modifying the cell wall structure (Figure 3.26A). In the multiple autolytic mutant combined with mutant *cwlO*, the poles of the cells were labeled more quickly in the presence of Mg compared to cells without Mg and to the wild type. However, it was difficult to determine whether this effect was due to the chaining of the cells or other factors influencing cell morphology (Figure 3.26B). Although the addition of Mg^{2+} rescued the growth defect caused by the absence of DacA, LytE, and LytF in the multiple autolytic mutant, it did not correct the twisting phenotype observed in this strain (Figure 3.26B). Consequently, the fluorescent images of the multiple autolytic mutant combined with mutant *lytE* showed stronger signals of HADA

and RADA compared to the wild type (*ΔdacA*). This could be attributed to the tangling of the twisting cell chains, resulting in a stronger signal, or it could be due to excessive accumulation of HADA or RADA on the twisted regions of the cell chains (potentially the reason for twisting occurring). Therefore, it was challenging to determine the precise source of the signal (Figure 3.26C). To overcome this complexity, a less complicated strain (*ΔlytF ΔlytE ΔdacA*) was utilised to monitor cell wall turnover and synthesis (Figure 3.26D). The fluorescent images of this strain showed that cells arranged in mid-chains with a lesser degree of twisting compared to the multiple autolytic mutant in the *dacA* background. The cells of the triple mutant *lytF lytE dacA*, when supplemented with Mg^{2+}, exhibited cell wall turnover and synthesis comparable to the wild type; however, cells started to lysis when depleted of Mg^{2+} (Figure 3.26D).

The analysis of fluorescence intensity measurements revealed signals for RADA and HADA of the cell population. The mean relative intensities plotted in the HADA and RADA graphs indicated the collocation of signals from cells in the same field. The RADA graphs represented the turnover of the cell wall, while the HADA graphs represented the cell wall synthesis. In the case of multiple autolytic mutants combined with the *lytE* mutant, the RADA and HADA signals were erratic, regardless of the addition of Mg^{2+}, due to the twisting phenotype of the cell chains (Figure 3.27A/B). However, when combined with *cwlO*, the multiple autolytic mutant was less affected by the twisting phenotype, so the HADA and RADA signals were reasonable. Otherwise, both autolytic mutants in the *dacA* background exhibited cell wall turnover and synthesis that were similar to the wild type (*ΔdacA*). Interestingly, the triple mutant *lytF lytE dacA* also underwent cell wall turnover and synthesis in a similar to the wild type, even though cells were lytic when the Mg^{2+} supplement was depleted, although here the analysis may be biased to the cells that had not lysed (Figure 3.27C/D).

A

Δ*dacA* (25 mM Mg^{2+})

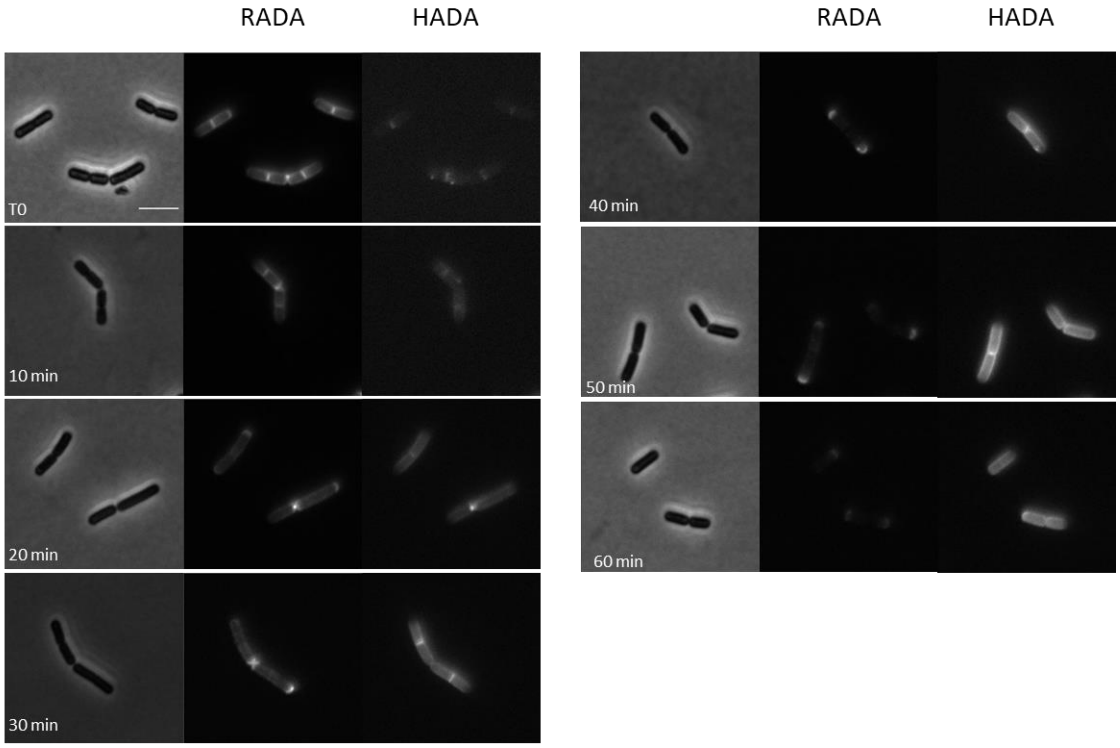

Δ*dacA*

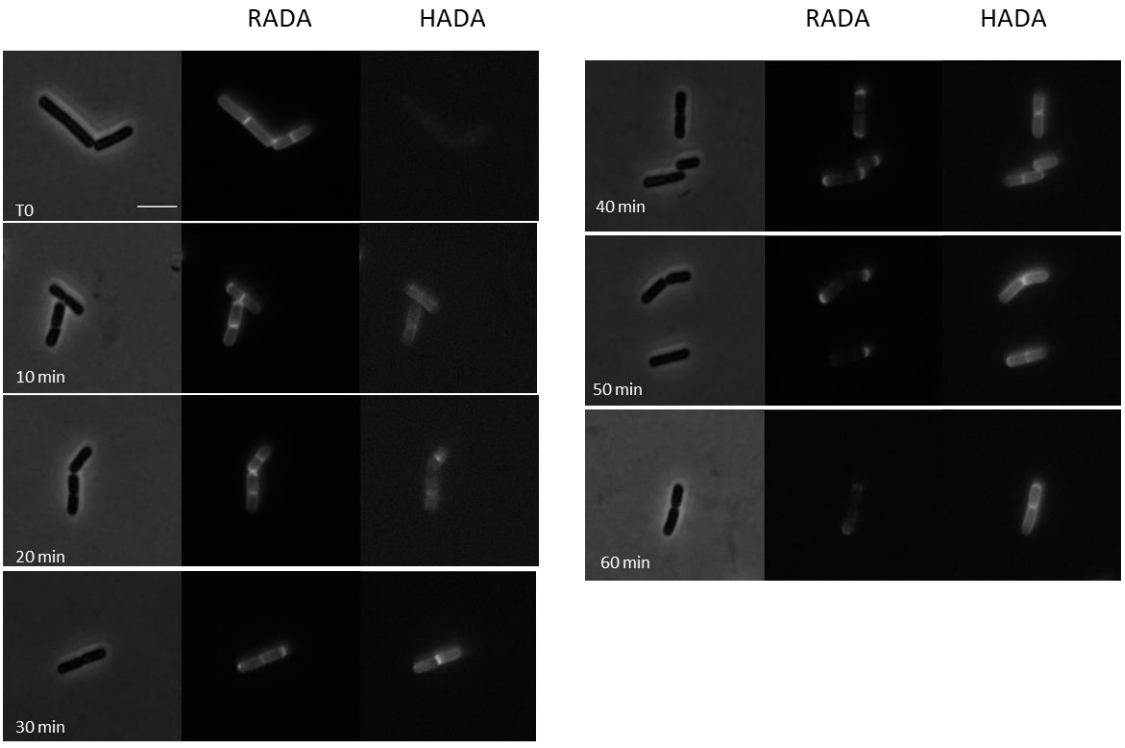

B

Δ*lytD* Δ*lytG* Δ*lytC* Δ*lytF* Δ*cwlS* Δ*cwlQ* Δ*cwlO* Δ*dacA* (25 mM Mg^{2+})

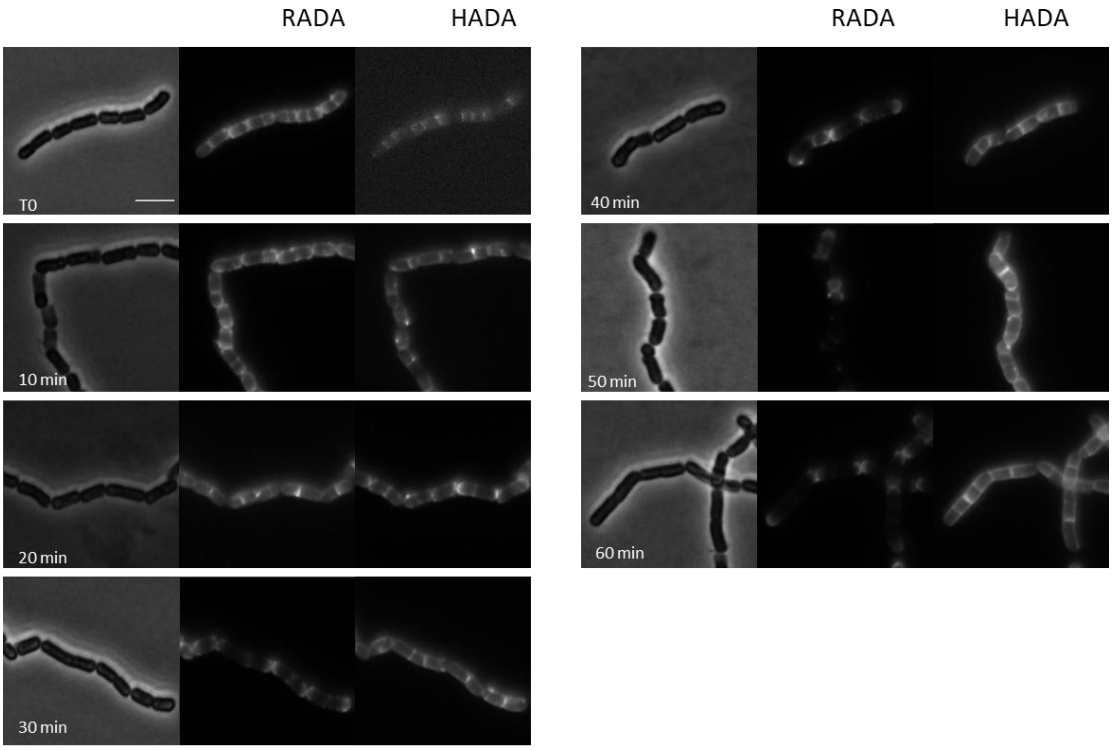

Δ*lytD* Δ*lytG* Δ*lytC* Δ*lytF* Δ*cwlS* Δ*cwlQ* Δ*cwlO* Δ*dacA*

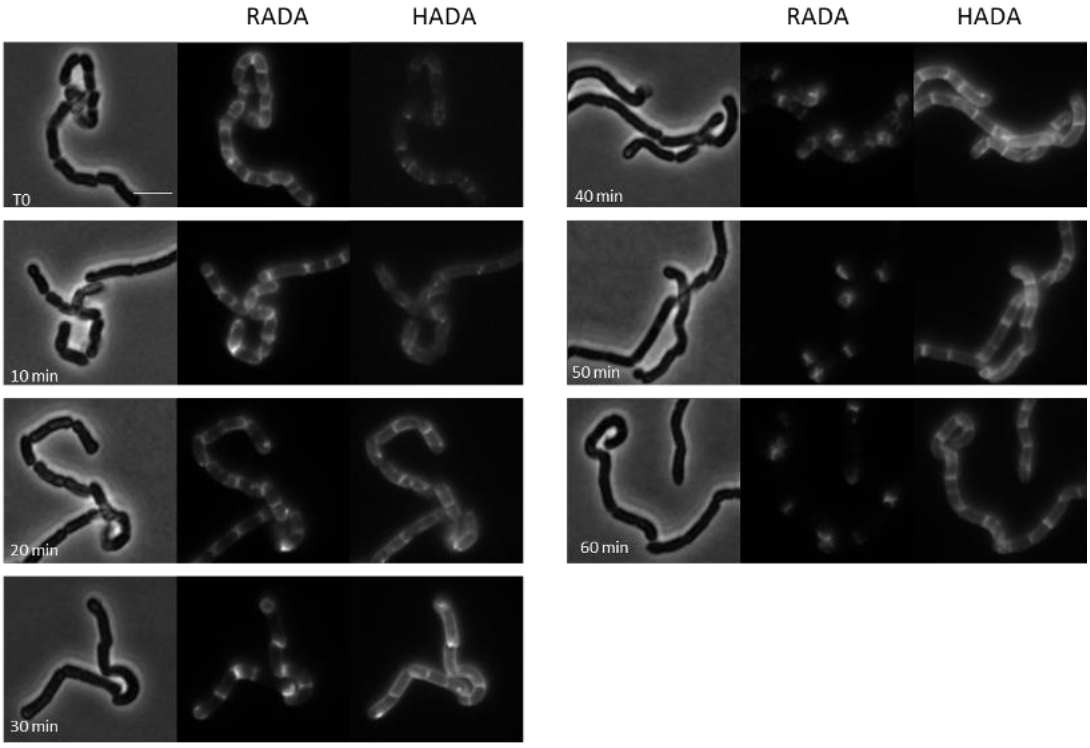

C

Δ*lytD* Δ*lytG* Δ*lytC* Δ*lytF* Δ*cwlS* Δ*cwlQ* Δ*lytE* Δ*dacA* (25 mM Mg^{2+})

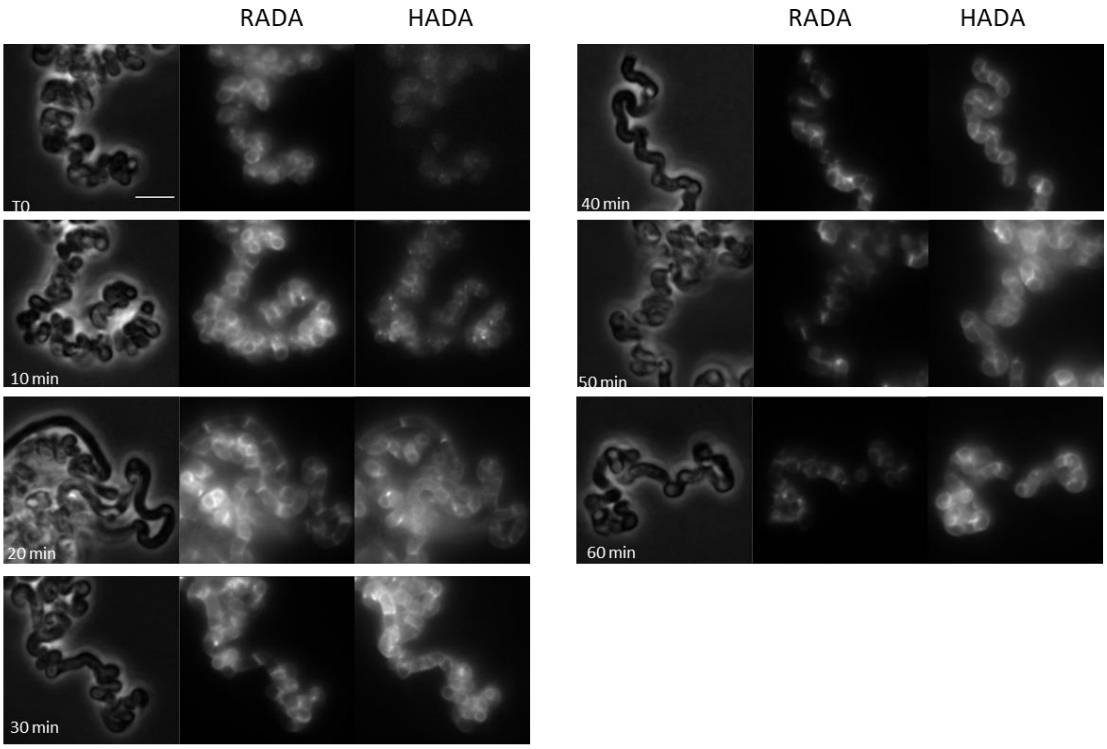

Δ*lytD* Δ*lytG* Δ*lytC* Δ*lytF* Δ*cwlS* Δ*cwlQ* Δ*lytE* Δ*dacA*

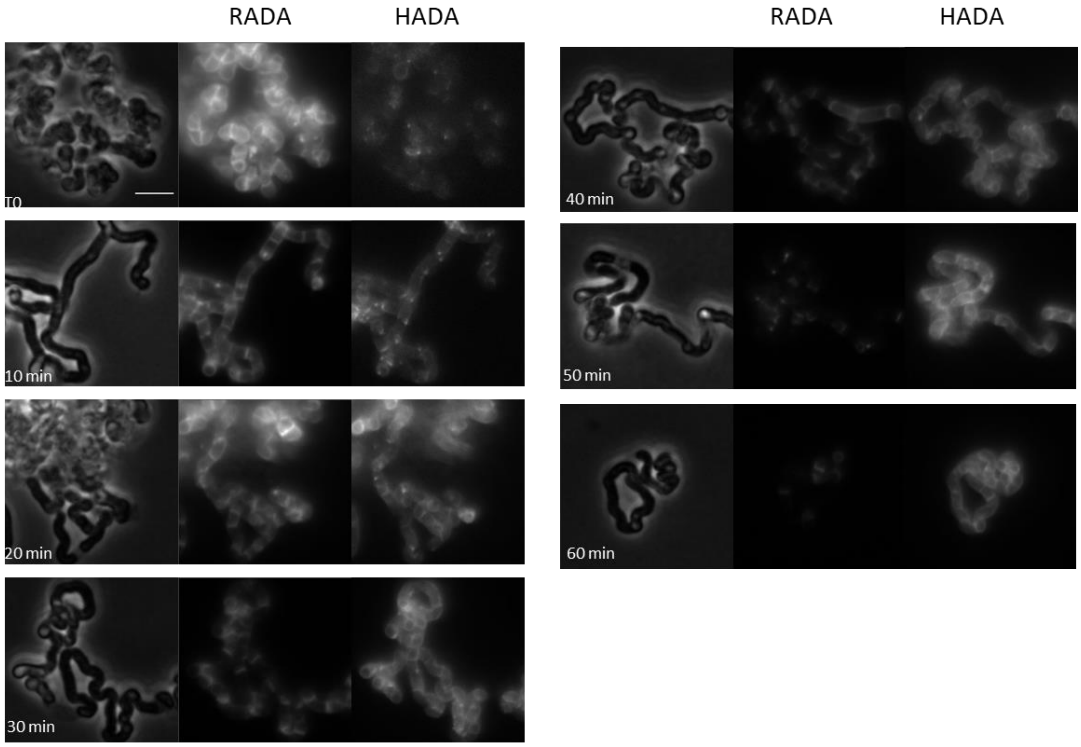

D

Δ*lytE* Δ*lytF* Δ*dacA* (25 mM Mg^{2+})

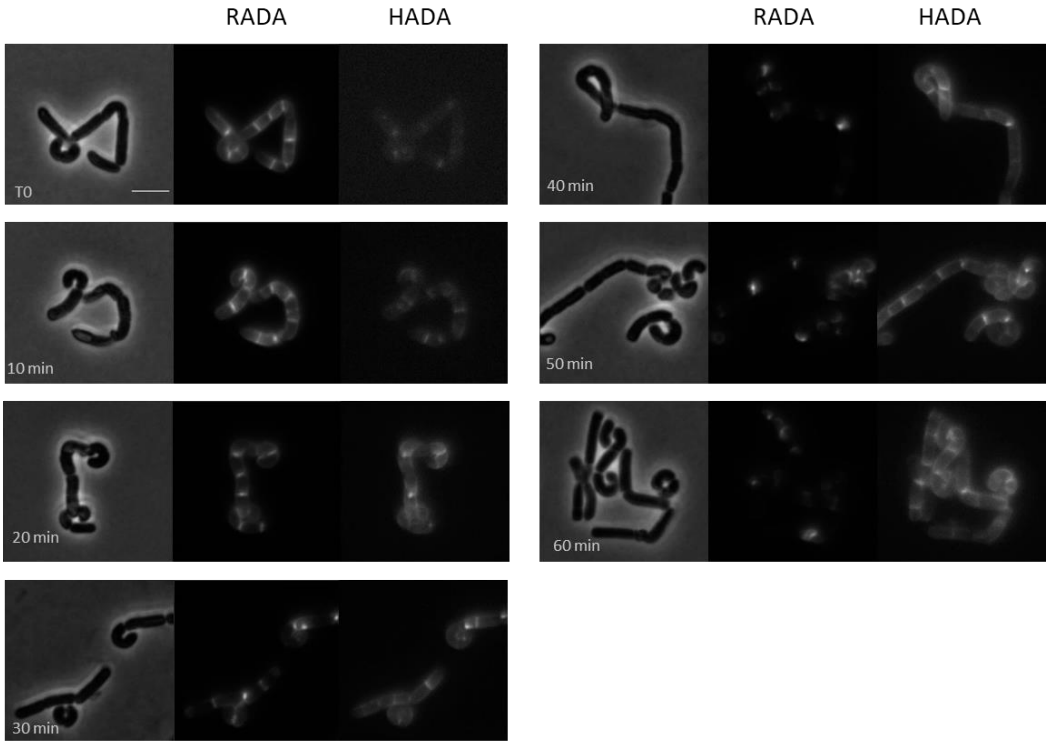

Δ*lytE* Δ*lytF* Δ*dacA*

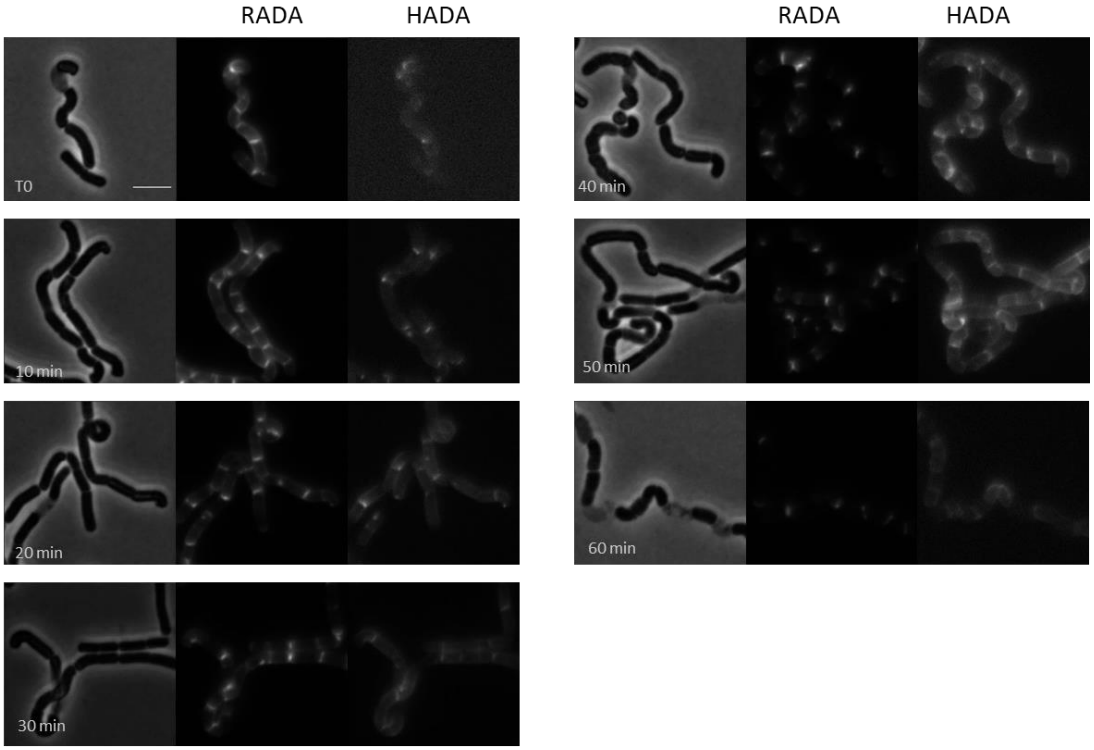

Figure 3.26 Cell wall turnover in the absence of major autolytic enzymes

Microscopy images show the cell wall turnover and cell wall synthesis in strains of **A-***ΔdacA* (wild type), the multiple autolytic mutants in *ΔdacA* background: **B-** *ΔlytD ΔlytG ΔlytC ΔlytF ΔcwlS ΔcwlQ ΔcwlO* and **C-** *ΔlytD ΔlytG ΔlytC ΔlytF ΔcwlS ΔcwlQ ΔlytE*, and **D-** *ΔlytFΔlytEΔdacA* growing with the presence and absence of 25 mM $MgSO_4$. The strains were incubated in LB with 20 μM RADA for an hour, then washed and allowed to grow in the presence of 20 μM HADA. Cell wall turnover was detected by the RADA signal emitting light in red, while cell wall synthesis was detected by the HADA signal emitting light in blue. Scale bar is 4 microns.

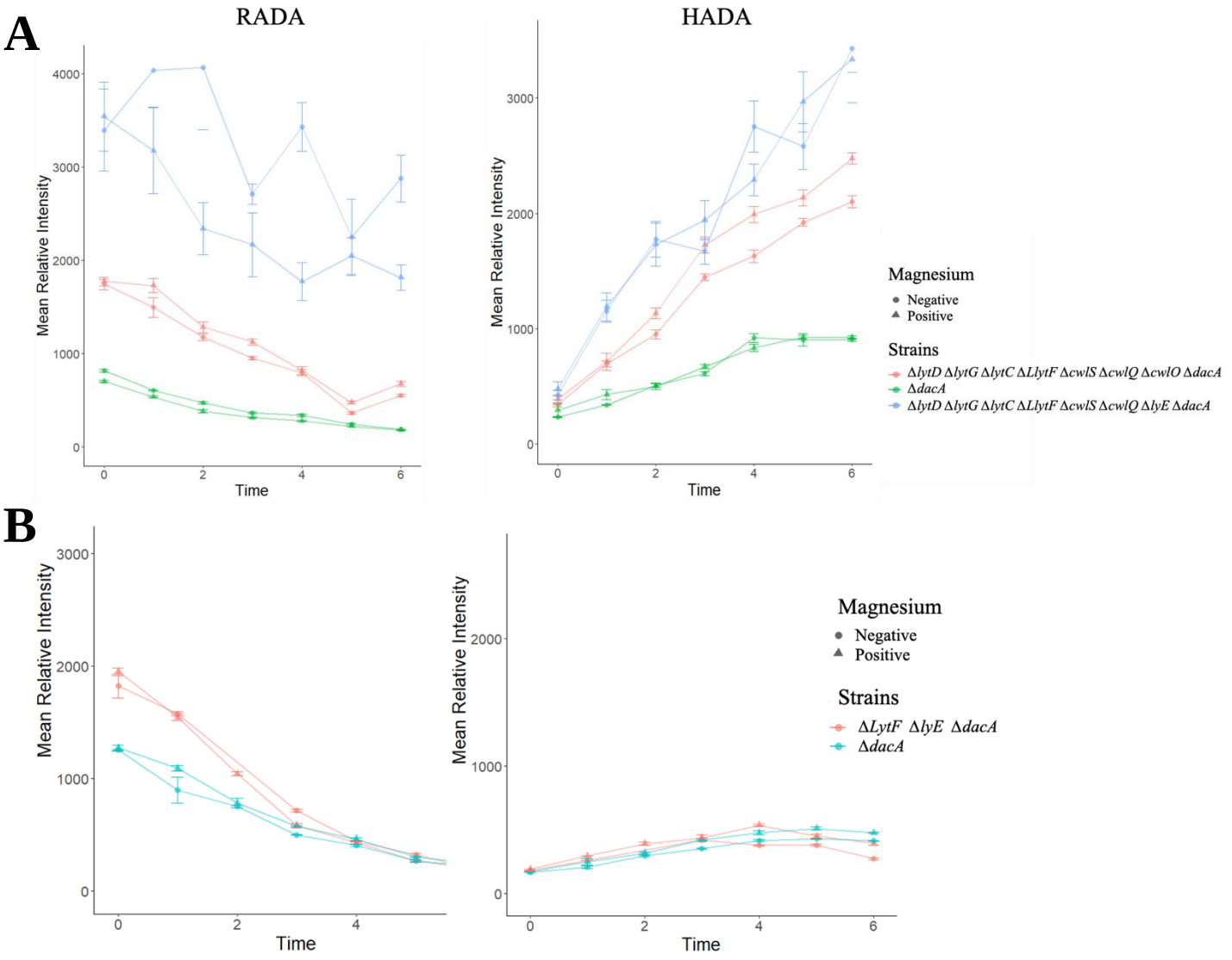

Figure 3.27 Analysis of fluorescence intensity measurements of FDAAs

Graphs represent the fluorescence intensity of RADA and HADA in *dacA* background strains: **A-** multiple vegetative autolytic mutants (Δ*lytD* Δ*lytG* Δ*lytC* Δ*lytF* Δ*cwlS* Δ*cwlQ* Δ*lytE* and Δ*lytD* Δ*lytG* Δ*lytC* Δ*lytF* Δ*cwlS* Δ*cwlQ* Δ*cwlO*), and **B-** Δ*lytF* Δ*lytE*.

3. 14 Discussion

This chapter focused on the autolytic enzymes expressed during the vegetative growth of *B. subtilis*, particularly LytD, LytG, LytC, LytF, CwlS, CwlQ, LytE, and CwlO, and their contribution to the processes required for cell growth: elongation, division, and cell wall turnover. The study used systematic deletions of these genes to define the minimum activities required for normal growth. Genetically, this confirmed that most autolysins are non-essential for cell growth, except for the semi-redundant pair CwlO and LytE, which were essential, as had been previously reported by Hashimoto (105). This observation is also supported by a recent study by Wilson and Garner (91) showing that the *B. subtilis* genome encodes a total number of 42 hydrolase enzymes, but the cell can carry out essentially normal cell growth with only LytE or CwlO. However, CwlO seems to have the most significant role on cell growth, as the cell growth of the multiple autolytic mutant combined with mutant *cwlO*, when diluted back, exhibited a significant lag in growth (two hours) before vegetative growth was initiated. This interrupted period was only detected when multiple autolytic mutant was combined with the *cwlO* allele but not *lytE*. Cell morphology analysis revealed that both multiple autolytic mutants displayed elongated cell chains that tangled, suggestive of a separation defect. Thus, one possible explanation was that the interruption in growth may result from the formation of cell clumps due to the tangled cell chains, which could potentially hinder accurate cell density measurements. However, this phenotype was observed in the other vegetative multiple autolytic mutant combined with the *lytE* mutation, which exhibited normal growth, like the wild type, as determined by optical density measurements. In addition, the viability, cell morphology analysis indicated that while most autolytic enzymes expressed during vegetative growth are redundant for cell division and separation, the absence of these autolytic enzymes led to slight variations in cell diameter, the most significant effects being observed in the absence of LytE or CwlO. According to Garti-Levi (232), cells mutated for *cwlO* were wider and shorter compared to the wild-type cells. In contrast, the cells lacking *lytE* were longer and slightly thinner than wild-type cells, with a mild effect on cell separation (233). These phenotypes were also observed in this study in any mutation combination combined with either mutant *lytE* or *cwlO*. In *B. subtilis*, cell elongation occurs through a coordinate process involving both the synthesis of new cell wall material and the breakdown of existing PG by autolytic enzymes. Two key autolytic enzymes, LytE and CwlO, are essential for this process, as they help maintain the cell shape by remodeling

the cell wall to allow for expansion. LytE and CwlO work in different areas of the cell wall: lytE is believed to function in the outer layers, while CwlO, associated with the FtsEX complex, acts in the inner layers. This difference in localisation explains the distinct changes in cell shape when these enzymes are missing. In the absence of LytE, cells become longer and thinner because the outer layer of the cell wall cannot properly expand, leading to elongated growth without an increase in width. On the other hand, when CwlO is missing, cells become shorter and wider, indicating that CwlO is crucial for the proper cross-linkage and inward pressure required for proper elongation. Without it, cells experience more radial growth, resulting in a wider and shorter shape. This complementary action of LytE and CwlO is vital for balancing cell length and width during growth. Our data further suggest that DacA, which is involved in the CwlO system, contributes to cell shape regulation, as its absence also produces shorter and wider cells. Additionally, LytF partially compensates for the loss of LytE, and its absence likewise results in thinner and longer cells. Overall, CwlO has a particularly strong influence on cell growth, with its absence causing the most significant changes to both cell length and width. The breakage of cross-linkages is believed to be mediated by LytE and CwlO. However, the mechanism by which CwlO and LytE compensate for each other's functions, considering their different locations of activity, is still not fully understood. The results presented here imply a "substrate mediated" repression of CwlO that is not seen for LytE and, as such, is an indication that their proposed functional redundancy is mediated through different mechanisms.

Surprisingly, no significant growth or change in morphology had been previously attributed to the loss of DacA (60). However, the cell morphology analysis in this study showed that DacA plays a role in controlling cell diameter. This result is supported by a recent study that employed a high-content screening (HCS) fluorescence microscopy and semi-automated techniques for measuring the dimensions of single-cell was able to analyse the cell morphology of 13 new mutations significantly altering cell diameter, and mutant *dacA* was one of them (83). Thus, DacA activity does seem to have a role in maintaining normal cell morphology that is masked by the functional redundancy of the autolytic enzymes.

However, cell diameters were notably exaggerated in the mid-exponential and the stationary phases. The single mutant *cwlO* was found shorter in the mid-exponential phase but exhibited a comparable length to the wild type in the stationary phase. In contrast, the mutant

lytE length was similar to the wild type in the mid-exponential and was longer in the stationary phase. Similar variations in cell dimensions were observed in single mutants *lytF* and *mreB*, with shorter cells during the mid-exponential and longer cells during the stationary phase. These observations perhaps shed light on the reasons behind the discrepancies in cell dimension reports across different publications. Of these, the most recent is a study by Dimitri Juillot (83) that employed high-content microscopy screening to identify *B. subtilis* genes involved in cell diameter, and their findings showed that the *lytE* mutant exhibited a phenotype comparable to the wild type. Conversely, Domínguez-Cuevas (11) reported that *lytE* mutant cells were thinner and longer compared to the wild type. The probable variations being differences in the growth medium and incubation conditions, although there is also a possibility that the genetic backgrounds used in the studies were slightly different.

Having established these morphological differences, it was surprising that muropeptide analysis by RP-HPLC revealed no significant difference in peptidoglycan profiles of the two vegetative multiple autolytic mutants and the wild type. This suggests that the autolytic enzymes LytD, LytG, LytC, LytF, CwlS, and CwlQ are not involved in the modification of the wall structure but are probably required for recycling, separation, division, and/or insertion of cellular appendages (see later chapters) where the changes may be lost in the overall average of the material analysed. CwlO and LytE were seemingly specifically responsible for cell elongation.

This study also aimed to investigate the contribution of vegetative autolytic enzymes to cell wall turnover in *vivo* by utilising fluorescent D-amino acids (FDAAs) to label newly synthesised peptidoglycan. The FDAAs are thought to be incorporated by PBPs while not actively engaged in PG synthesis through a nonproductive exchange of the terminal D-alanine of the pentapeptide; this incorporation allows new synthesis to be visualised by incorporation and turnover to be detected by loss of signal in live bacteria. Previous studies have shown that these fluorescent probes can be efficiently incorporated into the entire cell wall in the absence of DacA activity, the major DD-carboxypeptidase involved in peptidoglycan maturation during vegetative growth in *B. subtilis* (60, 226). Muropeptide analysis revealed that cells of mutant *dacA* showed a significant increase in pentapeptide appearance with a decrease in tetrapeptide chains compared to the wild type. However, it remains unclear if DacA acts to remove the labeled FDAAs, limiting labeling, or simply prevents the labeling by acting to remove the pentapeptides before

labeling can occur. However, for wild-type *B. subtilis*, labeling generally results in most of the signal being located at forming division sites and cell poles that were formed in the presence of the FDAA. To achieve more uniform incorporation of cell wall labeling and analyse the behaviour of the multiple autolytic mutants in terms of cell wall degradation, the *dacA* mutation was introduced into these mutants. This approach was intended for both microscopy and HPLC analysis. However, during the construction of the required strains, an unexpected incompatibility between the *dacA* deletion and certain autolytic enzyme deletion strains was observed. This complicated the original approach for cell wall labeling using FDAAs as the results have to be interpreted carefully as CwlO activity will be impaired. It also meant that the HPLC analysis was not completed in this work as planned. This was primarily because it was necessary to first understand the functional role of DacA in the processes under study, and later time, constraints meant that this aspect of the project was not possible.

During the constructing the double mutant *lytE dacA*, two distinct populations, dark and light colonies, were observed. The result was of different genetics outcomes from the transformation. The dark transformants were observed to have regained functional copies of *lytE,*. This suggests that during the transformation process, there was a selective pressure or a recombination event that led to the restoration of *lytE* function, enabling better growth of these transformants. However, the growth defect associated with the combination of *dacA* with *lytF* and/or *lytE* was found to be conditional on the medium composition. The addition of millimolar concentrations of magnesium to the growth medium was found to suppress the cell wall-related defects, maintain viability, and restore a more rod-shaped morphology of *B. subtills* in certain mutants. Previous studies reported that high Mg^{2+} concentrations were able to rescue cell growth and morphology defects in gene mutations for various genes implicated in PG synthesis: MreB, a cytoskeletal cell shape-determining protein (207); MreD, the shape-determining protein that is part of the Rod complex (234); and PonA, penicillin-binding protein that is required for the control of cell diameter (235-237). The reason behind these rescues is still not clear, but some theories suggest that magnesium ions may influence the activity or stability of cell wall enzymes, reinforce the sacculus by linking negatively charged groups, or stabilize the cytoplasmic membrane and associated peptidoglycan biosynthetic complexes. Additionally, *B. subtilis* has a higher tolerance for magnesium ions compared to other divalent cations, and it is generally relatively abundant in the environment (~50 mmol in seawater) (238). Other divalent cations,

such as Ca, Ba, and Ni, could potentially be used; they are associated with toxicity issues at high concentrations that can adversely affect cell growth and viability (239-242). Excessive Fe^{2+} or Mn^{2+} is also toxic to the bacterial cell (243). In contrast, Mg^{2+} does not exhibit such regulatory complexity or toxicity, making it a more straightforward and reliable choice. Therefore, $MgSO_4$ was selected due to its historical efficacy, compatibility with *B. subtilis*, and lack of adverse side effects, making it the most suitable choice to test for cell viability and minimize potential confounding variables related to metal ion toxicity or regulatory interactions.

Fluorescent and transmission electron images revealed abnormal cell morphologies in strains lacking DacA in *lytE* background, generating bent cells and twisted cells in *lytF* background. The addition of the Mg^{2+} supplement was able to correct the binding phenotype in the *lytE* background, demonstrating the crucial role of Mg^{2+} in cell morphology. However, it was unable to correct the twisting phenotype in the *lytF* background. Although the addition of Mg^{2+} was able to rescue the lethal effect of the triple mutant *lytE lytF dacA*, cells still grew slower in very twisting chains compared to the wild type. When cells of the triple mutant were depleted of the addition of the Mg^{2+} supplement, they were able to grow to a certain degree and ultimately lysed. This could be explained as the cells were using the remaining Mg^{2+} from the old culture or trying to survive by the low concentration of Mg^{2+} used in the fresh LB medium. Taking advantage of this, we looked at these cells under this condition (depleting of Mg^{2+} supplement) using fluorescence and transmission microscopies, revealing abnormal division sites that might lead to their lysis.

The absence of DacA impairs the function of the CwlO system, as evidenced by genetics and the similarity in cell morphology observed in both the *cwlO* mutant and the *dacA* mutant. Additionally, the *dacA* mutant showed reduced efficiency in transformation, which underscores the intricate relationship between cell wall remodeling and competence. This observation aligns with the findings of Liu (227), which highlighted that deletion of CwlO or LytE results in severe impairment of transformation efficiency and downregulation of ComK. Notably, since CwlO activity relies on the FtsEX transporter (111), the deletion of *ftsX* similarly affects transformation efficiency and ComK expression (227). Competence pili are essential for DNA uptake during transformation, and their proper assembly requires effective peptidoglycan remodeling. Our findings suggest that the reduced transformation efficiency observed in autolytic enzyme mutants

could be due to disruptions in competence pilus assembly. Autolytic enzymes create the necessary structural modifications in the cell wall, allowing competence pili to traverse and facilitate DNA uptake. When these enzymes are impaired, the competence pilus cannot be properly assembled or function effectively, leading to a significant reduction in transformation efficiency. Previous studies, such as those by Young (196), have long suggested that autolytic enzymes are integral to competence development in *B. subtilis*. Young observed a correlation between autolytic activity and competence, proposing that these enzymes create local gaps in the peptidoglycan layer, facilitating DNA uptake. This correlation was further supported by similar findings in group H streptococci by Ranhand (197) and expanded upon by Guillen (65), who demonstrated that competence development is co-regulated with autolytic activity and flagellar assembly. An indirect link between competence and peptidoglycan metabolism in *S. pneumoniae* was identified through a signaling pathway that controls both PBPs and competence (198). Our study corroborates these early findings, revealing that mutations in autolytic enzymes such as LytE and CwlO, or their regulators (DacA and FtsX), impair transformation efficiency. This reinforces the role of peptidoglycan remodeling in competence for effective transformation. The connection between peptidoglycan remodeling and competence is not unique to *B. subtilis*. Similar processes have been observed in Gram-negative bacteria. For example, in *H. influenzae*, competence genes are clustered with a gene involved in peptidoglycan metabolism (PBP1a), and inactivation of these genes significantly reduces transformation efficiency (200). This indicates a conserved mechanism across bacterial species. In *Neisseria gonorrhoeae*, natural transformation competence is closely linked to piliation, with several type IV pili assembly genes also crucial for transformation, supporting the idea of a pseudopilus in *B. subtilis* competence (201, 202). Additionally, Tpc and ComL in *Neisseria gonorrhoeae* are necessary for transformation and may function similarly to peptidoglycan hydrolases in other bacteria (201, 202). These proteins are thought to assist in DNA transport across the peptidoglycan layer, suggesting a broader role for peptidoglycan-modifying proteins in competence development. However, to this date, this concept has not been directly tested and is a direction of future work that has been revealed by this project.

Further investigation revealed that disrupting LytE activity in mutant *dacA* background resulted in synthetic lethality, similar to what was previously observed by Hashimoto (105) in the double mutant *lytE cwlO*. MreB, a protein that determines cell shape, is required for LytE

activity, according to studies by Kawai (231) and Domínguez-Cuevas (11, 231). The synthetic lethality of the double mutant *mreB dacA* suggests that both proteins are essential for cell growth and survival. The observation of nearly cocci-like cells in the double mutant further supports the role of MreB in cell shape determination and further suggests that DacA is required for the proper functioning of the CwlO system in maintaining cell morphology. These observations suggest that some autolytic enzymes are dependent on modifications to the cell wall and that CwlO activity is impaired when the peptidoglycan has pentapeptides without the terminal D-alanine removed by DacA.

However, the overexpression of *cwlO* was able to rescue, to a certain degree, the growth defect caused by the absence of LytF, LytE, and DacA as the cells eventually lysed. Increased CwlO activity supports cell elongation, leading to the formation of long filamentous cells due to a defect in cell division, but was insufficient for sustained cell growth. This seems to imply that CwlO activity is reduced when the cell wall contains a significant level of pentapeptides, and that increases the abundance of the enzymes.

This study highlights the complexity of the cell wall regulatory network, emphasizing the interplay between cell wall modification and degradation enzymes and the importance of multiple factors working together to maintain cell shape and integrity.

Additionally, it was observed that the GFP used to tag the CwlO was separated, presumably resulting in an untagged CwlO in the 168CA background. This separation raises concerns about the previous experiments using this organism and a GFP-fusion to determine cellular localization. However, for the work described here, this is not a major issue, as the objective was to increase the abundance of "active" CwlO. Cleavage of GFP can occur either during physiological degradation/turnover of the protein or within the artificial link between the protein and GFP. Several approaches could be considered to address this issue: fusing the GFP tag differently to the N-terminal or use of a C-terminal fusion to the protein, if functional, might resolve the issue; determining at what stage the cleavage occurs, for instance, immediately processing cells in SDS lysis buffer and running on a gel might indicate if GFP remains attached or is already cleaved off. If cleavage occurs during sample preparation, modifying the method to minimize protease activity (e.g., using protease inhibitors) might be necessary. Careful consideration of these factors is essential to ensure the accurate interpretation of results and the

reliability of conclusions drawn from experiments involving GFP-fusion proteins. A similar observation was made for the DacA fusion with GFP (See Appendix 1).

3.14.1 Proposed model of DacA/CwlO system

Our proposed model for the CwlO and DacA system comprises several stages (Figure 3.28). Initially, newly synthesised peptidoglycan material is polymerised and deposited into the innermost layer of the old cell wall (Figure 3.28A). At the same time, penicillin-binding proteins use the energy from the D-alanine donor peptide to link the newly formed tetrapeptide with neighbouring pentapeptide, facilitating cross-linkage between the nascent and pre-existing peptidoglycan (Figure 3.28B). Following that, DacA (PBP5) becomes active and cleaves the fifth peptide (D-alanine), forming mature peptidoglycan (Figure 3.28C); this is then followed by the action of LdcB, which removes another D-alanine to leave a tripeptide. Finally, CwlO, a cell membrane protein, identifies the mature peptidoglycan and becomes active, cleaving the bond between the second (D-glutamic acid) and the third (*meso*-diaminopimelic acid) peptides, resulting in modification of the cross-linkage of the peptidoglycan (Figure 3.28D). The proposed model provides insights into the complex process of peptidoglycan synthesis and degradation in *B. subtilis* and seems to have parallels in other bacterial spp., in that CwlO and the proteins it interacts with are conserved, and DD-carboxypeptidases are also generally present. Interestingly, the loss of DD-carboxypeptidases activity in *E. coli* has been reported to result in unexplained morphological defects that may be relayed to the results obtained for Bacillus.

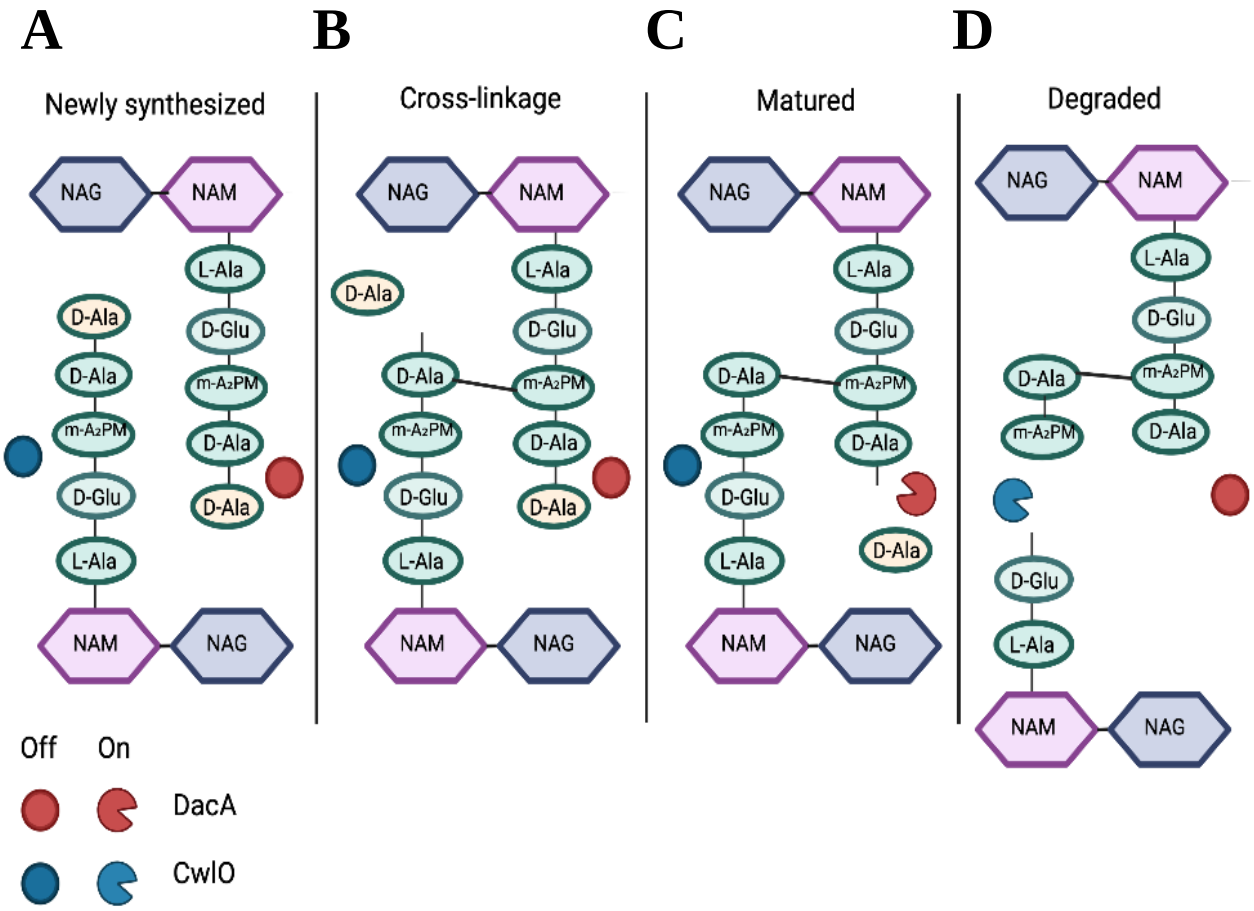

Figure 3.28 Schematic representation of the cell wall synthesis and turnover regulation in *B. subtilis*

Proposed model of the CwlO and DacA system. **A-** Newly synthesised material of peptidoglycan is polymerised and deposited into the innermost layer of the cell wall. **B-** The cross-linkage reaction mediated among the new material and pre-existing material by penicillin binding proteins using the energy of the donor peptide D-alanine to link the newly formed tetrapeptide with the neighbouring pentapeptide. **C-** DacA (Penicillin binding-protein 5) becomes active and cleaves the other 5th peptide to give matured peptidoglycan. **D-** CwlO (cell membrane protein) recognises the matured peptidoglycan and becomes active, cleaving the bond between the second (D-glutamic acid) and the third peptide (*meso*-diaminopimelic acid), resulting in degraded peptidoglycan. The illustration created was with BioRender.com.

3.14.2 DD-carboxypeptidases of *B. subtilis*

B. subtilis possesses four DD-carboxypeptidases (DacA, DacC, DacF, and DacB) that contain a very high sequence similarity to D-alanyl-D-alanine carboxypeptidase enzymes that have been biochemically characterized (87, 89, 244). DacA is the major DD-carboxypeptidase during

vegetative growth and is required for peptidoglycan maturation (6, 60, 83). However, DacB and DacF enzymes are different from DacA as they are expressed in the later stationary phase and are essential for proper spore wall development (86). While DacC is also expressed during stationery and sporulation phases, its function remains unknown (89). Even though DacB, DacC, and DacF share a very high sequence similarity to DacA, they could not compensate for DacA function as they were unable to rescue the lethal effect of the triple mutant *lytF lytE dacA*.

Sporulation relies on the degradation of the division septum and has its own autolytic system, as well as DacF and DacB that are expressed after division and are required for the correct formation of the spore wall. There is a possibility that these Dac proteins are targeted to the cell pole, which might alter the FDAAs labeling in the DacA background when expressed, potentially making the pole unlabeled. Interestingly, the expression of DacB was found to partially compensate for the loss of DacA function, as evidenced by poor labeling of the cell wall with the HADA fluorescent dye, which was similar to the labeling pattern observed in 168CA cells. This suggests that DacB is able to do DacA's function in cell wall modification "maturation" but not sufficiently to fully complement the loss of DacA. When DacC or DacF were expressed in the *dacA* mutant background, the cell wall was fully labeled by HADA, indicating that these enzymes are either not active in the removal of the terminal D-alanine on the pentapeptide or require some other factor to function. The observation of strong HADA signals at specific spots on the cell wall upon DacF expression suggests that cell wall modification may occur unevenly or in localised regions. This raises the possibility that DacF may be involved in spatially regulated cell wall modifications or that it acts in a more localised manner compared to DacA and DacC. The mild defective phenotypes observed upon ectopic expression of DacC or DacF in the DacA mutant seem to support this idea, but further analysis is required to confirm this observation.

3.14.3 Cell wall turnover and synthesis in the multiple autolytic mutants

The morphological defects behind the absence of most vegetative autolytic enzymes resulted in the formation of elongated chains, and the absence of DacA, LytE, and/or LytF resulted in a twisting phenotype affected the cell wall labeling by FADDs as the cell chains were tangled. It was observed that the multiple autolytic mutant combined with the *cwlO* mutant was less

affected by these phenotypes, likely due to the presence of LytE. Otherwise, the analysis of fluorescence intensity estimated similar rates of cell wall turnover and synthesis in both multiple autolytic mutants. However, to mitigate the potential accumulation of FADDs due to phenotypic complications, a less complex strain (Δ*lytF* Δ*lytE* Δ*dacA*) was utilised. Although the addition of Mg^{2+} helped restore cell growth, it did not fully resolve the issue, as cell morphology remained affected. Surprisingly, the triple mutant demonstrated normal cell wall turnover and synthesis despite the inability of cells to survive without Mg^{2+} supplementation. These findings suggest that none of the deleted autolytic genes were necessary for cell wall turnover and did not impact cell wall synthesis.

Previous studies have reported conflicting findings regarding the role of specific autolytic enzymes in cell wall turnover. For instance, Blackman (92) reported a decrease in the rate of cell wall turnover in a strain lacking the major amidase protein LytC. The same study found that the double mutant *lytD lytC* significantly reduced the rate of cell wall turnover, while the single mutant *lytD* had no impact on turnover. In contrast, Margot and Karamata (245) revealed that the absence of LytC delayed the release of radiolabeled wall material without affecting the turnover rate. Additionally, it was discovered that the endopeptidase LytF also plays a role in peptidoglycan turnover (92). A study by Wilson and Garner (91) has found that a strain lacking all 40 autolytic enzymes except CwlO and LytE showed no detectable cell wall turnover activities, indicating that LytE and CwlO were not directly involved in cell wall turnover. Thus, *B. subtilis* is capable of normal growth by relying on the cleavage of bonds for expansion without requiring extensive cell wall turnover processes.

Indeed, the cell wall labeling results in this study were limited due to the twisting phenotype observed in the examined strains. The accumulation of the FDAAs dye around the twisted chains or overlapping signals can lead to false signals and hinder accurate interpretation of the labeling data. These complications in cell wall labeling emphasize the challenges and limitations associated with studying cell wall dynamics and turnover in complex mutant backgrounds.

Chapter 4
Flagellum Assembly Through the Dynamic Cell Wall

4.1 Introduction

The cell wall defines the cell shape and is dynamic in that it is restructured during cell growth. It must also be modified to allow large cellular complexes, such as pili and flagella, to pass through without lysis. Among these structures, the flagella are the best characterised and are composed of a basal body embedded in the membrane and linked to the PG, providing a structural anchor, a rod that passes through the wall and links the basal body to the universal joint (hook), and a propeller-like filament. In *S. typhimurium* and *E. coli*, a specific autolytic enzyme is present (FlgJ) to allow the rod to pass through the peptidoglycan, presumably acting to "drill" through the wall and allow flagellar assembly (184, 185). However, in *Bacillus*, no gene corresponding to FlgJ is present in the flagellum operon, and it is unclear how the flagella are inserted.

Various hypotheses have been generated to explain the insertion of an appendage, such as flagella, through the thick multi-layered cell wall of *B. subtilis*. In simple terms, the flagella could be inserted actively by "drilling" a hole through the cell wall using the action of an autolytic enzyme, as is known in other species, or it could be more passive and depend on a normal growth process of cell wall synthesis and turnover (Figure 4.1A). In the latter case, the flagellar rod structure would be assembled in a newly formed wall and then pass through the cell wall linked with the peptidoglycan layer as it progresses to the outer surface through the normal molecular remodeling of the peptidoglycan (Figure 4.1B). A consequence of this would be that the "flagellum appearance" would be slow, comparable to the time taken for the complete turnover of the cell wall to allow it to progress to the outside. An alternative option might be, as suggested by a study in *E. coli* (246), in which the flexible peptides have the ability to adjust and deform in the direction of the long axis (247), and the glycan strands are arranged in a zigzag line to provide a layer with small pores (tesserae). These tesserae would then permit the basal rod of the flagella to push through the cell wall without the need for specific cutting of the PG crosslinks. This suggestion would work nicely in *E. coli*, which has a thin peptidoglycan layer and would involve passing through only one or two such "holes". However, in *B. subtilis*, it would be more complicated as there are multiple layers of peptidoglycan, requiring alignment of the tesserae in each layer. This mechanism would, however, allow for rapid assembly of the full flagellum structure, with minimal autolytic activity directly associated with the process.

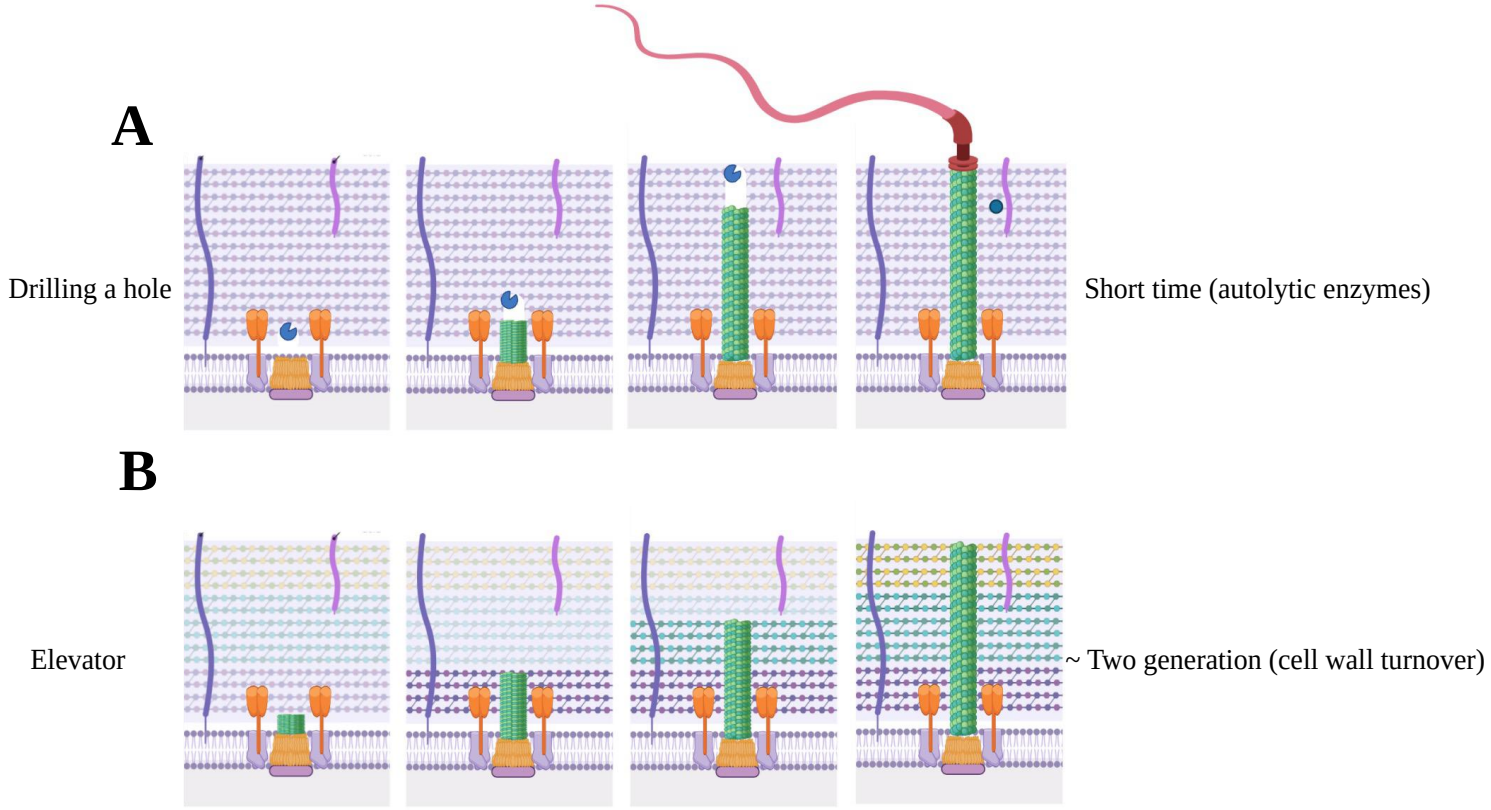

Figure 4.1 Postulated pathways of the flagellar rod

The postulated pathways of the flagellar rod reaching the outer surface of the cell wall either by **A-** drilling a hole through the peptidoglycan layers relying on autolytic enzyme activates (short time) or **B-** depending on the cell wall turnover system. As the cell wall undergoes turnover and new peptidoglycan layers are synthesised, the flagellar structure is elevated along with these layers. The lighter layers correspond to the old peptidoglycan, while the dark layers represent the newly synthesised peptidoglycan that carries the rod structure. In this scenario, the flagellar rod is incorporated into the growing cell wall from the inside to the outside (slow, about two generations). This illustration was created with BioRender.com.

Thus, this part of the project was to determine how the flagellum passes through the cell wall. The results shown in this chapter show that the flagellar assembly depends on a combination of enzymes, where one seems specific to the flagellar assembly (CwlQ) and the other is related to bacterial growth (CwlO). As such, it is apparent that no single autolytic enzyme is solely responsible for flagellar insertion, and it is possible that this is because the mechanisms function for several "appendages" (such as pili and DNA translocation systems, including the competence apparatus) and are to some degree functionally redundant, a common feature for many processes related to the cell wall in *B. subtilis*.

4.2 Initiating flagellar synthesis

In *B. subtilis* cells, flagella are not present throughout the entire growth cycle. Instead, they are assembled as a response to environmental conditions, particularly during periods of starvation. To study how the large, complex structure of the flagellum is inserted into the dynamic cell wall, it became necessary to develop methods that could induce cells to initiate flagellar assembly in a significant proportion of the cell population. In a standard growth medium like LB, flagella production is mainly seen to occur in the late stationary phase of growth, and the cells can also adapt to enter other developmental processes, e.g., sporulation, competence, and secondary metabolite production. To avoid these complications, two approaches were investigated. The first involved utilising a simple nutrition shift of exponentially growing cells in an LB medium to a glucose-rich nitrogen-limited medium (PTM), where it has been observed over time that a significant proportion of the cells becomes motile (described in Section 4.2.1). The second option was to genetically manipulate the strain to artificially express the genes required for flagellum biosynthesis (detailed in Section 4.2.2). These two methods were expected to result in the initiation of flagellum synthesis and formation of flagella on the cells. However, for this work, the requirement was to have the process "induced" in all cells as synchronously as possible to facilitate further investigation into the mechanisms of their assembly and insertion into the dynamics cell wall.

4.2.1 Induction of flagella using minimal medium

To test flagellar stimulation in a minimal medium using pre-transformation medium (PTM), we used a combination of scanning electron microscope (SEM) to image the cell wall surface of 168CA (Figure 4.2A/B) and the mutant *fliM*, as well as visualising the localisation of GFP fusions of some of the components of the flagellum basal body. The cells were prepared by growing overnight cultures in LB and then diluted back in both LB or PTM. The diluted cultures were incubated with shaking at 37 ºC for 40 mins, and then the cells were either directly visualised by phase contrast microscopy or fixed to be visualised under SEM. Preliminary experiments have shown that shifting an exponentially growing culture to the PTM media treatment resulted in the cells becoming motile, as determined by phase contrast microscopy. In contrast, growth and suspending the cells in fresh LB did not result in any obvious motility until

the culture reached the late stationary phase (Figure 4.2A). What was observed was a little unexpected in that the medium shift seemed to rapidly result in the formation of flagella. The cells become flagellated with complete long flagella within approximately 40 minutes (Figure 4.2B), and this was seen for a significant proportion of the cells examined (approx. 99%). These observations were initially made by looking for motile cells in liquid suspension, but later analysis looking at the localisation of flagellar subunits (see Section 4.3) confirmed the initial results and showed that assembly of the flagellum occurred earlier, and true motility, referring to the active swimming of the cells, was not evident until the culture was incubated for a longer period.

The analysis of SEM images of the cell wall surfaces of both the flagellated strain (168CA) and the non-flagellated mutant strain (*ΔfliM*) was used to confirm the initial visual observations and determine whether any indications of deformation in the cell wall were present where the flagella come out of the cells (Figure 4.2B). Consequently, the visual analysis was primarily focused on identifying cell surface features present on flagellated cells (168 grown in PTM), which were absent in cells lacking flagella (168 in LB) or in those genetically incapable of producing a flagellum (a FliM null mutant grown in PTM). However, the analysis of these SEM images did not reveal any clear changes in the area where flagella would be expected to emerge from the cells. In other words, there were no apparent deformations or noticeable differences in the cell wall structure between the flagellated and non-flagellated strains. It was challenging to precisely locate the origin of a flagellum on the cell surface in these samples.

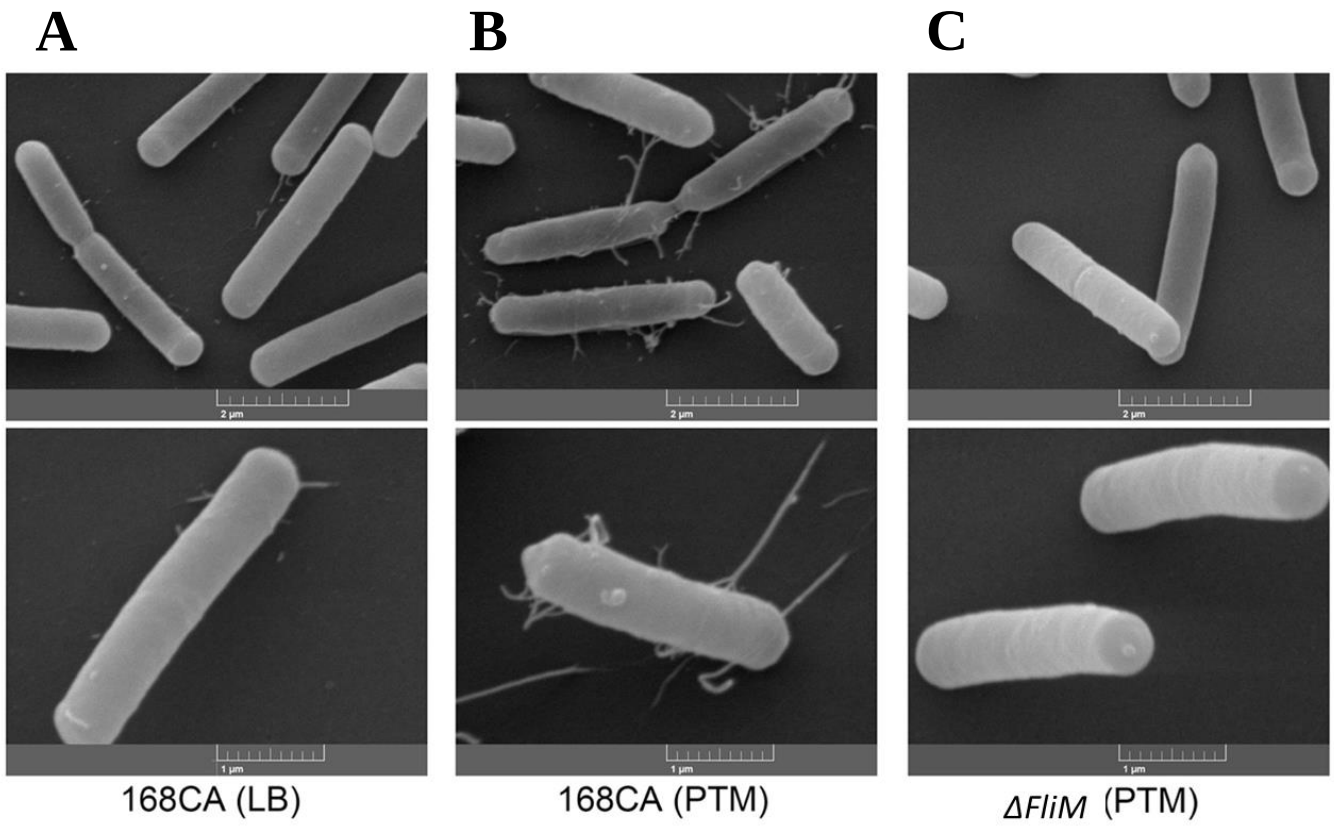

Figure 4.2 Flagellated and non-flagellated cells

Scanning electron microscopy images of: **A-** 168CA (flagellated strain) in LB. **B-** 168CA (flagellated strain) in PTM. **C-** *ΔfliM* strain (non-flagellated strain) in PTM. Scale bars represent 2 microns or 1 micron.

4.2.2 Inducible constructs

Utilising media shift from LB to PTM to stimulate the flagella worked reasonably well, but it was evident that the process of shifting between the two media resulted in a change in growth rate, presumably caused by the manipulation and the altered nutrient. This might potentially cause problems for later experiments where we wanted to relate the flagellum localisation and growth of the cells (see Chapter 5), so an alternative was to construct a strain where the flagellum gene expression was controlled by a repressible promoter that we could activate by a simple addition of an inducer to the culture medium and so avoid disrupting the culture growth. In order to construct a strain that is inducible for the expression of flagella (P_{xyl} inducible strain, $P_{fla/che}\Omega P_{xyl}$-$_{fla/che}$), a xylose promoter was introduced before the $P_{fla/che}$, replacing the P_{D3} (Figure

4.3A). Thus, a fragment of pRD96 containing P_{xyl} and a chloramphenicol resistance cassette was ligated to the amplified fragments of *codY* with a *Bam*HI tail and *flgB* with an *Xba*I tail (Figure 4.3B). It is important to note that *flgB* is the first gene of the *fla/che* operon, while *codY* is the gene immediately upstream of the *fla/che* operon. The ligated fragment was then used to transform 168CA to chloramphenicol resistance. One such transformant was designated strain AA035, and it was shown to have the inducible promoter correctly inserted by PCR amplification of the loci and agarose gel electrophoresis (Figure 4.3C). Growth curves (OD600 nm) of this constructed strain (AA035) and the wild type (168CA) were determined in LB with and without xylose (Figure 4.3D). Cells of AA035 grew normally in the presence or absence of xylose compared to the wild type.

Using light microscopy, we examined strain AA035 with and without the expression of the *fla/che* operon (with and without xylose). When the *fla/che* operon was expressed, a significant proportion of the cells were swimming, while the growth rate of the culture was not affected, indicating that having active flagella did not impact cell elongation and division. In contrast, without xylose, only a small proportion of the cells were swimming due to the leakiness of the P_{xyl} promoter. To address this issue, we constructed another strain under the control of the P_{spac} promoter, which generated strain AA036 and was found to have identical properties in that motility was dependent upon the presence of the inducer, in this case, IPTG, but the growth rates of the culture with or without IPTG were identical.

These results provide an alternative way to force cells to produce flagella and also provide a way to show that the insertion of multiple flagella into the wall of the growing cells did not impact the ability of the cells to proliferate. Thus, cell elongation and division are not perturbed by the assembly of the significant protein structures in the membrane that are attached to the cell wall and have projections through the thick cell wall.

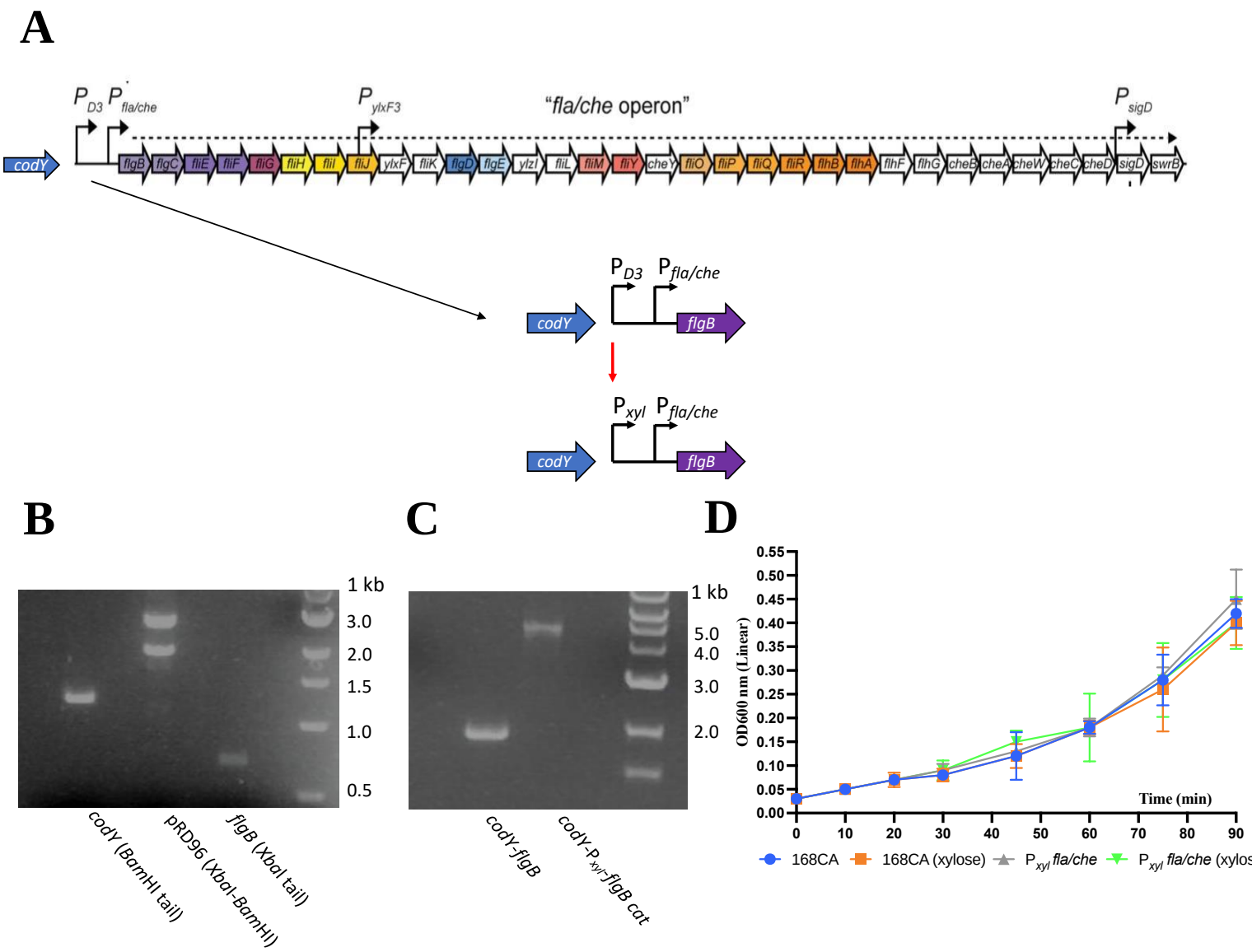

Figure 4.3 Inducible flagella construction

A- The genetic hierarchy of the flagella in *B. subtilis*. Coloured arrows represent the genes in the *fla/che* operon, and the bent arrows are the promoters. The red arrow indicates the insertion site of the artificial promoter (P_{xyl}) instead of (P_{D3}). This cartoon is adapted from (134). **B-** Agarose gel electrophoresis of PCR products (*codY*, pRD96, and *flgB*) before ligation. **C-** Agarose gel electrophoresis of PCR products after ligation, confirming the construction of AA035 strain. The DNA ladder is 1 kb. **D-** Growth curves of AA035 with and without xylose. Each plotted point corresponds to the average of cell growth (OD600 nm) based on three experimental replicates at the indicated time. Error bars represent the standard error of the mean. T0 is the time when xylose was added to the culture medium.

4.3 Visualisation of labeled flagellum subunits

As a way to determine the number and position of assembled flagella, fluorescently labeled alleles of specific genes were introduced into strains. Here, we exploited specific genetic modifications that had been previously published by Kearns (182) either in the form of chromosomal insertions or *E. coli* plasmids that on transformation into *B. subtilis* enable the labeling of components of the flagellum: *amyE::*$P_{fla/che}$*-fliM-gfp spec, amyE::*P_{hag}*-hag*^{T209C} *spec*, *amyE*::$P_{fla/che}$*-flgE*^{T123C} *cat amp* and plasmids permitting the insertion of manipulated genes; *thrC::*$P_{fla/che}$*-flgE*^{T123C} *ery amp* or *lacA::*P_{hag}*-hag*^{T209C} *ery amp.* These genetic constructs were transformed into our wild-type strain, 168CA, to generate isogenic strains and to remove the extra copy of *swrA* used as a background in the Kearns studies (182). SwrA is known to promote the production of multiple flagella (182, 183), a feature that is not desired in our strain as it mediates increased "flagellation" cells and could potentially complicate the analyses looking at the localisation and movement of the flagellar complex in live cells (see Section 5.4).

To visualise the flagellar basal body, FliM was fused to a green fluorescent protein, resulting in the formation of green dots on the cell membrane when observed under a fluorescence microscope (Figure 4.4A). FlgE, the hook protein, and Hag, the filament protein, had the coding sequence of the gene altered to introduce cysteine residues that could be stained with Alexa Fluor 488 C5-maleimide conjugated dye (green) or Alexa Fluor 594 C5-maleimide conjugated dye (red). This allowed the visualisation of FlgE as green or red dots on the cell wall surface (Figure 4.4B) and Hag as green/red filamentous appendages of the cell wall (Figure 4.4C) by fluorescence microscopy. For both of these extracellular proteins, GFP or other coloured variants were not possible as they are secreted, and the additional amino acid sequence would perturb the protein assembly and function. Unfortunately, this labeling is not perfectly clean as cysteine is present in other proteins in the cell envelope of *B. subtilis*, particularly at the division sites. Consequently, Alexa Fluor maleimide conjugated dyes, although able to label flagellar subunits such as FlgE and Hag, they also stain the cell wall and division sites of the bacterial cells but at a significantly lower level.

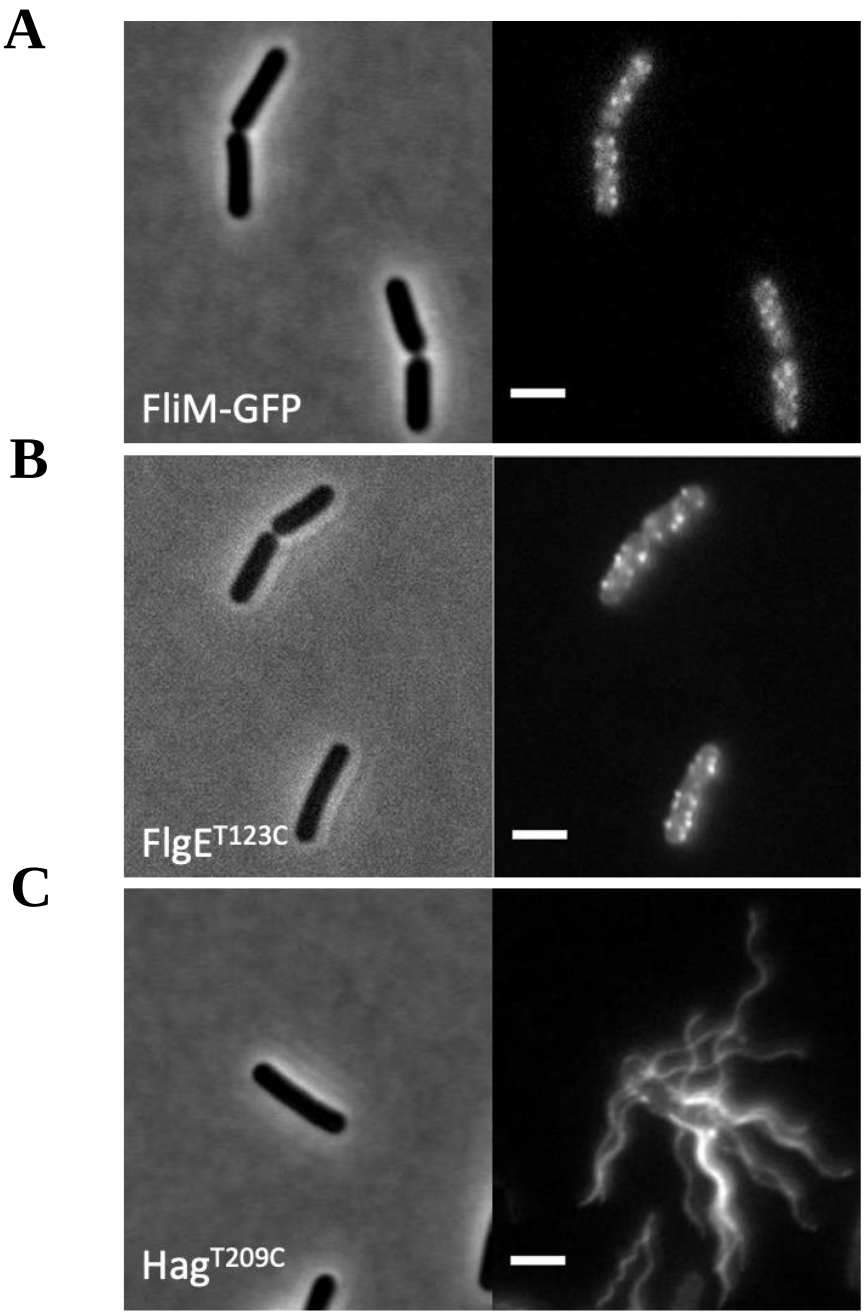

Figure 4.4 Fluorescent flagellar subunits

Fluorescent micrographs indicate the localisation of: **A-** FliM (basal body protein) utilising a strain background (AA028) containing a *fliM-gfp* fusion. **B-** FlgE (hook protein) of the modified strain (AA032) to introduce a single surface-exposed cysteine residue. **C-** Hag (filament protein) of the modified strain (AA031) to introduce a single surface-exposed cysteine residue. AA032 and AA031 were stained with Alexa Fluor 488 C5-maleimide conjugated dye (green). The strains were grown in LB, shifted into PTM, and sampled in 40 min later. Scale bars represent 2 microns.

4.4 The role of autolytic enzymes in the insertion of the flagella

It is presumed that the construction of flagella needs the action of one or more autolytic enzymes in order for them to pass through the thick and crosslinked peptidoglycan layers to be able to project out of the cell. To determine if this idea was correct, we assayed the ability of strains to produce flagellae that were deleted for sets of autolytic enzymes. As a starting point, we used the two multiple autolysin deletion strains Δ*lytD* Δ*lytG* Δ*lytC* Δ*lytF* Δ*cwlS* Δ*lytE* (+*cwlO*; strain AA020) and Δ*lytD* Δ*lytG* Δ*lytC* Δ*lytF* Δ*cwlS* Δ*cwlO* (+*lytE;* strain AA021) (described in Chapter 3 Section 3.2). For this assay, the *amyE* (P_{hag}-Hag^{T209C}) construction from Strain AA043 was introduced into the two autolytic mutant backgrounds; they were grown in LB, and then the cells shifted into pre-transformation medium (PTM) to induce the flagellar assembly. The cells were stained with Alexa Fluor 488 C5-maleimide conjugated dye (green) and visualised by fluorescence microscopy, using the wild-type strain AA043 as a positive control (Figure 4.5A). The cultures were then sampled at regular intervals to ensure that they exhibited similar growth rates, and cell samples that were taken at 45 min after being shifted to PTM (Figure 4.5D) were stained with the maleimide. This showed that the cells of the multiple autolytic mutant lacking *lytE* had an abundance of flagella (Figure 4.5B). But the cells of the multiple autolytic mutant lacking *cwlO* seemed to have very few flagella at the time they were sampled (Figure 4.5C). Repeating this experiment and sampling at multiple time points gave the same result. Thus, it had to be concluded that CwlO activity was important for the efficient extrusion of flagella, but there was the possibility that another enzyme (LytD, LytG, LytC, LytF, CwlS and/or CwlQ) was capable of permitting the extrusion of an occasional flagellum.

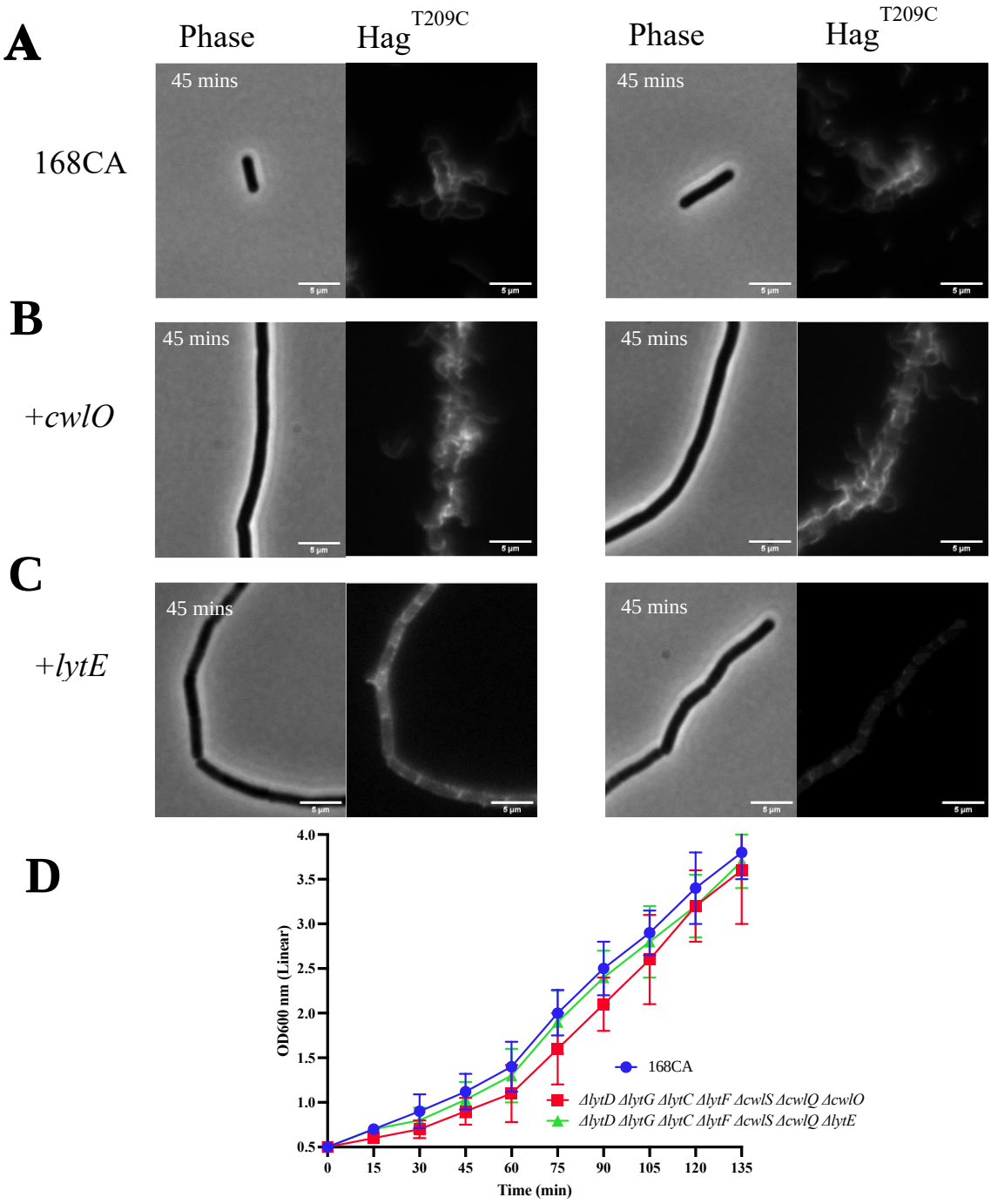

Figure 4.5 The flagellar insertion in the absence of vegetative autolytic enzymes

Fluorescent micrographs of: **A-** AA043 (wild type), **B-** Δ*lytD* Δ*lytG* Δ*lytC* Δ*lytF* Δ*cwlS* Δ*cwlQ* Δ*lytE*, and **C-** Δ*lytD* Δ*lytG* Δ*lytC* Δ*lytF* Δ*cwlS* Δ*cwlQ* Δ*cwlO* in a Hag^{T209C} background at 45 mins of shifting exponentially growing cells from LB to PTM. The strains were stained with Alexa Fluor 488 C5-maleimide conjugated dye (green). Scale bars represent 5 microns. **D-** Growth curves of these strains. Each plotted point corresponds to the average of cell growth (OD600 nm) based on three experimental replicates at the indicated time. Error bars represent the standard error of the mean.

This result presented three possible conclusions. Firstly, the lack of CwlO activity had an impact on the expression of the *fla* genes, and so there was insufficient synthesis of the components of the flagella to generate multiple filaments. Secondly, if the expression of the *fla* operon was normal, was the assembly of the basal body or the flagellum filament dependent on the CwlO activity? Finally, it was possible that although the basal body of the flagellum was assembled, it was unable to assemble the rod, hook, and filament components because the peptidoglycan was obstructing it and required the CwlO activity to open a path.

To differentiate between these possibilities, the localisation of the basal body and filament were investigated in the same cells. For this, the basal bodies were detected using a *fliM-gfp* fusion, and the filament assembly was determined by using the Hag^{T209C} allele, stained with Alexa Fluor 594 C5-maleimide conjugated dye. This resulted in the construction of 2 strains: one with *+cwlO* and the other with *+lytE*, with both strains having multiple deletions of other autolytic genes and carrying the GFP and Cysteine tags for FliM and Hag, respectively. The media were shifted as described previously, and samples were taken 45 min after the medium shift and imaged by microscopy after maleimide staining (Figure 4.6). From this, it was clear that both the basal bodies and filaments were easily detected in the culture where CwlO was present (Figure 4.6A). In contrast, the multiple autolytic mutant combined with *cwlO* mutant had a comparable number of basal bodies (green foci) but appeared to struggle in producing filaments (Figure 4.6B). Since the absence of CwlO was the only difference between these strains, this assay was repeated using a strain only deleted for *cwlO* (strain AA044); it was found that flagella were present (Figure 4.7A). Thus, it seems that flagellum extrusion can be mediated by a redundant set of autolytic enzymes, of which CwlO is functional alone.

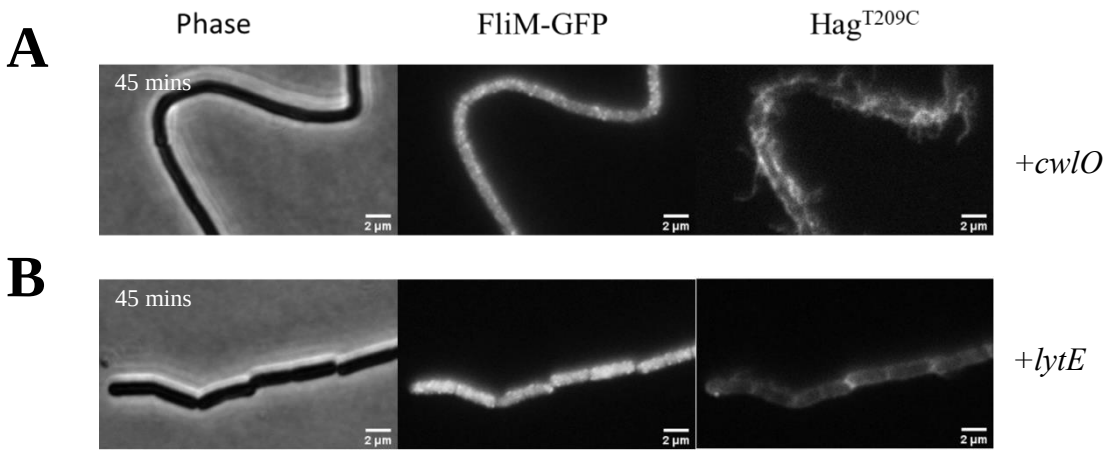

Figure 4.6 The flagellar basal bodies and filaments in multiple autolytic mutants

Fluorescent micrographs of FliM (basal body protein) and flagellin in strains **A-** +*cwlO* (Δ*lytD* Δ*lytG* Δ*lytC* Δ*lytF* Δ*cwlS* Δ*cwlQ* Δ*lytE*) and **B-** +*lytE* (Δ*lytD* Δ*lytG* Δ*lytC* Δ*lytF* Δ*cwlS* Δ*cwlQ* Δ*cwlO*) containing *fliM-gfp* fusion and the Hag^{T209C} allele of flagellin. Cells were collected in 45 mins after shifting the medium from LB to PTM. The cells were stained using Alexa Fluor 594 C5-maleimide conjugated dye (red). Scale bars represent 2 microns.

4.4.1 Specific autolysins required for the flagellum assembly

To identify the key autolytic mutants responsible for the flagellar insertion through the cell wall, double mutation combinations involving *cwlO* were constructed using the kanamycin resistance cassette insertions in *lytD, lytG, lytF, lytC, cwlS,* or *cwlQ* in a strain also carrying the Hag^{T209C} allele. The resulting strains were then induced to produce flagella by the growth shift into PTM and staining with a maleimide dye. From this systematic approach, fluorescence images for Hag^{T209C} showed that most double mutant combinations produced flagella at more or less normal levels, except the double mutant *cwlQ cwlO* where flagella were absent (Figure 4.7A) and a *cwlS cwlO* mutant that seemed to exhibit a delayed in the flagellar insertion (Figure 4.7B). Further characterisation revealed that the double mutant *cwlS cwlO* took over two hours to develop flagella compared to the wild type, which usually required only 40 minutes following the shift from LB to PTM medium. Since the single mutants of *cwlS, cwlQ,* and *cwlO* were as proficient in flagella as the wild type (Figure 4.8), the flagellar insertion process seems to require the

function of CwlO and either CwlQ or CwlS for effective penetration of the cell wall. However, CwlS seems to be either inefficient or not expressed at the time it is most needed, resulting in a long delay in the appearance of the flagellum.

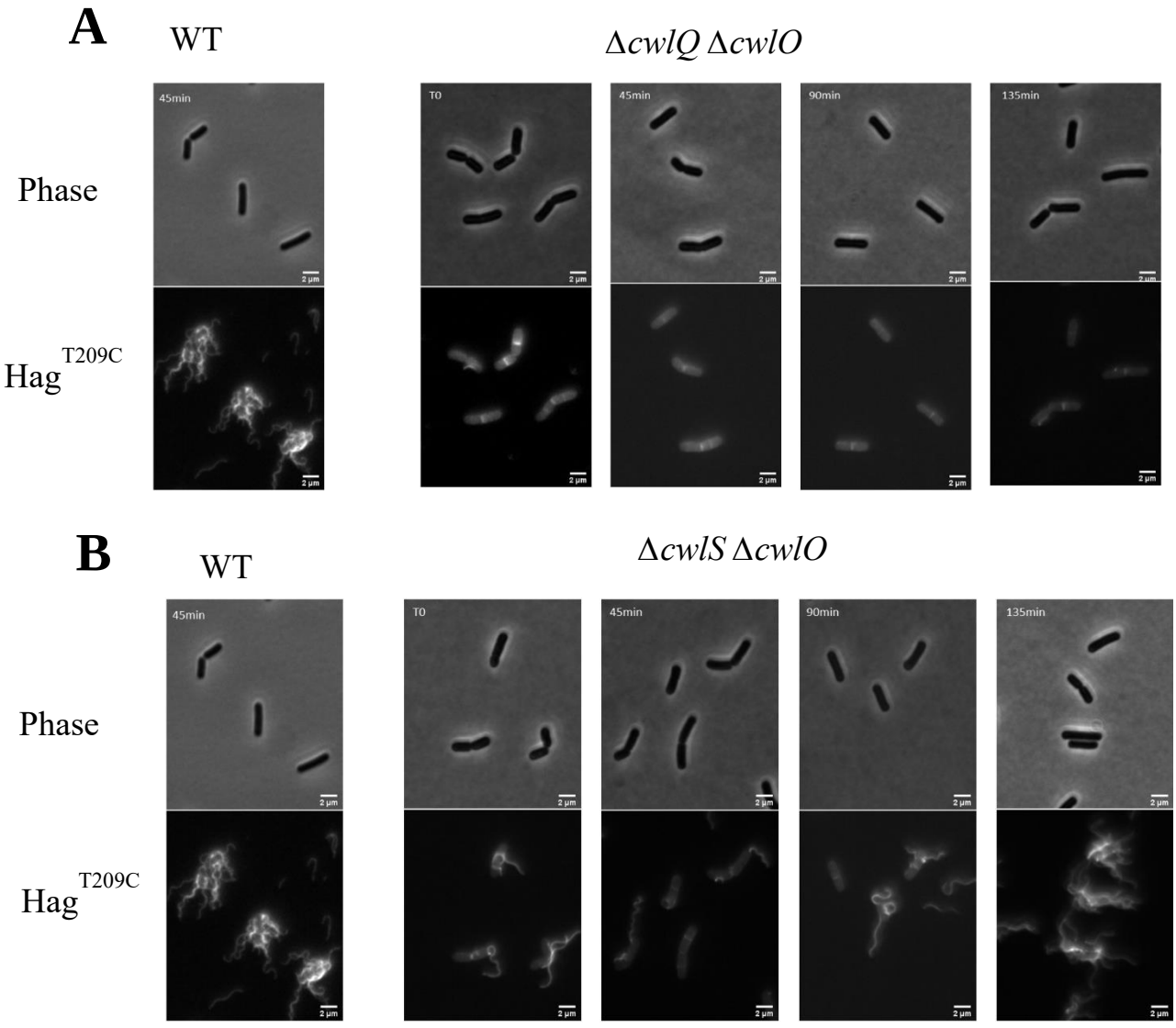

Figure 4.7 Specific autolytic enzymes required for flagellar insertion

Fluorescent micrographs of flagellin assembly in: **A-** Δ*cwlQ* Δ*cwlO*, and **B-** Δ*cwlS* Δ*cwlO*. All strains were in Hag^{T209C} backgrounds including the wild type 168CA. The strains were stained by Alexa Fluor 488 C5-maleimide conjugated dye (green). Scale bars represent 2 microns.

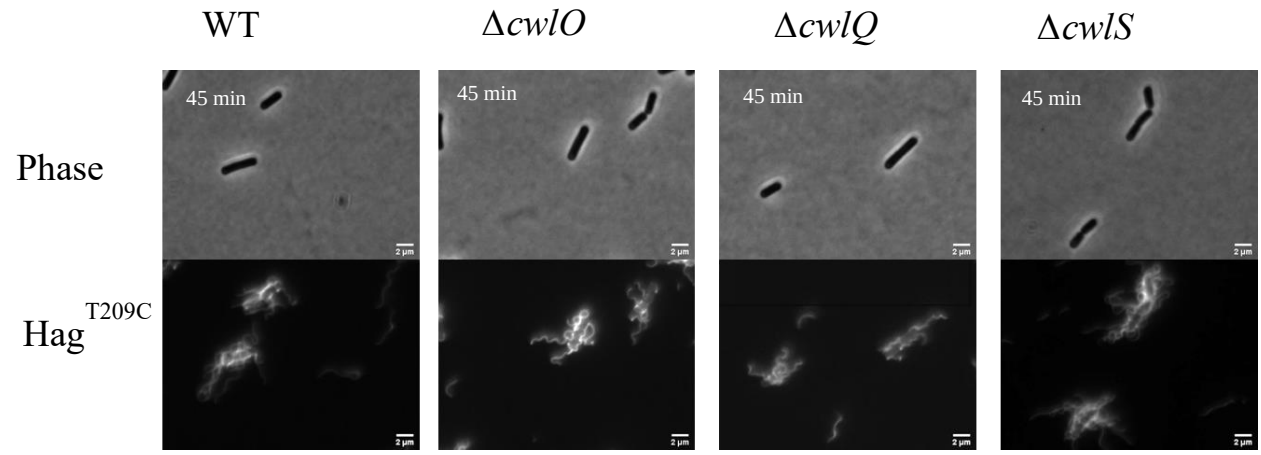

Figure 4.8 Flagella in single autolytic mutants

Fluorescent micrographs of flagellin assembly in single mutants Δ*cwlO*, Δ*cwlQ* and Δ*cwlS* compared to the wild type 168CA. All strain were in Hag^{T209C} backgrounds including the wild type 168CA. The strains were stained by Alexa Fluor 488 C5-maleimide conjugated dye (green). Scale bars represent 2 microns.

Since filament assembly was affected in the double mutants *cwlQ cwlO* and *cwlS cwlO,* the formation of the basal body and hook were assayed to determine if these mutations impair flagellum assembly. Using these double mutations *cwlQ cwlO* and *cwlS cwlO,* along with the wild-type strain (a positive control), in *fliM-gfp* fusion and *flgE*-cysteine backgrounds. The expression of flagella was induced by a medium shift, and samples were collected over a period of time and stained. From this, it was seen that the wild-type strain contained an identical number of basal bodies (FliM) and hooks (FlgE) in all time points (45, 90, and 135 minutes) (Figure 4.9A). In contrast, the strain lacking both CwlO and CwlQ had a normal number of basal bodies but failed to build the flagellar hook at the expected time (Figure 4.9B). The strain lacking both CwlO and CwlS showed a delay in hook assembly, which eventually became detectable approximately 2 hours after the shift from LB to PTM (Figure 4.9A/C), which corresponded to the time at which Hag was previously detected (Figure 4.7B). This indicates that CwlO and CwlQ are needed for the hook and filament assembly but not for the basal body formation. Thus, these autolytic enzymes are required to pave a way for the flagellar rod through the thick cell wall in order to allow the hook and then the filament assembly, while CwlS plays a

minor role. To try and genetically confirm that these phenotypes are solely due to the absence of the autolytic enzymes, a conditional allele of *cwlO* was introduced at the *amyE* locus of the double mutants *cwlQ cwlO* and *cwlS cwlO* under the control of a P_{xyl} promoter (see Figure 3.20, Chapter 3). However, complementing CwlO in this way did not correct the absence of the more distal components of the flagella (hook and filament) in the double mutant *cwlQ cwlO,* nor the delay of their assembly in *cwlS cwlO* (Figure 4.10). This is most probably due to the fact that CwlO was fused to GFP and potentially not fully functional.

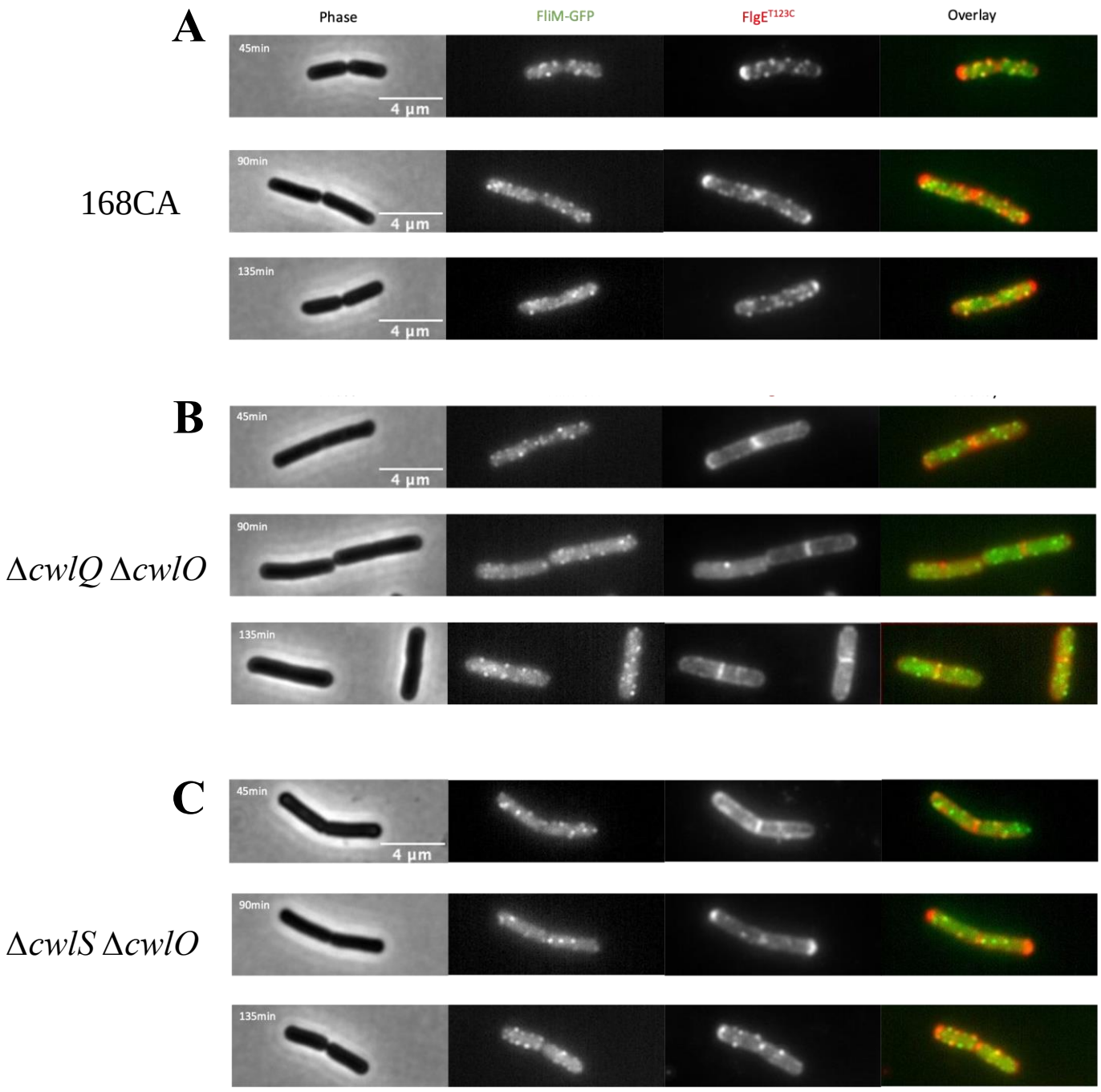

Figure 4.9 The flagellar basal bodies and hooks in the double mutants *cwlS cwlO* and *cwlQ cwlO*

Fluorescent micrographs showing the localisation of FliM (basal body protein) and FlgE (hook protein), utilising the following strains: **A-** 168CA, **B-** *ΔcwlQ ΔcwlO*, and **C-** *ΔcwlS ΔcwlO*. The strains contain a *fliM-gfp* fusion and *flgE*-cysteine labeled to introduce a single surface-exposed cysteine residue. The strains were stained using Alexa Fluor 594 C_5-maleimide conjugated dye

(red). The overlay panel indicates whether the flagella were able to pass through the thick peptidoglycan layers (yellow dots) or not. Scale bars represent 4 microns.

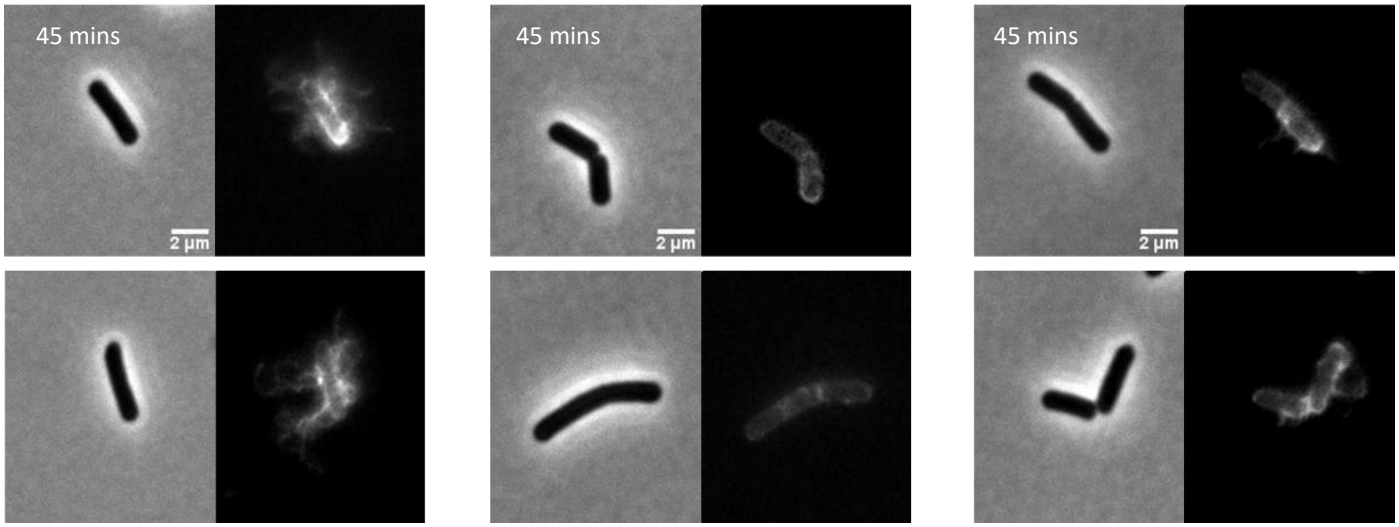

Figure 4.10 Complementing CwlO-P$_{xyl}$ regulated in the double mutants *cwlQ cwlO* and *cwlS cwlO*

Fluorescent microscopic images showing flagellar filaments in the presence and absence of CwlO expression, regulated by the xylose promoter, in the double mutants *cwlQ cwlO* and c*wlS cwlO*. All strains were in Hag^{T209C} and *amyE::*P$_{xyl}$*-gfp-cwlO* backgrounds, including the wild-type 168CA. Cells were collected 45 mins after shifting the medium from LB to PTM, with and without xylose. The cells were stained using Alexa Fluor 594 C5-maleimide conjugated dye (red). Scale bars represent 2 microns.

4.4.2 Motility of strains lacking specific autolysins

Swarming and swimming motilities on soft agar plates depend on the presence of flagella. However, in this case, the swimming cells grow in an "air-water" interface, where conditions are very different to liquid culture. In contrast, swarming cells move on solid surfaces, such as soft agar plates with higher concentrations. In this case, multicellular migration of cell rafts over the surface in a coordinated manner. Motility on soft agar plates is also a simple microscopy-independent assay for assessing motility, which has been established for a very long time. To determine whether the Cwl proteins are required for these forms of motilities, strains lacking CwlQ, CwlO, and/or CwlS were evaluated for swarming and swimming motilities on soft agar. These strains were compared to single mutants, a non-flagellated strain (*hag* mutant), and the flagellated wild-type strain. Previous analyses of various autolysin mutants had provided an

indication that motility was dependent upon the ability of the cells to become unicellular (i.e., not stuck together in chains), as well as having the ability to correctly assemble flagella. Therefore, multiple autolysin mutants, which were known to form chains were not included in previous motility analyses. However, in this study, deletion of the *cwl* gene did not result in cell separation defects, suggesting that the observed motility defects may be due to other factors.

The strains were inoculated as 5 µl drops of normalized cells on 0.5 % (w/v) swarm agar plate and 0.15% (w/v) swim agar plate. The swarm plate was incubated for 48 hours to promote the motility of all strains, while the swim agar plate was incubated for 12 hours to limit excessive strain spreading. Spreading diameters were measured in millimeters (mm) and compared to the wild type, with standard error of the mean indicated as $\sigma/\sqrt{n}$ (see Section 2.15). As can be seen from Figure 4.11, the wild-type strain spread over the surface of both swim and swarm agar plates; the spreading diameter on the swarm plate (38.6 mm, ± 0.8) was larger than that on the swim plate (20.17 mm, ± 0.4) due to the longer incubation period at 37 °C, attempting to enhance swarming motility of the other strains.

In contrast, the single mutants (*cwlO, cwlQ, cwlS*) and the double mutant *cwlQ cwlS* exhibited defects in swarming motility, forming tight colonies where the normalized cell cultures were dropped, similar to the non-flagellated *hag* mutant. However, these strains displayed swimming capability in very low agar concentrations. Mutant *cwlS* exhibited slightly reduced swimming motility (19 mm, ± 0.43) compared to the wild type (20.17 mm, ± 0.4), whereas swimming motility was significantly reduced in the single mutants *cwlQ* and *cwlO* (15.17 mm, ±0.18 and 15.86 mm, ±0.38, respectively). The double mutant *cwlS cwlQ* also showed a reduction in swimming motility (15 mm, ±0.21) compared to the wild type. As expected, the double mutant *cwlQ cwlO* exhibited defects in both swarming and swimming motilities, with cells confined to the drop site due to flagellar assembly impairment. Surprisingly, similar motility defects were observed in the double *cwlS cwlO,* which shows a delay in the flagella processing through the cell wall (Figure 4.11). Although the double mutant *cwlS cwlO* has flagella, they may not be present in sufficient numbers or have some other dysfunction, such that they cannot effectively provide swarming motility.

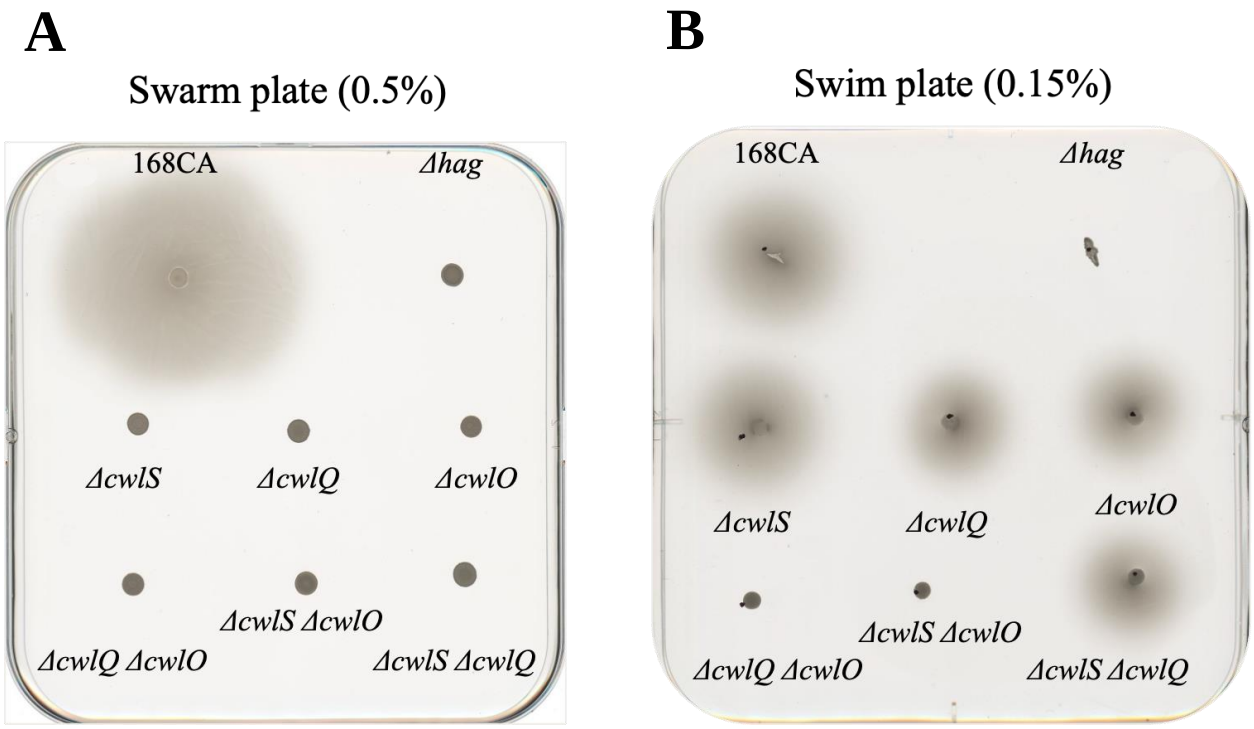

Figure 4.11 Swarming and swimming motility tests

A- A swarm agar plate (0.5%, w/v) incubated for 48 hours at 37 ºC. **B-** A swim agar plate (0.15%, w/v) incubated for 12 hours at 37 ºC. The plates were inoculated with 5 µL drop of cultures (OD600 nm ~0.03): 168CA (wild type), *Δhag*, single mutants *ΔcwlS*, *ΔcwlQ*, and *ΔcwlO*, and double mutants, *ΔcwlQ ΔcwlO*, *ΔcwlS ΔcwlO*, and *ΔcwlS ΔcwlQ* to evaluate the swarming and swimming motilities of these strains.

4.4.3 Flagellin expression in autolytic mutants

One possibility for the absence of the flagellar filaments in the double mutant *cwlQ cwlO* was that a transcriptional block in flagellin protein expression rather than preventing effective assembly of the flagellum filament. To determine if this was the case, the level of cell-associated flagellin protein (Hag with a molecular weight of 32.47 kDa) was assessed in cell pellets from the single mutants *cwlS*, *cwlQ*, and *cwlO* and the double mutants *cwlS cwlO* and *cwlQ cwlO*, including cells of the wild type and *hag* mutant. Cell lysates were resolved by SDS-PAGE, and Western blot analysis was preformed using anti-Hag and PBP2B antibodies to determine the level of flagellin subunit expression (Figure 4.12). PBP2B detection (a 79.12 kDa protein) served as a control to ensure comparable loading across all of the lysates.

This analysis showed that the level of flagellin was high in the wild type and single mutants *cwlS*, *cwlQ*, and *cwlO*, as well as in the double mutant *cwlS cwlO*. However, in the double mutant *cwlQ cwlO*, flagellin expression was severely reduced, despite the higher loading than the other samples, as confirmed by the PBP2B loading control (Figure 4.12, indicated by red arrows).

These findings suggest that the absence of flagellar filaments in the double mutant *cwlQ cwlO* may be attributed to a decrease in flagellin protein synthesis. Thus, it is possible that the double mutant experiences a disruption in the regulatory mechanisms or processes involved in flagellin production, leading to a significant reduction in flagellin levels compared to the other strains.

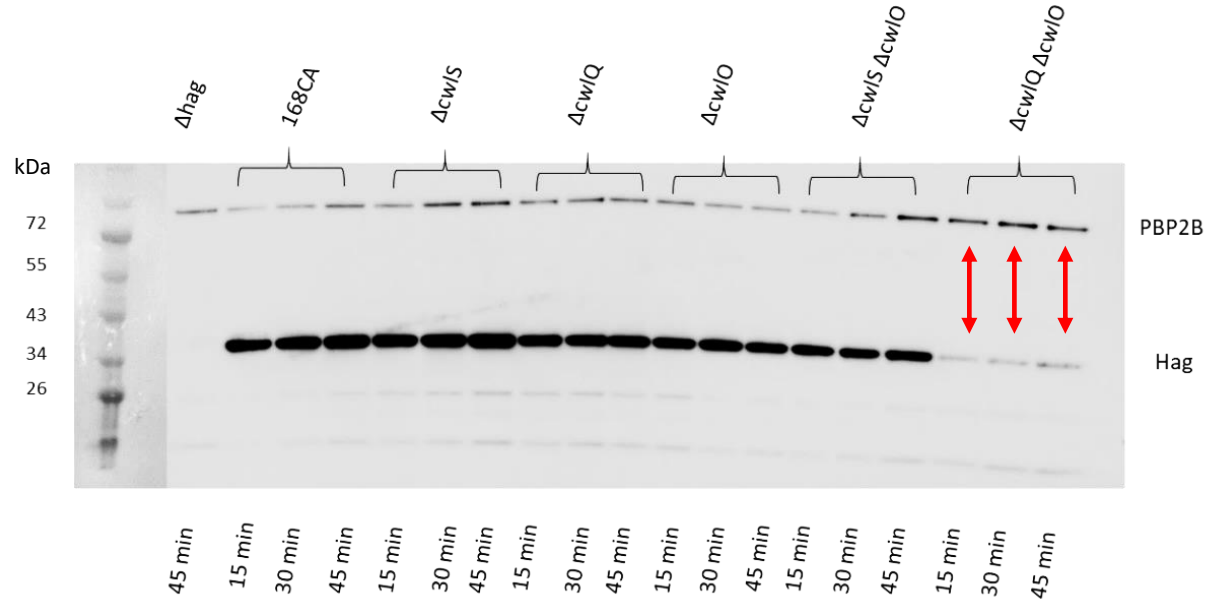

Figure 4.12 Flagellin (Hag) expression in autolytic mutants

Western blot analysis of cell lysates is shown to detect the level of flagellin (Hag) expression in the following strains: the wild-type 168CA, *Δhag*, *ΔcwlS*, *ΔcwlQ*, *ΔcwlO*, *ΔcwlS ΔcwlO*, and *ΔcwlQ ΔcwlO*, using a 1/10000 dilution of Hag antibody as the primary antibody, and 1/10000 dilution anti-rabbit as the secondary antibody. The upper bands indicate the control PBP2B detected by the PBP2B antibody as the primary, and anti-rabbit as the secondary (molecular weight 79.12 kDa). The lower bands indicated the level of Hag expression in each strain (molecular weight 32.47 kDa). Red arrows indicate the severe reduction in Hag expression level in the double mutant *cwlQ cwlO*, even though the loading of this strain was high at all-time points.

4.4.4 Transcriptional regulation of flagellum genes

To determine the underlying cause of the interruption in flagellin expression in the double mutant *cwlQ cwlO* and the delay in flagellar assembly in the double mutant *cwlS cwlO*, we conducted experiments to investigate whether there was altered transcriptional regulation caused by the loss of autolytic functions. Here, we exploited the fact that SigD is the key regulator of flagellar expression and used a lacZ reporter construct in the *yxkC* gene as a way to determine SigD activity. YxkC is a SigD dependent protein, and it was chosen as it is unrelated to flagella, ensuring that any observed effects were not influenced by potential interference from flagellar components (117). By measuring the activity of SigD through a β-galactosidase assay, our goal was to determine whether SigD activity was reduced in the autolytic mutant backgrounds and if this could account for the observed deficiency in flagellar assembly. As can be seen from the activity profile for the wild-type strain, the expression of *yxkC* is not solely regulated by SigD but is expressed at a significantly lower level in a *sigD* null mutant, without a spike in activity at 40 min after motility was induced by the medium shift (Figure 4.13). Analysing the transcriptional activity of this reporter in the double mutant *cwlQ cwlO* and *cwlS cwlO*, in combination with a *ΔflgM* background (where FlgM acts as an inhibitor of SigD), activity levels similar to the wild-type strain were obtained (Figure 4.13, indicated in orange and yellow lines). This suggesting that the expression of flagellar proteins was not affected in these double mutants *cwlQ cwlO* and *cwlS cwlO*, where SigD activity was constitutively active. In contrast, the double mutants in the *ΔsigD* background exhibited no β-galactosidase activity, indicating that the expression of flagellar genes was blocked due to the absence of SigD function (Figure 4.13, indicated in grey and dark blue lines).

Based on these observations, the disruption of flagellar hook and filament assembly in the double mutants *cwlQ cwlO* and *cwlS cwlO* was not attributable to transcriptional effects on the flagellar genes as the expression levels imply that the expression of flagellar genes, including those responsible for flagellin synthesis, was not the primary cause of the observed phenotype. Instead, the hook and the filament assembly rely on the proper functioning of either CwlO or CwlQ, with a minor contribution from CwlS. The absence or malfunction of either of these autolytic enzymes results in a disruption of the flagellar assembly process, leading to the observed defects in the flagellar structure. The reduced expression of flagellin seen in the CwlQ

CwlO strain could potentially be related to the fact that FlgM is not lost in this strain as it is exported from the cell when the basal body is assembled correctly, resulting in SigD activity driving the expression of the flagellin protein, Hag. This was why the transcriptional activity assays were done in a *flgM* null strain to avoid this level of regulation.

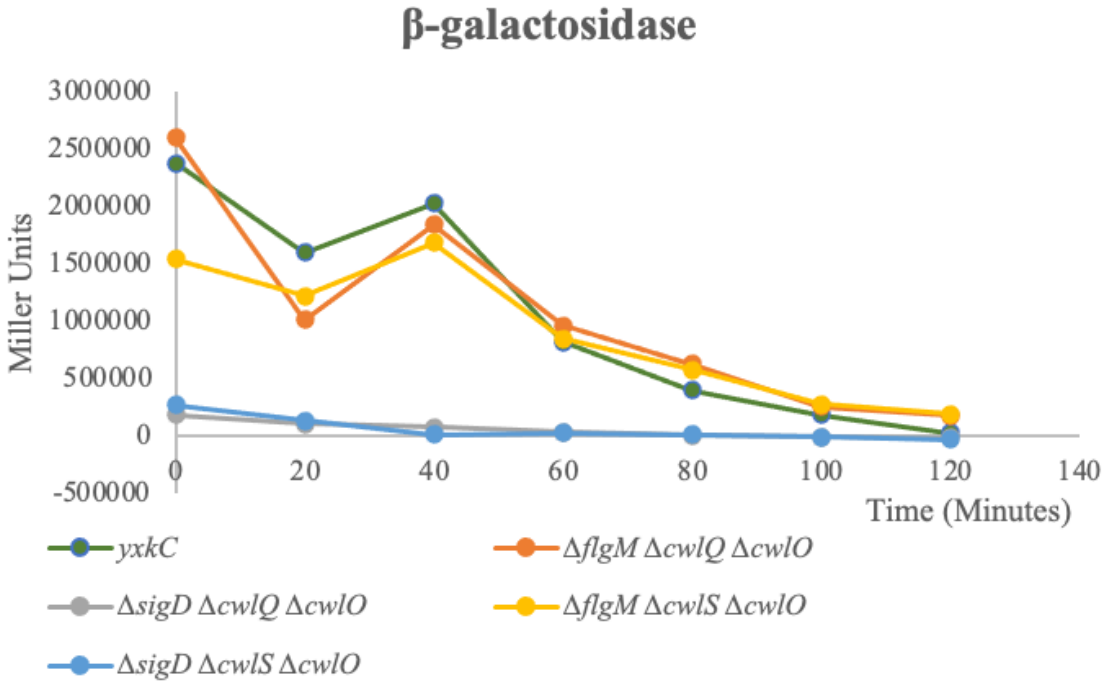

Figure 4.13 Transcriptional regulation of flagellum genes

β-galactosidase activity of SigD was assessed in the double mutants *cwlQ cwlO* and *cwlS cwlO* in *sigD* or *flgM* backgrounds using a lacZ reporter construct in the *yxkC* gene. The growth of these mutants was conducted in liquid media using the shift from LB to PTM media as the starting point for sampling and was incubated at 37 ºC with shaking.

4.5 CwlO has two functions in cell wall modification

Since the DD-carboxypeptidase (DacA) is involved in the CwlO activity (as discussed in the previous chapter), it was expected that the absence of DacA might affect the function of CwlO in relation to flagellar assembly. To investigate this hypothesis, the presence of flagella was assessed in mutants of *cwlQ dacA* and *cwlQ cwlS dacA* compared to the wild type and single mutants *cwlO* and *dacA*. All strains were in the Hag^{T209C} background and were stained with

Alexa Fluor 488 C5-maleimide conjugated dye to expose flagella under fluorescence microscopy (Figure 4.14). Surprisingly, all strains exhibited proficient flagella comparable to the wild type, indicating that the role CwlO plays in flagellar insertion does not require DacA. This finding suggests that CwlO has two distinct functions in cell wall modification: one related to cell growth and another involved in the insertion of flagellar filaments through the cell wall.

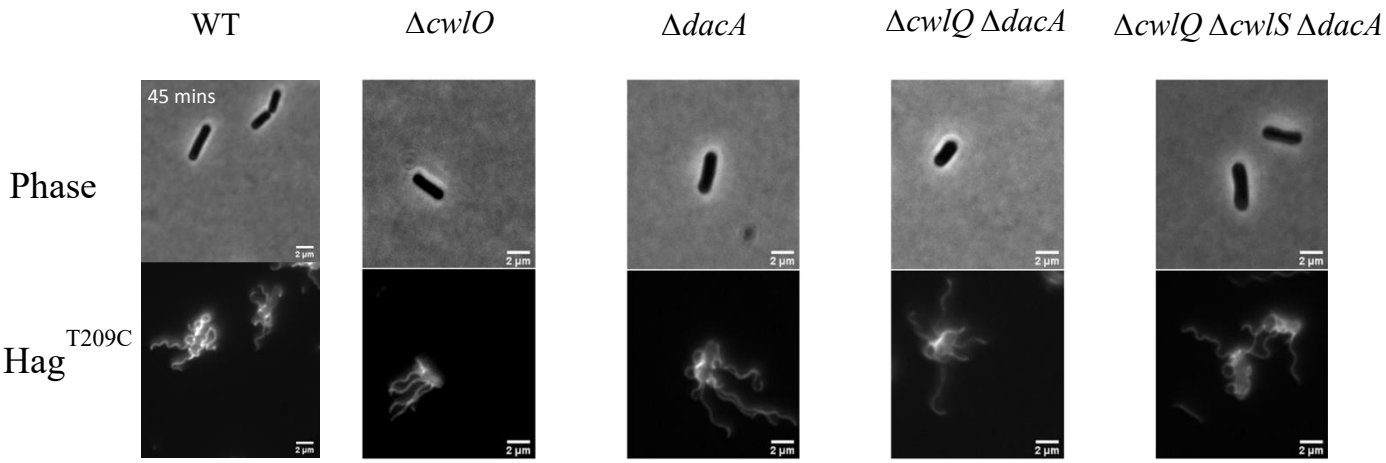

Figure 4.14 The flagellar assemble in *dacA* background

Fluorescent micrographs of flagellin assembly in the following strains: Δ*cwlO,* Δ*dacA,* Δ*cwlQ* Δ*dacA,* and Δ*cwlQ* Δ*cwlS* Δ*dacA* with the Hag^{T209C} allele of flagellin compared to their wild type (AA043). Scale bars represent 2 microns. Cells were collected in 45 mins after shifting the medium from LB to PTM. The cells were stained with Alexa Fluor 488 C5-maleimide conjugated dye (green).

4.6 Discussion

This chapter explores the intricate mechanism by which flagella penetrate the mesh-like structure of the cell wall of *B. subtilis*. Studying the mechanisms of flagellar assembly and insertion required a way to stimulate their formation rapidly and synchronously in the growing culture. These processes are tightly regulated and primarily initiated in response to specific environmental conditions, particularly during periods of starvation. In a standard growth medium like LB, flagella production is a late process that mainly occurs during the stationary phase. However, by shifting the medium to a semi-defined medium, it is possible to create optimised conditions that promote rapid flagellar assembly and initiate response to starvation. This shift leads to the rapid formation of complete, long flagella within approximately 40

minutes. However, true motility, indicated by active swimming of the cells, only becomes evident after a significantly longer period of time. This observation suggests that other signaling processes or factors are required to enable functional motility.

Flagella assembly involves a complex interplay of various proteins, starting from embedding the basal body into the cell membrane, which serves as a core of the specialised secretion apparatus. The secretion apparatus exports proteins necessary for the formation of the flagellar rod, hook, and filament. The polymerisation and arrangement of rod proteins through the thick cell wall are crucial for constructing the more distal compartments (hook and filament). However, prior to this assembly, the action of autolytic enzymes is required to create a suitable pore for the flagellar rod formation. In other bacterial species, flagellar formation relies on the action of autolytic enzymes to facilitate their insertion through the cell wall. In *E. coli*, the autolytic enzyme FlgJ facilitates the passage of the flagellar rod through the peptidoglycan layer, potentially acting as a "drill" to allow flagellar rod assembly (185), but in *B. subtilis*, no FlgJ homolog has been identified. In this study, flagellar formation in *B. subtilis* was investigated in the absence of vegetative autolytic enzymes. Through systematic deletions of vegetative autolytic genes, it was determined that no single autolytic enzyme is responsible for facilitating flagellar rod formation. Instead, the formation was severely affected in the double mutant *cwlQ cwlO*, where CwlQ is specific to the flagellar assembly, and CwlO is best characterised as having a role in cell elongation. It is worth mentioning that a recent study by Sandra (118) reported that the absence of CwlQ and CwlO resulted in a swarming motility defect but not in flagellar formation. However, it should be noted that this work was performed in a different genetic background (*swrA+*), which is known to promote an increased number of flagellar production (183, 248) and does not contradict the results presented here as our analysis did not look at swarming directly as our background is swarming defective.

The glycosaminidase CwlQ and the DL-endopeptidase CwlO are redundant for flagellar formation. The double mutant *cwlQ cwlO* exhibited the basal body but failed to assemble the flagellar hook and filaments. This observation suggests that cells have the genetic potential to respond to environmental changes by forming flagellar basal bodies, as this phenotype is not caused by significant transcriptional changes in flagellar gene expression. Instead, it seems that the flagellar rod encounters difficulties in passing through the thick peptidoglycan layers without

the function of either CwlQ or CwlO, resulting in the failure in hook and filament assembly. Another possibility is that a complete mutation in *cwlQ* and\or *cwlO* may result in other secondary protein complex formation issues that may lead to the observed phenotypes. Thus, active site mutations in these genes should be carried out to assess the phenotypes more accurately.

Intriguingly, our findings suggest that the DL-endopeptidase CwlS is also involved in flagellar assembly. The double mutant *cwlS cwlO* displayed a significant delay of approximately two hours in the formation of the flagellar hook and subsequent filament assembly, even though this strain exhibited the basal bodies at the expected time. This suggests that CwlQ alone is insufficient to facilitate the passage of the flagellar rod through the cell wall, and the assistance of CwlS or CwlO is necessary. These observations indicate that CwlS likely plays a minor role in compensating for the function of CwlQ in flagellar assembly. Thus, the absence or malfunction of these autolytic enzymes results in a disruption of the flagellar assembly process, leading to the observed defects in the flagellar structure. However, when CwlO was complemented in the double mutant *cwlQ cwlO,* the more distal components of the flagella, such as the hook and filament, were not restored to their normal state. Similarly, in the *cwlS cwlO* mutant, the delay in the assembly of these components was not fully corrected. This suggests that the artificially induced CwlO is insufficient for rescuing the flagellar assembly defect.

Notably, the single mutants *cwlO, cwlQ,* and *cwlS,* as well as the double mutant *cwlQ cwlS,* exhibited defects in swarming motility. This indicates that the presence of Cwl proteins is essential for the coordinated swarming behaviour of bacteria on soft agar surfaces. Interestingly, despite the swarming defects, these mutants retained swimming capability at low agar concentrations, albeit with varying degrees of impairment. This suggests a differential requirement for Cwl proteins in swarming versus swimming motilities and highlights the specific roles of these proteins in facilitating efficient bacterial movement in solid and liquid environments. The slight reduction in swimming motility in the *cwlS* mutant suggests a partial involvement of this protein in swimming behaviour. The double mutant *cwlS cwlQ* displayed a swimming defect comparable to the single mutant *cwlQ,* indicating a possible dominant effect of the *cwlQ* mutation on swimming motility. The flagella of *cwl* mutants may not be fully functional in supporting proper motility, possibly due to a defect in flagellar rotation. Moreover,

the double mutant *cwlS cwlO* also exhibited defects in both motility behaviours. Despite the eventual flagella formation, the inability of this mutant to exhibit proper swarming or swimming motilities suggests that flagellar assembly and function are separate processes.

Our earlier genetic studies provided evidence suggesting that DacA is essential for the activity of CwlO in cell morphology, particularly in relation to the width and elongation of the cell (see Chapter 3). This implies that CwlO's functionality is impaired when the peptidoglycan contains pentapeptides in the absence of DacA, as DacA is responsible for removing the terminal D-alanine from the pentapeptide chain in the peptidoglycan structure. Considering this, it was initially anticipated that the absence of DacA might have an impact on the function of CwlO in relation to flagellar assembly. However, mutants of *cwlQ* and *cwlQ cwlS* in the *dacA* background exhibited proficient flagella. Interestingly, the involvement of DacA in swarming motility has been indicated through transposon mutagenesis and high-throughput sequencing (TnSeq) analysis (85). This analysis demonstrated that the absence of DacA led to a defect in swarming, which implies that while DacA is not directly required for flagellar insertion, it plays a role in facilitating efficient swarming motility. Nevertheless, our observations indicate that CwlO has dual roles in cell wall modification: one involved in cell growth that relies on DacA activity and another involved in the insertion of flagellar filaments through the cell wall, which appears to be independent of DacA.

4.6.1 Proposed model

The assembly of the flagellum structure involves the basal body, which acts as an anchor to the cell membrane, and the secretion apparatus coming together (Figure 4.15A). At the same point, modifications are required in the peptidoglycan structure. These modifications primarily rely on the action of CwlO or CwlQ, with a minor involvement of CwlS (Figure 4.15B/C), assuming that the absence of these proteins dose not disrupt a secondary protein complex necessary for flagellar insertion. CwlO, a cell membrane protein, interacts with other proteins and is believed to act near the cell membrane, while CwlS continues its function on the outer layers (Figure 4.15B/C). CwlQ appears to be active in both the inner and outer layers (Figure 4.15A/B/C). The autolytic enzymes (CwlO, CwlQ, and CwlS) play a crucial role in modifying the peptidoglycan at the site where the basal bodies are assembled, potentially creating a cavity for the subsequent

assembly of the flagellar rod. This modification then facilitates the formation of the more distal compartments, such as the hook and filament (Figure 4.15D). Through this well-coordinated process, fully functional flagella are constructed, enabling the bacterium to become mobile in its environment. Considering these complex protein structures are inserted through the cell wall in multiple places, it is surprising that this does not seem to have a significant impact on the cells ability to continue to elongate and divide.

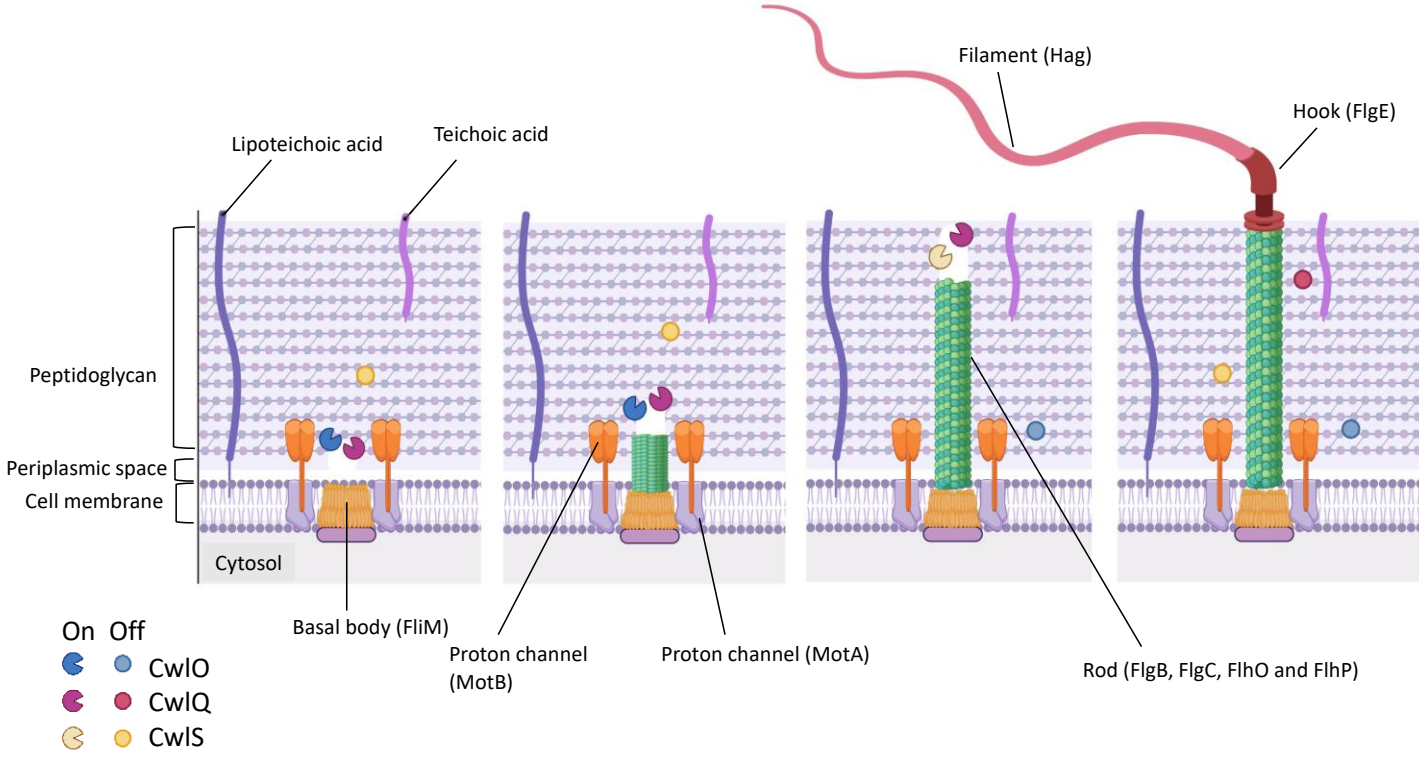

Figure 4.15 Proposed model of flagellar insertion in *B. subtilis*

Cartoon diagram of the *B. subtilis* cell wall showing the process of flagellar assembly through the PG. **A-** The assembly of the basal body and the secretion apparatus represents the initial steps of flagellar assembly. **B** and **C-** The involvement of CwlO, CwlQ, and CwlS in modifying the peptidoglycan structure at different layers of the cell wall. CwlO is primarily active near the cell membrane, while CwlS operates in the outer layers. CwlQ is active across all layers. These autolytic enzymes create a pore at the site of basal body assembly, facilitating the subsequent assembly of the flagellar rod. **D-** The formation of distal components, such as the hook and filament, through this modification process. The illustration was created with BioRender.com.

Chapter 5
Flagella as a Landmark within the Dynamic Cell Wall

5.1 Introduction

Flagella are long whip-like structures that protrude from the surface of bacterial cells. *B. subtilis* is known for its highly organized and complex flagellar system, in which its subunits are arranged in a distinctive (helicoidal) pattern, forming a bundle that allows the bacterium to swim through its environment. The flagellum assembly is a multi-step process that involves the sequential synthesis and export of flagellar components (basal body, rod, hook, and filament) and their subsequent assembly into a functional structure (described in detail in Section 1.6/ Chapter 1). This structure extends from the cytoplasmic membrane, traversing the thick peptidoglycan layers, and finally projects out into the external environment (see Chapter 4).

Regardless of the mechanism by which flagella pass through the cell wall, they must be fixed landmarks on the cell surface, extending from the cytoplasmic membrane of the cell to the environment. The peptidoglycan in *B. subtilis* is relatively thick, measuring approximately 20-35nm and consisting of around 30 dynamic layers (3, 249, 250). Previous studies have reported that peptidoglycan architecture elongates through the movement of the layers relative to each other, resulting in twisted action, potentially mediated by the peptidoglycan strands being arranged in a helix-like structure (235, 251). This was then used to explain how certain strains of *B. subtilis* (presumably defective in aspects of cell wall metabolism) formed fiber-like structures that appeared to be made up of long chains of cells that intertwined like the fibers in a cotton thread (252, 253). To try and determine if these concepts were correct and obtain a different perspective of the cell wall dynamics, it was possible that visualising the distribution and movement of functional flagella on the cell surface could potentially provide evidence to support this concept of the cell wall dynamics. In addition, modeling cell growth in terms of surface movement also raises the question of whether the insertion of multiple flagella through the lateral wall occurs during cell growth and is restricted to non-growing cells. This was partially answered in the last chapter, but it raised the question, how does the cell wall synthetic apparatus "work around" large membrane-embedded structures that project out of the cell? Thus, it was important to investigate whether the flagella exhibit relative movement on the cell surface during cell growth, given that the layers of the cell wall are thought to be dynamic in nature. Additionally, the idea of growth with flagella poses the question as to how these structures are evenly distributed, such that cell division results in equal numbers being inherited by the

daughter cell. Something that again addresses aspects of the overall organization and dynamics of the cell wall.

The aim of this chapter is to utilise the flagellar structure located on the cell surface as a tool to enhance our understanding of the dynamics of the cell wall of *B. subtilis.* By studying the behaviour of flagella in relation to cell growth, insights into the dynamics and organization of the cell wall will be revealed, contributing to our overall understanding of bacterial cell biology. For this analysis, the flagellum was divided into two visualisable components as landmarks on a dynamic cell surface: the basal body and the hook/flagellum filament. The formation of the basal bodies is an initial step in flagellar assembly, and they are membrane-associated, but at some point, they must become attached to the cell wall. Thus, the appearance and dynamics of these structures were investigated in relation to cell growth. Conversely, the hook and filament are assembled essentially on the outside of the wall and represent the point where the assembly has passed through the wall and would then fix in position.

5.2 Basal body number and cell growth

A strain expressing a FliM-GFP (green fluorescent protein) functional fusion was utilised to track the formation and number of basal bodies. For this analysis, cells were induced to synthesise flagella by growth in LB medium and "resuspension" in pre-transformation medium (PTM; described previously (Section 4.2.1/ Chapter 4). This was defined as time 0, and samples were collected at different time points relative to this.

By fluorescence microscopy, the basal bodies were visualised as green dots. Analysis of these images showed an increase in the number of basal bodies after the shift to PTM, reaching an apparent maximum after about 1-2 h (Figure 5.1A). Close inspection of multiple images from several independent experiments showed that after two hours of incubation in PTM, nearly 99% of cells had multiple basal bodies, and the culture was still exhibiting exponential growth (Figure 5.1B). This observation suggests that cells were able to continue to grow and divide even though they had assembled a significant number of flagella basal bodies and presumably had fully assembled flagella passing through the cell wall.

However, measuring the optical density as a proxy for the bacterial growth used to estimate cell growth might reflect changes in cell density rather than the actual increase in the

number of cells. To confirm that cells were still able to grow by elongation when flagella were assembled in multiple places over the cylindrical portion of the cell, time-lapse imaging of a single cell was used. Analyses of these time series showed that the assembly of multiple basal bodies had no significant effect on the growth of the cells. Taking individual cells and determining the time taken for these cells to elongate and divide indicated that there was no significant difference between cells having multiple FliM foci and cells with few or none (Figure 5.2). This observation seems to support the notion that despite basal body assembly and presumably fully assembled flagella passing through the cell wall, cells were not arrested in growth.

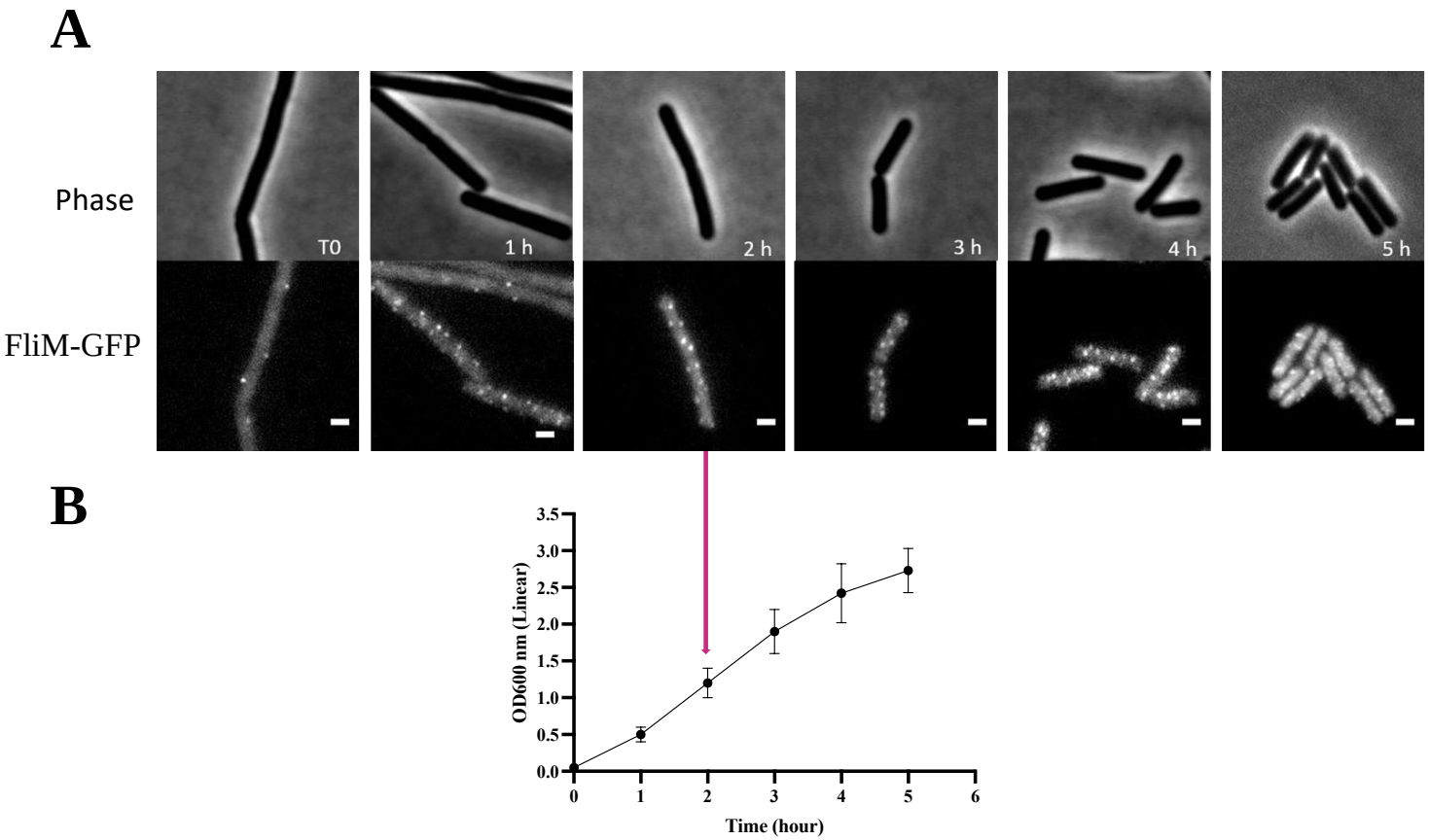

Figure 5.1 The basal body number in relation to cell growth

A- Fluorescent micrographs of FliM (basal body protein) in a strain background (AA028) containing a *fliM-gfp* fusion, used to detect the number of basal bodies in relation to cell growth. The scale bars represent 1 micron. **B-** A growth graph of AA028 strain at the time of microscopy images were obtained. Each plotted point corresponds to the average of cell growth (OD600 nm) based on three experimental replicates at the indicated time. Error bars represent the standard

error of the mean. The pink arrow indicates that the cells were exponentially growing while they have flagella, and this occurred in 99% of the cell population at this time. The T0 sample refers to when exponentially growing cells diluted back from LB to PTM.

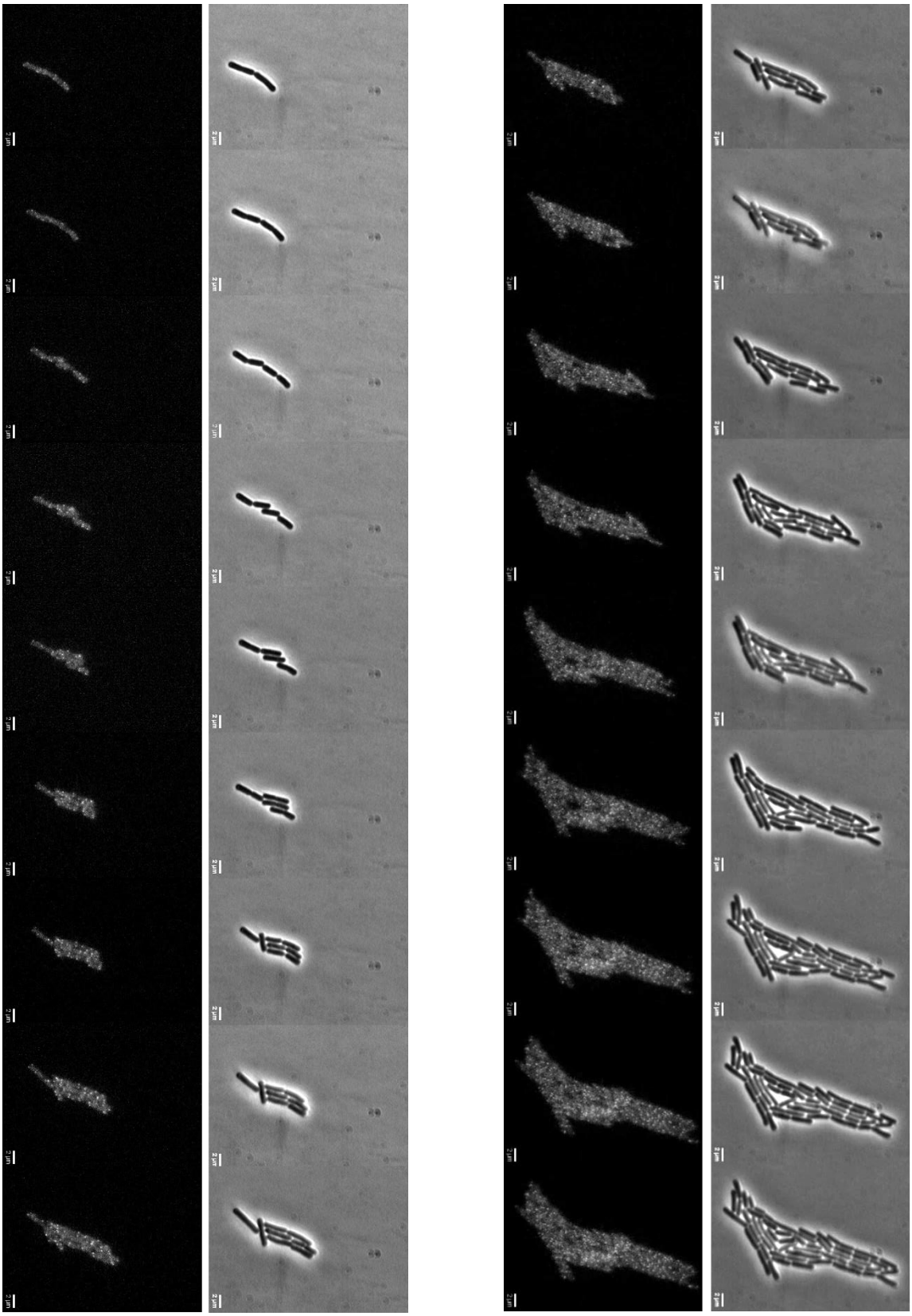

Figure 5.2 Time-lapse of cells growing and developing basal bodies

Fluorescent micrographs of FliM (basal body protein) in a strain background (AA028) containing a *fliM-gfp* fusion, used to detect the number of basal bodies in relation to the cell growth. The T0 image refers to when exponentially growing cells were diluted back from LB to PTM. The time-lapse was recorded for 4 hours, with images taken every 10 mins. Scale bars represent 2 microns.

5.3 Hook and flagellin localisation relative to basal body formation

The basal body, represented by the FliM protein, serves as the anchor for the flagella to the cell membrane. Hence, it was possible that although the basal body had assembled, it was not attached to the cell wall, and the rest of the flagellum structure was absent. In this state, cell growth, mediated by cell wall synthesis, may not be impeded as the basal bodies would not be fixed obstructions in the membrane, impeding the movement of the cell wall synthetic apparatus.

The assembly of the hook (FlgE) and the filament (Hag) indicates the successful passage of the rod through the peptidoglycan layers and the completion of the flagellum. To determine if there was a significant delay between FliM focus formation and the presence of a fully assembled flagellum, co-localisation of FliM with FlgE or Hag was used. Initial experiments used the Hag^{T209C} allele combined with the FliM-GFP fusion (AA048 strain). Flagellum assembly was induced by shifting the growth medium from LB to PTM as before. The cells were then either directly imaged for green fluorescence, corresponding to the FliM fusion, or stained with Alexa Fluor 594 C5-maleimide to label the exposed cysteine tag on the flagellum subunits (Hag), resulting in a red fluorescent signal associated with this protein. However, determination of the number and origin of Hag filaments proved to be impossible by fluorescence microscopy images because filaments were generally tangled together or wrapped over the surface of the cell (Figure 5.3A).

Consequently, the localisation of the basal body protein (FliM) in relation to the hook protein (FlgE) was used since both took the form of reasonably discrete foci. Cells expressing the FliM-GFP fusion protein and the $FlgE^{T123C}$ allele in the AA035 strain were visualised using fluorescence microscopy. The FlgE protein (hook protein) was labeled with cysteines and stained with Alexa Fluor 594 C5-maleimide conjugated dye, resulting in a red fluorescence signal. Imaging cells was found to be possible by conventional epifluorescence microscopy, and it was clear that, in general, each basal body protein was associated with a hook protein, albeit

with a slight shift in their localisation (Figure 5.3B). This could be attributed to a technical artifact in the imaging method generally referred to as a chromatic shift. As a way to avoid this problem and obtain a higher level of resolution imaging, structured illumination microscopy (SIM) was used (Figure 5.3C). From this, it was clear that using the flagella as landmarks on the cells was feasible, although the fluorescence signal from the GFP fluorophore exhibited a problematic degree of photobleaching, meaning that time-lapse imaging would be limited using these techniques.

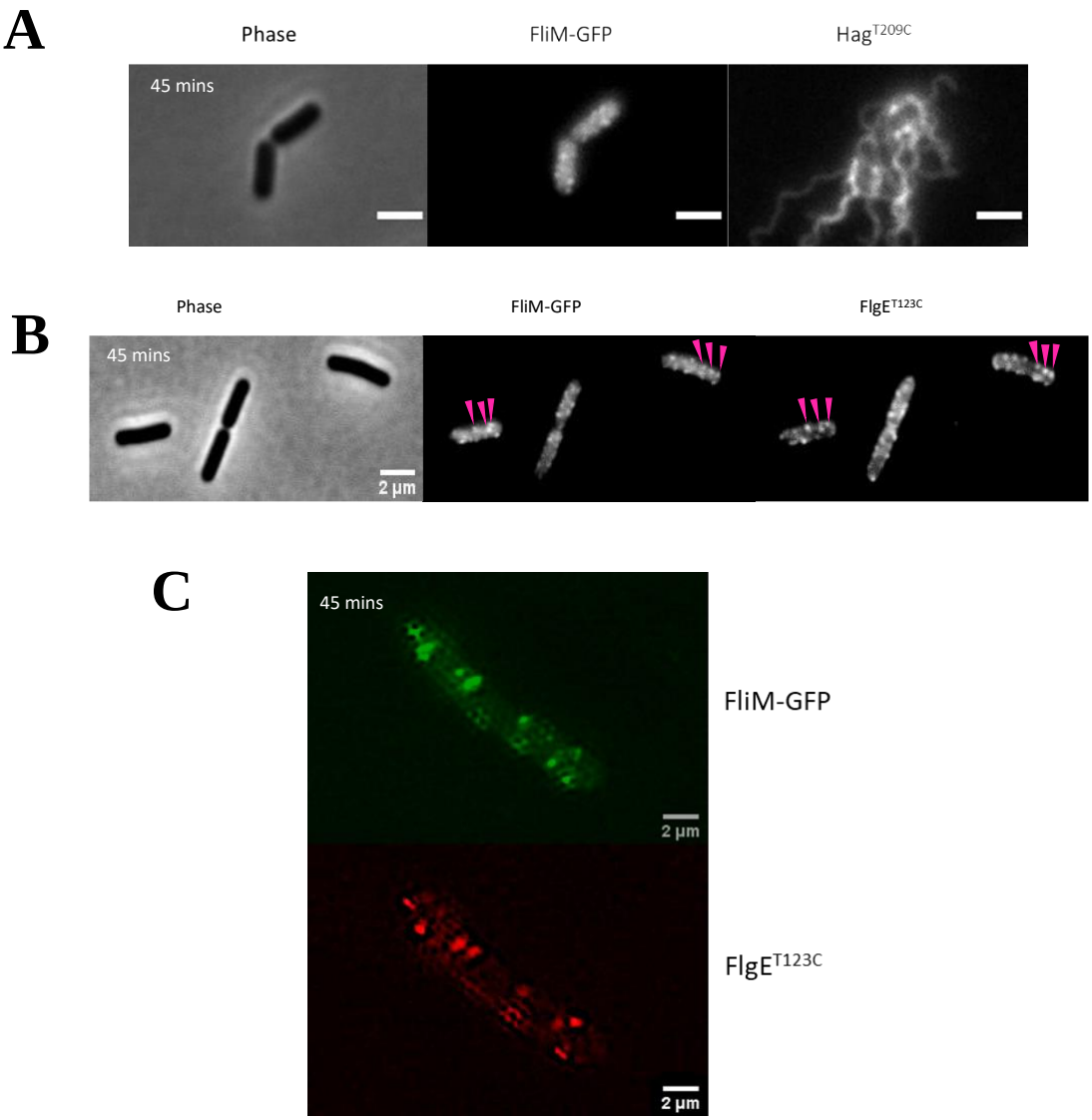

Figure 5.3 Localisation of the basal body, hook, and filament

A- Fluorescent micrographs of FliM (basal body protein) in a strain background (AA048) containing a *fliM-gfp* fusion and Hag^{T209C} allele of flagellin, used to detect the localisations of the basal body in relation to flagellin. **B-** Fluorescent micrographs indicate the localisation of FliM (basal body protein) in relation to FlgE (hook protein) in a strain background (AA035) containing a *fliM-gfp* fusion and *flgE* (hook protein) cysteine labeled with a single surface-exposed cysteine residue. Cells were collected in 45 mins after shifting the medium from LB to PTM. The cells were stained with Alexa Fluor 594 C5-maleimide conjugated dye (red). Pink arrows indicate the locations of FliM and FlgE. **C-** Structured Illumination microscopy images of FliM-GFP and FlgE^{T123C}. Scale bars represent 2 microns.

5.4 Visualising cell growth and surface movement of the flagellar hook

To track cell growth and the relative position of flagella, strains were constructed with a fluorescent fusion that labeled the cell membrane, WalP23-GFP, and tagged components of the flagellum complex. The pattern of cell wall expansion was determined by analysing the movement of the flagellar hook during cell growth. Cells with a *walP23-gfp* fusion and *flgE* ^{T123C} allele were stained with Alexa Fluor 594 C5-maleimide conjugated dye (red) and observed under a fluorescence microscope as they grew. Time-lapse sequences of images captured the cell dimensions and septum, indicated by WalP23-GFP, as well as the flagellar hook represented by red dots (Figure 5.4). The flagellar hooks were observed to be located either near the edge of the cell poles (represented by red boxes) or scattered further away from them along the cell axis (represented by green boxes) (Figure 5.5A).

To analyse the distance between the flagellar hooks and/or cell poles, lines were drawn in micrometres (µm) using the fluorescent images at T0 (representing the parent cell) and after 75 minutes of growth (representing the daughter cells) of growth, and then the length of these lines was compared. The distance between hooks 1 and 3 (represented by the green line) increased from 0.5 to 0.7 µm, and the distance between hooks 4 and 5 (represented by the grey line) increased from 0.7 to 1.3 µm (Figure 5.5 B/C/D). Similarly, the distance between the flagellar hooks and the cell septum (hooks no.5, no.7, and no.6) increased from 0.8 to 1.4 µm (blue line), 0.7 to 1.2 µm (pink line), and 5.1 to 8.9 µm (yellow line), respectively. The white line between flagellar hook no. 5 and the cell pole increased from 1.5 to 2.4 µm, and the distance between flagellar hook no.7 and the cell pole increased from 1.6 to 2.6 µm (represented by the orange line) (Figure 5.5 B/C/D).

The flagellar hooks 1 and 2 that were very close to the cell poles remained relatively constant, indicating low cell wall synthesis in this area (Figure 5.5E, purple arrows). The movement of the flagellar hooks along the lateral cell wall, as shown by the black horizontal line linking hooks 5 and 6, indicated that the cell wall elongates along the axial direction of the cell (Figure 5.5E). The distance between the cell pole and the flagellar hooks located further away from the cell poles increased as the cells elongated, suggesting ongoing cell wall synthesis in these areas.

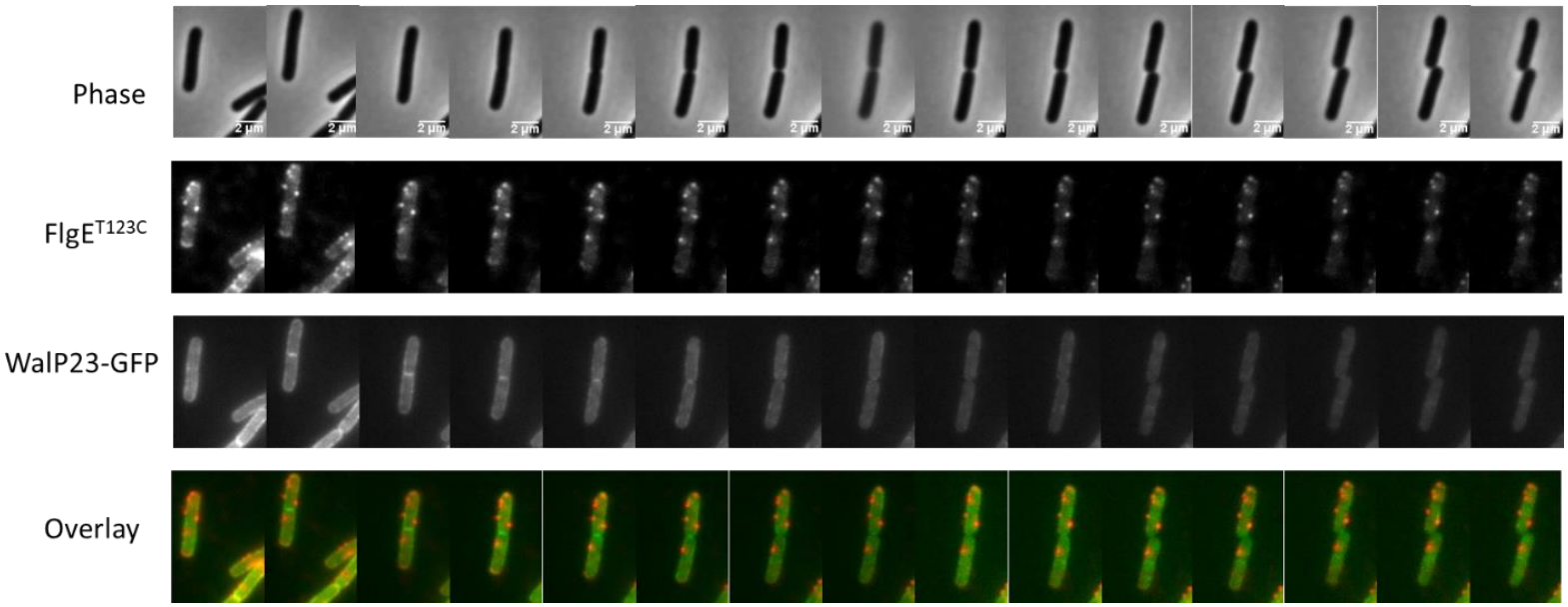

Figure 5.4 Tracking flagella on a cell surface

Time-lapse fluorescent images showing the universal joint protein (FlgE) of the flagella used as a landmark on the cell surface, utilising a strain with a *walP*$_{23}$*-gfp* and FlgE^{T123C} allele. The T0 image refers to when exponentially growing cells diluted back from LB to PTM. The strain was stained with Alexa Fluor 594 C5-maleimide conjugated dye (red) to introduce a single surface-exposed cysteine residue. Scale bars represent 2 microns. Images were captured at 5-minute intervals.

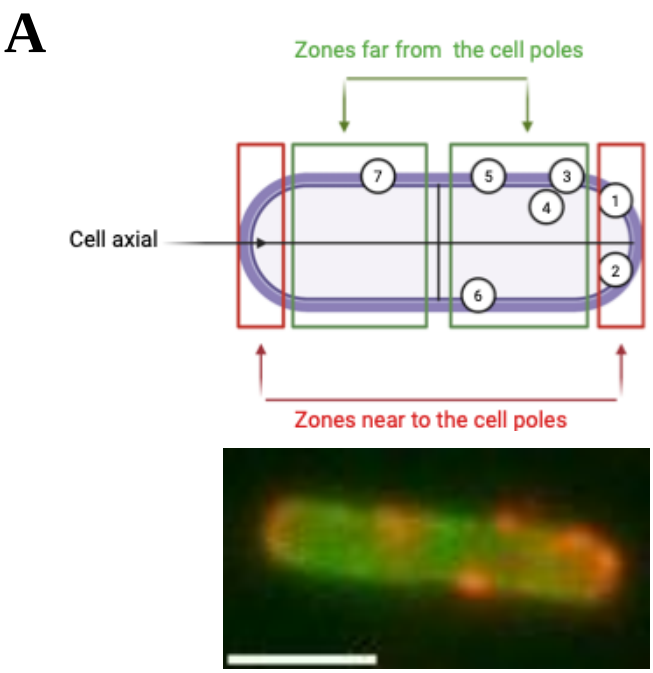
A
Zones far from the cell poles
Cell axial
Zones near to the cell poles
B
T0
1.5
0.5
0.7
0.8
0.4
0.7
1.6 µm
75 min
2.4
0.7
1.3
1.4
0.9
1.2
2.6 µm
C

D

Line and a hook number	Distance in microns at T0	Distance in microns at 75 min
Green line (1to 3)	0.5	0.7
Grey line (4 to 5)	0.7	1.3
Blue line (5 to division site)	0.8	1.4
Pink line (7 to division site)	0.7	1.2
Yellow line (6 to a cell pole)	0.4	0.9
White line (6 to a cell pole)	1.6	2.6
Orange line (7 to a cell pole)	1.5	2.4

E

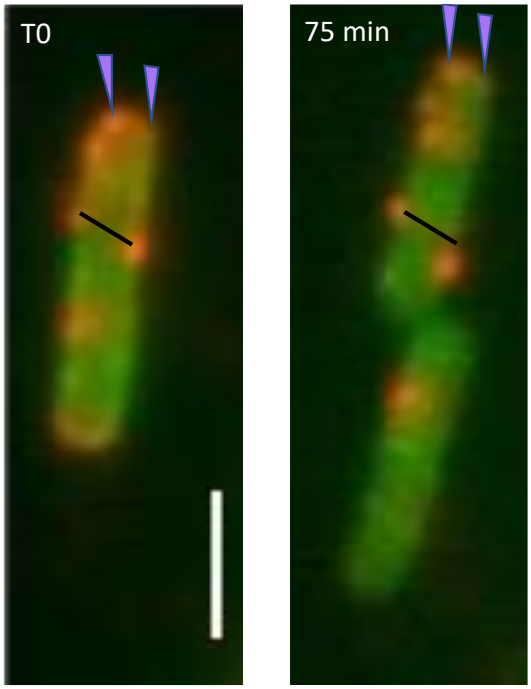

Figure 5.5 Tracking flagellar hooks on the cell surface

A- A fluorescent image from the time-lapse at T0 is shown, displaying the FlgE protein, along with a corresponding cartoon. The red boxes show the zones near the poles, while the green boxes are the further zones. The strain, with *walP23-gfp* and *flgE*^{T123C} backgrounds, was stained with Alexa Fluor 594 C5-maleimide conjugated dye (red) to introduce a single surface-exposed cysteine residue. **B-** Fluorescent images from the time-lapse images at T0 and 75 minutes are presented, depicting the parent cell initially and later the daughter cells, respectively. Coloured lines represent the changing distances, in microns (µm), between hooks and division or polar sites, as well as the changing distances between two hooks. **C-** Corresponding cartoons of the fluorescent images illustrate the images at T0 and 75 minutes. **D-** A table presents measurements of the varying distances, in microns (µm), that occur between hooks and division or polar sites. **E-** Fluorescent images show the static hooks (indicated by purple arrows) and the movement of the hooks within the lateral cell wall, represented by a black line. The illustration was created with BioRender.com. Scale bars represent 2 microns.

5.5 Discussion

This chapter investigated the pattern of cell wall expansion in *B. subtilis* by examining the fixed landmarks provided by the flagella projections on the cell wall. The flagella are complex structures consisting of inner components (basal body and rod) and outer components (hook and filament) within the bacterial cell. Considering the structure of the flagella, it was initially expected that their insertion into the cell wall would interfere with the orientation of the cytoskeleton and hinder the synthesis and lateral movement of the peptidoglycan layers relative to each other. However, during this study, it was observed that cells exhibiting a significant number of flagellar basal bodies were able to grow and divide normally, exhibiting a significant number of flagellar basal bodies. The basal body is the base of the flagellum that is constructed in the cell membrane, so it was possible that the rest of the flagellar structure was absent and not yet attached to the cell wall during cell growth. A study by Guttenplan (182) showed that the assembly of a fully functional flagellum when artificially induced, takes approximately 40 minutes. This process involves the basal body assembly, which takes up to 5 minutes, followed by the hook assembly (10 minutes), and the first appearance of the filament is in 15 minutes, which then grows into a longer filament within an additional 10 minutes. This indicates that during rapid growth, the mother cell develops flagella that become functional in the daughter cells. The use of a shift media technique from LB to PTM was also found to stimulate the formation of full flagella within 40 minutes. During this time period, it was observed that each basal body contained a hook. However, it was challenging to detect flagellin in relation to the basal body and hook as the flagella often appeared tangled together or wrapped over the cell surface.

Understanding how cell growth copes with and encompasses the flagella is a novel way to address the mechanisms behind cell wall expansion. Preliminary observations have indicated that the flagella can be found either near the cell caps region or further away on the lateral cell wall. A similar study conducted on *E. coli* proposed a model that utilises the flagella as fixed landmarks, showing that the flagella are located either in the inert zones (spherical caps) specified as 0.27 μm from the cell poles' tips or the active zones (cylindrical body) (254). In the inert zones, the flagella remain fixed, whereas in the active zones, they undergo movement during cell elongation. Similar observations were made in the current study using *B. subtilis* as a

model organism, indicating that cell wall synthesis is slower at the cell caps but more active at the lateral cell wall during cell elongation. This aligns with the observations made by Koch and Doyle (8) supporting the concept that *B. subtilis* elongates cylindrically during growth, with the poles serving as fixed support points that do not undergo significant changes in the peptidoglycan structure.

Earlier studies have reported that the peptidoglycan architecture elongates in a twisted manner, with the peptidoglycan strands arranged in a helix-like structure (235, 251). Given that the flagella move along the axial direction of the cell (Figure 5.6A), it is believed that the flagella remained static at the cell wall, and cell wall synthesis occurs in a twisted manner around the flagella, pushing them along the axial direction (Figure 5.6B). This model explains why the flagella remains constant close to the cell poles, as the cell wall synthesis in these regions is very slow.

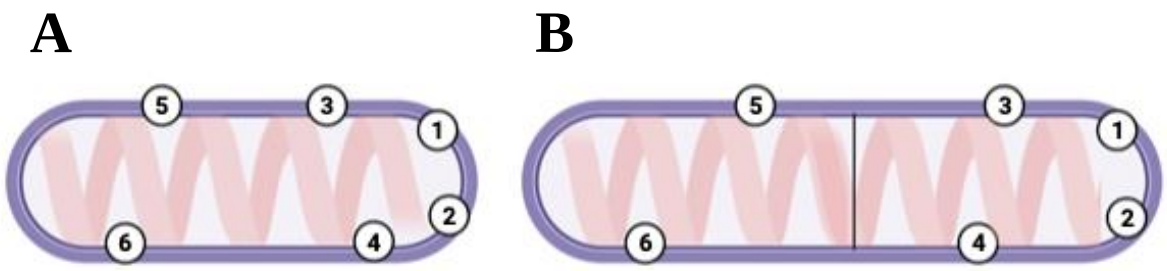

Figure 5.6 Proposed model of the cell wall elongation in a flagellated cell

A- A mother cell devolves flagella during cell growth. **B-** The peptidoglycan expands in a twisted manner, allowing the mother cell to elongate and divide, giving two daughter cells. During cell wall expansion, the flagella on the lateral cell wall are pushed and moved toward the axial direction of the cell, whereas the flagella at the cell poles remain constant as there is no cell wall expansion in those regions. The illustration was created with BioRender.com.

From the limited data obtained in this work, which was unfortunately impacted by the Covid-19 pandemic crisis, there is no clear indication that there is axial separation of pairs of flagella during growth. Also, there were challenges during our attempts to trace the flagella. This experiment employing fluorescence microscopy was hindered by cell rotation, which affected the accuracy and resolution of the observations. To overcome this challenge and obtain

more precise results, the decision was made to repeat the experiment using Total Internal Reflection Fluorescence (TIRF) microscopy. Necessary adjustments were made to set up the TIRF microscopy experiment. The experimental conditions were carefully prepared to ensure optimal usage of the TIRF microscopy technique. Unfortunately, despite the preparations and efforts made to utilise TIRF microscopy, unforeseen constraints limited the available time for conducting the experiment. As a result, the experiment could not be completed within the allocated time frame.

Chapter 6
Concluding Remarks and Future Directions

Bacillus subtilis is a bacterial species that is very common, often isolated from soil, and has been extensively studied as a model organism for bacterial research due to its fully sequenced genome, ease of genetic manipulation, and the fact that it exhibits cellular differentiation during sporulation. It is also widely exploited industrially for the production of secreted enzymes, e.g., proteases and small metabolites such as riboflavin. More recently, research has started to unravel the mechanisms by which this bacterial species is able to faithfully maintain its distinctive rod-shaped morphology through coordinated cell wall synthesis without compromising its structural integrity. It is also clear that the mechanisms employed are conserved in a wide range of bacteria, particularly Gram-positive species, both rod-shaped and coccoid, but also many processes seem to be similar in the structurally different Gram-negative bacteria. Thus, having a comprehensive understanding of how *B. subtilis* functions is more than just academic curiosity; it has application clinically through understanding how to perturb bacterial growth and industrially, through the optimisation of bio-processes as greener alternatives for both pharmaceutical and chemicals that currently directly or indirectly rely on petrochemicals.

The thesis presents a set of findings related to how *B. subtilis* can degrade the cell wall in a controlled way such that cell enlargement is possible under standard lab conditions. From this work, it is shown that growth requires only one of two key autolytic enzymes, LytE or CwlO. The other comparable enzymes, meaning having the ability to degrade the cell wall, that are expressed in vegetative growth (LytD, LytG, LytC, LytF, CwlS, and CwlQ) are dispensable for growth but clearly have other roles. LytE and CwlO have long been known to be important and purportedly functionally redundant (105). However, the fact that functional analysis of CwlO clearly indicates that it is membrane-associated and this interaction (with other proteins - FtsEX and SweCD) is required for its activity (107, 111). In contrast, LytE is secreted and seems to be functional without regulation; hence, it can function anywhere in the wall, making it hard to see how they were functionally interchangeable. In this respect, the results presented here resolve the conflicting concept of having an active autolytic enzyme near the site of new wall synthesis, in that CwlO has a probable substrate preference (requires the terminal D-alanine to be removed from the peptidoglycan by DacA and LdcB (60, 69)). In addition, this work clearly shows that although one is able to permit cell growth to occur, the resulting cells have distinctive, though potentially subtle morphologies, depending on the growth conditions (Figure 3.4); the results

also indicate that the functional redundancies are much more complicated (Chapter 3/ Sections 3.3 and 3.7). At the simplest level, the loss of CwlO results in problems with both cell morphology and LytE, while LytF acts to minimize the consequences of this defect during normal cell growth. In addition to these differences in vegetative growth, CwlO was found to play a key but, again, partially redundant role in permitting the assembly of flagella (CwlQ and CwlS also having at least partially overlapping activities). Interestingly, both CwlO and LytE are suggested to be important for other processes where the passage of material must cross the cell wall; of this, genetic competence is one which was encountered in this work but not investigated in detail. The observation that the loss of either LytE or CwlO has a significant impact on the ability of *B. subtilis* to be naturally transformed (227) and our observation that *dacA* has a similar effect potentially implies that the DNA uptake channel requires these two enzymes in different ways to allow DNA to reach the cell membrane. Perhaps CwlO allows the channel to assemble correctly, and LytE opens the wall to allow the DNA to reach the channel!

In summary, this work has tried to address cell wall metabolism from a different perspective, which was discussed in detail in each chapter. Most previous research had focused on the synthetic aspect of peptidoglycan and had not addressed how controlled cell degradation might be modulated. Perhaps unsurprisingly, it was found that this aspect of bacterial cell biology, like most other essential processes in *B. subtilis*, has many functionally redundant components. Here, the best guess would be that this ensures functionality under all conditions, such as extreme environmental changes, but equally could suggest that the mechanisms have been duplicated for specific processes, but in so doing, the original function is still maintained. This latter option could apply to the activities of CwlO, CwlS and, CwlQ, where they clearly have overlapping functions in some aspects but not all. However, perhaps the most important aspect that this work has provided is an insight into how old and new cell walls may be differentiated. This has potentially interesting applications, as the ability to disrupt the control of the autolytic system represents a novel route to the development of antibiotics. The idea being that autolysins are essential, but if uncontrolled, they are lethal to the cell under normal conditions. Thus, resistance cannot be attained by simple loss of function, and the alternative mechanism to repurpose the mechanism is likely to be complex and unlikely to occur rapidly. Thus, one direction of research would be to confirm how much of this mechanism is common to other bacteria. Current literature, to some degree, suggests that DD-carboxypeptidases have

important roles in *E. coli* (255-257), *M. tb.* (258), and *Caulobacter* (259), although it is unclear if these roles are linked to the function of CwlO like autolytic enzymes.

Despite these insights, a deeper understanding of each autolytic enzyme's precise role during vegetative growth requires further investigation. This analysis now seems possible, given the fact that the absence of DacA will have an impact. It would allow an understanding of how the wall is recycled and which enzymes are important in this process. A possible approach could involve exploring at the biochemical level to determine if there are alterations in cell wall composition or if the culture medium of autolytic mutants contains detectable fragments of the cell wall. Efficiently labeling the cell wall could permit visualisation of any changes in local turnover within living cells and also enable easy detection of cell wall fragments released into the culture medium during growth by utilising advanced techniques like High-Performance Liquid Chromatography (HPLC) and mass spectrometry.

Furthermore, the presence of growth defects and twisting phenotypes in *dacA* background strains emphasizes the importance of accounting for morphological abnormalities during cell wall labeling analysis. In this instance, these phenotypes hindered the precise assessment of cell wall turnover and synthesis based on fluorescent signals. It is crucial to recognise such limitations and explore alternative approaches or additional techniques to complement the cell wall labeling data. By integrating multiple approaches, researchers can achieve a more comprehensive understanding of cell wall dynamics, thereby overcoming the limitations posed by specific phenotypes or challenges in labeling.

Considering *B. subtilis'* conjugation mechanism for DNA transport through the cell wall, facilitated by specific pili structures, raises intriguing questions about autolytic enzyme involvement in their assembly (191, 260). These pili are capable of traversing the layers of the cell wall in a manner reminiscent of flagellar insertion. It is plausible that the extension of these pili necessitates the involvement of autolytic enzymes, enabling them to successfully traverse the cell wall and facilitate the uptake of DNA into the cell. Thus, do the autolytic enzymes responsible for flagellar assembly (CwlO, CwlQ, and CwlS) also play a role in the pili assembly? Would an inhibitor of CwlO or its interactors (DacA?) result in pathogen adhesion being lost? Further investigations are required to contribute significantly to the broader understanding of *B. subtilis* and its intricate cell wall dynamics.

To extend the significance of these findings, it's crucial to broaden the investigation beyond *B. subtilis* to other bacterial species. Examining the roles of DD-carboxypeptidases and autolysins in diverse microbial contexts, including Gram-negative bacteria and pathogens, could provide valuable insights into conserved or divergent functions. Such comparative studies will contribute to a broader understanding of cell wall dynamics across different microbial systems.

References

1. Hobot J, Carlemalm E, Villiger W, Kellenberger E. Periplasmic gel: new concept resulting from the reinvestigation of bacterial cell envelope ultrastructure by new methods. Journal of bacteriology. 1984;160(1):143-52.
2. Silhavy TJ, Kahne D, Walker S. The bacterial cell envelope. Cold Spring Harbor perspectives in biology. 2010;2(5):a000414.
3. Rohde M. The Gram-positive bacterial cell wall. Microbiology Spectrum. 2019;7(3):10.1128/microbiolspec. gpp3-0044-2018.
4. Zerbib D. Bacterial cell envelopes: composition, architecture, and origin. Handbook of Electroporation. 2017;25:417-36.
5. Panawala L. Difference between gram positive and gram negative bacteria. Epedıaa. 2017;3:1-13.
6. Vollmer W, Joris B, Charlier P, Foster S. Bacterial peptidoglycan (murein) hydrolases. FEMS microbiology reviews. 2008;32(2):259-86.
7. Höltje J-V. Growth of the stress-bearing and shape-maintaining murein sacculus of *Escherichia coli.* Microbiology and molecular biology reviews. 1998;62(1):181-203.
8. Koch AL, Doyle RJ. Inside-to-outside growth and turnover of the wall of gram-positive rods. Journal of theoretical biology. 1985;117(1):137-57.
9. van Heijenoort J. Peptidoglycan hydrolases of *Escherichia coli*. Microbiology and Molecular Biology Reviews. 2011;75(4):636-63.
10. Yang DC, Peters NT, Parzych KR, Uehara T, Markovski M, Bernhardt TG. An ATP-binding cassette transporter-like complex governs cell-wall hydrolysis at the bacterial cytokinetic ring. Proceedings of the National Academy of Sciences. 2011;108(45):E1052-E60.
11. Domínguez-Cuevas P, Porcelli I, Daniel RA, Errington J. Differentiated roles for MreB-actin isologues and autolytic enzymes in *Bacillus subtilis* morphogenesis. Molecular microbiology. 2013;89(6):1084-98.
12. Pooley H. Layered distribution, according to age, within the cell wall of *Bacillus subtilis*. Journal of Bacteriology. 1976;125(3):1139-47.
13. Milewski S, Gabriel I, Olchowy J. Enzymes of UDP-GlcNAc biosynthesis in yeast. Yeast. 2006;23(1):1-14.
14. He X, Agnihotri G, Liu H-w. Novel enzymatic mechanisms in carbohydrate metabolism. Chemical reviews. 2000;100(12):4615-62.
15. Teplyakov A, Leriche C, Obmolova G, Badet B, Badet-Denisot M-A. From Lobry de Bruyn to enzyme-catalyzed ammonia channelling: molecular studies of D-glucosamine-6P synthase. Natural Product Reports. 2002;19(1):60-9.
16. Jolly L, Pompeo Fdr, van Heijenoort J, Fassy F, Mengin-Lecreulx D. Autophosphorylation of phosphoglucosamine mutase from *Escherichia coli.* Journal of Bacteriology. 2000;182(5):1280-5.
17. Brown K, Pompeo F, Dixon S, Mengin-Lecreulx D, Cambillau C, Bourne Y. Crystal structure of the bifunctional N-acetylglucosamine 1-phosphate uridyltransferase from *Escherichia coli*: a paradigm for the related pyrophosphorylase superfamily. The EMBO journal. 1999.
18. Walter A, Mayer C. Peptidoglycan structure, biosynthesis, and dynamics during bacterial growth. Extracellular sugar-based biopolymers matrices. 2019:237-99.

19. El Zoeiby A, Sanschagrin F, Levesque RC. Structure and function of the Mur enzymes: development of novel inhibitors. Molecular microbiology. 2003;47(1):1-12.
20. Bugg T, Walsh C. Intracellular steps of bacterial cell wall peptidoglycan biosynthesis: enzymology, antibiotics, and antibiotic resistance. Natural product reports. 1992;9(3):199-215.
21. Du W, Brown JR, Sylvester DR, Huang J, Chalker AF, So CY, *et al.* Two active forms of UDP-N-acetylglucosamine enolpyruvyl transferase in gram-positive bacteria. Journal of Bacteriology. 2000;182(15):4146-52.
22. Kock H, Gerth U, Hecker M. MurAA, catalysing the first committed step in peptidoglycan biosynthesis, is a target of Clp-dependent proteolysis in *Bacillus subtilis.* Molecular Microbiology. 2004;51(4):1087-102.
23. Blake KL, O'Neill AJ, Mengin-Lecreulx D, Henderson PJ, Bostock JM, Dunsmore CJ, *et al.* The nature of *Staphylococcus aureus* MurA and MurZ and approaches for detection of peptidoglycan biosynthesis inhibitors. Molecular microbiology. 2009;72(2):335-43.
24. Benson TE, Marquardt JL, Marquardt AC, Etzkorn FA, Walsh CT. Overexpression, purification, and mechanistic study of UDP-N-acetylenolpyruvylglucosamine reductase. Biochemistry. 1993;32(8):2024-30.
25. Walsh C. Enzymes in the D-alanine branch of bacterial cell wall peptidoglycan assembly. Journal of biological chemistry. 1989;264(5):2393-6.
26. Marquardt J, Siegele D, Kolter R, Walsh C. Cloning and sequencing of *Escherichia coli murZ* and purification of its product, a UDP-N-acetylglucosamine enolpyruvyl transferase. Journal of Bacteriology. 1992;174(17):5748-52.
27. Bouhss A, Mengin-Lecreulx D, Blanot D, van Heijenoort J, Parquet C. Invariant amino acids in the Mur peptide synthetases of bacterial peptidoglycan synthesis and their modification by site-directed mutagenesis in the UDP-MurNAc: L-alanine ligase from *Escherichia coli*. Biochemistry. 1997;36(39):11556-63.
28. Patin D, Boniface A, Kovač A, Hervé M, Dementin S, Barreteau H, *et al.* Purification and biochemical characterization of Mur ligases from *Staphylococcus aureus.* Biochimie. 2010;92(12):1793-800.
29. Mahapatra S, Yagi T, Belisle JT, Espinosa BJ, Hill PJ, McNeil MR, *et al.* Mycobacterial lipid II is composed of a complex mixture of modified muramyl and peptide moieties linked to decaprenyl phosphate. Journal of bacteriology. 2005;187(8):2747-57.
30. Hu Y, Chen L, Ha S, Gross B, Falcone B, Walker D, *et al.* Crystal structure of the MurG: UDP-GlcNAc complex reveals common structural principles of a superfamily of glycosyltransferases. Proceedings of the National Academy of Sciences. 2003;100(3):845-9.
31. Mengin-Lecreulx D, Texier L, Rousseau M, van Heijenoort J. The *murG* gene of *Escherichia coli* codes for the UDP-N-acetylglucosamine: N-acetylmuramyl-(pentapeptide) pyrophosphoryl-undecaprenol N-acetylglucosamine transferase involved in the membrane steps of peptidoglycan synthesis. Journal of bacteriology. 1991;173(15):4625-36.
32. Rogers H, Perkins H, Ward J, Rogers H, Perkins H, Ward J. Biosynthesis of peptidoglycan. Microbial cell walls and membranes. 1980:239-97.
33. Maidhof H, Reinicke B, Blümel P, Berger-Bächi B, Labischinski H. femA, which encodes a factor essential for expression of methicillin resistance, affects glycine content of peptidoglycan in methicillin-resistant and methicillin-susceptible *Staphylococcus aureus* strains. Journal of bacteriology. 1991;173(11):3507-13.

34. Henze U, Sidow T, Wecke J, Labischinski H, Berger-Bächi B. Influence of *femB* on methicillin resistance and peptidoglycan metabolism in *Staphylococcus aureus*. Journal of bacteriology. 1993;175(6):1612-20.
35. Rohrer S, Ehlert K, Tschierske M, Labischinski H, Berger-Bächi B. The essential *Staphylococcus aureus* gene *fmhB* is involved in the first step of peptidoglycan pentaglycine interpeptide formation. Proceedings of the National Academy of Sciences. 1999;96(16):9351-6.
36. Schneider T, Senn MM, Berger-Bächi B, Tossi A, Sahl HG, Wiedemann I. In *vitro* assembly of a complete, pentaglycine interpeptide bridge containing cell wall precursor (lipid II-Gly5) of *Staphylococcus aureus.* Molecular microbiology. 2004;53(2):675-85.
37. Thumm G, Götz F. Studies on prolysostaphin processing and characterization of the lysostaphin immunity factor (Lif) of *Staphylococcus simulans biovar staphylolyticus.* Molecular microbiology. 1997;23(6):1251-65.
38. Tschierske M, Ehlert K, Stranden A, Berger-Bächi B. Lif, the lysostaphin immunity factor, complements FemB in *staphylococcal* peptidoglycan interpeptide bridge formation. FEMS microbiology letters. 1997;153(2):261-4.
39. Filipe SR, Pinho MG, Tomasz A. Characterization of the *murMN* operon involved in the synthesis of branched peptidoglycan peptides in *Streptococcus pneumoniae*. Journal of Biological Chemistry. 2000;275(36):27768-74.
40. Bouhss A, Josseaume N, Severin A, Tabei K, Hugonnet J-E, Shlaes D, *et al.* Synthesis of the L-alanyl-L-alanine cross-bridge of *Enterococcus faecalis* peptidoglycan. Journal of Biological Chemistry. 2002;277(48):45935-41.
41. Kresge N, Simoni RD, Hill RL. tRNA Involvement in Peptidoglycan Synthesis: the Work of Dieter Söll. Journal of Biological Chemistry. 2007;282(26):e20-e1.
42. Mahapatra S, Crick DC, Brennan PJ. Comparison of the UDP-N-acetylmuramate: L-alanine ligase enzymes from *Mycobacterium tuberculosis* and *Mycobacterium leprae.* Journal of bacteriology. 2000;182(23):6827-30.
43. Chopra I, Storey C, Falla TJ, Pearce JH. Antibiotics, peptidoglycan synthesis and genomics: the c*hlamydial anomaly* revisited. Microbiology. 1998;144(10):2673-8.
44. Vollmer W, Blanot D, De Pedro MA. Peptidoglycan structure and architecture. FEMS microbiology reviews. 2008;32(2):149-67.
45. Figueiredo TA, Sobral RG, Ludovice AM, de Almeida JMF, Bui NK, Vollmer W, *et al.* Identification of genetic determinants and enzymes involved with the amidation of glutamic acid residues in the peptidoglycan of *Staphylococcus aureus.* PLoS pathogens. 2012;8(1):e1002508.
46. Münch D, Roemer T, Lee SH, Engeser M, Sahl HG, Schneider T. Identification and in *vitro* analysis of the GatD/MurT enzyme-complex catalyzing lipid II amidation in S*taphylococcus aureus.* PLoS pathogens. 2012;8(1):e1002509.
47. Boniface A. Etude des relations structure-activité au sein de la famille des Mur synthétases, enzymes de la voie de biosynthèse du peptidoglycane 2007.
48. Hammes WP, Neukam R, Kandler O. On the specificity of the uridine diphospho-N-acetylmuramyl-alanyl-D-glutamic acid: diamino acid ligase of *Bifidobacterium globosum.* Archives of Microbiology. 1977;115:95-102.
49. Boniface A, Bouhss A, Mengin-Lecreulx D, Blanot D. The MurE synthetase from Thermotoga maritima is endowed with an unusual D-lysine adding activity. Journal of Biological Chemistry. 2006;281(23):15680-6.

50. Duncan K, Van Heijenoort J, Walsh CT. Purification and characterization of the D-alanyl-D-alanine-adding enzyme from *Escherichia coli.* Biochemistry. 1990;29(9):2379-86.
51. Neuhaus FC, Struve WG. Enzymatic synthesis of analogs of the cell-wall precursor. I. Kinetics and specificity of uridine diphospho-N-acetylmuramyl-L-alanyl-D-glutamyl-L-lysine: D-alanyl-D-alanine ligase (adenosine diphosphate) from *Streptococcus faecalis* R. Biochemistry. 1965;4(1):120-31.
52. Healy VL, Lessard IA, Roper DI, Knox JR, Walsh CT. Vancomycin resistance in *enterococci:* reprogramming of the d-Ala–d-Ala ligases in bacterial peptidoglycan biosynthesis. Chemistry & biology. 2000;7(5):R109-R19.
53. Ruiz N. Bioinformatics identification of MurJ (MviN) as the peptidoglycan lipid II flippase in *Escherichia coli.* Proceedings of the National Academy of Sciences. 2008;105(40):15553-7.
54. Ruiz N. *Streptococcus pyogenes* YtgP (Spy_0390) complements *Escherichia coli* strains depleted of the putative peptidoglycan flippase MurJ. Antimicrobial agents and chemotherapy. 2009;53(8):3604-5.
55. Sham L-T, Butler EK, Lebar MD, Kahne D, Bernhardt TG, Ruiz N. MurJ is the flippase of lipid-linked precursors for peptidoglycan biogenesis. Science. 2014;345(6193):220-2.
56. Meeske AJ, Sham L-T, Kimsey H, Koo B-M, Gross CA, Bernhardt TG, *et al.* MurJ and a novel lipid II flippase are required for cell wall biogenesis in *Bacillus subtilis.* Proceedings of the National Academy of Sciences. 2015;112(20):6437-42.
57. Van Heijenoort J. Biosynthesis of the bacterial peptidoglycan unit. New Comprehensive Biochemistry. 27: Elsevier; 1994. p. 39-54.
58. Ward JB, Perkins HR. The direction of glycan synthesis in a bacterial peptidoglycan. Biochemical Journal. 1973;135(4):721-8.
59. McPherson DC, Driks A, Popham DL. Two class A high-molecular-weight penicillin-binding proteins of *Bacillus subtilis* play redundant roles in sporulation. Journal of bacteriology. 2001;183(20):6046-53.
60. Atrih A, Bacher G, Allmaier Gn, Williamson MP, Foster SJ. Analysis of peptidoglycan structure from vegetative cells of *Bacillus subtilis* 168 and role of PBP 5 in peptidoglycan maturation. Journal of bacteriology. 1999;181(13):3956-66.
61. Blattner FR, Plunkett III G, Bloch CA, Perna NT, Burland V, Riley M, *et al*. The complete genome sequence of *Escherichia coli* K-12. science. 1997;277(5331):1453-62.
62. Kunst F, Ogasawara N, Moszer I, Albertini A, Alloni G, Azevedo V, *et al.* The complete genome sequence of the gram-positive bacterium *Bacillus subtilis.* Nature. 1997;390(6657):249-56.
63. Spratt BG, Cromie KD. Penicillin-binding proteins of gram-negative bacteria. Clinical Infectious Diseases. 1988;10(4):699-711.
64. Goffin C, Ghuysen J-M. Multimodular penicillin-binding proteins: an enigmatic family of orthologs and paralogs. Microbiology and molecular biology reviews. 1998;62(4):1079-93.
65. Guillen N, Weinrauch Y, Dubnau D. Cloning and characterization of the regulatory *Bacillus* subtilis competence genes *comA* and *comB.* Journal of bacteriology. 1989;171(10):5354-61.
66. Macheboeuf P, Contreras-Martel C, Job V, Dideberg O, Dessen A. Penicillin binding proteins: key players in bacterial cell cycle and drug resistance processes. FEMS microbiology reviews. 2006;30(5):673-91.

67. Sauvage E, Kerff F, Terrak M, Ayala JA, Charlier P. The penicillin-binding proteins: structure and role in peptidoglycan biosynthesis. FEMS microbiology reviews. 2008;32(2):234-58.
68. Scheffers D-J, Pinho MG. Bacterial cell wall synthesis: new insights from localization studies. Microbiology and molecular biology reviews. 2005;69(4):585-607.
69. Hoyland CN, Aldridge C, Cleverley RM, Duchêne M-C, Minasov G, Onopriyenko O, *et al.* Structure of the LdcB LD-carboxypeptidase reveals the molecular basis of peptidoglycan recognition. Structure. 2014;22(7):949-60.
70. Spratt BG. Distinct penicillin binding proteins involved in the division, elongation, and shape of *Escherichia coli* K12. Proceedings of the National Academy of Sciences. 1975;72(8):2999-3003.
71. Denome SA, Elf PK, Henderson TA, Nelson DE, Young KD. *Escherichia coli* mutants lacking all possible combinations of eight penicillin binding proteins: viability, characteristics, and implications for peptidoglycan synthesis. Journal of bacteriology. 1999;181(13):3981-93.
72. Young KD. Approaching the physiological functions of penicillin-bindingproteins in *Escherichia coli.* Biochimie. 2001;83(1):99-102.
73. Dowson C, Jephcott A, Gough K, Spratt B. Penicillin-binding protein 2 genes of non-β-lactamase-producing, penicillin-resistant strains of *Neisseria gonorrhoeae*. Molecular microbiology. 1989;3(1):35-41.
74. Ropp PA, Hu M, Olesky M, Nicholas RA. Mutations in *ponA*, the gene encoding penicillin-binding protein 1, and a novel locus, *penC,* are required for high-level chromosomally mediated penicillin resistance in *Neisseria gonorrhoeae*. Antimicrobial agents and chemotherapy. 2002;46(3):769-77.
75. Stefanova ME, Tomberg J, Olesky M, Höltje J-V, Gutheil WG, Nicholas RA. Neisseria gonorrhoeae penicillin-binding protein 3 exhibits exceptionally high carboxypeptidase and β-lactam binding activities. Biochemistry. 2003;42(49):14614-25.
76. Vicente M, Berenguer J, De Pedro M, Perez-Diaz J, Baquero F. Penicillin binding proteins in Listeria monocytogenes. Acta Microbiologica Hungarica. 1990;37(2):227-31.
77. Korsak D, Vollmer W, Markiewicz Z. *Listeria monocytogenes* EGD lacking penicillin-binding protein 5 (PBP5) produces a thicker cell wall. FEMS microbiology letters. 2005;251(2):281-8.
78. Zawadzka-Skomiał J, Markiewicz Z, Nguyen-Disteche M, Devreese B, Frere J-M, Terrak M. Characterization of the bifunctional glycosyltransferase/acyltransferase penicillin-binding protein 4 of *Listeria monocytogenes*. Journal of bacteriology. 2006;188(5):1875-81.
79. Goffin C, Ghuysen J-M. Biochemistry and comparative genomics of SxxK superfamily acyltransferases offer a clue to the mycobacterial paradox: presence of penicillin-susceptible target proteins versus lack of efficiency of penicillin as therapeutic agent. Microbiology and molecular biology reviews. 2002;66(4):702-38.
80. Bernard E, Rolain T, Courtin P, Guillot A, Langella P, Hols P, *et al.* Characterization of O-acetylation of N-acetylglucosamine: a novel structural variation of bacterial peptidoglycan. Journal of Biological Chemistry. 2011;286(27):23950-8.
81. Davis KM, Weiser JN. Modifications to the peptidoglycan backbone help bacteria to establish infection. Infection and immunity. 2011;79(2):562-70.
82. Park SH, Choi U, Ryu S-H, Lee HB, Lee J-W, Lee C-R. Divergent effects of peptidoglycan carboxypeptidase DacA on intrinsic β-lactam and vancomycin resistance. Microbiology Spectrum. 2022;10(4):e01734-22.

83. Juillot D, Cornilleau C, Deboosere N, Billaudeau C, Evouna-Mengue P, Lejard V, *et al.* A high-content microscopy screening identifies new genes involved in cell width control in *Bacillus subtilis.* Msystems. 2021;6(6):e01017-21.
84. Todd J, Roberts A, Johnstone K, Piggot P, Winter G, Ellar D. Reduced heat resistance of mutant spores after cloning and mutagenesis of the *Bacillus subtilis* gene encoding penicillin-binding protein 5. Journal of bacteriology. 1986;167(1):257-64.
85. Sanchez S, Snider EV, Wang X, Kearns DB. Identification of genes required for swarming motility in *Bacillus subtilis* using transposon mutagenesis and high-throughput sequencing (TnSeq). Journal of Bacteriology. 2022;204(6):e00089-22.
86. Atrih A, Zöllner P, Allmaier G, Foster SJ. Structural analysis of *Bacillus subtilis* 168 endospore peptidoglycan and its role during differentiation. Journal of bacteriology. 1996;178(21):6173-83.
87. Buchanan CE, Ling M-L. Isolation and sequence analysis of *dacB*, which encodes a sporulation-specific penicillin-binding protein in *Bacillus subtilis.* Journal of bacteriology. 1992;174(6):1717-25.
88. Popham DL, Gilmore ME, Setlow P. Roles of low-molecular-weight penicillin-binding proteins in *Bacillus subtilis* spore peptidoglycan synthesis and spore properties. Journal of bacteriology. 1999;181(1):126-32.
89. Pedersen LB, Murray T, Popham DL, Setlow P. Characterization of *dacC*, which encodes a new low-molecular-weight penicillin-binding protein in *Bacillus subtilis*. Journal of bacteriology. 1998;180(18):4967-73.
90. Duez C, Zervosen A, Teller N, Melkonian R, Banzubaze E, Bouillenne F, *et al.* Characterization of the proteins encoded by the *Bacillus subtilis yoxA-dacC* operon. FEMS microbiology letters. 2009;300(1):42-7.
91. Wilson SA, Tank RK, Hobbs JK, Foster SJ, Garner EC. An exhaustive multiple knockout approach to understanding cell wall hydrolase function in *Bacillus subtilis.* Mbio. 2023;14(5):e01760-23.
92. Blackman SA, Smith TJ, Foster SJ. The role of autolysins during vegetative growth of *Bacillus subtilis* 168. Microbiology. 1998;144(1):73-82.
93. Smith TJ, Blackman SA, Foster SJ. Autolysins of *Bacillus subtilis*: multiple enzymes with multiple functions. Microbiology. 2000;146(2):249-62.
94. Nicolas P, Mäder U, Dervyn E, Rochat T, Leduc A, Pigeonneau N, *et al.* Condition-dependent transcriptome reveals high-level regulatory architecture in *Bacillus subtilis.* Science. 2012;335(6072):1103-6.
95. Litzinger S, Mayer C. The murein sacculus. Prokaryotic cell wall compounds: structure and biochemistry. 2010:3-52.
96. Duchêne M-C, Rolain T, Knoops A, Courtin P, Chapot-Chartier M-P, Dufrêne YF, *et al.* Distinct and specific role of NlpC/P60 endopeptidases LytA and LytB in cell elongation and division of *Lactobacillus plantarum*. Frontiers in microbiology. 2019;10:713.
97. von Heijne G. The signal peptide. The Journal of membrane biology. 1990;115:195-201.
98. Tjalsma H, Bolhuis A, Van Roosmalen ML, Wiegert T, Schumann W, Broekhuizen CP, *et al*. Functional analysis of the secretory precursor processing machinery of *Bacillus subtilis*: identification of a eubacterial homolog of archaeal and eukaryotic signal peptidases. Genes & development. 1998;12(15):2318-31.

99. Park S, Schumann W. Optimization of the secretion pathway for heterologous proteins in *Bacillus subtilis*. Biotechnology and bioprocess engineering. 2015;20:623-33.
100. Luirink J, ten Hagen-Jongman CM, Van Der Weijden CC, Oudega B, High S, Dobberstein B, *et al*. An alternative protein targeting pathway in *Escherichia coli:* studies on the role of FtsY. The EMBO journal. 1994;13(10):2289-96.
101. Tjalsma H, Antelmann H, Jongbloed JD, Braun PG, Darmon E, Dorenbos R, *et al.* Proteomics of protein secretion by *Bacillus subtilis:* separating the "secrets" of the secretome. Microbiology and molecular biology reviews. 2004;68(2):207-33.
102. Tjalsma H, Bolhuis A, Jongbloed JD, Bron S, van Dijl JM. Signal peptide-dependent protein transport in *Bacillus subtilis*: a genome-based survey of the secretome. Microbiology and molecular biology reviews. 2000;64(3):515-47.
103. Hashimoto M, Matsushima H, Suparthana IP, Ogasawara H, Yamamoto H, Teng C, *et al.* Digestion of peptidoglycan near the cross-link is necessary for the growth of *Bacillus subtilis*. Microbiology. 2018;164(3):299-307.
104. Margot P, Pagni M, Karamata D. *Bacillus subtilis* 168 gene *lytF* encodes a 7-D-muropeptidase expressed by the alternative vegetative sigma factor, cD. Microbiology. 1999;145:57-65.
105. Hashimoto M, Ooiwa S, Sekiguchi J. Synthetic lethality of the *lytE cwlO* genotype in *Bacillus subtilis* is caused by lack of D, L-endopeptidase activity at the lateral cell wall. Journal of bacteriology. 2012;194(4):796-803.
106. Carballido-López R, Formstone A, Li Y, Ehrlich SD, Noirot P, Errington J. Actin homolog MreBH governs cell morphogenesis by localization of the cell wall hydrolase LytE. Developmental cell. 2006;11(3):399-409.
107. Brunet YR, Wang X, Rudner DZ. SweC and SweD are essential co-factors of the FtsEX-CwlO cell wall hydrolase complex in *Bacillus subtilis.* PLoS Genetics. 2019;15(8):e1008296.
108. Bisicchia P, Noone D, Lioliou E, Howell A, Quigley S, Jensen T, *et al.* The essential YycFG two-component system controls cell wall metabolism in *Bacillus subtilis*. Molecular microbiology. 2007;65(1):180-200.
109. Yamaguchi H, Furuhata K, Fukushima T, Yamamoto H, Sekiguchi J. Characterization of a new *Bacillus subtilis* peptidoglycan hydrolase gene, *yvcE* (named *cwlO*), and the enzymatic properties of its encoded protein. Journal of bioscience and bioengineering. 2004;98(3):174-81.
110. Reith J, Mayer C. Peptidoglycan turnover and recycling in Gram-positive bacteria. Applied microbiology and biotechnology. 2011;92(1):1-11.
111. Meisner J, Montero Llopis P, Sham LT, Garner E, Bernhardt TG, Rudner DZ. FtsEX is required for CwlO peptidoglycan hydrolase activity during cell wall elongation in *Bacillus subtilis*. Molecular microbiology. 2013;89(6):1069-83.
112. Chen R, Guttenplan SB, Blair KM, Kearns DB. Role of the σD-dependent autolysins in *Bacillus subtilis* population heterogeneity. Journal of bacteriology. 2009;191(18):5775-84.
113. Lazarevic V, Margot P, Soldo B, Karamata D. Sequencing and analysis of the *Bacillus subtilis lytRABC* divergon: a regulatory unit encompassing the structural genes of the N-acetylmuramoyl-L-alanine amidase and its modifier. Journal of general microbiology. 1992;138(9):1949-61.

114. Shah IM, Dworkin J. Induction and regulation of a secreted peptidoglycan hydrolase by a membrane Ser/Thr kinase that detects muropeptides. Molecular microbiology. 2010;75(5):1232-43.
115. Horsburgh GJ, Atrih A, Williamson MP, Foster SJ. LytG of *Bacillus subtilis* is a novel peptidoglycan hydrolase: the major active glucosaminidase. Biochemistry. 2003;42(2):257-64.
116. Sudiarta IP, Fukushima T, Sekiguchi J. *Bacillus subtilis* CwlQ (previous YjbJ) is a bifunctional enzyme exhibiting muramidase and soluble-lytic transglycosylase activities. Biochemical and Biophysical Research Communications. 2010;398(3):606-12.
117. Serizawa M, Yamamoto H, Yamaguchi H, Fujita Y, Kobayashi K, Ogasawara N, *et al.* Systematic analysis of SigD-regulated genes in *Bacillus subtilis* by DNA microarray and Northern blotting analyses. Gene. 2004;329:125-36.
118. Sanchez S, Dunn CM, Kearns DB. CwlQ is required for swarming motility but not flagellar assembly in *Bacillus subtilis.* Journal of Bacteriology. 2021;203(10):10.1128/jb. 00029-21.
119. Merad T, Archibald AR, Hancock IC, Harwood CR, Hobot JA. Cell wall assembly in *Bacillus subtilis*: visualization of old and new wall material by electron microscopic examination of samples stained selectively for teichoic acid and teichuronic acid. Microbiology. 1989;135(3):645-55.
120. Irazoki O, Hernandez SB, Cava F. Peptidoglycan muropeptides: release, perception, and functions as signaling molecules. Frontiers in microbiology. 2019;10:500.
121. Borisova M, Gaupp R, Duckworth A, Schneider A, Dalügge D, Mühleck M, *et al.* Peptidoglycan recycling in Gram-positive bacteria is crucial for survival in stationary phase. MBio. 2016;7(5):10.1128/mbio. 00923-16.
122. Mobley H, Koch A, Doyle R, Streips U. Insertion and fate of the cell wall in *Bacillus subtilis*. Journal of bacteriology. 1984;158(1):169-79.
123. Nayyab S, O'Connor M, Brewster J, Gravier J, Jamieson M, Magno E, *et al.* Diamide inhibitors of the *Bacillus subtilis* N-acetylglucosaminidase LytG that exhibit antibacterial activity. ACS infectious diseases. 2017;3(6):421-7.
124. Piepenbrink KH, Sundberg EJ. Motility and adhesion through type IV pili in Gram-positive bacteria. Biochemical Society Transactions. 2016;44(6):1659-66.
125. Kearns DB, Losick R. Swarming motility in undomesticated *Bacillus subtilis*. Molecular microbiology. 2003;49(3):581-90.
126. Burrage AM, Vanderpool E, Kearns DB. Assembly order of flagellar rod subunits in *Bacillus subtilis*. Journal of bacteriology. 2018;200(23):10.1128/jb. 00425-18.
127. Zhou J, Lloyd SA, Blair DF. Electrostatic interactions between rotor and stator in the bacterial flagellar motor. Proceedings of the National Academy of Sciences. 1998;95(11):6436-41.
128. Macnab RM. Type III flagellar protein export and flagellar assembly. Biochimica et Biophysica Acta (BBA)-Molecular Cell Research. 2004;1694(1-3):207-17.
129. Kutsukake K, Ohya Y, Iino T. Transcriptional analysis of the flagellar regulon of *Salmonella typhimurium.* Journal of bacteriology. 1990;172(2):741-7.
130. DePamphilis M, Adler J. Fine structure and isolation of the hook-basal body complex of flagella from *Escherichia coli* and *Bacillus subtilis.* Journal of Bacteriology. 1971;105(1):384-95.
131. Dimmitt K, Simon M. Purification and thermal stability of intact *Bacillus subtilis* flagella. Journal of Bacteriology. 1971;105(1):369-75.

132. Stallmeyer MB, Aizawa S-I, Macnab RM, DeRosier DJ. Image reconstruction of the flagellar basal body of *Salmonella typhimurium*. Journal of molecular biology. 1989;205(3):519-28.
133. Kubori T, Okumura M, Kobayashi N, Nakamura D, Iwakura M, Aizawa SI. Purification and characterization of the flagellar hook–basal body complex of *Bacillus subtilis.* Molecular microbiology. 1997;24(2):399-410.
134. Mukherjee S, Kearns DB. The structure and regulation of flagella in *Bacillus subtilis*. Annual review of genetics. 2014;48(1):319-40.
135. Ohnishi K, Kutsukake K, Suzuki H, Lino T. A novel transcriptional regulation mechanism in the flagellar regulon of *Salmonella typhimurium*: an anti-sigma factor inhibits the activity of the flagellum-specific Sigma factor, σF. Molecular microbiology. 1992;6(21):3149-57.
136. lyoda S, Kutsukake K. Molecular dissection of the flagellum-specific anti-sigma factor, FlgM, of *Salmonella typhimurium*. Molecular and General Genetics MGG. 1995;249:417-24.
137. Bertero MG, Gonzales B, Tarricone C, Ceciliani F, Galizzi A. Overproduction and characterization of the *Bacillus subtilis* anti-sigma factor FlgM. Journal of Biological Chemistry. 1999;274(17):12103-7.
138. Caramori T, Barilla D, Nessi C, Sacchi L, Galizzi A. Role of FlgM in sigma D-dependent gene expression in *Bacillus subtilis*. Journal of bacteriology. 1996;178(11):3113-8.
139. Fan F, Ohnishi K, Francis NR, Macnab RM. The FliP and FliR proteins of *Salmonella typhimurium*, putative components of the type III flagellar export apparatus, are located in the flagellar basal body. Molecular microbiology. 1997;26(5):1035-46.
140. Minamino T, Macnab RM. Components of the *Salmonella* flagellar export apparatus and classification of export substrates. Journal of Bacteriology. 1999;181(5):1388-94.
141. Li H, Sourjik V. Assembly and stability of flagellar motor in *Escherichia coli.* Molecular microbiology. 2011;80(4):886-99.
142. Barker CS, Meshcheryakova IV, Kostyukova AS, Samatey FA. FliO regulation of FliP in the formation of the *Salmonella enterica* flagellum. PLoS genetics. 2010;6(9):e1001143.
143. Zhu K, González-Pedrajo B, Macnab RM. Interactions among membrane and soluble components of the flagellar export apparatus of *Salmonella.* Biochemistry. 2002;41(30):9516-24.
144. Bange G, Kümmerer N, Engel C, Bozkurt G, Wild K, Sinning I. FlhA provides the adaptor for coordinated delivery of late flagella building blocks to the type III secretion system. Proceedings of the National Academy of Sciences. 2010;107(25):11295-300.
145. Fraser GM, González-Pedrajo B, Tame JR, Macnab RM. Interactions of FliJ with the *Salmonella* type III flagellar export apparatus. Journal of bacteriology. 2003;185(18):5546-54.
146. Jones CJ, Macnab RM, Okino H, Aizawa S-I. Stoichiometric analysis of the flagellar hook-(basal-body) complex of *Salmonella typhimurium.* Journal of molecular biology. 1990;212(2):377-87.
147. Ueno T, Oosawa K, Aizawa S-I. Domain structures of the MS ring component protein (FliF) of the flagellar basal body of *Salmonella typhimurium*. Journal of molecular biology. 1994;236(2):546-55.
148. Müller V, Jones CJ, Kawagishi I, Aizawa S-i, Macnab RM. Characterization of the fliE genes of *Escherichia coli* and *Salmonella typhimurium* and identification of the FliE protein as a component of the flagellar hook-basal body complex. Journal of bacteriology. 1992;174(7):2298-304.

149. Suzuki H, Yonekura K, Murata K, Hirai T, Oosawa K, Namba K. A structural feature in the central channel of the bacterial flagellar FliF ring complex is implicated in type III protein export. Journal of structural biology. 1998;124(2-3):104-14.
150. Francis NR, Irikura VM, Yamaguchi S, DeRosier DJ, Macnab RM. Localization of the *Salmonella typhimurium* flagellar switch protein FliG to the cytoplasmic M-ring face of the basal body. Proceedings of the National Academy of Sciences. 1992;89(14):6304-8.
151. Lee LK, Ginsburg MA, Crovace C, Donohoe M, Stock D. Structure of the torque ring of the flagellar motor and the molecular basis for rotational switching. Nature. 2010;466(7309):996-1000.
152. Kubori T, Yamaguchi S, Aizawa S-i. Assembly of the switch complex onto the MS ring complex of *Salmonella typhimurium* does not require any other flagellar proteins. Journal of bacteriology. 1997;179(3):813-7.
153. Bischoff DS, Ordal GW. Identification and characterization of FliY, a novel component of the *Bacillus subtilis* flagellar switch complex. Molecular microbiology. 1992;6(18):2715-23.
154. Francis NR, Sosinsky GE, Thomas D, DeRosier DJ. Isolation, characterization and structure of bacterial flagellar motors containing the switch complex. Journal of molecular biology. 1994;235(4):1261-70.
155. Irikura V, Kihara M, Yamaguchi S, Sockett H, Macnab R. *Salmonella typhimurium fliG* and *fliN* mutations causing defects in assembly, rotation, and switching of the flagellar motor. Journal of bacteriology. 1993;175(3):802-10.
156. Lloyd SA, Blair DF. Charged residues of the rotor protein FliG essential for torque generation in the flagellar motor of *Escherichia coli*. Journal of molecular biology. 1997;266(4):733-44.
157. Lloyd SA, Tang H, Wang X, Billings S, Blair DF. Torque generation in the flagellar motor of *Escherichia coli:* evidence of a direct role for FliG but not for FliM or FliN. Journal of bacteriology. 1996;178(1):223-31.
158. Homma M, Kutsukake K, Hasebe M, Iino T, Macnab RM. FlgB, FlgC, FlgF and FlgG: a family of structurally related proteins in the flagellar basal body of *Salmonella typhimurium*. Journal of molecular biology. 1990;211(2):465-77.
159. Kubori T, Shimamoto N, Yamaguchi S, Namba K, Aizawa S-I. Morphological pathway of flagellar assembly in *Salmonella typhimurium*. Journal of molecular biology. 1992;226(2):433-46.
160. Saijo-Hamano Y, Uchida N, Namba K, Oosawa K. In vitro characterization of FlgB, FlgC, FlgF, FlgG, and FliE, flagellar basal body proteins of *Salmonella*. Journal of molecular biology. 2004;339(2):423-35.
161. Jones C, Homma M, Macnab R. L-, P-, and M-ring proteins of the flagellar basal body of *Salmonella typhimurium*: gene sequences and deduced protein sequences. Journal of bacteriology. 1989;171(7):3890-900.
162. Ueno T, Oosawa K, Aizawa S-I. M ring, S ring and proximal rod of the flagellar basal body of *Salmonella typhimurium* are composed of subunits of a single protein, FliF. Journal of molecular biology. 1992;227(3):672-7.
163. Minamino T, Yamaguchi S, Macnab RM. Interaction between FliE and FlgB, a proximal rod component of the flagellar basal body of *Salmonella*. Journal of bacteriology. 2000;182(11):3029-36.

164. Okino H, Isomura M, Yamaguchi S, Magariyama Y, Kudo S, Aizawa S. Release of flagellar filament-hook-rod complex by a *Salmonella typhimurium* mutant defective in the M ring of the basal body. Journal of bacteriology. 1989;171(4):2075-82.
165. Zuberi AR, Ying C, Bischoff DS, Ordal GW. Gene-protein relationships in the flagellar hook-basal body complex of *Bacillus subtilis*: sequences of the *flgB, flgC, flgG, fliE* and *fliF* genes. Gene. 1991;101(1):23-31.
166. Courtney CR, Cozy LM, Kearns DB. Molecular characterization of the flagellar hook in *Bacillus subtilis*. Journal of bacteriology. 2012;194(17):4619-29.
167. Iino T, Komeda Y, Kutsukake K, Macnab RM, Matsumura P, Parkinson JS, *et al.* New unified nomenclature for the flagellar genes of *Escherichia coli* and *Salmonella typhimurium*. Microbiological reviews. 1988;52(4):533-5.
168. Bonifield HR, Yamaguchi S, Hughes KT. The flagellar hook protein, FlgE, of *Salmonella enterica* serovar *Typhimurium* is posttranscriptionally regulated in response to the stage of flagellar assembly. Journal of Bacteriology. 2000;182(14):4044-50.
169. Ohnishi K, Ohto Y, Aizawa S, Macnab RM, Iino T. FlgD is a scaffolding protein needed for flagellar hook assembly in *Salmonella typhimurium.* Journal of bacteriology. 1994;176(8):2272-81.
170. Hirano T, Yamaguchi S, Oosawa K, Aizawa S-I. Roles of FliK and FlhB in determination of flagellar hook length in *Salmonella typhimurium*. Journal of bacteriology. 1994;176(17):5439-49.
171. Minamino T, González-Pedrajo B, Yamaguchi K, Aizawa SI, Macnab RM. FliK, the protein responsible for flagellar hook length control in *Salmonella*, is exported during hook assembly. Molecular microbiology. 1999;34(2):295-304.
172. Ferris HU, Furukawa Y, Minamino T, Kroetz MB, Kihara M, Namba K, *et al.* FlhB regulates ordered export of flagellar components via autocleavage mechanism. Journal of Biological Chemistry. 2005;280(50):41236-42.
173. Williams AW, Yamaguchi S, Togashi F, Aizawa S-I, Kawagishi I, Macnab RM. Mutations in *fliK* and *flhB* affecting flagellar hook and filament assembly in *Salmonella typhimurium*. Journal of bacteriology. 1996;178(10):2960-70.
174. Silverman MR, Simon MI. Flagellar assembly mutants in *Escherichia coli*. Journal of Bacteriology. 1972;112(2):986-93.
175. Samatey FA, Matsunami H, Imada K, Nagashima S, Shaikh TR, Thomas DR, *et al.* Structure of the bacterial flagellar hook and implication for the molecular universal joint mechanism. Nature. 2004;431(7012):1062-8.
176. Chevance FF, Hughes KT. Coordinating assembly of a bacterial macromolecular machine. Nature reviews microbiology. 2008;6(6):455-65.
177. LaVallie ER, Stahl ML. Cloning of the flagellin gene from *Bacillus subtilis* and complementation studies of an in *vitro*-derived deletion mutation. Journal of Bacteriology. 1989;171(6):3085-94.
178. Auvray F, Thomas J, Fraser GM, Hughes C. Flagellin polymerisation control by a cytosolic export chaperone. Journal of molecular biology. 2001;308(2):221-9.
179. Mukherjee S, Babitzke P, Kearns DB. FliW and FliS function independently to control cytoplasmic flagellin levels in *Bacillus subtilis*. Journal of bacteriology. 2013;195(2):297-306.

180. Oshiro R, Rajendren S, Hundley H, Kearns D. Robust stoichiometry of FliW-CsrA governs flagellin homeostasis and cytoplasmic organization in *Bacillus subtilis.* MBio. 2019;10(3):10.1128/mbio. 00533-19.
181. Yonekura K, Maki S, Morgan DG, DeRosier DJ, Vonderviszt F, Imada K, *et al.* The bacterial flagellar cap as the rotary promoter of flagellin self-assembly. Science. 2000;290(5499):2148-52.
182. Guttenplan SB, Shaw S, Kearns DB. The cell biology of peritrichous flagella in *Bacillus subtilis*. Molecular microbiology. 2013;87(1):211-29.
183. Patrick JE, Kearns DB. Swarming motility and the control of master regulators of flagellar biosynthesis. Molecular microbiology. 2012;83(1):14-23.
184. Nambu T, Minamino T, Macnab RM, Kutsukake K. Peptidoglycan-hydrolyzing activity of the FlgJ protein, essential for flagellar rod formation in *Salmonella typhimurium*. Journal of bacteriology. 1999;181(5):1555-61.
185. Herlihey FA, Moynihan PJ, Clarke AJ. The essential protein for bacterial flagella formation FlgJ functions as a β-N-acetylglucosaminidase. Journal of biological chemistry. 2014;289(45):31029-42.
186. Dubnau D. Genetic competence in *Bacillus subtilis*. Microbiological reviews. 1991;55(3):395-424.
187. Veening J-W, Smits WK, Kuipers OP. Bistability, epigenetics, and bet-hedging in bacteria. Annu Rev Microbiol. 2008;62(1):193-210.
188. Whitchurch CB, Hobbs M, Livingston SP, Krishnapillai V, Mattick JS. Characterisation of a Pseudomonas aeruginosa twitching motility gene and evidence for a specialised protein export system widespread in eubacteria. Gene. 1991;101(1):33-44.
189. Albano M, Breitling R, Dubnau D. Nucleotide sequence and genetic organization of the B*acillus subtilis comG* operon. Journal of bacteriology. 1989;171(10):5386-404.
190. Chung Y, Dubnau D. All seven comG open reading frames are required for DNA binding during transformation of competent *Bacillus subtilis.* Journal of bacteriology. 1998;180(1):41-5.
191. Kilb A, Burghard-Schrod M, Holtrup S, Graumann PL. Uptake of environmental DNA in *Bacillus subtilis* occurs all over the cell surface through a dynamic pilus structure. Plos Genetics. 2023;19(10):e1010696.
192. Inamine G, Dubnau D. ComEA, a *Bacillus subtilis* integral membrane protein required for genetic transformation, is needed for both DNA binding and transport. Journal of bacteriology. 1995;177(11):3045-51.
193. Provvedi R, Dubnau D. ComEA is a DNA receptor for transformation of competent *Bacillus subtilis*. Molecular microbiology. 1999;31(1):271-80.
194. Hahn J, Maier B, Haijema BJ, Sheetz M, Dubnau D. Transformation proteins and DNA uptake localize to the cell poles in *Bacillus subtilis.* Cell. 2005;122(1):59-71.
195. Draskovic I, Dubnau D. Biogenesis of a putative channel protein, ComEC, required for DNA uptake: membrane topology, oligomerization and formation of disulphide bonds. Molecular microbiology. 2005;55(3):881-96.
196. Young F, Tipper DJ, Strominger JL. Autolysis of cell walls of *Bacillus subtilis:* Mechanism and possible relationship to competence. Journal of Biological Chemistry. 1964;239(10):PC3600-PC2.
197. Ranhand JM. Autolytic activity and its association with the development of competence in group H streptococci. Journal of bacteriology. 1973;115(2):607-14.

198. Guenzi E, Gasc AM, Sicard MA, Hakenbeck R. A two-component signal-transducing system is involved in competence and penicillin susceptibility in laboratory mutants of *Streptococcus pneumoniae*. Molecular microbiology. 1994;12(3):505-15.
199. Londoño-Vallejo J, Dubnau D. *comF,* a *Bacillus subtilis* late competence locus, encodes a protein similar to ATP-dependent RNA/DNA helicases. Molecular microbiology. 1993;9(1):119-31.
200. Pugsley AP. Translocation of a folded protein across the outer membrane in *Escherichia coli.* Proceedings of the National Academy of Sciences. 1992;89(24):12058-62.
201. Fussenegger M, Facius D, Meier J, Meyer TF. A novel peptidoglycan-linked lipoprotein (ComL) that functions in natural transformation competence of *Neisseria gonorrhoeae.* Molecular microbiology. 1996;19(5):1095-105.
202. Hamilton HL, Dillard JP. Natural transformation of *Neisseria gonorrhoeae*: from DNA donation to homologous recombination. Molecular microbiology. 2006;59(2):376-85.
203. Balachandran P, Hollingshead SK, Paton JC, Briles DE. The autolytic enzyme LytA of *Streptococcus pneumoniae* is not responsible for releasing pneumolysin. Journal of bacteriology. 2001;183(10):3108-16.
204. Koo B-M, Kritikos G, Farelli JD, Todor H, Tong K, Kimsey H, *et al.* Construction and analysis of two genome-scale deletion libraries for *Bacillus subtilis*. Cell systems. 2017;4(3):291-305. e7.
205. Kobayashi K, Ehrlich SD, Albertini A, Amati G, Andersen KK, Arnaud M, *et al.* Essential *Bacillus subtilis* genes. Proceedings of the National Academy of Sciences. 2003;100(8):4678-83.
206. Middlemiss S, Blandenet M, Roberts DM, McMahon A, Grimshaw J, Edwards JM, *et al.* Molecular motor tug-of-war regulates elongasome cell wall synthesis dynamics in *Bacillus subtilis*. Nature Communications. 2024;15(1):5411.
207. Formstone A, Errington J. A magnesium-dependent *mreB* null mutant: implications for the role of *mreB* in *Bacillus subtilis*. Molecular microbiology. 2005;55(6):1646-57.
208. Kondorosi A, Kondorosi E, Pankhurst C, Broughton W, Banfalvi Z. Mobilization of a *Rhizobium meliloti* megaplasmid carrying nodulation and nitrogen fixation genes into other rhizobia and Agrobacterium. Molecular and General Genetics MGG. 1982;188:433-9.
209. Lewis PJ, Marston AL. GFP vectors for controlled expression and dual labelling of protein fusions in *Bacillus subtilis*. Gene. 1999;227(1):101-9.
210. Anagnostopoulos C, Spizizen J. Requirements for transformation in *Bacillus subtilis*. Journal of bacteriology. 1961;81(5):741-6.
211. Hamoen LW, Smits WK, Jong Ad, Holsappel S, Kuipers OP. Improving the predictive value of the competence transcription factor (ComK) binding site in *Bacillus subtilis* using a genomic approach. Nucleic acids research. 2002;30(24):5517-28.
212. Hanahan D, Glover D. DNA cloning: a practical approach. DNA cloning: a practical approach. 1985;1:109-35.
213. Bergmans H, Van Die I, Hoekstra W. Transformation in *Escherichia coli*: stages in the process. Journal of bacteriology. 1981;146(2):564-70.
214. Glauner B. Separation and quantification of muropeptides with high-performance liquid chromatography. Analytical biochemistry. 1988;172(2):451-64.
215. Desmarais SM, De Pedro MA, Cava F, Huang KC. Peptidoglycan at its peaks: how chromatographic analyses can reveal bacterial cell wall structure and assembly. Molecular microbiology. 2013;89(1):1-13.

216. Porfírio S, Carlson RW, Azadi P. Elucidating peptidoglycan structure: an analytical toolset. Trends in microbiology. 2019;27(7):607-22.
217. Bui NK, Gray J, Schwarz H, Schumann P, Blanot D, Vollmer W. The peptidoglycan sacculus of *Myxococcus xanthus* has unusual structural features and is degraded during glycerol-induced myxospore development. Journal of Bacteriology. 2009;191(2):494-505.
218. Zhao G, Meier TI, Kahl SD, Gee KR, Blaszczak LC. BOCILLIN FL, a sensitive and commercially available reagent for detection of penicillin-binding proteins. Antimicrobial agents and chemotherapy. 1999;43(5):1124-8.
219. Zapun A, Philippe J, Abrahams KA, Signor L, Roper DI, Breukink E, *et al.* In vitro reconstitution of peptidoglycan assembly from the Gram-positive pathogen *Streptococcus pneumoniae*. ACS chemical biology. 2013;8(12):2688-96.
220. Lupoli TJ, Tsukamoto H, Doud EH, Wang T-SA, Walker S, Kahne D. Transpeptidase-mediated incorporation of D-amino acids into bacterial peptidoglycan. Journal of the American Chemical Society. 2011;133(28):10748-51.
221. Kuru E, Tekkam S, Hall E, Brun YV, Van Nieuwenhze MS. Synthesis of fluorescent D-amino acids and their use for probing peptidoglycan synthesis and bacterial growth in situ. Nature protocols. 2015;10(1):33-52.
222. Kuru E, Hughes HV, Brown PJ, Hall E, Tekkam S, Cava F, *et al.* In situ probing of newly synthesized peptidoglycan in live bacteria with fluorescent D-amino acids. Angewandte Chemie. 2012;124(50):12687-91.
223. Tsui HCT, Boersma MJ, Vella SA, Kocaoglu O, Kuru E, Peceny JK, *et al.* Pbp2x localizes separately from Pbp2b and other peptidoglycan synthesis proteins during later stages of cell division of *Streptococcus pneumoniae* D 39. Molecular microbiology. 2014;94(1):21-40.
224. Bisson-Filho AW, Hsu Y-P, Squyres GR, Kuru E, Wu F, Jukes C, *et al.* Treadmilling by FtsZ filaments drives peptidoglycan synthesis and bacterial cell division. Science. 2017;355(6326):739-43.
225. Hsu Y-P, Rittichier J, Kuru E, Yablonowski J, Pasciak E, Tekkam S, *et al.* Full color palette of fluorescent d-amino acids for in situ labeling of bacterial cell walls. Chemical science. 2017;8(9):6313-21.
226. Morales Angeles D, Liu Y, Hartman AM, Borisova M, de Sousa Borges A, de Kok N, *et al.* Pentapeptide-rich peptidoglycan at the *Bacillus subtilis* cell-division site. Molecular microbiology. 2017;104(2):319-33.
227. Liu T-Y, Chu S-H, Shaw G-C. Deletion of the cell wall peptidoglycan hydrolase gene *cwlO* or *lytE* severely impairs transformation efficiency in *Bacillus subtilis.* The Journal of General and Applied Microbiology. 2018;64(3):139-44.
228. Beadle BM, Nicholas RA, Shoichet BK. Interaction energies between β-lactam antibiotics and *E. coli* penicillin-binding protein 5 by reversible thermal denaturation. Protein Science. 2001;10(6):1254-9.
229. Sharifzadeh S, Dempwolff F, Kearns DB, Carlson EE. Harnessing β-lactam antibiotics for illumination of the activity of penicillin-binding proteins in *Bacillus subtilis*. ACS chemical biology. 2020;15(5):1242-51.
230. Davies C, White SW, Nicholas RA. Crystal structure of a deacylation-defective mutant of penicillin-binding protein 5 at 2.3-Å resolution. Journal of Biological Chemistry. 2001;276(1):616-23.

231. Kawai Y, Asai K, Errington J. Partial functional redundancy of MreB isoforms, MreB, Mbl and MreBH, in cell morphogenesis of *Bacillus subtilis.* Molecular microbiology. 2009;73(4):719-31.
232. Garti-Levi S, Hazan R, Kain J, Fujita M, Ben-Yehuda S. The FtsEX ABC transporter directs cellular differentiation in *Bacillus subtilis*. Molecular microbiology. 2008;69(4):1018-28.
233. Ishikawa S, Hara Y, Ohnishi R, Sekiguchi J. Regulation of a new cell wall hydrolase gene, *cwlF*, which affects cell separation in *Bacillus subtilis.* Journal of bacteriology. 1998;180(9):2549-55.
234. Rogers H, Thurman P, Buxton R. Magnesium and anion requirements of *rodB* mutants of *Bacillus subtilis.* Journal of Bacteriology. 1976;125(2):556-64.
235. Mendelson NH. Helical growth of *Bacillus subtilis*: a new model of cell growth. Proceedings of the National Academy of Sciences. 1976;73(5):1740-4.
236. Scheffers D-J, Errington J. PBP1 is a component of the *Bacillus subtilis* cell division machinery. Journal of bacteriology. 2004;186(15):5153-6.
237. Scheffers DJ, Jones LJ, Errington J. Several distinct localization patterns for penicillin-binding proteins in *Bacillus subtilis.* Molecular microbiology. 2004;51(3):749-64.
238. Mewes A, Langer G, de Nooijer LJ, Bijma J, Reichart G-J. Effect of different seawater Mg2+ concentrations on calcification in two benthic foraminifers. Marine micropaleontology. 2014;113:56-64.
239. Isshiki K, Azuma K. Microbial growth suppression in food using calcinated calcium. Japan Agricultural Research Quarterly. 1995;29:269-74.
240. Dominguez DC. Calcium signalling in bacteria. Molecular microbiology. 2004;54(2):291-7.
241. Souza A, Parnell M, Rodriguez BJ, Reynaud EG. Role of pH and Crosslinking Ions on Cell Viability and Metabolic Activity in Alginate–Gelatin 3D Prints. Gels. 2023;9(11):853.
242. Sanjaya A, Praseptiangga D, Zaman M, Umiati V, Baraja S, editors. Effect of pH, temperature, and salt concentration on the growth of *Bacillus subtilis* T9-05 isolated from fish sauce. IOP Conference Series: Earth and Environmental Science; 2023: IOP Publishing.
243. Guo T, Herman JK. Magnesium modulates *Bacillus subtilis* cell division frequency. Journal of Bacteriology. 2023;205(1):e00375-22.
244. Wu J, Schuch R, Piggot P. Characterization of a *Bacillus subtilis* sporulation operon that includes genes for an RNA polymerase sigma factor and for a putative DD-carboxypeptidase. Journal of bacteriology. 1992;174(15):4885-92.
245. Margot P, Karamata D. Identification of the structural genes for N-acetylmuramoyl-L-alanine amidase and its modifier in *Bacillus subtilis* 168: inactivation of these genes by insertional mutagenesis has no effect on growth or cell separation. Molecular and General Genetics MGG. 1992;232:359-66.
246. Koch A. Orientation of the peptidoglycan chains in the sacculus of *Escherichia coli.* Research in microbiology. 1998;149(10):689-701.
247. Boulbitch A, Quinn B, Pink D. Elasticity of the rod-shaped gram-negative eubacteria. Physical Review Letters. 2000;85(24):5246.
248. Kearns DB, Chu F, Rudner R, Losick R. Genes governing swarming in *Bacillus subtilis* and evidence for a phase variation mechanism controlling surface motility. Molecular microbiology. 2004;52(2):357-69.

249. Matias VR, Beveridge TJ. Cryo-electron microscopy reveals native polymeric cell wall structure in *Bacillus subtilis* 168 and the existence of a periplasmic space. Molecular microbiology. 2005;56(1):240-51.
250. Vollmer W, Seligman SJ. Architecture of peptidoglycan: more data and more models. Trends in microbiology. 2010;18(2):59-66.
251. Hayhurst EJ, Kailas L, Hobbs JK, Foster SJ. Cell wall peptidoglycan architecture in Bacillus subtilis. Proceedings of the National Academy of Sciences. 2008;105(38):14603-8.
252. Mendelson NH. Dynamics of *Bacillus subtilis* helical macrofiber morphogenesis: writhing, folding, close packing, and contraction. Journal of Bacteriology. 1982;151(1):438-49.
253. Mendelson NH, Favre D, Thwaites J. Twisted states of *Bacillus subtilis* macrofibers reflect structural states of the cell wall. Proceedings of the National Academy of Sciences. 1984;81(11):3562-6.
254. Sun Y-J, Bai F, Luo A-C, Zhuang X-Y, Lin T-S, Sung Y-C, *et al.* Probing bacterial cell wall growth by tracing wall-anchored protein complexes. Nature Communications. 2021;12(1):2160.
255. Nelson DE, Young KD. Penicillin binding protein 5 affects cell diameter, contour, and morphology of *Escherichia coli.* Journal of bacteriology. 2000;182(6):1714-21.
256. Peters K, Kannan S, Rao VA, Biboy J, Vollmer D, Erickson SW, *et al.* The redundancy of peptidoglycan carboxypeptidases ensures robust cell shape maintenance in *Escherichia coli*. MBio. 2016;7(3):10.1128/mbio. 00819-16.
257. Choi U, Park SH, Lee HB, Son JE, Lee C-R. Coordinated and distinct roles of peptidoglycan carboxypeptidases DacC and DacA in cell growth and shape maintenance under stress conditions. Microbiology Spectrum. 2023;11(3):e00014-23.
258. Bourai N, Jacobs Jr WR, Narayanan S. Deletion and overexpression studies on DacB2, a putative low molecular mass penicillin binding protein from *Mycobacterium tuberculosis* H37Rv. Microbial pathogenesis. 2012;52(2):109-16.
259. Markiewicz Z, Glauner B, Schwarz U. Murein structure and lack of DD-and LD-carboxypeptidase activities in *Caulobacter crescentus*. Journal of bacteriology. 1983;156(2):649-55.
260. Miguel-Arribas A, Hao J-A, Luque-Ortega JR, Ramachandran G, Val-Calvo J, Gago-Córdoba C, *et al.* The *Bacillus subtilis* conjugative plasmid pLS20 encodes two ribbon-helix-helix type auxiliary relaxosome proteins that are essential for conjugation. Frontiers in Microbiology. 2017;8:2138.
261. Puyet A, Sandoval H, Lopez P, Aguilar A, Martin J, Espinosa M. A simple medium for rapid regeneration of *Bacillus subtilis* protoplasts transformed with plasmid DNA. FEMS microbiology letters. 1987;40(1):1-5.

Appendices

Appendix 1- DacA is a secreted protein

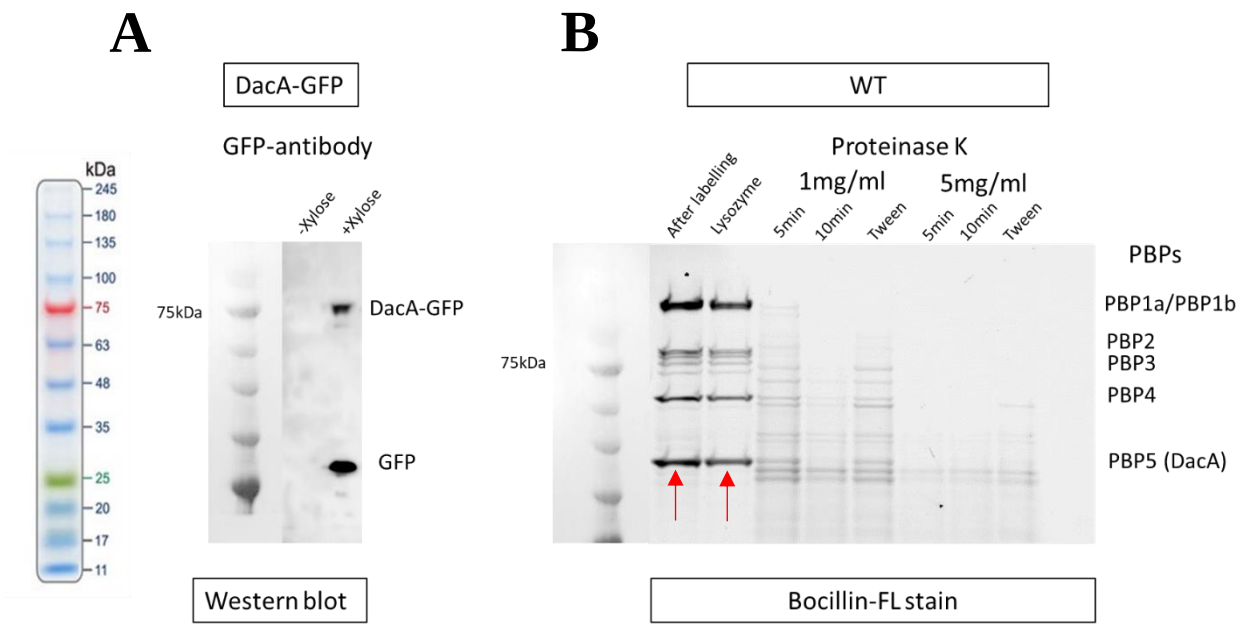

Supplementary Figure 1.1 DacA is a secreted protein

A- Western blot analysis of cell lysates is shown to detect GFP-DacA expression in the following strain (AA101) with the *dacA* 'P_{xyl}-*gfp-dacA*, using a 1/10000 dilution of GFP antibodies. The upper band indicated GFP-DacA (molecular wight 75.47 kDa), while the lower band indicated the cleavage GFP (molecular wight 27 kDa). **B-** SDS PAGE of the168CA cell lysate shows the PBPs labeled by the Bocillin FL stain. Red arrows are the bands corresponding to DacA.

To determine whether DacA is a cell membrane or secreted protein, strain AA101 with the *dacA* 'P_{xyl}-*gfp-dacA* was used. The correct construct was first checked via western blot (as described in Chapter 2/ Section 2.16). However, it was observed that GFP was cleaved off, which could lead to incorrect DacA detection (Supplementary Figure 1.1A). Consequently, Bocillin FL (Invitrogen) was used as a labeling reagent to detect penicillin binding proteins (PBPs), specifically DacA (PBP5) (218).

Samples were prepared as: 20 mL LB was inoculated with 168CA cells and incubated at 37 °C overnight. The following day, the growing culture was diluted back in fresh LB (OD600 nm ~0.05) and incubated until reaching (OD600 nm ~0.5-1). The culture was labeled by 20 µl of Bocillin FL penicillin stain (Invitrogen) and allowed to incubate for 2 minutes. Subsequently, 1

mL of the culture was centrifuged at 13,300 x *g* for 3 minutes. The supernatant was discarded, and the cell pellets were placed in ice. The remaining 29 mL culture was centrifuged, and the cells were suspended in 20 mL MSM (1 M sucrose, 0.04 M malic acid, 0.04 $MgCl_2.6H_2O$, pH 6.5) (261). Next, 0.4% (w/v) lysozyme (4 mg/mL) was added, and the sample was incubated with light shaking for 20 mins. 1 mL of the sample was collected and centrifuged, and the cell pellets were kept in ice. The remaining sample was divided into two tubes, with one receiving 1 mg/mL of proteinase K and the other receiving 5 mg/mL. After 5 and 10 minutes, 1 mL of each sample was collected, centrifuged, and placed in ice. The remaining samples were treated with 0.01%, (v/v) Tween detergent for 10 min, collected, centrifuged, and kept in ice.

Subsequently, all samples were suspended in SDS buffer containing a proteinase K inhibitor, sonicated and resolved via SDS-PAGE (as described previously in Chapter 2/ Section 2.16.1). The labeled penicillin binding proteins were visualised via a Typhoon scanner - FITC channel (488 nm- blue) with an absorbance peak of 490 nm.

Distinct bands of PBPs labeled with Bocillin FL were identified (Supplementary Figure 1.1B). The DacA band was still observed even after lysates were treated with lysozyme (protoplast cells), confirming that DacA is a secreted protein (red arrows).

Appendix 2- Reserved-phase high-performance liquid chromatography (RP-HPLC) profile

Supplementary Table 2.1

Muropeptide*	Muropeptide identification	168CA	168CA (25mM Mg)	*ΔdacA*	*ΔlytE ΔlytF ΔdacA* (25mM Mg)	*lytE***	*cwlO****
1	Tri	0.91	1.73	0	0	0.87	1.19
2	Tri (NH_2) (PO_4)	1.13	1.33	0.55	1.08	0.44	0.64
3	Tri (NH_2)	16.11	17.57	1.6	0.86	17.08	17.4
4	Tri (NH_2)	0	0	0	0	0	0
5	Di	2.19	2.11	2.55	1.75	2.63	3.67
6	Tri-Ala-mDap (NH_2)	0.74	0.94	0	0.43	0.7	1.21
7	tetra (NH_2)	0.83	0.76	0.39	0	0.86	0.91
8	Tri-Ala-mDap (NH2)2	1.79	0.97	0.26	0.26	2.52	3.44
9	penta (Gly5 (NH2)	0	0.24	4.43	8.47	0	0
10	Tri Tetra (-GM) (NH2)2	0.66	0.43	0	0.48	0.57	0
11	penta (NH2)	0	0	16.56	19.06	0	0
12	Tri Tetra (-G)	0	0	1.34	1.28	0	0
13	Tri Tetra (NH2) (PO4)	0.81	1.21	4.27	2.01	0.77	0.57
14	Tetra Tetra (-GM) (NH2)2	0.9	1.19	3.12	1.62	0.89	0.81
15	Tri Tetra (NH2)	11.67	21.02	5.55	11.01	10.01	12.94
18	Tri Tetra (NH2) (deAc)	1.95	2.48	1.46	0.77	1.07	1.19
19	Tri Tetra (NH2) (deAc)	2.02	2.58	1.4	2.86	0.87	1.15
20	Tri Tetra (NH2)	1.32	2.11	3.05	5.46	2.15	1.93
21	Tri Tetra (NH2)2	28.42	18.22	20.49	15.58	38.36	30.21
22	Tri Tetra (NH2)2 (deAc)	4.3	1.7	7.01	3.06	3.09	2.58
23	Tri Tetra (NH2)2 (deAc)	0.52	0.75	0.57	0.31	0.67	0.57
24	Penta (Gly5) Tetra	0	0.66	0.18	0	0	0
25	Penta (Gly5) Tetra (NH2)2	0.56	0.56	0.33	0.54	0.82	0.5
26	TetraTetra (NH2)2	0.66	0.47	0.6	0.73	0.81	0.73
27	PentaTetra (NH2)2	0.5	0.31	1	1.15	0.7	0.54
28	TriTetraTetra (NH2)2	0.42	0.69	0.52	0.79	0	0.4
29	TriTetraTetra (-G)	1.06	1.49	1.34	1.67	0.75	0.64
30	TriTetraTetra (NH2)2	0.59	0.56	0	0	0	0
31	TriTetraTetra (NH2)3	2.51	3.18	1.96	1.05	1.51	2.03
32	TriTetraTetra (NH2)3 (deAc)	3.4	1.89	0.51	0	2.86	2.57
33	TriTetraTetra (NH2)3 (deAc)	0.87	0.34	0	0	0.53	0.49
34	Penta(Gly5)TetraTetra (NH2)2-3	0.52	0	0.32	0	0	0
35	TriTetraTetraTetra (NH2)2-3	0.66	0.81	0.27	0.36	0	0.58
36	TriTetra(Anh) (NH2)2	0	0	0	0	0	0
37	TriTetraTetraTetra (NH2)4	1.08	0.92	0.24	0.18	1.5	1.3
38	TriTetraTetra(Anh) (NH2)2	0	0	0.7	0.20	0	0

* Muropeptide are numbered from the RP-HPLC profile of muropeptides (Supplementary Figure 2.1) and as described by Atrih (60).

** *lytE* is the multiple vegetative autolytic mutant that only expressed LytE and lacked LytD, LytG, LytC, LytF, CwlS, CwlQ, and CwlO enzymes (*ΔlytD ΔlytG ΔlytC ΔlytF ΔcwlS ΔcwlQ ΔcwlO*)

****cwlO* is the multiple vegetative autolytic mutant that only expressed CwlO and lacked LytD, LytG, LytC, LytF, CwlS, CwlQ, and LytE (*ΔlytD ΔlytG ΔlytC ΔlytF ΔcwlS ΔcwlQ ΔlytE*).

A

168CA

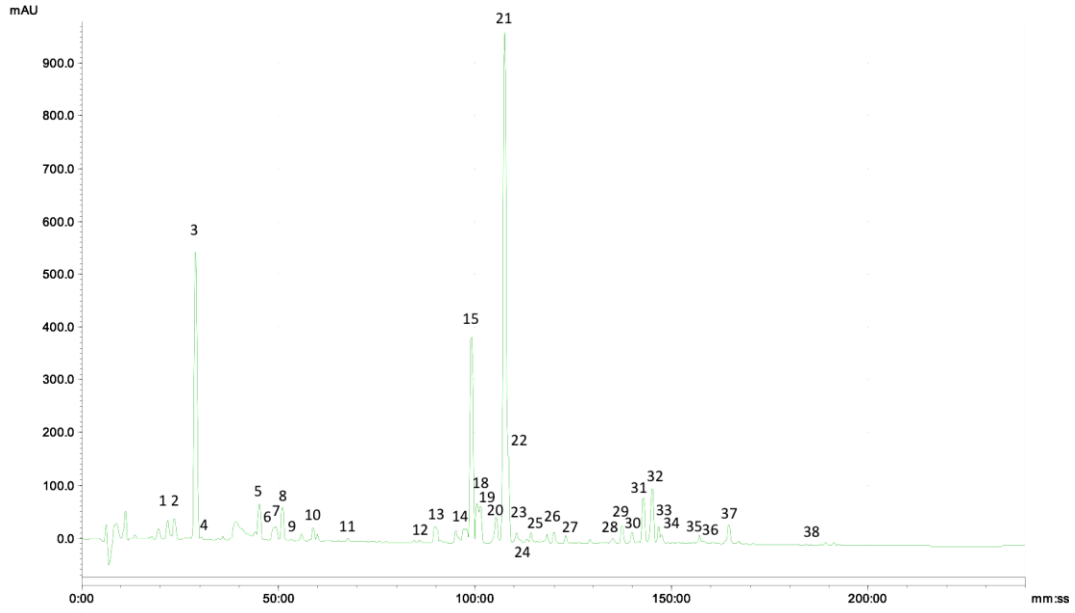

B

168CA (25 mM Mg^{2+})

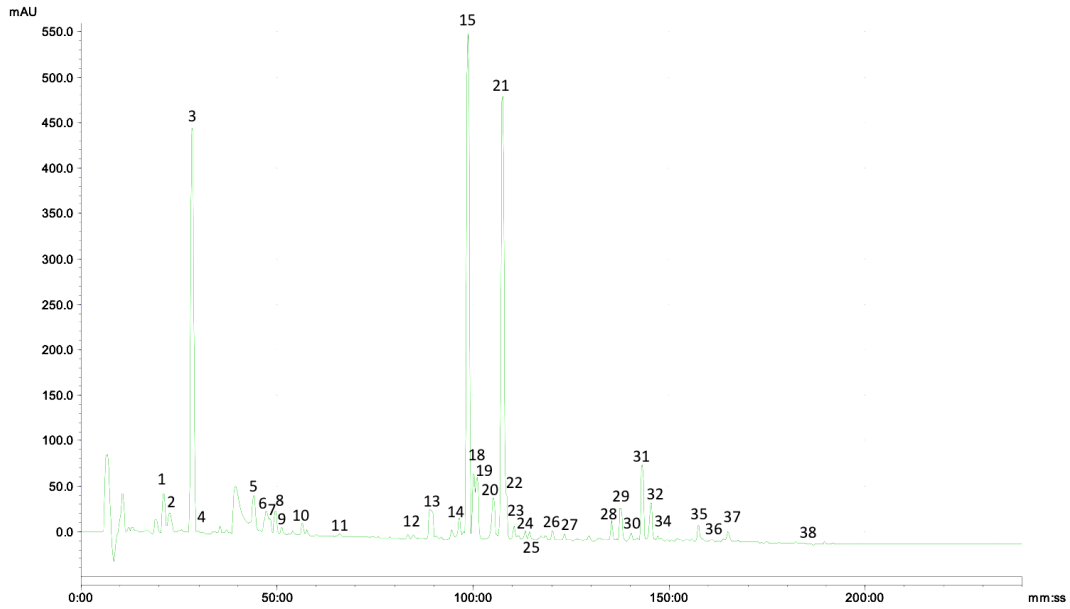

C

Δ*dacA*

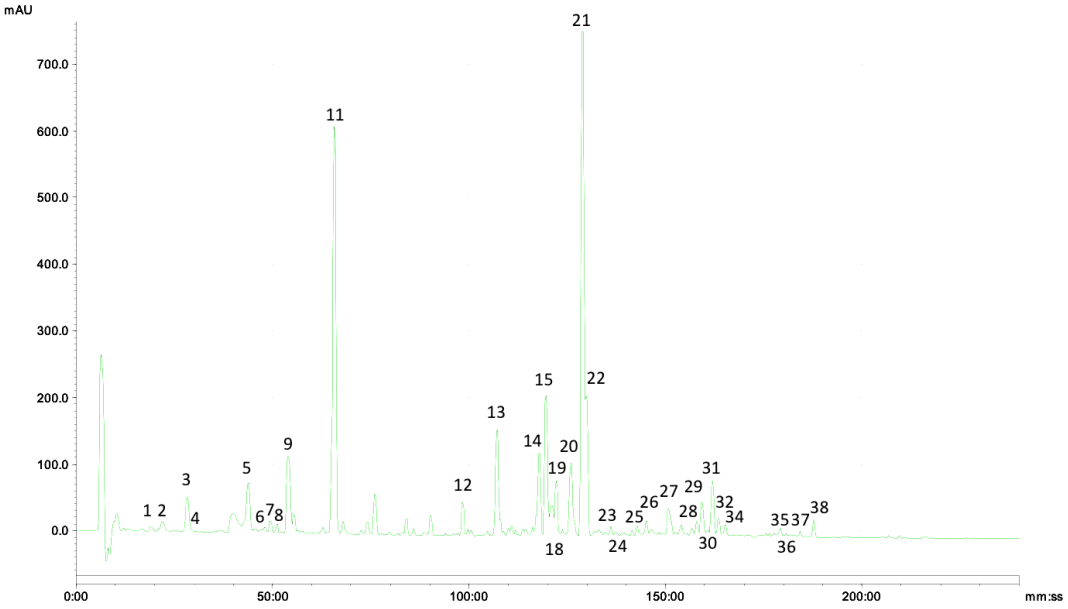

D

Δ*lytE* Δ*lytF* Δ*dacA* (25 mM Mg^{2+})

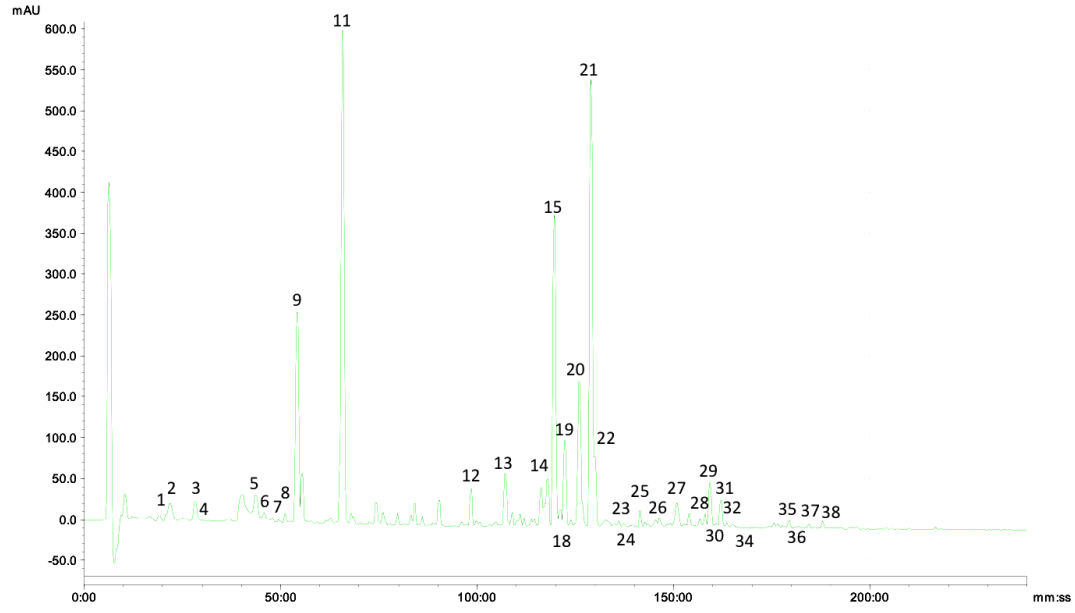

E

Δ*lytD* Δ*lytG* Δ*lytC* Δ*lytF* Δ*cwlS* Δ*cwlQ* Δ*cwlO*

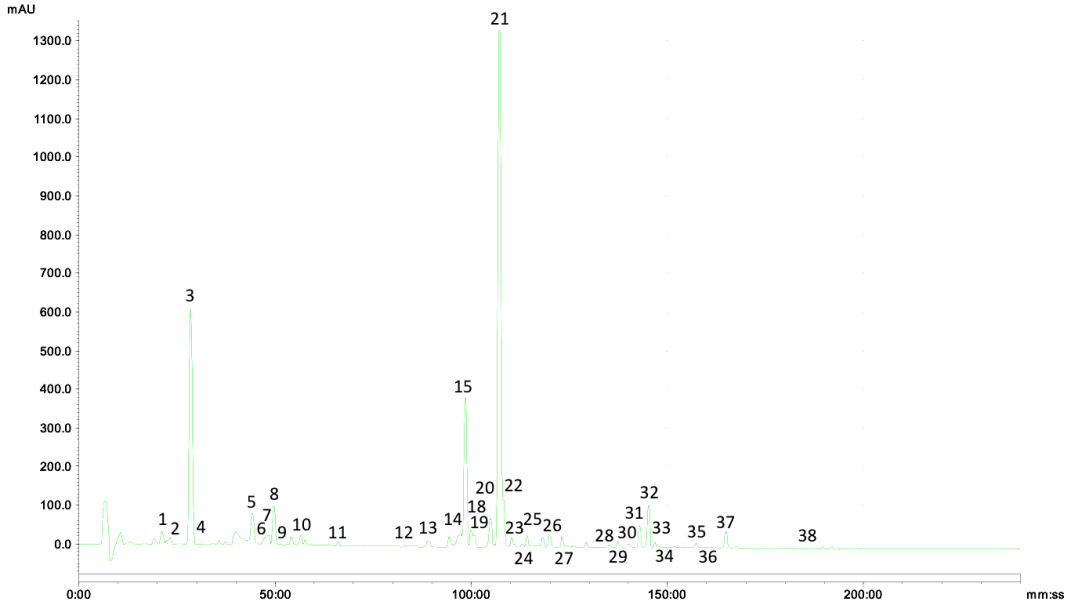

F

Δ*lytD* Δ*lytG* Δ*lytC* Δ*lytF* Δ*cwlS* Δ*cwlQ* Δ*lytE*

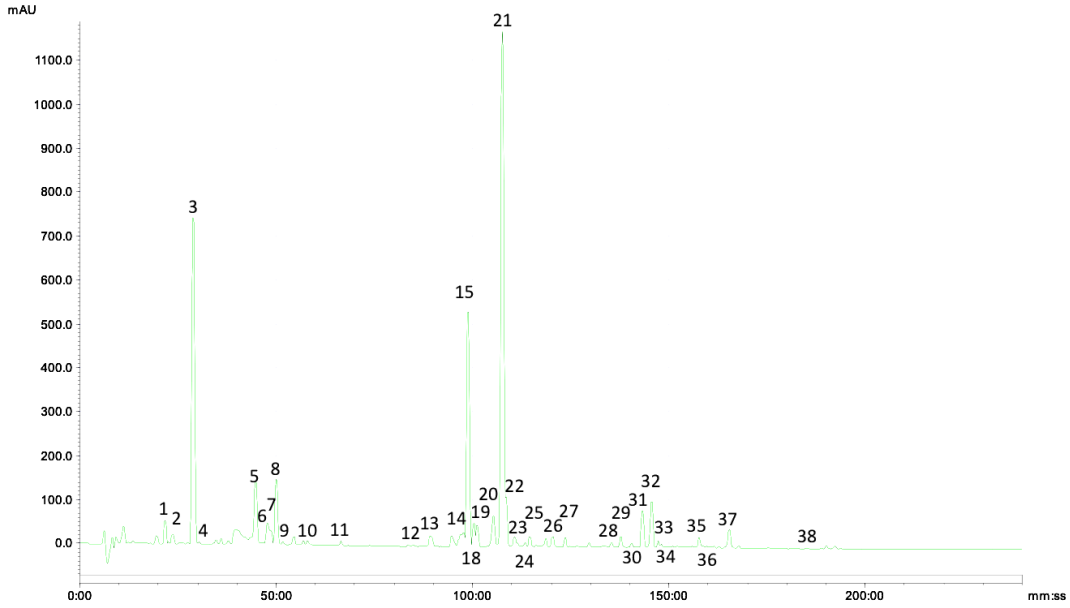

Supplementary Figure 2.1 Muropeptide analysis

RP-HPLC profile of muropeptides for the following strains: **A-** 168CA, **B**-168CA (25 mM Mg^{2+}), **C-** Δ*dacA*, **D-** Δ*lytE* Δ*lyF* Δ*dacA* (25 mM Mg^{2+}), **E-** Δ*lytD* Δ*lytG* Δ*lytC* Δ*lytF* Δ*cwlS* Δ*cwlQ* Δ*cwlO,* and **F-** Δ*lytD* Δ*lytG* Δ*lytC* Δ*lytF* Δ*cwlS* Δ*cwlQ* Δ*lytE*.

Appendix 3- Width and length variations between different genotypes

Supplementary Tables 3.1 Width and length variations of strains in a *dacA* background

A- Percentage of width variation in mid-exponential phase

Strains	*ΔdacA*	*ΔlytF*	*ΔlytE*	*ΔlytE ΔdacA* (+Mg^{2+})	*ΔlytF ΔdacA*	*ΔlytF ΔdacA* (+Mg^{2+})
ΔdacA	-	17.74	24.8	-13.05	-8.26	-17.79
ΔlytF	-15.07	-	5.99	-26.15	-22.08	-30.18
ΔlytE	-19.87	-5.65	-	-30.33	-26.49	-34.12
***ΔlytE ΔdacA* (+Mg^{2+})**	15.01	35.41	43.53	-	5.51	-5.45
ΔlytF ΔdacA	9.00	28.34	36.03	-5.22	-	-10.39
***ΔlytF ΔdacA* (+Mg^{2+})**	21.64	43.22	51.8	5.76	11.59	-

B- Percentage of width variation in stationary phase

Strains	*ΔdacA*	*ΔlytF*	*ΔlytE*	*ΔlytE ΔdacA* (+Mg^{2+})	*ΔlytF ΔdacA*	*ΔlytF ΔdacA* (+Mg^{2+})
ΔdacA	-	10.99	16.28	-17.96	-18.51	-21.97
ΔlytF	-9.90	-	4.76	-26.09	-26.58	-29.70
ΔlytE	-14.00	-4.54	-	-29.45	-29.92	-32.90
***ΔlytE ΔdacA* (+Mg^{2+})**	21.90	35.30	41.75	-	-0.66	-4.89
ΔlytF ΔdacA	22.71	36.20	42.69	0.67	-	-4.25
***ΔlytF ΔdacA* (+Mg^{2+})**	28.16	42.25	49.03	5.14	4.44	-

C- Percentage of length variation in mid-exponential phase

Strains	***ΔdacA***	***ΔlytF***	***ΔlytE***	***ΔlytE ΔdacA* (+Mg^{2+})**	***ΔlytF ΔdacA***	***ΔlytF ΔdacA* (+Mg^{2+})**
ΔdacA	-	-20.93	-36.39	1.25	-11.99	-2.11
ΔlytF	26.47	-	-19.56	28.05	11.30	23.79
ΔlytE	57.21	24.31	-	59.18	38.36	53.89
***ΔlytE ΔdacA* (+Mg^{2+})**	-1.23	-21.90	-37.18	-	-13.08	-3.32
ΔlytF ΔdacA	13.63	-10.15	-27.72	15.05	-	11.23
***ΔlytF ΔdacA* (+Mg^{2+})**	2.16	-19.22	-35.02	3.43	-10.09	-

D- Percentage of length variation in stationary phase

Strains	***ΔdacA***	***ΔlytF***	***ΔlytE***	***ΔlytE ΔdacA* (+Mg^{2+})**	***ΔlytF ΔdacA***	***ΔlytF ΔdacA* (+Mg^{2+})**
ΔdacA	-	-18.55	-28.76	-1.04	5.92	7.60
ΔlytF	22.77	-	-12.53	21.49	30.04	32.11
ΔlytE	40.37	14.33	-	38.90	48.67	51.04
***ΔlytE ΔdacA* (+Mg^{2+})**	1.05	-17.69	-28.01	-	7.03	8.74
ΔlytF ΔdacA	-5.59	-23.10	-32.74	-6.57	-	1.59
***ΔlytF ΔdacA* (+Mg^{2+})**	-7.07	-24.30	-33.79	-8.04	-1.57	-

Supplementary Tables 3.2 Width and length variations of strains in *dacA* and/or *mreB* backgrounds

A- Percentage of width variation in mid-exponential phase

Strains	*ΔdacA*	*ΔmreB*	*ΔmreB ΔdacA*
ΔdacA	-	-16.40	-43.15
ΔmreB	19.62	-	-32.00
***ΔmreB ΔdacA* (+Mg^{2+})**	75.90	47.05	-

B- Percentage of width variation in stationary phase

Strains	*ΔdacA*	*ΔmreB*	*ΔmreB ΔdacA*
ΔdacA	-	-13.60	-36.50
ΔmreB	15.74	-	-26.50
***ΔmreB ΔdacA* (+Mg^{2+})**	57.47	36.05	-

C- Percentage of length variation in mid-exponential phase

Strains	*ΔdacA*	*ΔmreB*	*ΔmreB ΔdacA*
ΔdacA	-	-11.76	25.74
ΔmreB	13.33	-	42.51
***ΔmreB ΔdacA* (+Mg^{2+})**	-20.47	-29.83	-

D- Percentage of length variation in stationary phase

Strains	*ΔdacA*	*ΔmreB*	*ΔmreB ΔdacA*
ΔdacA	-	-14.91	-10.76
ΔmreB	17.52	-	4.87
***ΔmreB ΔdacA* (+Mg^{2+})**	12.06	-4.65	-

Supplementary Tables 3.3 Width and length variations of strains in *dacA* and/or *cwlO* backgrounds

A- Percentage of width variation in mid-exponential phase

Strains	*ΔdacA*	*ΔlytF*	*ΔcwlO*	*ΔcwlO ΔdacA*	*ΔlytF ΔcwlO*	*ΔlytF ΔdacA*
ΔdacA	-	17.74	-3.27	-12.13	-4.87	-8.26
ΔlytF	-15.07	-	-17.85	-25.37	-19.21	-22.08
ΔcwlO	3.38	21.72	-	-9.16	-1.66	-5.16
ΔcwlO ΔdacA	13.80	33.99	10.08	-	8.26	4.40
ΔlytF ΔcwlO	5.12	23.77	1.69	-7.63	-	-3.56
ΔlytF ΔdacA	9.00	28.34	5.44	-4.22	3.69	-

B- Percentage of width variation in stationary phase

Strains	*ΔdacA*	*ΔlytF*	*ΔcwlO*	*ΔcwlO ΔdacA*	*ΔlytF ΔcwlO*	*ΔlytF ΔdacA*
ΔdacA	-	10.99	-2.72	-19.12	-12.46	-18.51
ΔlytF	-9.91	-	-12.36	-27.13	-21.13	-26.58
ΔcwlO	2.80	14.10	-	-16.86	-10.01	-16.23
ΔcwlO ΔdacA	23.64	37.23	20.28	-	8.24	0.75
ΔlytF ΔcwlO	14.23	26.79	11.12	-7.61	-	-6.92
ΔlytF ΔdacA	22.71	36.21	19.38	-0.75	7.43	-

C- Percentage of length variation in mid-exponential phase

Strains	*ΔdacA*	*ΔlytF*	*ΔcwlO*	*ΔcwlO ΔdacA*	*ΔlytF ΔcwlO*	*ΔlytF ΔdacA*
ΔdacA	-	-20.93	5.02	44.84	-14.13	-11.99
ΔlytF	26.47	-	32.81	83.17	8.60	11.30
ΔcwlO	-4.78	-24.71	-	37.92	-18.23	-16.20
ΔcwlO ΔdacA	-30.96	-45.41	-27.49	-	-40.71	-39.24
ΔlytF ΔcwlO	16.45	-7.92	22.30	68.67	-	2.49
ΔlytF ΔdacA	13.63	-10.15	19.33	64.58	-2.43	-

D- Percentage of length variation in stationary phase

Strains	*ΔdacA*	*ΔlytF*	*ΔcwlO*	*ΔcwlO ΔdacA*	*ΔlytF ΔcwlO*	*ΔlytF ΔdacA*
ΔdacA	-	-18.55	-13.16	19.23	10.64	5.92
ΔlytF	22.77	-	6.62	46.38	35.84	30.04
ΔcwlO	15.15	-6.21	-	37.29	27.41	21.96
ΔcwlO ΔdacA	-16.13	-31.68	-27.16	-	-7.20	-11.16
ΔlytF ΔcwlO	-9.62	-26.38	-21.51	7.76	-	-4.27
ΔlytF ΔdacA	-5.59	-23.10	-18.01	12.57	4.46	-

Appendix 4- Multiple autolytic mutants

A Δ*lytD* Δ*lytG* Δ*lytC* Δ*lytF* Δ*cwlS* Δ*cwlQ* Δ*lytE*

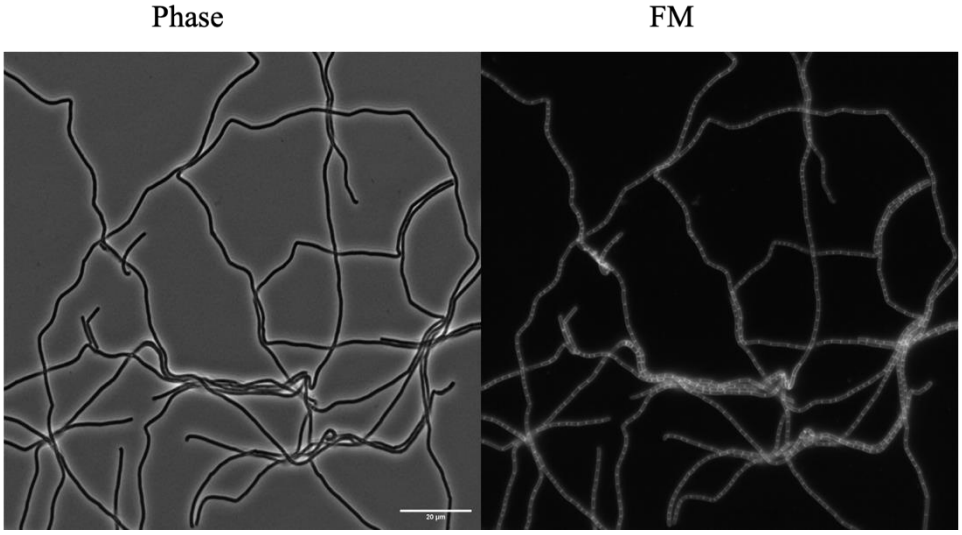

B Δ*lytD* Δ*lytG* Δ*lytC* Δ*lytF* Δ*cwlS* Δ*cwlQ* Δ*cwlO*

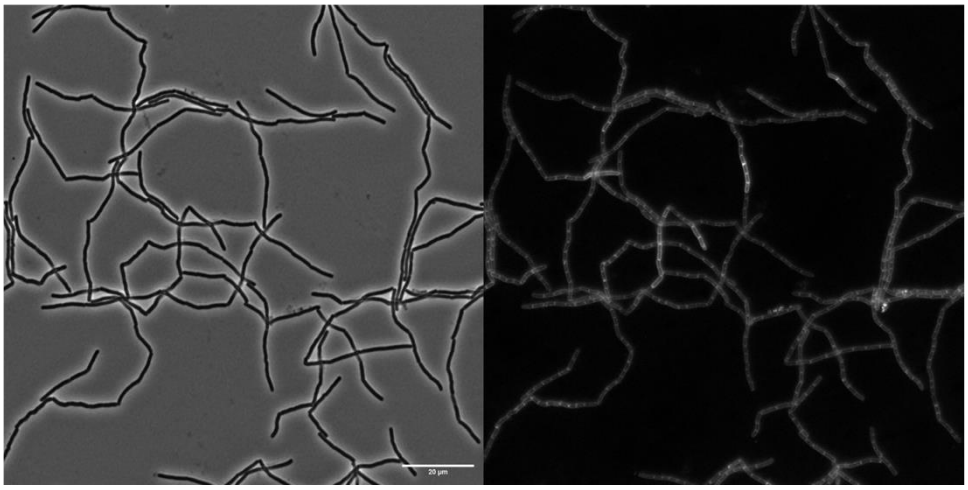

Supplementary Figure 4.1 Brightfield and fluorescence microscopy images of multiple autolytic mutants

Full field of view of multiple autolytic mutants of: **A-** Δ*lytD* Δ*lytG* Δ*lytC* Δ*lytF* Δ*cwlS* Δ*cwlQ* Δ*lytE* and **B-** Δ*lytD* Δ*lytG* Δ*lytC* Δ*lytF* Δ*cwlS* Δ*cwlQ* Δ*cwlO.* Cells of these strains are in very long chains that are tangled, giving a network-like appearance. Scale bars represent 20 microns. The cells were stained with FM5-95 dye.

Appendix 5- Cell phenotypes in the absence of LdcB in *lytE* and/or *lytF* backgrounds

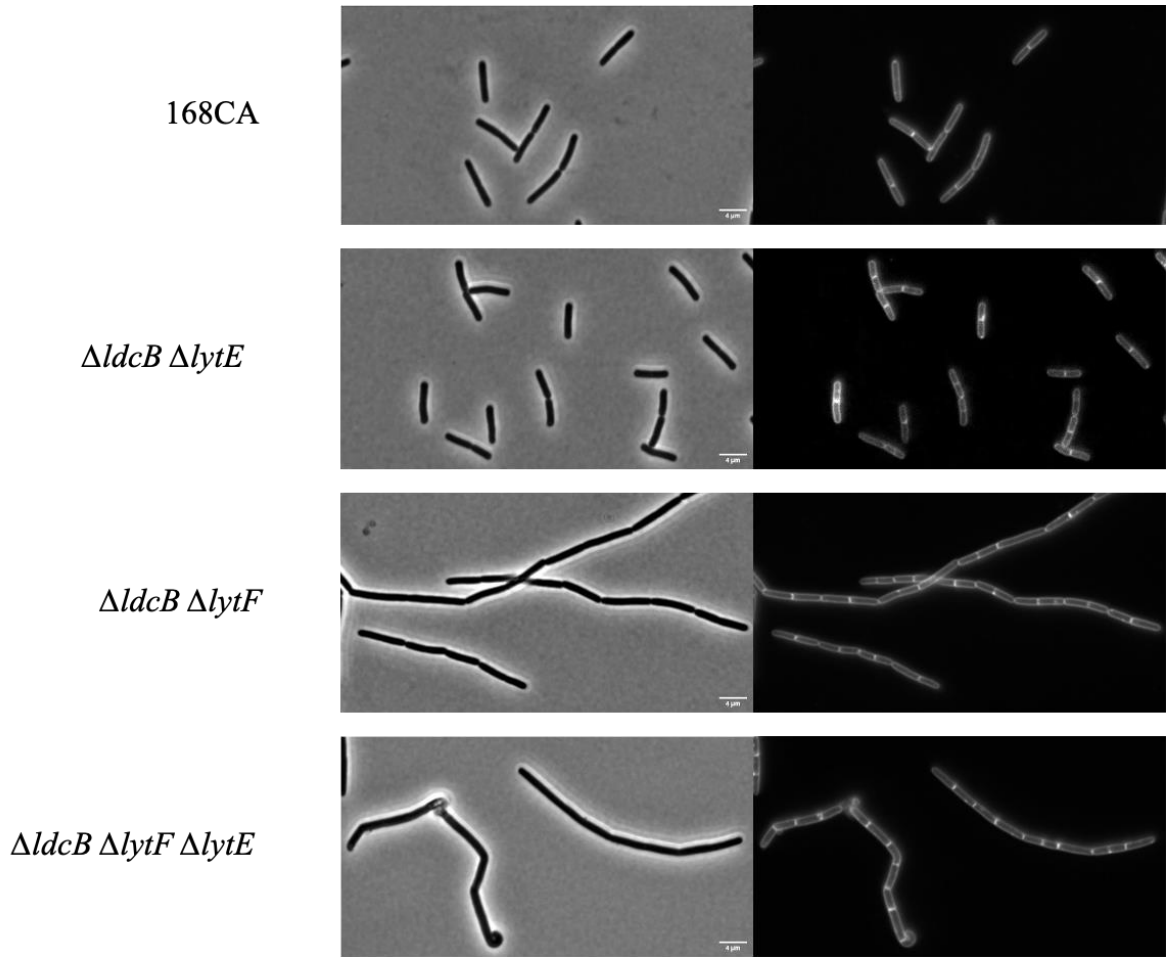

Supplementary Figure 5.1 Morphological effect of the absence of LdcB in different mutant

Fluorescence microscopy images show the cell morphology of strains lacking *ldcB lytE*, *ldcB lytF* and *ldcB lytF lytE* compared to the wild type (168CA). The cells were stained with FM5-95 dye. Scale bars represent 4 microns.

To investigate whether the absence of LD-carboxypeptidase, LdcB, affects the CwlO activity similar to DacA, cells of the mutant *ldcB* in *lytF* and/or *lytE* backgrounds were grown in LB medium until reaching the exponential phase. The cells were visualised under fluorescence microscopy using FM dye. The absence of LdcB in *lytF* and/or *lytE* backgrounds exhibited moderate effects. Notably, cells of the triple mutant *ldcB lytF lytE* displayed a distinctive twisting phenotype, indicating that CwlO function is slightly affected by the absence of LdcB activity.